‘‘Biocompatible and Biodegradable Nanogels and Hydrogels for Protein/Peptide Delivery’’

Von der Fakultät für Mathematik, Informatik und Naturwissenschaften der RWTH Aachen University zur Erlangung des akademischen Grades einer Doktorin der Naturwissenschaften genehmigte Dissertation

vorgelegt von

M.Tech, M.Sc
Smriti Singh

aus
Indien

Berichter: Universitätsprofessor Prof. Dr. Martin Möller
Universitätsprofessor Prof. Dr. Andrij Pich

Tag der mündlichen Prüfung: 21.11.2013

To my loved ones

Table of Contents

List of Abbreviations

Acrylate-sP(EO-*stat*-PO)	Acrylate functionalized star shaped poly (ethylene oxide-*stat*-propylene oxide)
AFM	Atomic force microscopy
AGE	Allyl glycidyl ether
AMPS	2-acrylamido-2-methyl-1-propanesulfonic acid
ANS	Ammonium salt of 8-anilinonaphthalene-1-sulfonic acid
AOT	Bis(2-ethylhexyl) sulfosuccinate
APTMACl	3-acrylamidopropyl-trimethylammonium chloride
APTT	Activated partial thromboplastin time
ASTM	American Society for Testing and Materials
ATRP	Atom transfer radical polymerization
BCA	Bicinchoninic acid
BS3	BS3 Bis(sulfosuccinimidyl) suberate
BSA	Bovine serum albumin
C57BL/6	Inbred strain of laboratory mice
CCR1	C-C chemokine receptor type 1
CCR5	C-C chemokine receptor type 5
CD31 staining	Cluster of differentiation 31 staining
CHP	Cholesterol-bearing PuL
CHPANG	Cholesterol-bearing pullulan
CHPNG	Cholesterol-bearing PuL nanogels
CL	Cellulose
cmc	Critical micelle concentrations
cRGDfC	Cyclo(Arg–Gly–Asp–D-Phe–Cys)
CS	Chitosan
CSF	Cerebro Spinal Fluid
CSKC	Ac-Cys-Ser-Lys-Cys-NH_2
CXCL12	CXCL12 C-X-C motif chemokine 12/ Stromal Cell Derived Factor 1
CYKC	Ac-Cys-Tyr-Lys-Cys-NH_2
DCC	DCC dicyclohexylcarbodiimide
DCC	DCC dicyclohexylcarbodiimide
DDC	N,N-Dicyclohexylcarbodiimide
DDS	Drug delivery system
Dex	Dextran
DHU	Dicyclohexylurea
DIC	Differential interference contrast
DLS	Dynamic light scattering
DMAc	N,N-dimethylacetamide
DMAP	DMAP 4-Dimethylaminopyridine

DMEM	Dulbecco's Modified Eagle Medium
DMF	N,N-dimethylformamide
DMSO	Dimethyl sulfoxide
DOPE	Di-oleoylphosphatidyl ethanol amine
DOX	Doxorubicin
DPPIV/CD26	Dipeptidyl peptidase IV
DSP	Dithiobis(succinimidyl propionate)
DTME	Dithio-bis-maleimidoethane
DTNB	5,5'-dithio-bis(2-nitrobenzoic acid)
DTPA	DTPA 3,3'- Dithiopropionic acid
DTT	Dithiothreitol
ELP	Elastin like polymers
EPO	Erythropoietin
EPR	Enhanced permeability and retention
eq.	Equivalent
EthD -1	Ethidium homo dimer
FAM	Carboxyflourescein
FBS	Fetal bovine serum
FDH	Fast degradable hydrogels
FESEM	Field Emission Scanning Electron Microscopy
GALA	Glutamic acid-alanine-leucine-alanine
GSH	Glutathione
HA	Hyaluronan
Hb	Haemoglobin
HEPES	4-(2-hydroxyethyl)-1-piperazineethanesulfonic acid
HLB	Hydrophilic-Lipophilic BalanceI
HPC	Hydroxypropylcellulose
HRP	Horseradish peroxidase
HS-PEG	Thiolated poly (ethylene glycol)
HS-PG	Thiolated poly(glycidol)
HS-sP(EO-*stat*-PO)	Thiol functionalized star shaped poly (ethylene oxide-*stat*-propylene oxide)
HUVECs	Human umbilical vein endothelial cells
Hy	Hydrazine
IL-12	Interleukin-12
IR	Infrared
LCST	Lower critical solution temperature
MAS-S	N,N'-bis(methacryloyl)-L-cystine
Met- CCL5	Chemokine N-terminal methionine- (C-C motif) ligand 5
MI	Myocardial infarction
MMP-2	Matrix metalloproteinase-2
MWCO	Molecular weight cut off
NAC	N-Acetylcysteine

NF-κB	Nuclear factor
NG	Nanogel
NHS	N-hydroxysuccinimid
NODAGA	2,2'-(7-(1-carboxy-4-((2-(2,5-dioxo-2,5-dihydro-1H-pyrrol-1-yl)ethyl)amino)-4-oxobutyl)-1,4,7-triazonane-1,4-diyl) diacetic acid
NP	Nanoparticle
O.D.	Optical density
O/W	Oil-in-water
OEOMA	Oligo(ethylene glycol) monomethyl ether methacrylate
ONP	o-nitrophenol
ONPG	o-nitrophenyl- β-D-galactopyranoside
OVA	Ovalbumin
PBS	PBS Phosphate buffer saline
PBS	Phosphate buffered saline
PDI	Polydispersity index
PEEGE	Poly(glycidol) acetal
PEG	Poly(ethylene glycol)
PEG-DGE	Poly(ethylene glycol) diglycidyl ether
PET	positron emission tomography
PGA	Polyglycolides
PHEMA	Poly(2-hydroxyethyl methacrylate)
PLA	Polylactides
PLGA	Poly(lactide-co-glycolides)
PMA	Phorbol 12-myristate 13-acetate
PT	Prothrombin time
RBC	Red blood cells
RPMI	Roswell Park Memorial Institute media
SDH	Slow degradable hydrogels
sP(EO-*stat*-PO)	Star shaped poly (ethylene oxide-*stat*-propylene oxide)
STS	Sulfanylthiocarbonylsulfanyl
t-BuGE	*tert*-butyl glycidyl ether
t-BuOK	Potassium *tert*-butoxide
THP1	Human monocytic cell line
VPT	Volume phase transition
VPTT	Volume phase transition temperature
VS	Vinyl sulphone
W/O	Water in oil
β-Gal	β-Galactosidase

Summary

In the present work nanogels and hydrogels composed of functional hydrophilic polymers or proteins crosslinked with degradable crosslinkers are prepared and characterized. The nanogels and hydrogel systems could be modified with targeting molecules for the delivery of peptides or proteins.

As building blocks shaped poly (ethylene oxide-stat-propylene oxide) **(sP(EO-stat-PO)**), linear poly(glycidol) (**PG**) and α-Elastin polypeptide are used. Linear PG was synthesised via anionic polymerization and then functionalizated with thiol groups. **sP(EO-stat-PO)**) was received from Dow chemicals and was functionalised with thiol and acrylate end groups. While α-Elastin was used as recived. Bulk hydrogels were prepared by crosslinking of **HS-sP(EO-stat-PO)** and **HS-PG** via oxidation of thiol groups to disulfide bonds as well as by Michael addition with PEG-diacrylate. The disulfide bonds formed in the process are known to be cleaved in the reductive environment of the cytosol and the ester bonds formed in the Michael addition process can be hydrolyzed over a period of several days or weeks depending on pH. Thus the presence of these two segments ensures the biodergadability of such hydrogels. To show the biodegrability and use of such hydrogels, **HS-sP(EO-*stat*-PO)** hydrogel crosslinked by oxidation and Micheal addition was loaded with engineered chemokines. Under the cytosolic condition the hydrogels showed triggered release of chemokines which to a considerable extent could prevent injury extension after myocardial infarction.

The oxidation in air normally takes several hours which in many cases is too slow in order to maintain stable miniemulsion for the production of nanogels. Therefore hydrogen peroxide was used as an oxidizing agent and studies were performed in order to optimise the parameters for the synthesis of nanogels in the inverse miniemulsion. The formed gels were characterized for their size, dipersity, degradation behaviour, *in vitro* cytotoxicity and hemocmpatibility. Scanning electron microscopy (SEM), dynamic light scattering (DLS) in the water solution and scanning force microscopy (SFM) in the dry state were used to characterize the gels size and polydispersity. The stability of nanogels was monitored by DLS measurements.The live/dead viability/cytotoxicity assay was used to examine the cytotoxicity of nanogels and hemocompatibility tests were performed according to 1SO 10993-4.

Further different formulation strategies were used to control the particle size and polydisperstiy of crosslinked PG nanogel prepared via inverse miniemulsion. Comparative investigation of the use of alloxan, a mild oxidation catalyst, and hydrogen peroxide is discussed. Going a step further horseradish peroxidase (HRP) one of the most studied oxidation-catalyzing enzymes was used for synthesis of hydrogel and nanogels from **HS-PG** polymers. Nanogels were shown to entrap two different enzymes HRP and β-Galactosidase without affecting the enzyme activity and cells were successfully encapsulated in the hydrogel.

Biohybrid nanogels were constructed by immobilization of protein ovalbumin by crosslinking acrylate functionalized star shaped poly (ethylene oxide-*stat*-propylene oxide) (**Acrylate-sP(EO-*stat*-PO)**) resulting in the formation of biohybrid nanogel. Biohybrid nanogels systems based on soluble α-elastin polypeptides were also prepared by using two different amine-reactive cross-linkers; poly(ethylene glycol) diglycidyl ether (PEG-DGE) and bis(sulfosuccinimidyl) suberate (BS3). Thermo- and pH responsivity of such nanogels was explored. An elastase-triggered degradation profile of such nanogels was monitored by DLS measurements against time, while the colloidal stability was investigated by sedimentation analysis. Texas Red conjugated dextran was used as a model drug to load the nanogels and its loading and release kinetics was studied.

In the last part of the thesis synthesis of radiolabeled nanogels for nuclear molecular imaging is reported using **HS-sP(EO-*stat*-PO)**. Simple and efficient ^{68}Ga-labeling procedure was used to radiolabel the nanogels containing chelating groups for ^{68}Ga with high radio chemical yield and *in vitro* studies were performed to study the biocompatibility of the nanogels.

Zusammenfassung

Im Rahmen dieser Arbeit werden Nanogele und Hydrogele aus funktionalen hydrophilen Polymeren oder Proteinen, die mit abbaubaren Vernetzungseinheiten verknüpft sind, hergestellt und charakterisiert. Diese können mit Zielmolekülen modifiziert werden für die Abgabe von Peptiden und Proteinen.

Als Bausteine werden Poly(ethyleneoxid-*stat*-propylenoxid) (sP(EO-stat-PO)), lineares Poly(glycidol) (PG) und α-Elastinpolypeptid eingesetzt. Das lineare PG wurde über anionische Polymerisation hergestellt und danach mit Thiolgruppen funktionalisiert. sP(EO-stat-PO) stammt von Dow Chemicals und wurde mit Thiol- und Acrylatendgruppen funktionalisiert. α-Elastin wurde wie erhalten eingesetzt. Makroskopische Hydrogele wurden durch die Vernetzung von HS-sP(EO-stat-PO) und HS-PG erreicht, entweder durch Oxidation von Thiolgruppen zu Disulfiden oder über eine Michaeladdition mit PEG-Diacrylaten. Es ist bekannt dass sich die bei diesem Prozess gebildeten Disulfid-Bindungen in reduktiver Umgebung des Cytosols spalten lassen. Die Esterbindungen aus der Michael-Addition lassen sich abhängig vom pH-Wert innerhalb von Tagen oder Wochen hydrolysieren. Somit gewährleisten beide Segmente die biologische Abbaubarkeit solcher Hydrogele. Zum Beweis der biologischen Abbaubarkeit und der möglichen Anwendbarkeit solcher Hydrogele wurde das Hydrogel HS-sP(EO-stat-PO) oxidativ und über Michael-Addition vernetzt und mit veränderten Chemokinen beladen. Unter den Bedingungen im Cytosol ermöglichen die Hydrogele eine kontrollierte Freisetzung von Chemokinen, wodurch sich Folgeschäden nach einem Herzinfarkt erheblich vorbeugen lassen sollten.

An Luft dauert die Oxidation zu Gelen mehrere Stunden. Daher lassen sich in vielen Fällen die zur Herstellung von Nanogelen erforderlichen Miniemulsionen nicht stabil aufrechterhalten. Demzufolge wurde Wasserstoffperoxid als Oxidationsmittel eingesetzt und weitere Studien durchgeführt um die Synthese der Nanogele in inversen Miniemulsionen zu optimieren. Die dabei entstandenen Gele wurden nach Größe, Dispersität, Degradationsverhalten, in vitro Cytotoxizität und Blutverträglichkeit charakterisiert. Zur Bestimmung der Größe der Gele und ihrer Polydispersität wurden die Rasterelektronenmikroskopie (Scanning Electron Microscopy, SEM), Dynamische Lichtstreuung (DLS) in wässriger Lösung und die Rasterkraftmikroskopie (Scanning

Force Microscopy, SFM) im trockenen Zustand eingesetzt. Die Stabilität der Nanogele wurde über DLS kontrolliert. Zur Bestimmung der Zelltoxizität der Nanogele und der Blutverträglichkeit wurden Zellviabilität/Zytotoxizitäts-Tests- nach ISO 10993-4 durchgeführt.

Weitere Strategien wurden angewandt, um die Partikelgröße und Polydispersität quervernetzter PG-Nanogele aus inverser Miniemulsion zu kontrollieren. Eine vergleichende Untersuchung der Verwendung von Alloxan, einem milden Oxidationskatalysator und Wasserstoffperoxid wird diskutiert. Zudem wurde Meerrettichperoxidase (HRP) als eines der am meisten erforschten katalytischen Enzyme zur Synthese der Hydrogele und Nanogele aus HS-PG-Polymeren eingesetzt. Beobachtet wurde, dass die Nanogele zwei Enzyme, HRP and β-Galactosidase, einschließen ohne deren Aktivitäten zu beeinflussen. Die Zellen wurden erfolgreich in Hydrogele eingeschlossen.

Biohybridn-Nanogele wurden durch Immobilisierung des Proteins Ovalbumin über Vernetzung von acrylatefunktionalisiertem sternförmigem Poly(ethylenoxid-stat-propylenoxid) (Acrylate-sP(EO-stat-PO)) hergestellt. Biohybrid-Nanogel-Systeme aus löslichen α-Elastin-Polypeptiden wurden mit Hilfe von zwei gegenüber Aminen reaktiven Vernetzern, Poly(ethylenglycol) Diglycidylether (PEG-DGE) und Bis(sulfosuccinimidyl)suberat (BS3), hergestellt. Die thermische pH-Beständigkeit wurde untersucht. Zeitabhängige DLS-Messungen zeigten ein durch Elastase ausgelöstes Abbauprofil solcher Nanogele. Gleichzeitig wurde die Stabilität der Kolloide durch Sedimentationsanalyse ermittelt. Die Nanogele wurden mit Texasrot-konjugiertes Dextran als Modellverbindung beladen. Untersucht wurde die Kinetik des Beladens und der Freilassung.

Der letzte Teil dieser Arbeit beschreibt die Synthese radioaktiv markierter Nanogele für die nuklearmolekulare Abbildung (Imaging) mit Hilfe von HS-sP(EO-stat-PO). Ein einfaches und effizientes Verfahren zur Isotopenmarkierung mit 68Ga wurde eingesetzt, um Nanogele mit chelatisierenden Gruppen mit einem hohen Anteil an 68Ga zu versehen. *In vitro* Untersuchungen zur Biokompatibilität der Nanogele wurden durchgeführt.

CHAPTER 1

Introduction

Rapid progress in synthetic and recombinant DNA technology, as well as in peptide and protein production technologies has resulted in the availability of a wide variety of protein- and peptide-based drugs targeting poorly controlled diseases. Several hundred protein drugs are currently undergoing clinical trials. However, the use of these potentially beneficial compounds as drugs may be severely limited by their fragile structure and the body's ability to rapidly remove them from the bloodstream. The structure, physicochemical properties, stability, pharmacodynamics, and pharmacokinetics of these new bio pharmaceutics place stringent demands on the way they are delivered into the body. More specifically, peptides and proteins must retain their structural integrity until they reach their target site and should not be degraded enzymatically.

Targeted drug delivery is emerging as a powerful tool for the treatment of various ailments compared to the conventional methods as it enhances the specificity of delivery to a particular site, protects the active agent of the drugs and controls the release kinetics. Over the last 30 years different types of nano-carriers were proposed as drug carriers and have received growing attention since due to their stability, loading capabilities and physicochemical properties. With respect to the emerging field of the delivery of peptides and proteins, the most crucial challenges are:

- Creating a delivery vehicle for the polymeric, hydrophilic molecules that protects them from degradation without irreversibly affecting their native structure.
- Improving the stability of peptide and protein drugs in vivo as well as the specificity of their transport to the intended delivery site.
- Decreasing the nonspecific delivery to non-targeted tissues as well as the dose that has to be applied and their immunogenicity.

Nanogels, hydrophilic, cross-linked polymeric particles, are an extremely interesting class of materials for the delivery of peptides and proteins. They can be tuned regarding their chemical composition and three-dimensional physical structure enabling

control over water content, mechanical properties, and biocompatibility. Moreover, microgel particles offer significant opportunities for targeted applications as a consequence of their tuneable size and their large surface area which enable multivalent bio conjugation. In addition, biodegradability of nanogels can be tailored to respond to external stimuli such as enzymes, pH change, ion strength or redox potential, which offers a number of benefits for their use as selective drug delivery carriers. This could facilitate controllable release of encapsulated molecules from the interior of nanogels and ensure the removal of empty vehicles after the drug release.

The aim of this thesis is to prepare and characterize nanogel carriers composed of functional hydrophilic polymeric / proteinic building blocks that are crosslinked with degradable crosslinkers and can be modified with targeting molecules for the delivery of peptides or proteins **(Figure 1.1)**.

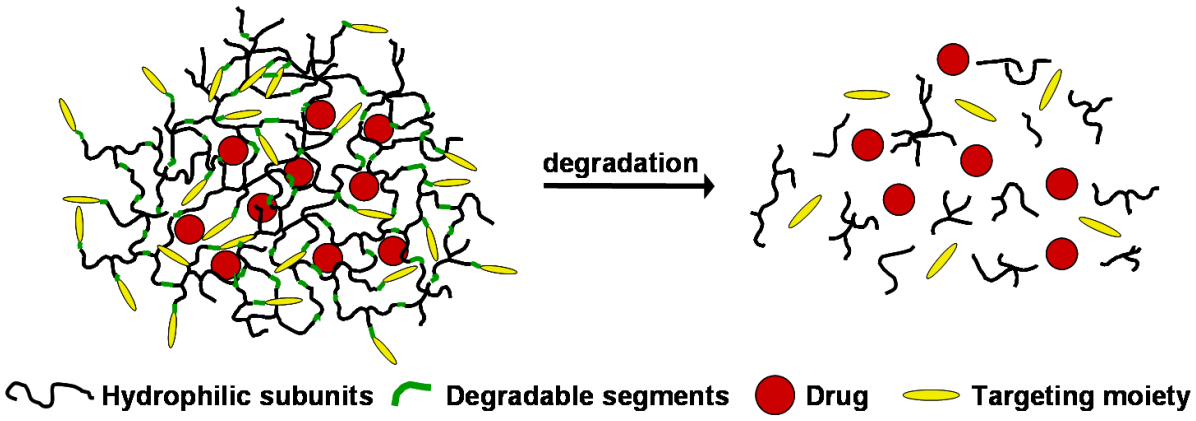

Figure 1.1: Underlying concept of this thesis. Biodegradable gels for targeted delivery of drugs.

Chapter 2 gives a literature overview on current approaches for targeted delivery of drugs, as well as nanogel systems and the disulfide crosslinking chemistry that is used in this study.

Chapter 3 deals with synthesis of thiol functionalized polymers, and use of **HS-sP(EO-*stat*-PO)** based hydrogel for chemokine delivery. Chemokine-derivatives **Met-CCL5** and recombinant protease-resistant **CXCL12 (S4V)** were used for the inhibition of neutrophil infiltration and concomitant improvement of hematopoietic stem cell recruitment to sustain neovascularization after myocardial infraction.

Chapter 4 describes the preparation of the nanogels via inverse miniemulsion and their characterisation regarding particle size distribution, degradation behaviour and chemical composition, *in vitro* cytotoxicity as well as hemocompatibility studies.

Chapter 5 focuses on the comparative investigation of alloxan, a mild oxidation catalyst, and hydrogen peroxide as oxidation catalyst for the formation of disulphide cross-linked hydrogels and nanogels. Further formulation strategies to control the size of the disulphide cross-linked poly(glycidol) (**PG)** nanogel prepared via inverse miniemulsion for both catalyst systems is presented and the differences are discussed. Investigations on nanogel stability and degradation behaviour in presence of glutathione as well as *in vitro* cytocompatibility studies are shown.

Chapter 6 deals with enzymatically mediated cross-linking of redox-sensitive, reversibly crosslinked hydrogel and nanogels and to embed (bio-)functional moieties such as peptide sequences. Self-encapsulation of the enzyme horseradish peroxidase (HRP) into the nanogels in functional form is shown. Double encapsulation of HRP with β- galactosidase was done in the nanogels. Further *in vitro* cytocompatibility of nanogels and cell encapsulation in the hydrogel are studied.

Chapter 7 focuses on nanogels that are constructed by immobilization of the protein Ovalbumin by crosslinking with a reactive prepolymer, acrylate functionalized star shaped poly (ethylene oxide-*stat*-propylene oxide) (**Acrylate-sP(EO-*stat*-PO**)) in inverse miniemulsion which results in the formation of a biohybrid nanogels. This type of biohybrid nanogel introduces hydrophobic pockets into the hydrophilic nanogels which can be a potential candidate for drug delivery application.

Chapter 8 is concerned with enzyme degradable novel biohybrid nanogels/nanogels systems based on α-elastin polypeptides *via* facile inverse miniemulsion approach using two different amine-reactive cross-linkers; poly(ethylene glycol) diglycidyl ether (PEG-DGE) and bis(sulfosuccinimidyl) suberate (BS3). Nanogels were fabricated at various compositions of the precursors (elastin and cross-linker), drug loading and dual stimulus responsivity (temperature and pH) were studied.

Chapter 9 reports the synthesis of radiolabeled biodegradable nanogels and the physiochemical and biological properties relevant to nuclear molecular imaging. Nanogels were synthesized by self-assembly of **HS-sP(EO-*stat*-PO)** prepolymers in aqueous medium without using organic solvents and surfactants, and crosslinked *via* disulfide bonds.

CHAPTER 2

Literature Overview on Nanoparticles as Controlled Drug Delivery Devices

2.1 Role of the Drug Delivery Systems

Way back to early civilisations, humans have put tremendous efforts to overcome ailments, discomfort and pain. This led them to use and test substances occurring in nature against the diseases. Significant advancement in science has resulted in the identification of these active ingredients of the long used natural products and their structure and mechanism of action were elucidated. With the progress of humanity more and more effort is being put to find new or more potent tools against diseases. Although the exact mechanism of how a drug works may not be known for all the known compounds but it has been understood that their functions are highly specific and complex. Mostly drug activity is the result of their induced molecular interaction in specific cells. Therefore it is utmost important that the drug reaches the site of action, in right concentration and for the right period of time. When it is not possible to achieve it by simple administration (oral, intravenous, local, transdermal etc.) or if such administration causes patient discomfort, strategies based on the association of the drug with a carrier (a drug delivery system-DDS) have to be considered.[1,2] The idea behind DDS is to control the pharmacokinetics, pharmacodynamics,[3,4] non-specific toxicity, immunogenicity, bio-recognition and efficacy of the drug for minimising drug degradation and loss, prevention of harmful-side effects, increase drug bioavailability, counter problems arising from low drug solubility, fast clearance rates, non-specific toxicity, inability to cross biological barriers, just to mention a few.[2,5] For tackling these challenges various drug delivery and drug targeting systems are currently under development like microcapsules, liposome, micelles, nanogels made from synthetic or natural polymers and dendrimes.[1,6] These

systems are exploited for therapeutic purpose to carry drug in the body in a controlled manner from the site of application to the therapeutic target.

2.2 Targeting Drug Delivery System

2.2.1 Passive Targeting:

Passive targeting refers to targeting of the systemic circulation due to physiochemical or pharmacological factors. When the tissue is diseased, variety of pathological conditions can alter its physiology and result in its vascular remodelling and permeability **(Figure 2.1 (left))**. This allows extravasation and selective localisation of long circulating drug carriers from the blood to these sites, as was shown by Lamprecht *et al.* that polymeric carrier administered orally could target the inflamed colonic mucosa in inflammatory bowel disease.[7] In tumors, this condition is more pronounced as rapidly growing tumors develop new blood vessels through active angiogenesis to meet the nutritional demands of increasing number of cells. These newly formed blood vessels are irregular, defective or leaky and unlike the tight endothelium of normal blood vessels, these are disordered creating large fenestration (≤ 300 nm).[8] This increased vascular permeability along with impaired or absent lymphatic drainage in tumors allows an enhanced permeability and retention (EPR) effect of the carrier in the tumor.[9] But several factors are important for passive tumor accumulation using the EPR effect, like long blood circulation time of carrier and activity of loaded drug for that time, degree of tumor vascularization/angiogenesis and the size of the carrier system. But EPR effect is only applicable for high-molecular-weight drugs since low-molecular-weight drugs can rapidly diffuse into the circulating blood followed by renal clearance. Although leaky vasculature and modelling of carrier system can enhance passive targeting, a major part of the nanosystems injected intravenously are lost to reticulo-endothelial system (RES), mainly by fixed macrophages in the liver and spleen after opsonization by proteins present in the blood stream.[10] This tendency of the RES can excellently be used for passive targeting of drugs.

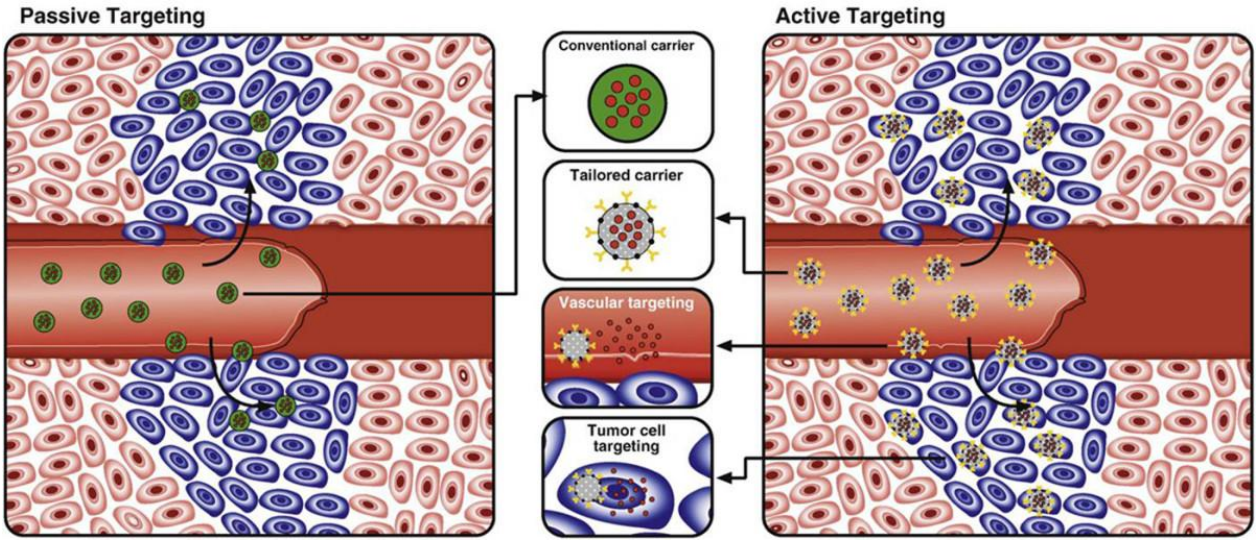

Figure 2.1: Passive versus active targeting. (Left) In passive targeting, particles tend to passively diffuse through the leaky vasculature of the tumor bed and accumulate primarily through the enhanced permeability effect. (Right) In active targeting, once particles have extravagated in the target tissue, the presence of ligands on the particle surface facilitates their interaction with receptors that are present on tumor or other cells, resulting in enhanced accumulation and preferential cellular uptake through receptor-mediated processes. This approach can be used either for vascular targeting and/or tumor cell targeting purposes. Reprinted from Ref.11

2.2.2 Active Targeting:

Since passive targeting approaches are limited, tremendous effort has been put towards developing active approaches for drug targeting which focuses on specific modification of a drug carrier nanosystem with ligands or engineered homing devices to increase receptor mediated localisation of the drug.[12]

Drug targeting to specific cells has been explored in this way by taking the advantage of various receptors, antigens/proteins present on the plasma membrane of cells and of different lipid components of the cell membrane (**Figure 2.1 (right)**). Active agents, such as ligands specific for the receptors have been used extensively to target specific cells which also facilitates the uptake of the carrier via receptor mediated endocytosis.[13] Targeting molecules can be either an antibody or non-antibody ligands like peptides, sugars or vitamins which are of low cost and easily available. But relatively unselective expression of non-antibody ligands to the targeted receptors could be major drawback of their use. On the other hand antibodies are higher specific and a wide range of

binding affinities can be achieved by them. However, the production of antibodies is expensive and time-consuming, and problems with stability and storage have to be overcome.[14]

2.3 Cellular Uptake

Uptake and internalisation nano carrier can occur through receptor-mediated bio-events once it reaches the targeted tissue or cell population, either passive or active targeting or a combination of both. Along with receptor mediated endocytosis phagocytosis and pinocytosis can contribute to the uptake and internalisation of the drug. Receptor-mediated endocytosis has higher selectivity in cellular targeting, since the cellular membrane is decorated with number of receptors, which upon extracellular binding to their respective ligands (or to nanoparticles whose surface is functionalized with ligands), transduce a signal to the intracellular spaces which can in return trigger a multitude of biochemical pathways. This may also cause internalization of the ligand and its appended nanoparticle via endocytosis. Cross-linking of receptors via ligands attached to nanoparticles also results in a pronounced pit in the membrane which is followed by subsequent enfolding and reunification of the cellular membrane forming an endosome. It has been reported that nanoparticle in the range between 25 and 50 nm are most suitable for optimal endocytosis and intracellular localization.[15-18]

Furthermore, on selective active targeting of nanocarriers several other bio-events are possible **(Figure 2.2)**. After the endocytosis of a DDS either in a receptor-mediated or in an unspecific way results in a significant drop in pH from the extracellular 7.2 to 7.4 to 6.5 to 5.0 in the early stages in the endosomal processing pathway. Another drop in pH to about 4.0 occurs upon fusion with lysosomes which additionally contain a great number of enzymes, e.g. phosphatases, nucleases, proteases, esterases, that become active at acidic pH.[19,20] This environment is developed for protein processing via proteolysis and disulfide bond reduction[21,22] and therefore is extremely harmful for most active substances, which could also lead to degradation or inactivation of the therupatic agent. On the other hand, these are the properties which are widely used for release of the DDS/drug from the endosome into the cytosol. For example, using pH sensitive peptides like glutamic acid-alanine-leucine-alanine (GALA)[23,24] which results in the destabilization of the endosome through carrier-membrane interaction or use of dioleoylphosphatidylethanolamine

(DOPE)[25,26] a fusogenic phospholipids which fuses the liposomal carrier with the endosomal membrane or by using amine-containing polymers which can be highly protonated during endosome acidification, causing chloride influx into the vesicle resulting in osmotic swelling and vesicle lysis.[27]

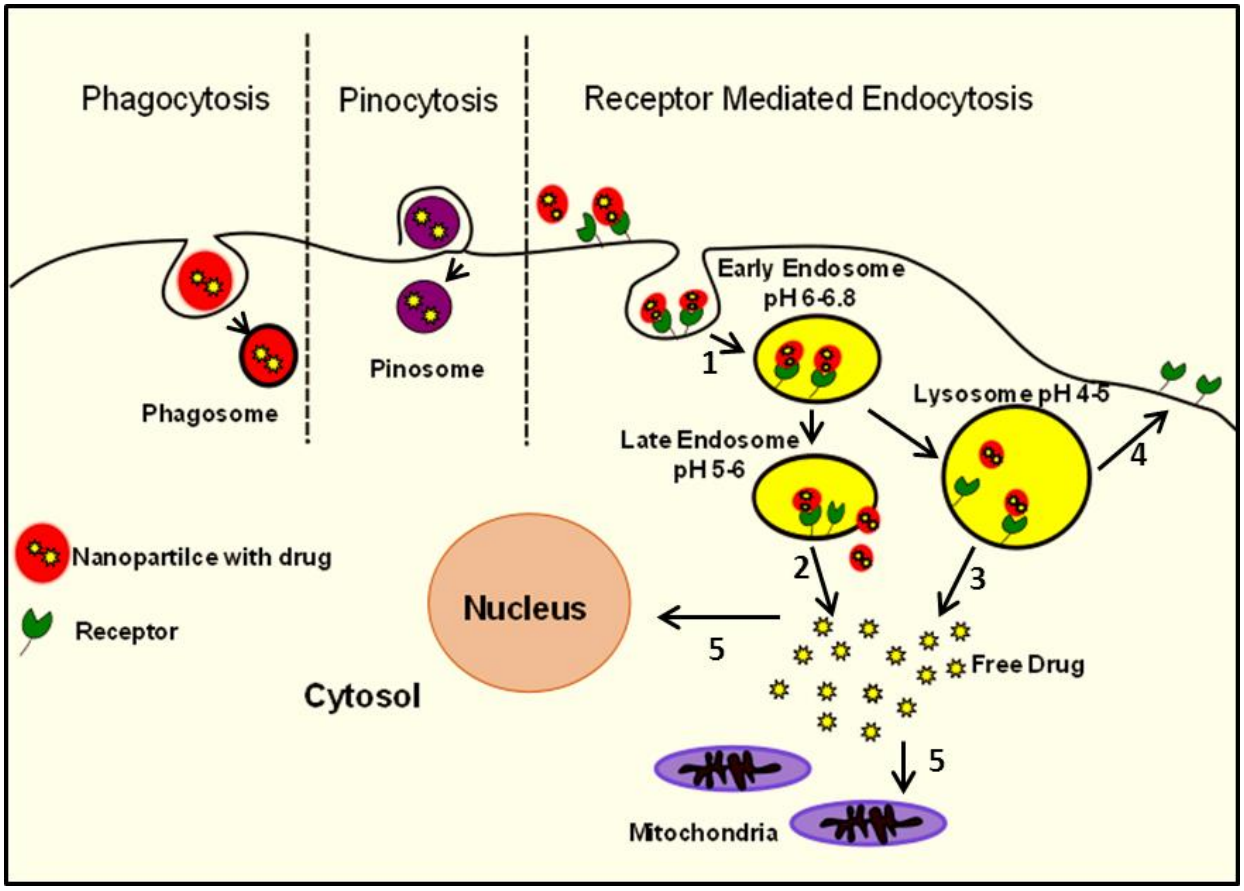

Figure 2.2: Cytosolic delivery of therapeutic agents via nanoparticle carriers. (1) Endocytosis resulting into internalisation of nanoparticles, (2) endosomal escape of nanoparticles (3) lysosomal degradation of nanoparticle, (4) recycling of the receptors (5) drugs freely diffuses into cytoplasm and cytoplasmic transport of therapeutic agent to target organelle. Reproduced and reprinted from Ref. 20.

Apart from endocytic pathway to deliver drugs directly to the cytosol, another method most widely explored is using cell-penetrating peptides like the HIV-1 derived TAT protein transduction domain.[28, 29] Use of cell-penetrating peptides bypasses the endocytic pathway completely and facilitates cytoplasmic localization; increasing the bioavailability of a drug in cytosol.

2.4 Nano Drug Carriers

Nano drug carriers are a major class of DDS.[1,5] They are mainly defiend as colloidal particles in the range of 10 to 1000nm. Administration of the nano carriers in the body can be done by different routes like intravenous, intramuscular or subcutaneous.The carrier should be small to access all locations in the body by these administration routes as the diameter of the smallest blood capillary in human boday is about 4µm. Carrier larger than a few micrometers accumulate in the lung capillaries, while sufficiently small structures could escape from circulation through intercellular junctions of healthy endothelium (e.g. lymph nodes endothelium[30]), or may be removed by the sinus endothelium of the bone marrow.[31] It should be bioacceptable, should be able to carry an optimal drug load and should have a long circulation time for effective targeting.[32,33] Ultimately physiological properties of drug and the therapeutic goal influence the final choice of a nano carrier.

Nanocarriers in general protect a drug load from degradation and hence enhances cellular uptake, modify pharmacokinetic and drug distribution and improves intracellular penetration. Nanocarriers have also been widely used to improve the performance of imaging techniques applied for the *in vivo* diagnosis of tumors. Many of the current "nano" drug carriers used as drug delivery systems are liposomes, polymeric micelles, nanoparticles, dendrimers, and nanocrystals (**Figure 2.3**).

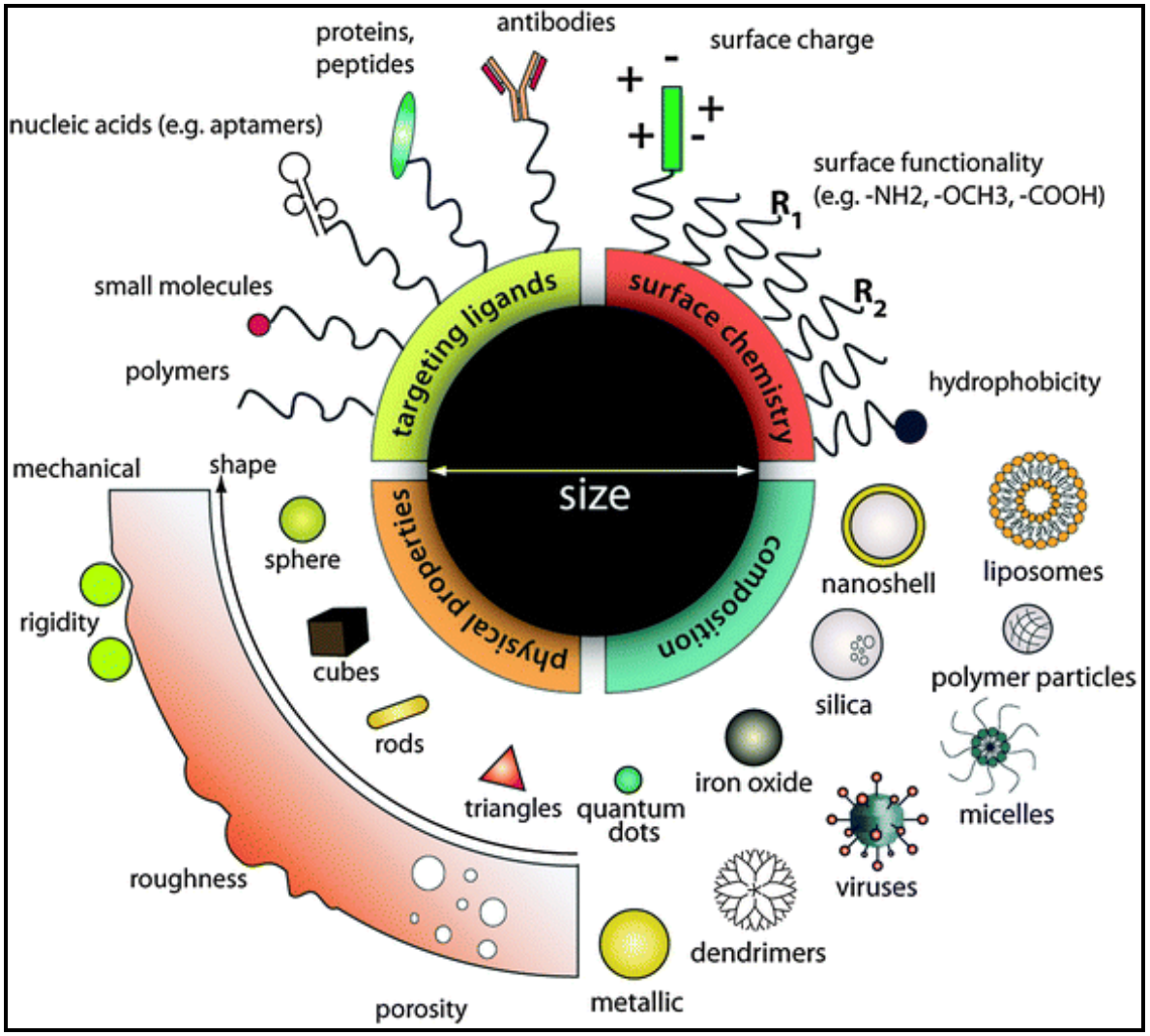

Figure 2.3: Designing nanoparticles for intracellular applications. Nanoparticles can be modularly assembled from different materials composition with different physical and chemical properties and functionalized with a myriad of ligands for biological targeting. Such flexibility in design freedom enables researchers to tailor nanoparticle for specific intracellular applications as contrast agents, drug delivery vehicles, and therapeutics**.** Reprinted from Ref. 34.

2.4.1 Liposomes

Liposomes are nano size artificial vesicles of spherical shape consisting of a lipid bilayer (or multiple bilayers) composed generally of phospholipids and internal aqueous pools. Lipids self assemble to liposomes by spontaneous self-organization, during this process drugs are incorporated. Hydrophilics drugs get trapped inside the liposomal cavity while hydrophobic drugs are incorporated within lipid bilayer but similar to biological membranes liposomes have low permeability to hydrophilic drugs and high

permeability to hydrophobic drugs. This bilayer of liposomes can fuse with other bilayers such as the cell membrane, which promotes release of its contents.

A number of anticancer and antibacterial agents have been effectively entrapped in liposomes eg. Doxorubicin was loaded by ion-trapping methods. At present, number of liposomal formulations are available in the market like DaunoXome® loaded with daunorubicin for the treatment Kaposi's sarcoma, breast, ovarian.[35] Epaxal-Berna Vaccine loaded with inactivated hepatitis A virions for active immunization against hepatitis.[36] Liposomes acting as drug depots take the advantage of the EPR effect to reach the tumor. But many drugs cannot cross cell membranes to gain access to their intracellular site of action, to achieve this liposomes are modified with membrane active lipide or membrane active peptides which fuse with or disrupt the cell membrane to result in the cytoplasmic delivery of the drug. Extensive studies have been done on liposomal drug delivery systems to increase the solubility and therapeutic index of chemotherapeutic agents while minimising the side effects.[37] However, several disadvatages have been shown with these conventional vehicles like physical/chemical drug leakage, short biological activity, low therapeutic index and dose effectiveness, all of which have limited the use of the conventional liposomes in clinical applications.[38,39]

2.4.2 Polymeric Nanoparticles

Nanoparticles are solid colloidal drug carriers ranging from 10 to 100 nm in diameter, typically made of a single material. The drug is either attached or entrapped to nanoparticles and depending upon the method of preparation, they can be obtained in different forms and shapes.[40]

The majority of microparticle preparation techniques have been tailored for the fabrication of nano - sized particles. Conventialy they are formed either by polymerization of monomers or by dispersion of preformed polymers. In spite of development of various synthetic and semi synthetic polymers, natural polymers like chitosan, gelatin, albumin, sodium alginate are widely used in drug delivery. A variety of materials have been employed for the synthesis of the synthetic polymeric nanoparticle as delivery of therapeutic agents. Main requirement of using such materials is they must be non-toxic, chemically inert and free of leachable impurities with suitable physical structure, good processiablity and undesired aging. Nanoparticles posses a stable structure, in contrast to self-assembled systems.[41] This advantageous stability must however be coupled to a long-term degradation under physiological conditions, in

order to prevent undesired body accumulation. Ideally, nanoparticles should break down into non-toxic products which can have renal excreation, or are absorbed by the body.[42] Some nanoparticles in market are Risperidal® Consta, Nutropin® and Trelstar® Depot.

2.4.3 Polymeric Micelles

Amphiphilic copolymers with large solubility difference between hydrophilic and hydrophobic segments self assemble in aqueous medium to form micelles. The size of the micelles can range from few to tens of nanometer. They consist of a densely packed hydrophobic inner core capable of physically entrapping lipophilic substances and a dense hydrophilic shell which serves as as a stabilizing the micelle in external aqueous environment.[43] Furthermore the hydrophilic shell of the micelle prevents protein adsorbtion and hence recognition by the immune system in the body. Compared to surfactant micelles, polymeric micelles are generally more stable, with a lowered critical micellar concentration and slower dissociation rate. This not only allows longer period of retention of loaded drugs but also higer accumulation at the target site particularly due to EPR effect. Active targeting of the micelles is also possible by modifying the peripheral chain ends of the polymer with conjugating ligands further the polymer can also functionalized with crosslinkable groups which can increase the stability of the micelles. Moreover control of the size and morphology of the micelles can be easily be adjusted by changing the chemical composition, molecular weight and block length ratios of the copolymer. Several micellar compositions for various applications are under clinical study eg. Genexol PM® Samyang, Novavax® Estrasorb, Medicelle® NanoCarrier, Flucide® NanoViricides, Basulin®, Flamel Technologies.[44]

2.4.4 Dendrimers

Dendrimers are tree like macromolecules branching out from central core unit. Dendrimers have a uniform size, well-defined molecular weight, highly functionalized terminal surface and water solubility. With modification of the cavities inside the core and branches successful encapsulation of hydrophobic or hydrophilic drugs could be attained. The terminal groups on the surface can be adapted to carry drugs or antibodies for neutralizing or targeting purpose.[45] They are prepared either from the central initiator core, layer by layer or are built from small building blocks that end up at the surface of the sphere, reaction in this case proceeds inward and the block are

finally attached to a core. With each subsequent growth step a new "generation" of polymer is formed which has larger molecular diameter, more reactive surface sites, and approximately double the molecular weight of the previous generation. Dendrimers thus provide platforms for drug attachment and have the ability to encapsulate or bind drugs via several mechanisms such as electrostatic interaction, physical encapsulation and covalent conjugation. The encapsulation / complexation of drug molecules into/with dendrimers can be widely used in different routes of drug administration. Use of dendrimers as parenteral injections is most common, either directly into the tumor tissue or intravenously for systemic delivery.Some of the marketed products are Vivagel® a vaginal Gel for preventing HIV, Starpharma, Stratus CS® a cardiac marker, Dade Behring SuperFect® for gene transfection.

2.4.5 Nanogels

Another emerging class of nanodevice which could be used for the drug delivery are nanogels suggested to be used as carriers to carry the cargo\drug. These gels are insoluble in water, but swell when immersed. In recent years, these carriers have been considered in sustained and controlled release devices for the delivery of water soluble drugs. Thus minimising the toxic effect caused by the use of organic solvents.[46]

2.4.5.1 Nanogels via Disulphide Bridging

The nanogels properties can be tailored by using different polymers and co-polymers or proteins. The new strategies use synthetic polymers with biodegradable conjugation like disulphide and from natural products such as chitosan, hyaluronic acid, heparin, dextran and albumin or combination of both.[47]

In a novel approach stable biodegradable nanogels cross-linked with biodegradable disulfide linkages were prepared by inverse miniemulsion atom transfer radical polymerization (ATRP) by Matyjaszewski et al.[48,49] In this process, water-soluble monomer oligo(ethylene glycol) monomethyl ether methacrylate (OEOMA) with different molecular weights were crosslinked in the ATRP reaction with the disulfide-functionalized crosslinker. The nanogels formed were considered to have a uniformly cross-linked network, which was supposed to improve, control the release of encapsulated agents, and the nanogels were shown to be biodegradable into water-soluble polymers in the presence of a biocompatible glutathione tripeptide, which is commonly found in cells. The biodegradation of nanogels thus could trigger the release

of encapsulated drugs, as well as facilitate the removal of empty vehicles. Cytotoxicity assays of nanogel loaded with drug on HeLa cancer cells was performed. Results obtained from this suggested that the released drug molecules penetrated cell membranes and could suppress the growth of cancer cells. Further, OH-functionalized nanogels were also prepared to demonstrate facile applicability toward bio conjugation with biotin. Stable PEG/DNA nanogels were prepared by using a thiol-functionalized six-arm branched PEG for DNA solubilization in DMSO followed by oxida-tive cross-linking.[50] In the presence of a reducing agent, intact plasmid DNA was released from the nanogels. The PEG/DNA nanogels exhibited appreciable gene transfection efficiency. Morimoto et al. prepared dual stimuli-responsive nanogels based on polysaccharides lightly grafted with thiol-terminated poly(N -isopropylacrylamide) (PNIPAM), which was synthesized via RAFT polymerization of NIPAM using 2-(1-isobutyl)-sulfanylthio-carbonylsulfanyl-2-methyl propionyl acid chloride conjugated pullulan followed by aminolysis.[51] Moore and coworkers developed chymotrypsin and reduction responsive polyacrylamide microscopic hydrogels using a tetra-peptide sequence, Ac-Cys-Tyr-Lys-Cys-NH2 (CYKC), as a cross-linker.[52] These microscopic hydrogels dissolved when exposed to a solution of R-chymotrypsin, while control hydrogels cross-linked with the tetrapeptide, Ac-Cys-Ser-Lys-Cys-NH_2 (CSKC), were not affected by R-chymotrypsin. Both the CYKC and CSKC cross-linked hydrogels were eroded in the presence of the disulfide reducing agent tris(2-carboxyethyl) phosphine (TCEP). Galaev et al. prepared biodegradable macroporous PHEMA cryogels by combining two crosslinkers, PEG diacrylate and a disulfide-containing water soluble crosslinker, N,N'-bis(methacryloyl)-L-cystine (MAS-S).[53] Aliyar et al. describe nanogels prepared by intramolecular crosslinking of high molecular weight polyacrylamide.[54] Thiol-functional polyacrylamide was synthesized by copolymerization of acrylamide and N,N' -bisacryloylcystamine, and subsequent reduction of the obtained gel using DTT. Dissolution of the thiomer in water at very low concentrations followed by air oxidation at pH 7.5 resulted in crosslinked particles. Diluted solution conditions favored the formation of intramolecular crosslinks so that mainly single-chain nanogel particles were obtained. Recently, a report on nanogels prepared from star-shaped poly(ethylene oxide-stat-propylene oxide) (sP(EO-stat-PO)) or from linear PG[55] was published. Nanogels were prepared in inverse miniemulsion and the disulfide bond formation was accelerated by addition of catalytic amounts of the hydrogen peroxide.

The group of Bernkop-Schnürch describes the preparation of thiolated chitosan (CS) microparticles loaded with insulin as a potential carrier for nasal delivery. Thiolated CS showed higher mucoadhesive and permeation-enhancing properties than unmodified CS,[56-58] which makes them ideal precursors for nasal or oral drug delivery systems. Thiolated CS/DNA complexes have been prepared in aqueous solution.[59] In comparison to the particles prepared by complexation of DNA with thiol-free CS, the oxidized particles with DNA showed an increased stability to artificial intestinal fluid, a triggered release in a reducing environment, and improved transfection efficiency. Chitosan-N-acetylcysteine (CS-NAC) nanoparticles were investigated as a nonviral gene carrier.[60] The CS–NAC/DNA particle have been prepared in water and the oxidation of free thiol groups was catalyzed by the addition of hydrogen peroxide. They showed enhanced stability in comparison to the non-crosslinked particles against polyanionic heparin as well as alkaline pH. The same thiolation of CS was applied by Atyabi et al.[61] Lee at al. describes the preparation of thiolated CS/pDNA nanocomplexes using an aqueous homogeneous chemical gelation process.[62] Although the non-crosslinked thiolated CS provided higher transfection efficiency in vitro, the disulfide-crosslinked complexes showed a more sustained pDNA release profile and significantly higher gene expression in comparison to non-crosslinked systems, especially at 14 days post-intranasal administration in a mouse model. Another strategy was pursued by Shu et al., who prepared CS-based disulfide solidified polyelectrolyte nanogels through mild ionic gelation.[63] The resulting coacervates were covalently fixed by chloramine-T-mediated disulfide formation. Such nanogels were successfully loaded with insulin and showed a pH-dependent size variation, indicating a suitability of these particles for oral drug delivery applications. Preparation of erythropoietin (EPO)-loaded hyaluronic acid (HA) nanogels was described by Hahn et al.[64] Lee et al. demonstrated the preparation of disulfide-crosslinked nanogels for entrapment of green fluorescence protein siRNA. These nanogels effectively protected the encapsulated siRNA from enzymatic degradation.[65] The siRNA/HA nanoparticles showed a considerable gene silencing effect in serum conditions. Recently, dual stimuli-responsive disulfide-crosslinked nanogels were prepared by covalently linking sulfanylthiocarbonylsulfanyl (STS) to 100 kDa Pullan and subsequent grafting of short PNIPAM chains through reversible addition-fragmentation chain transfer (RAFT) polymerization of NIPAM.[66] Aminolysis of the STS functionalities at the PNIPAM chain ends with isopropylamine yields thiol groups. Disulfide-crosslinked heparin nanogels

were prepared for efficient cellular uptake of heparin in order to induce apoptotic cell death.[67] The obtained stable nanogels, with an average diameter of 250 nm in water, rapidly disintegrated and released free heparin upon reduction with GSH. These nanogels enhanced the internalization of heparin and, in addition, significantly reduced the proliferation of mouse melanoma cells.

Self assembled acrylate group-modified cholesterol-bearing pullulan (CHPANG) were crosslinked with thiolated poly (ethylene glycol) (PEGSH) by Michael type addition yielding nanogels (A-CHPNG) in the size range of 40–120 nm depending on the concentration of CHPANG and PEGSH. A-CHPNG was shown to be degraded by hydrolysis under physiological condition and dissociate back to original nanogels with efficient encapsulation of interleukin-12 (IL-12).[68] Poly(N-isopropylacrylamide) (PNIPAAm) grafted Dex nanogels with dodecyl and thiol end groups was synthesized by RAFT polymerisation. Dodecyl-terminated polymers (Dex-PNIPAAm) can be readily self-assembled to form nanogels. Dex-PNIPAAm nanogels showed volume phase transition due to PNIPAAm side chains which was dependent on PNIPAAm chain length and polymer concentration. Aminolysis of trithiocarbonate groups rendered thiol functionality in the polymer resulting into crosslinking of the nanogels though disulphide bond formation (SS-Dex-PNIPAAm). Dual responsiveness of the Dex-PNIPAAm nanogels make them intriguing candidate for coating on different nanomaterials.[69] Dually functionalized HA by hydrazine and thiol (HA-hy-SH) was first converted by click chemistry to HA-hy-pyrene. HA-hy-pyrene self assemble in water and lead to the formation of physical nanogels which were chemically cross-linked by amide coupling between the hydrazide and carboxylate group.

Physically associated nanogels composed of HA with 5% of the pyrene-tethered disaccharide units were decreased in size from 450 nm to 390 nm upon the EDC mediated crosslinking. When the pyrene content was decreased to 0.5% the size of nanogels reduced to 248 nm. DOX was physically loaded into nanogels either by electrostatic binding of cationic DOX in salt form or by entrapment of the neutral DOX within the hydrophobic pyrene cores. The loading efficiency of 66% and 82% was achieved respectively. Nanogels loaded with DOX showed an anti-proliferating effect on cell analogous type. Further an enzymatic degradation approach was reported to obtain the nanogels via degradation of the pyrene-immobilized HA hydrogel.[70] HA-based nanogels with positive and negative charges on the surface prepared using an aqueous solution of linear HA in a sodium bis(2-ethylhexyl) sulfosuccinate (AOT)-

isooctane microemulsion system. The prepared HA particles were post modified to aldehyde (HA-O) by $NaIO_4$ treatment and then particles were reacted with cysteamine (CY) to obtain thiol groups on the surface. The thiolated HA particles (HA-CY) were further exposed to radical polymerization with an anionic monomer, 2-acrylamido-2-methyl-1-propanesulfonic acid (AMPS), and with a cationic monomer, 3-acrylamidopropyl-trimethylammonium chloride (APTMACl), to generate HA-based ionic hydrogel particles, HA-CY-AMPS and HA-CY-APTMACl, respectively. The prepared HA-based anionic and cationic particles illustrated strong pH dependent size variations. Trimethoprim (TMP) and naproxen (NN) were used as model drugs in the drug delivery experiments.[71]

Different proteins have been used as building blocks for the synthesis of biohybrid nanogels. Nanogels with diameter of 250nm were prepared by complexation of thiolated heparin and poly (ethylene glycol) (PEG) in DMSO followed by intermolecular crosslinking induced by disulfide bond formation between adjacent heparin molecules. Under reductive environment nanogels disintegrated and released free heparin. These nanogels showed significant inhibition in proliferation of mouse melanoma cells by inducing caspase -mediated apoptotic cell death.[72] *The RNase A-loaded heparin–Cystamine–Pluronic–cRGDfC nanogels with mean diameter of 116 nm were prepared according to the direct dissolution method. The heparin–Pluronic (HP) conjugate was coupled via redox-sensitive disulphide. Heparin was conjugated with cystamine (Cys) and the terminal hydroxyl groups of Pluronic were activated with the vinyl sulphone (VS) group, followed by coupling of VS groups of Pluronic with cystamine of heparin. Cyclo(Arg–Gly–Asp–D-Phe–Cys) (cRGDfC) peptide was efficiently conjugated to VS groups of HP nanogel and exhibited higher cellular uptake than unmodified nanogels.*[73]

2.5 Disulfide Crosslinking in Drug Delivery

Thiols oxidise to form disulphide bond, relatively this bond is quite stable in oxidising environment but can be readily cleaved under reductive condition to generate free thiols. Since disulphide bond formation is initiated by deprotonation of thiols in neutral or basic conditions, acidic conditions stabilize free thiols. For reduction of disulfides to thiols in an aqueous environment, dithiothreitol (DTT), 2-thioethanol, triscarboxyethylphosphin (TCEP), or glutathione (GSH) are commonly used as reduction reagents. GSH is a tripeptide composed of L- Glutamate, L-Cysteine and

Glycine with an unusual peptide linkage between the γ-carboxy group of glutamate and the amino group of cysteine.[74,75] In mammalian cellular fluids it is present in the range of 0.5 - 10 mM[76-78] and acts as major protection against oxidants such as reactive oxygen species. When reacting with oxidants, GSH itself is oxidized and forms disulfides (GSSG). In a healthy cell, 90% of GSH is present in the reduced form. In contrast to its concentration in the cytosol, the concentration of GSH in plasma and other extracellular fluid is only in micromolar (20 - 40μM) and even lower in the blood (about 2 μM). This high redox potential difference between the neutral or oxidizing extracellular space and the reducing intracellular space makes disulfide-crosslinked nano and nanogels especially attractive as drug delivery systems due to the possibility of controlled biodegradation of the crosslinked network, and thus quantitative drug release in the cytosol.[79-82]

Disulfides can form spontaneously by autoxidation of thiols upon exposure to air. This process is, however, relatively slow and not useful for most microgel preparation techniques. Thus, oxidizing catalysts such as diamide,[83] peroxides,[84] alloxan,[85] and sodium tetrathionate,[86] or a catalyst based on Fenton chemistry,[87] are often applied in order to shorten the oxidation time.

2.6 Emulsions as System for the Nanoparticle Synthesis

An emulsion is defined as a system of two immiscible liquid phases mostly oil and water, where one of the phase is dispersed in the other as microscopic or colloidal size drops typically around 1 μm: there are two kinds of simple emulsion, oil-in-water (o/w) and water in oil (w/o), depending on which phase comprises the disperse phase.[88] Unstable emulsions are formed if they are made just by stirring of the pure immiscible liquids. Such emulsions tend to break promptly into their respective phases either due to molecular diffusion degradation (Ostwald ripening) or coalescence. To protect the emulsion from destabilisation surfactants should be added which provide either electrostatic or steric stabilization to the formed droplets and protect the emulsions against coalescence. Although surfactants provide stabilisation, preparation emulsion leads to size distribution which is determined by Laplace pressure difference between droplets of different size resulting in a net mass flux by diffusion between the droplets thereby reducing the total free energy of the system. If the droplets are not

stabilized against diffusional degradation, Ostwald ripening occurs which is a process where small droplet will disappear leading to an increase of the average droplet size.[89] There are three different types of emulsions, based upon the size of the dispersed particles (1) macroemulsion, opaque emulsion with particle size >400 nm, easily visible under microscope; (2) microemulsion, transparent dispersions with particles <100 nm in size and (3) mini- or nanoemulsion with a particle size between 100-400 nm. In the formation of macroemulsion one of the two immiscible liquids is broken up into particles that are dispersed in the second liquid. Since the interfacial tension between the two immiscible pure liquids is always greater than zero, this dispersion of the inner liquid, which produces a tremendous increase in the area of the interphase between them, results in a correspondingly large increase in the interfacial free energy of the system. The macroemulsion produced is highly unstable therefore an emulsifying agent is added to stabilize this basically unstable system. Microemulsions are transparent dispersions containing two immiscible liquids with particles of 10-100 nm diameters. The main difference macro-/miniemulsions and microemulsions are that the former, although exhibit excellent kinetic stability, are thermodynamically unstable. In addition, there are marked differences in their method of preparation in terms of energy input to make them. Miniemulsions are prepared by shearing a system of oil, water, a surfactant and a hydrophobe. The dispersions formed are of stabilized disperse phase with droplets in the size range of 50 and 500 nm. The emulsifier is generally 1-3 % of the oil phase, in contrast to the 15-30% in microemulsions.[90] Miniemulsions have been used widely used for the synthesis of the nanoparticles. On careful preparation, polymerizations in such miniemulsions results in monodispersed latex particles which have about the same size as the initial droplets since the polymerization time is usually shorter than the growth of the droplets by collisions. This implies that the appropriate formulation of a miniemulsion suppresses coalescence of droplets or Ostwald ripening. The principle of miniemulsion polymerization is schematically shown in **Figure 2.4.** The density of the surfactant layer controls the growth of droplets by collision. Freshly prepared miniemulsions are critically balanced and show a gradual but marked growth whereas a miniemulsion in equilibrium exhibit constant particle size on longer time scales. Polymerization in the dispersed droplets of such miniemulsions has turned out to be very promising for the synthesis of nanoparticles and has drawn attention towards their use as containers for drug delivery. [91,92-96]

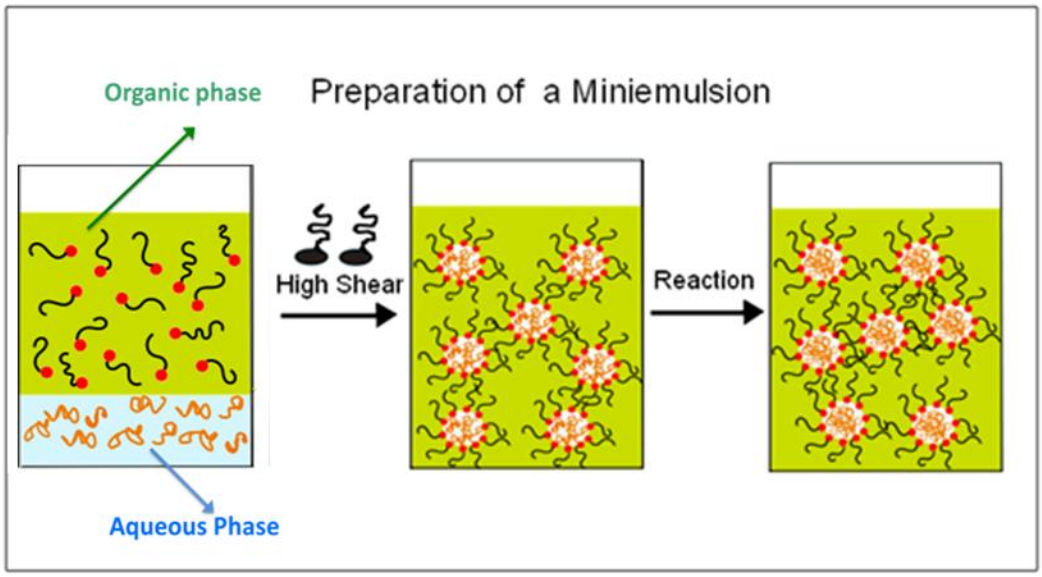

Figure 2.4: Schematic of miniemulsion polymerization. Mechanical agitation of a heterogeneous fluid containing surfactants always leads to a distribution of droplet sizes results.

2.6 References

[1] M. Ferrari, *Nature Reviews Cancer* **2005**, 5, 161.

[2] T. M. Allen, P. R. Cullis, *Science* **2004**, 303, 1818.

[3] M. A. Moses, H. Brem, R. Langer, *Cancer Cell* **2000**, 4, 337.

[4] G. Orive, A.R. Gascón, R.M. Hernández, A. Domínguez-Gil, J. L. Pedraz, *Pharmacol. Sci.* **2004**, 25, 382.

[5] S. M. Moghimi, A. C. Hunter, J. C. Murray, *The FASEB Journal* **2005**, 19, 311.

[6] K. Kostarelos, *Adv. Colloid Interface Sci.* **2003**, 106, 147.

[7] A. Lamprecht, N. Ubrich, H. Yamamoto, U. Schafer, H. Takeuchi, P. Maincent, Y. Kawashima, C. M. Lehr, *J. Pharmacol. Exp. Ther.* **2001**, 299, 775.

[8] T. M. Allen, P. R. Cullis, *Science* **2004**, 303, 1818.

[9] M. Meridio, J. M. Irache, F. Eclancher, M. Mirshahi, H. Villarroya, *J. Drug Target* **2000**, 8, 289.

[10] R. L. Juliano, *Adv. Drug Deliv. Rev*. **1998**, 2, 31.

[11] G. Orive, O. A. Ali, E. Anitua, J. L. Pedraz, D. F. Emerich, *Biochim. Biophys. Acta* **2010**, 1806, 96.

[12] Y. Nishioka, H. Yoshino, *Adv. Drug Deliv. Rev.* **2001**, 47, 55.

[13] B. Rihova, *Adv. Drug Deliv. Rev.* **1998**, 29, 273.

[14] T. M. Allen, *Nature Rev. Cancer* **2002**, 2, 750.

[15] Y. Aoyama, T. Kanamori, T. Nakai, T. Sasaki, S. Horiuchi, S. Sando, T. Niidome, *J. Am. Chem. Soc*. **2003**, 125, 3455.

[16] T. Nakai, T. Kanamori, S. Sando, Y. Aoyama, *J. Am. Chem. Soc*. **2003**, 125, 8465.

[17] B. D. Chithrani, A. A. Ghazani, W. C. W Chan, *Nano Lett.* **2006**, 6, 662.

[18] W. Jiang, B. Y. S. Kim, J. T. Rutka, W. C. W Chan, *Nat. Nanotechnol.* **2008**, 3, 145.

[19] C. S. Pillay, E. Elliot, C. Dennison, *J. Biochem.* **2002**, 363, 417.

[20] A. H. Faraji, P. Wipf, *Bioorganic Med. Chem.* **2009**, 17, 2950.

[21] D. S. Collins, E. R. Unanue, C.V. Harding, *J. Immunology* **1991**, 147, 4054.

[22] E. P. Feener, W. C. Shen, H. J. P. Ryser*, J. Biol. Chem.* **1990**, 265, 18780.

[23] R. A. Parente, L. Nadeasdi, N. K. Subabrao, F.C. Szoka, *J. Biochem*. **1990**, 29, 8713.

[24] E. Wagner, *Adv Drug Delivery Rev*. **1999**, 38, 279.

[25] D. C. Litzinger, L. Huang, *Biochim. Biophys. Acta* **1992**, 1113, 201.

[26] P. Venugopalan, S. Jain, S. Sankar, P. Singh, A. Rawat ,S. P. Vyas, *Pharmazie* **2002**, 57, 659.

[27] O. Boussif, F. Lezoualch, M. A. Zanta, M. D. Mergny, D. Scherman, B. Demeneix, J. P. Behr, *Proc. Natl. Acad. Sci.* **1995**, 92, 7297.

[28] M. Green, P. M. Loewenstein, *Cell* **1988**, 55, 1179.

[29] A. D. Frankel, C. O. Pabo, *Cell* **1998**, 55, 1189.

[30] S. M. Moghimi, B. Bonnemain, *Adv. Drug Delivery Rev*. **1999**, 37, 295.

[31] S. M. Moghimi, *Adv. Drug Delivery Rev*. **1995**, 17, 61.

[32] S. M. Moghimi, J. Szebeni, *Progress in Lipid Research* **2003**, 42, 463.

[33] S. M. Moghimi, A. C. Hunter, J. C. Murray, *Pharmacol. Rev.* **2001**, 53, 283

[34] L. Y. T. Chou, K. Ming, W. C. W. Chan, *Chem. Soc. Rev.* **2011***,* 40, 233.

[35] J. W. Park, *Breast Cancer Research* **2002**, 4, 95.

[36] A. Gabizon, H. Shmeeda, Y. Barenholz, *Clin. Pharmacokinet*. **2003**, 42, 419.

[37] V. P Torchilin, *Nat. Rev. Drug Discov.* **2005**, 4, 145.

[38] S. K. Sahoo, V. Labhasetwar, *Drug Discov. Today* **2003**, 8, 1112.

[39] T. M. Allen, *Trends Pharmacol. Sci.* **1994**, 15, 215.

[40] K. S. Soppimath, T. M. Aminabhavi, A. R. Kulkarni, W. E. Rudzinski, *J. Control. Rel.* **2001**, 70, 1.

[41] J. Kreuter, *Pharmaceutica Acta Helvetiae* **1983**, 58, 196.

[42] J. Boyd, C. Parkinson, P. Sherman, *J. Colloid Interface Sci.* **1972**, 41*,* 359.

[43] M. F Francis, M. Cristea, F. M. Winnik, *Pure Appl. Chem.* **2004**, 76, 1321.

[44] D. W. Kim, S. Y. Kim, H. K. Kim, S. W. Kim, S. W. Shin, J.S. Kim, K. Park, M. Y Lee, D. S. Heo, *Ann Oncol*. **2007**, 18*,* 2009.

[45] B. Klajnert, M. Bryszewska, *Acta Biochimica Polonica.* **2001**, 48, 199.

[46] S. V. Vinogradov, T. K. Bronich, A. V. Kabanov, *Adv. Drug Delivery Rev*. **2002**, 54, 135.

[47] K. Albrecht, M. Moeller, J. Groll, *Adv. Polym. Sci.* **2010**, 234, 65.

[48] J. K. Oh, D. J. Siegwart, H. I. Lee, G. Sherwood, L. Peteanu, J. O. Hollinger, *J. Am. Chem. Soc.* **2007**, 129, 5939.

[49] J. K. Oh, D. J. Siegwart, K. Matyjaszewski, *Biomacromolecules* **2007**, 8, 3326.

[50] H. Mok, T. G. Park, *Bioconjugate Chem.* **2006**, 17, 1369.

[51] N. Morimoto, X. P. Qiu, F. M. Winnik, K. Akiyoshi, *Macromolecules* **2008**, 41, 5985.

[52] K. N. Plunkett, K. L. Berkowski, J. S. Moore, *Biomacromolecules* **2005**, 6, 632.

[53] M. Andac, F. M. Plieva, A. Denizli, I.Y. Galaev, B. Mattiasson, *Macromol. Chem. Phys.* **2008**, 209, 577.

[54] H. A. Aliyar, P. D. Hamilton, E. E. Remsen, N. Ravi, *J. Bioact. Compat. Polym.* **2005**, 20, 169.

[55] J. Groll, S. Singh, K. Albrecht, M. Moeller, *J. Polym. Sci. A: Polym. Chem.* **2009**, 47, 5543.

[56] A. Bernkop-Schnürch, V. Schwarz, S. Steininger, *Pharm. Res.* **1999**, 16, 876.

[57] A. Bernkop-Schnürch, M. Hornof, Y. Pinter, *Int. J. Pharm.* **2003**, 260, 229.

[58] A. Bernkop-Schnürch, D. Guggi, Y. Pinter, *J. Control. Rel.* **2004**, 94, 177.

[59] T. Schmitz ,I. Bravo-Osuna, C. Vauthier, G. Ponchel, B. Loretz, A. Bernkop-Schnürch, *Biomaterials* **2007**, 28, 524.

[60] B. Loretz, M. Thaler, A. Bernkop-Schnürch, *Bioconjug. Chem*. **2007**, 18, 1028.

[61] F. Atyabi, F. Talaie, R. Dinarvand, *J. Nanosci. Nanotechnol*. **2009**, 9, 4593.

[62] D. Lee, W. Zhang, S. A. Shirley, X. Kong, G. R. Hellermann, R. F. Lockey, S. S. Mohapatra, *Pharm. Res.* **2007**, 24, 157.

[63] S. Shu, X. Wang, X. Zhang, X. Zhang, Z. Wang, C. Li, *New J. Chem*. **2009**, *33*, 1882.

[64] S. K. Hahn, J. S. Kim, T. Shimobouji, *J. Biomed. Mater. Res.* **2006**, 80A, 916.

[65] H. Lee, H. Mok, S. Lee, Y-K Oh, T. G. Park*, J. Control. Rel.* **2007**, 119, 245.

[66] N. Morimoto, X-P. Qui, F. M. Winnik, K. Akiyoshi, *Macromolecules,* **2008**, 41, 5985.

[67] K. H. Bae, H. Mok, T. G. Park, *Biomaterials* **2008**, 29, 3376.

[68] U. Hasegawa, S. I. Sawada, T. Shimizu, T. Kishida, E. Otsuji, O. Mazda, K. Akiyoshi, *J. Control. Rel.* **2009**, 140, 312.

[69] W. Lv, S. Liu, W. Feng, J. Qi, G. Zhang, F. Zhang, X. Fan, *Macromol. Rapid Comm.* **2011**, 32, 1101.

[70] X. Yang, S. Kootala, J. Hilborn, D. A. Ossipov, *Soft Matter* **2011**, 7, 7517.

[71] S. Ekici, P. Ilgin, S. Butun, N. Sahiner, *Carbohydr. Polym*. **2011**, 84, 1306.

[72] K. H. Bae, H. Mok, T.G. Park, *Biomaterials* **2008**, 29, 3376.

[73] D. H. Nguyen, Y. K. Joung, J. H. Choi, H. T. Moon, K. D. Park, *Biomed. Mater.* **2011**, 6, 1.

[74] A. Meister, M. E. Anderson, *Annu. Rev. Biochem*. **1983**, 52, 711.

[75] G. Wu, Y-Z Fang, S. Yang, J. R. Lupton, N. D.Turner, *J. Nutr.* **2004**, 134, 489.

[76] A. Meister, M. E. Anderson, *Annu. Rev. Biochem.* **1983**, 52, 711.

[77] F. Q. Schafer, G. R. Buettner, *Free Radical Biol. Med*. **2001**, 30, 1191.

[78] C. V. Smith, D. P. Jones, T. M. Guenthner, L. H. Lash, B. H. Lauterburg, *Toxicol. Appl. Pharmacol.* **1996**, 140, 1.

[79] G. Saito, J. A. Swanson, K-D Lee, *Adv. Drug Deliv. Rev.* **2003**, 55, 199.

[80] F. Meng, W. E. Hennink, Z. Zhong, *Biomaterials* **2009**, 30, 2180.

[81] P. Kuppusamy, M. Afeworki, R. A. Shankar, D. Coffin, M. C. Krishna, S. M. Hahn, J. B. Mitchel, J. L. Zweier, *Cancer Res.* **1998**, 58, 1562.

[82] P. Kuppusamy, H. Li, G. Ilangovan, A. J. Cardounel, J. L. Zweier, K. Yamada, M. C. Krishna, J. B. Mitchell, *Cancer Res.* **2002**, 62, 307.

[83] N. S. Kosower, E. M. Kosower, *Meth. Enzymol.* **1995**, 251, 123.

[84] X. Z. Shu, Y. Liu, Y. Luo, M. C. Roberts, G. D. Prestwich, *Biomacromolecules* **2002**, 3, 1304.

[85] AplaGen, Process for Forming Disulphide Bridges US Patent Application 20100203001, August 12, **2010**.

[86] S. K. Hahn, J. K. Park, T. Tomimatsu, T. Shimobouji, *Int. J. Biol. Macromol*. **2007**, 40, 374.

[87] A. Goessl, N. Tirelli, J. A. Hubbell, *J. Biomater. Sci. Polym. Ed.* **2004**, 15, 895.

[88] K. Landfester, *Adv. Mater*. **2001**, 13, 765.

[89] M. J. Rosen, *Surfactants and Interfacial Phenomena Third Ed*.; John Wiley & Sons, Inc. New York, **2004**.

[90] K. Landfester, M. Willert, M. Antonietti, *Macromolecules* **2000**, 33*,* 2370.

[91] F. Tiarks, K. Landfester, M. Antonietti, *J. Polym. Sci. Part A: Polym. Chem.* **2001**, 39, 2520.

[92] L. Torini, J. F. Argillier, N. Zydowick, *Macromolecules* **2005**, 38*,* 3225.

[93] M. Barrère, K. Landfester, *Macromolecules* **2003**, 36*,* 5119.

[94] K. Landfester, U. Pawelzik, M. Antonietti, *Polymer* **2005**, 46*,* 9892.

[95] D. Crespy, K. Landfester, *Macromol. Chem. Phys.* **2007**, 208, 457.

[96] A. Taden, M. Antonietti, K. Landfester, *Macromol. Rapid Comm.* **2003***,* 24*,* 512.

CHAPTER 3

Synthesis of Thiol Functionalized Polymers, and use of HS-sP(EO-*stat*-PO) based Hydrogels for Chemokine Delivery

Part of this work which deals with chemokines delivery form the hydrogels was performed in the work group of Prof. Christian Weber, Institute for Molecular Cardiovascular Research (IMCAR), RWTH Aachen and Institute for Cardiovascular Prevention (IPEK), Hospital of the LMU Munich.

3.1 Introduction

Disulfide bonds as key features in drug delivery systems are being investigated in a wide variety of forms and applications. Because of the easy reversibility but relative stability, disulfide bonds have mostly been used to attach functional moieties to an already existing drug delivery system. However, these exact same properties also present an interesting opportunity as a basis for a reductively degradable bulk carrier material. In this chapter first we investigate the possibility to functionalize branched star shaped poly(ethylene oxide-*stat*-propylene oxide) (**sP(EO-*stat*-PO)**) and poly(glycidol) (**PG**) macromolecules with thiol groups, in order to then crosslink them via formation of disulfide bonds or by Micheal addition to form hydrogels. **PG** was synthesized via poly (ethoxyethylglycidylether) by anionic ring-opening polymerisation followed by subsequent deprotection. Thiol functionalization was introduced by Steglish Esterification of prepolymers. The prepolymers were first crosslinked via esterification to form disulphide crosslinked hydrogels. The hydrogels formed were subsequently reduced by cleaving the disulfide cross-linkage (–S–S–) to thiol groups (–SH HS–) by using tris(2-carboxyethyl) phosphine (TCEP) as reductant. Secondly we show the release of engineered chemokines from **HS-sP(EO-*stat*-PO)** hydrogel crosslinked by oxidation and Micheal addition to prevent injury extension after myocardial infarction. The hydrogel was loaded with two chemokine-derivatives, Met-CCL5 (7.98 kDa) and recombinant protease-resistant CXCL12 (S4V) (8.07 kDa), for the inhibition of

neutrophil infiltration and concomitant improvement of hematopoietic stem cell recruitment to sustain neovascularization after myocardial infraction.

Myocardial infarction (MI), following the occlusion of an atherosclerotic coronary artery, causes death of the cardiomyocytes and initiation of an inflammatory reaction, activation of the nuclear factor (NF)-κB and toll like receptor (TLR)-mediated pathways, which up-regulates chemokines, cytokines as well as adhesion of molecules in endothelial cells and leukocytes.[1] All these processes lead to the infiltration of polymorphonuclear cells, monocytes and lymphocytes into the infarcted area and are of crucial importance in the proper healing and scar formation. The cardiac repair, or so-called "remodeling", of the heart muscle is in fact the replacement of the adjacent myocardium with connective tissue and consecutive dilation of the ventricles.

Neutrophil and macrophage derived inflammatory signals initiate the phagocytosis of dead cells and degradation products from matrix. During this proliferation phase, the expression of inflammatory mediators is inhibited; which causes the infiltration of fibroblasts and endothelial cells into the infarcted area, resulting into promotion of collagen deposition and angiogenesis.[2] Current clinical therapies include only cause-dependent interventions, which are not always efficient in reducing myocardial necrosis and optimizing cardiac repair following infarction. New strategies have been proposed such as progenitor cell therapy, which was considered as a very promising therapeutic approach to provide an alternative way to regenerate the heart structure after MI. Animal studies have shown that transplantation of adult stem cells after acute MI improves neovascularization and reduces fibrosis, preserving the left ventricular heart function.[3-5] Unfortunately, these promising results were not obtained in clinical studies in patients,[6-9] probably due to incorrect translation of the knowledge from animal to human system. New data suggest that the main mechanism of improving the heart function by cell therapy is in fact due to the inflammation and its consecutive effects.[10] These findings are of notable significance, since they selectively control and manipulate the inflammatory reaction through chemokines.[11]

Chemokines are small signaling proteins that trigger migration (chemotaxis) of different cells. They can both prevent apoptosis of cardiomyocytes and promote angiogenesis in the infarcted area.[11] The inhibition of neutrophil infiltration by blocking CCR1 or by Met-CCL5 treatment leads to improved left ventricular function and reduction of infarct extension,[12,13] possibly by decreasing myeloperoxidase expression and preventing further expansion of the resulting tissue damage.[14] CXCL12 (Stromal Cell-Derived

Factor 1/SDF-1) and its protease-resistant mutants are well established agents for recruiting hematopoietic stem cells from the circulating blood, resulting in a significant increase in vessel formation, vascularization in the scar tissue, and a consecutive improvement of left ventricular function after MI.[15-18]

In this study, combined approach implementing Met-CCL5 and recombinant protease-resistant CXCL12 (S4V), for the inhibition of neutrophil infiltration and concomitant improvement of hematopoietic stem cell recruitment to sustain neovascularization is provided. To avoid any unwanted effects of a systemic administration, the chemokine-derivatives were added to biodegradable hydrogels and administered locally in the infarcted myocardium.

3.2 Experimental

3.2.1 Materials and Methods

Six arm, star shaped **sP(EO-*stat*-PO)** with a backbone consisting of 80% ethylene oxide and 20% propylene oxide (Mn = 12000 g/mol, Mw/Mn=1.12 g/mol) was purchased from Dow Chemicals. Prior to functionalization **sP(EO-*stat*-PO**) has been purified by precipitation in THF/cold diethylether as solvent/non solvent system. 1, 3-dicyclohexylcarbodiimide (DCC), (99%) was purchased from Acros and used as received. 4-Dimethylaminopyridine (DMAP) (99 + %), 3, 3'-dithiopropionic acid (DTPA), tris(2-carboxyethyl) phosphine (TCEP) (99%), dichloromethane (HPLC grade), DMSO (Biotech grade) (99.9 + %), potassium *tert*-butoxide (1 M solution in THF) were purchased from Aldrich and used as received. HCl and *p*-toluene sulphuric acid were purchased from VWR and used as received. THF used was distilled over $LiAlH_4$ and dried with n-BuLi, 2,3-epoxypropan-1-ol (glycidol) (99%, Fluka) was dried over molecular sieves (4Å) and distilled over CaH_2 under reduced pressure and ethyl vinyl ether (99%, Fluka) was purified by distillation at atmospheric pressure under dry nitrogen atmosphere, ethoxy ethyl glycidyl ether (EEGE) was synthesized from glycidol and ethyl vinyl ether according to Fitton *et al.*[19] Hydrogen peroxide 30% (p.A) (VWR), PEG diacrylate (Mn = 700 g/mol) (Sigma) were used as received. Phosphate buffered saline (PBS) from Sigma has been dissolved in water to 0.01 M concentration (pH 7.4). Dialysis membrane, MWCO = 3500 and 1000 Dalton, has been purchased from Spectrum Laboratories, Inc. Demineralised water was used throughout the work.

^{1}H-NMR spectra were carried out on a Bruker DPX 300 at 300 MHz. DMSO-d6 with TMS as internal standard was used as solvents. ^{1}H spectra were recorded in D_2O, DMSO-d6 and $CDCl_3$ with a Bruker spectrometer operating at 400 MHz (Bruker AV 400). Tetramethylsilane was added as the internal standard. Chemical shifts are reported in parts per million (ppm) relative to the internal standard.

Size Exclusion Chromatography (SEC) was performed in THF with addition of 250 mg/L 2, 6-di-tert-butyl-4-methylphenol. A high pressure liquid chromatography pump (PL-LC 1120 HPLC) and a refractive index detector (ERC 7515A) were used at 35 °C with a flow rate of 1.0 mL/min. Five columns with MZ gel were applied. The length of the first column was 50 mm, and 300 mm for the other four columns. The diameter of each column was 8 mm, the diameter of the gel particles 5 mm, and the nominal pore widths were 50, 50, 100, 1000, and 10 000 Å, respectively. Calibration was achieved using poly(methyl methacrylate) standards.

For **PG** and **HS-PG**, SEC analyses were carried out at 80°C using a high-pressure liquid chromatography pump (Bischoff HPLC 2200) and a refractive index detector (Waters 410). The eluting solvent was *N,N*-dimethylacetamide (DMAc) with 2.44 g L-1 LiCl and a flow rate of 0.8 mL min-1. Four columns with MZ-DVB gel were applied. The length of each column was 300 mm, the diameter 8 mm, the diameter of the gel particles 5 mm, and the nominal pore widths were 100, 1000, and 10000 Å. Calibration was achieved using poly(methyl methacrylate) standards.

Raman Spectroscopy Raman spectra were recorded on Bruker RFS 100/S spectrometer. The laser used was Nd:YAG at 1064 nm wavelength at a power of 250 mW. On an average 1000 scans were taken at a resolution of 4 cm^{-1}. For sample holding aluminium pans of 2 mm bore were used. Software used for data processing was OPUS 4.0.

3.2.2 Synthesis of Protected Glycidol (Ethoxy Ethyl Glycidyl Ether)

The monomer, ethoxy ethyl glycidyl ether (EEGE) was synthesized as follows. Under inert gas conditions 117 mL (1.75 mol) of freshly distilled glycidol and 567 mL (5.93 mol) of ethyl vinyl ether were added in a 1000mL 3-neck flask. To prevent overheating the reaction mixture was cooled in ice bath to 0°C followed by addition of 2.66 g (0.0153 mol) of *p*-toluene sulphuric acid added drop by drop with constant stirring. The

reaction was continued under stirring at room temperature for 4h. After which, the reaction mixture was extracted with an excess of saturated $NaHCO_3$. The organic phase was collected and dried over magnesium sulphate. The solid was filtrated off and excess of ethyl vinyl ether was removed under vacuum. The crude product ethoxy ethyl glycidyl ether (EEGE) **(Scheme 3.1)** was fractionated under reduced pressure and stored over CaH_2. Yield: 97% of crude product, 72% after fractionation.

1H NMR (CDCl3): δ = 1.1-1.5 Hz (t, 3H, CH3-7), 1.2-1.25 Hz (q, 3H, CH3-5), 2.5-2.8 Hz (m, 2H CH2-6), 3.1-3.8 Hz (m, 5H, CH2-1, 3, CH-2), 4.7-4.75 Hz (m, 1H, CH-4).

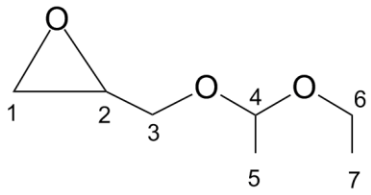

Scheme 3.1: Schematic representation of ethoxy ethyl glycidyl ether (EEGE)

3.2.3 Synthesis of Linear Poly(glycidol) acetal

Anionic polymerisation of EEGE was initiated by *t*-BuOK according to Dworak *et al.*[20] to form poly(glycidol) acetal (PEEGE) **(Scheme 3.2).** Schlenk flask used for reactions was evacuated and flushed with nitrogen prior to polymerization. Under nitrogen atmosphere EEGE (50 mL, 342 mmol) was mixed with 50 mL of dry THF. *t*-BuOK (0.43 mL of a 1 M solution in THF, 0.43 mmol) was added and the reaction mixture stirred at 60 °C for 24 h. On completion of polymerization the reaction was cooled down to RT and polymerisation was terminated by addition of excess of methanol. Solvents were removed in vacuum. From SEC (THF): Mn = 9500 g/mol, degree of polymerization (DP) = 60, Mw/Mn = 1.11.

1H NMR (CDCl3): δ = 1.21 Hz (s, br, 9H, CH3-1), 3.34-3.67 Hz (m, 7 H, CH2-2, 4, 7, CH-3), 1.18 Hz (t, 3H, CH3-8), 1.29 Hz, (d, 3 H, CH3-6), 4.70 (q, 1H, CH-5).

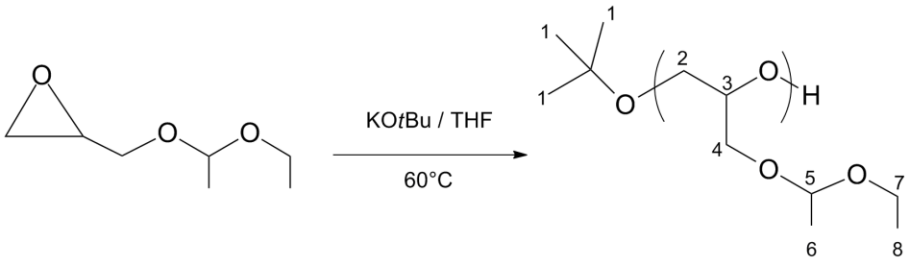

Scheme 3.2: Schematic representation of anionic polymerization of ethoxy ethyl glycidyl ether to poly(glycidol) acetal.

3.2.4 Deprotection of Poly(glycidol) acetal to Poly(glycidol)

PEEGE was dissolved in 5 L of THF to the concentration of 4 g/L. 100 mL of concentrated HCl was added to this solution and after 2 h of stirring at RT the deprotected polymer was precipitated. THF was removed and the polymer was dissolved in minimum quantity of methanol followed by drying under vacuum for 12 h. Poly(glycidol) was obtained in good yields of 85%. The deprotection reaction is presented in **Scheme 3.3**. SEC (DMF): Mn = 4500 g/mol, Mw/Mn = 1.06.

^{1}H NMR (DMSO): δ = 1.25 Hz (s, br, 9H, CH_3-1), 3.37-3.64 Hz (m, 5 H, CH_2-2, 4, CH-3).

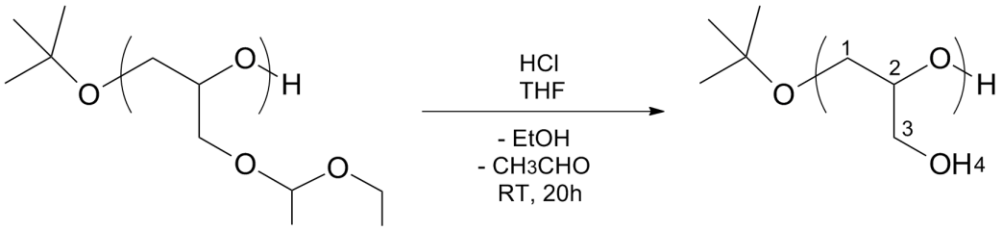

Scheme 3.3: Schematic representation of deprotection of poly(glycidol) acetal to poly(glycidol)

3.2.5 Synthesis of Thiol Functionalized Star-shaped Poly(ethylene oxide-*stat*-propylene oxide) (sP(EO-*stat*-PO))

The thiol functionalized **sP(EO-*stat*-PO))** (**HS-sP(EO-*stat*-PO))**, **(Scheme 3.4)** has been prepared in a two step synthesis. In the first step **sP(EO-*stat*-PO))** have been crosslinked with disulfide crosslinker followed by the reduction of disulfide bonds to thiol groups in the second step. Typically the functionalization of four –OH groups has been performed. This lead to unreacted two -OH groups which can be used for further functionalization, for example with targeting molecules or drugs.

Step 1. For crosslinking of four -OH groups of **sP(EO-*stat*-PO))**, a solution consisting of 3,3'-dithiopropionic acid (DTPA) (1.0 eq with respect to one –OH) (0.1051 g, 0.5 mmol) in dried THF (4 mL) was added drop wise to a solution consisting of the purified **sP(EO-*stat*-PO)** (M=12000 g/mol, 3g, 0.25 mmol × 4 –OH = 1.0 mmol), dicyclohexylcarbodiimide (DCC) (1.1 eq with respect to one -COOH) (0.2269 g, 1.1 mmol) and dimethylaminopyridine (DMAP) (1.1 eq with respect to one -COOH) (0.1343 g, 1.1 mmol) in CH_2Cl_2 (6 mL) in an ice bath at 0 °C over 10 min. The resulting mixture was allowed to stir at RT for 12 h. The formed hydrogel was washed three times with CH_2Cl_2, twice with THF, ethanol and water followed by evaporation of remaining solvents on the rotary evaporator. Finally, the product was dried in a vacuum oven at 35 °C for 12 h.

Step 2. Tris (2-carboxyethy) phosphine (TCEP) has been used for the reduction of disulfide bonds. TCEP (1.5 eq. with respect to the disulfide units) (0.429 g, 1.5 mmol) was reacted with the crosslinked polymer in PBS buffer at room temperature for 2 h (pH of the solution ~ 4) under inert gas atmosphere. Subsequently, the solution was dialyzed (membrane pore size MWCO = 3500 Da) for two days at RT against aqueous HCl solution at pH ~ 3.5. Finally, the polymer solution have been lyophilized and stored at +4 °C for further use. The free thiol content of the polymer was determined by NMR. SEC (THF): Mn = 12900 g/mol, Mw/Mn = 1.12.

^{1}H NMR (D_2O): δ = 1.21 Hz (s, br, 9H, CH_3-1), 3.34-3.67 Hz (m, 7 H, CH_2-2, 4, 7, CH-3), 1.18 Hz (t, 3H, CH_3-8), 1.29 Hz, (d, 3 H, CH_3-6), 4.70 (q, 1H, CH-5).

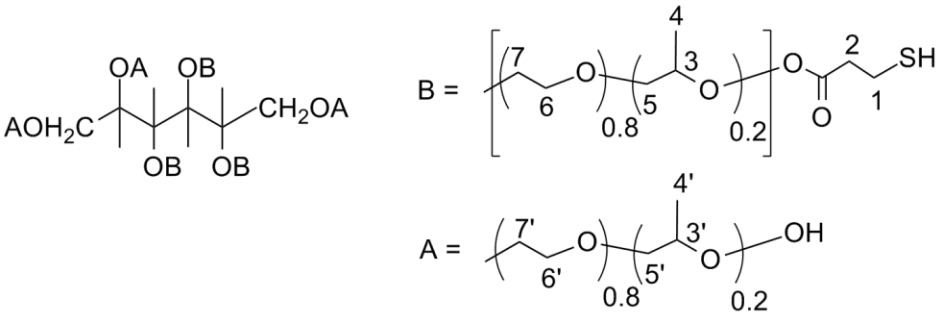

Scheme 3.4: Schematic representation of Thiolated six armed **sP(EO-*stat*-PO)**

3.2.6 Synthesis of Thiolated Poly(glycidol)

Functionalization of 25% of –OH groups in **PG** (Mn = 4500 g/mol, DP = 60) was done in a similar way as done as with **sP(EO-*stat*-PO)**. However, since the **PG** is not soluble in CH_2Cl_2, DMF was used as a solvent instead. The thiol content has been determined by ^{1}H-NMR.

^{1}H NMR (D_2O): δ = 1.13 Hz (s, br, 9H, CH_3-1), 3.4-3.9 Hz (m, 7 H, CH_2 2, 7, 9, CH-3, 8), 2.65 Hz (t, 4H, CH_2-5, 6)

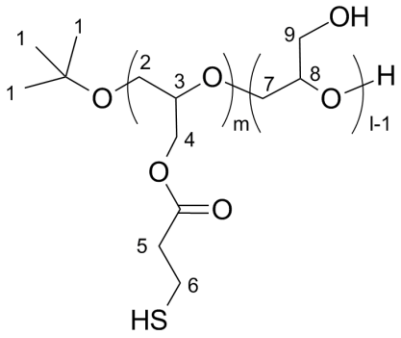

Scheme 3.5: Schematic representation of Thiol functionalized linear poly(glycidol) (**HS-PG**).

3.2.7 Synthesis of Hydrogels.

The synthesis of hydrogels from thiol-functionalized biodegradable **sP(EO-*stat*-PO)** and **PG** prepolymer was performed as:

HS-sP(EO-*stat*-PO) (0.025 g, 2.08×10^{-3} mmol, 6.25×10^{-3} mmol with respect to SH groups (3 SH per molecule)) was dissolved in PBS buffer pH 7.4 (63μL). The solution was mixed followed by the addition of the oxidation catalyst H_2O_2 (3×10^{-3} mmol). Gelation time was qualitatively determined by the vial inversion method.

HS-sP(EO-*stat*-PO) (0.025 g, 2.08×10^{-3} mmol, 6.25×10^{-3} mmol with respect to SH groups (3 SH per molecule)) was dissolved in PBS buffer pH 7.4 (63μL) and was mixed thoroughly. To this solution PEG diacrylate (0.00218 g, 2.0×10^{-3} mmol with respect to acrylate (ACR) groups (2 ACR groups per molecule)) was added. This equals a molar ratio 1:1 SH: ACR functional groups. All the components were homogenized fast.

HS-PG (0.025 g, 4.1×10^{-3} mmol, 6.14×10^{-2} mmol with respect to SH groups (15 SH per molecule)) was dissolved in PBS buffer pH 7.4 (63μL). The solution was mixed followed by the addition of the oxidation catalyst H_2O_2 (3×10^{-3} mmol). Gelation time was qualitatively determined by the vial inversion method.

HS-PG (0.025 g, 4.1×10^{-3} mmol, 6.14×10^{-2} mmol with respect to SH groups (15 SH per molecule)) was dissolved in PBS buffer pH7.4 (63μL) and was mixed thoroughly. To this solution PEG diacrylate (0.0215 g, 3.07×10^{-2} mmol, with respect to ACR groups (2 ACR groups per molecule)) was added. This equals a molar ratio 1:1 SH: ACR functional groups. All the components were homogenized fast.

3.2.8 Procedure for Hydrogel Synthesis with Chemokines

HS-sP(EO-*stat*-PO) hydrogels were prepared in similar manner as described above. H_2O_2 crosslinked hydrogels were used to encapsulate Met-CCL5 mentioned as FDH (fast degradable hydrogels) while diacrylate crosslinked hydrogels were used to encapsulate CXCL12 (S4V) mentioned as SDH (slow degradable hydrogels) further in the text. The FDH was prepared by dissolving **HS-sP(EO-*stat*-PO)** (0.0125 g, 1.04×10^{-3} mmol) in PBS buffer pH 7.4 (31.5μL) supplemented with Met-CCL5 1.47μg (1.83×10^{-3} μmoles). The solution was mixed followed by the addition of the oxidation catalyst H_2O_2 (1.5×10^{-3} mmol). While SDH was prepared by dissolving **HS-sP(EO-*stat*-PO)** (0.0125 g, 1.04×10^{-3} mmol) in PBS buffer pH 7.4 (31.5μL) supplemented with CXCL12 (S4V) 8.8μg (1.09×10^{-2} μmoles) followed by addition of PEG diacrylate (0.00109 g, 1.0×10^{-3} mmol).

3.2.9 Biocompatibility of CXCL12 (S4V), Met-CCL5 and HS-sP(EO-*stat*-PO)

HUVECs were seeded in collagen-G coated 96-well plates with Endothelial Cell Growth Medium (PromoCell, Heidelberg, Germany) and cells were allowed to attach prior to treatment with 5 μg/mL Met-CCL5, 30 μg/mL CXCL12 (S4V) and 0.45 g/mL **HS-sP(EO-*stat*-PO)**. Proliferation between 0-72h was determined using BrdU Proliferation Assay (Novagen / Merck Bioscience, Darmstadt, Germany) and cytotoxicity was detected using the CellTiter-Blue® cell viability assay (Promega, Mannheim, Germany) at time points ranging from 0-24 h. All procedures were performed according to the manufacturer's instructions. The data were expressed as the relative signal (RFU) after subtraction of the relative signal of the appropriate buffer or medium controls.

3.2.10 Release of CXCL12 (S4V) and Met-CCL5 from HS-sP(EO-*stat*-PO) Hydrogels.

FDH (15μL) containing 3 μg CXCL12 (S4V), were incubated at 37°C in 250 μL PBS containing 5 mM reduced glutathione (Sigma) for 24h. While SDH with 0.5 μg Met-

CCL5 were incubated at 37°C in 250 μL PBS only, for over 4 weeks. At suitable time points 250 μL PBS containing 5 mM reduced glutathione was replaced and the supernatant was analyzed by DuoSet ELISA kit (R&D Systems) for mouse CXCL12 (S4V) or human Met-CCL5 according to manufacturer's instructions.

3.2.11 Mouse Model of Myocardial Infarction and Injection of Hydrogels Containing Chemokines

Eight weeks old male C57BL/6 mice (n = 6-9 per group) were subjected to coronary occlusion as described earlier.[21,22] Briefly, mice were intubated under general anesthesia and positive pressure ventilation was maintained using a rodent respirator. Hearts were exposed by left thoracotomy and myocardial infarction (MI) was induced by suture occlusion of the left anterior descending artery (LAD) over a silicone tube. FDH/ SDH (15μL), alone or loaded with 0.5 μg Met-CCL5 and/or 3μg CXCL12 (S4V), were injected into the myocardium of the mice directly after MI. The muscle layer and skin incision were closed with a silk suture. The animals were kept in standard conditions one day or 4 weeks after MI until further investigation. Heart function of the mice was evaluated 1 day before, and 4 weeks after MI. All animal experiments and study protocols were approved by local authorities, complying with German animal protection laws.

3.3 Results and Discussion

3.3.1 Synthesis of Linear Poly(glycidol) acetal

A defined molecular structure as well a narrow polydispersity index (PDI) of polymer is very important for using it in biomedical applications. Living anionic polymerization allows the synthesis of polymers with PDIs of approximately one (**Equation 3.1**), following Poisson-distribution which is the ratio of weight-average molecular weight ($\bar{M}_w$) to number-average molecular weight (M_n).

$$PDI = \frac{\bar{M}_w}{M_n} \qquad \text{Eq.3.1}$$

Glycidol (2, 3-epoxypropanol-1) is an oxirane monomer containing a hydroxyl group. Polyethers obtained from this monomer contain a hydroxyl group in each structural repeating unit. In order to obtain linear polymers of glycidol its hydroxyl group has to be protected. Living anionic polymerization of monomer proceeds via ring-opening,

resulting into polymer with narrow PDI, the degree of polymerization only depends on the monomer $[M]_0$ and initiator $[I]_0$ concentration as well as the conversion X_p and can be calculated by **Equation 3.2**.

$$DP_0 = \frac{[M]_o}{[I]_o} \cdot x_p \qquad \text{Eq.3.2}$$

While polymerizing unprotected glycidol would lead to equilibrium between three active species and in the following steps to a highly branched polymer **(Scheme 3.6)**.

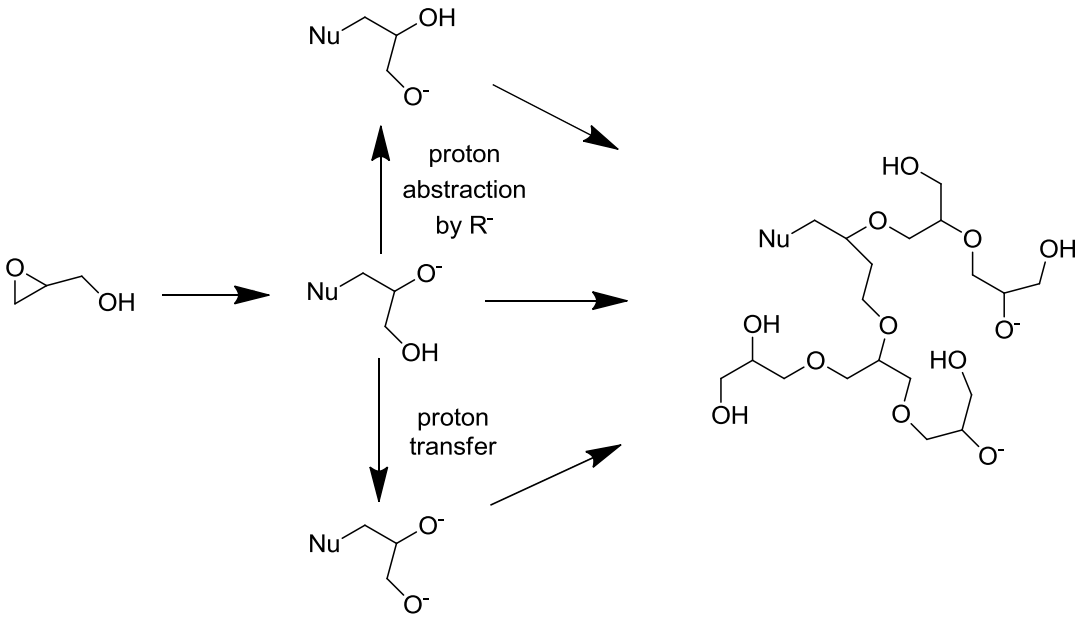

Scheme 3.6: Schematic representation for formation of highly branched polyglycidol

Thus to obtain well defined linear polyglycidol, monomers with protected hydroxyl group like ethoxy ethyl glycidyl ether (EEGE), allyl glycidyl ether (AGE) or *tert* -butyl glycidyl ether (*t*-BuGE) are used.

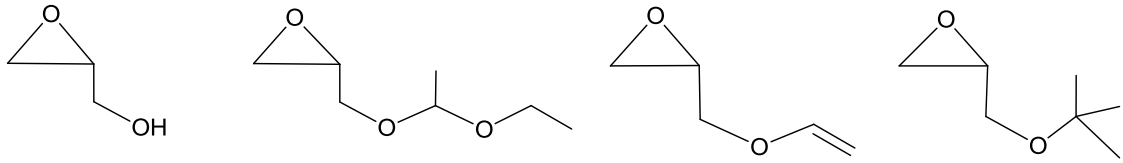

(a) Gylcidol (b) EEGE (c) AGE (d) *t*-BuGE

Scheme 3.7: Structure of (a) unptotcted glycidol and different protected glycidoly (b) ethoxy ethyl glycidyl ether (EEGE), (c) allyl glycidyl ether (AGE) (d) *tert* -butyl glycidyl ether (*t*-BuGE)

The polymerization mechanism is illustrated in **Scheme 3.8**. The reaction is initiated by a nucleophillic attack of potassium *tert*-butoxide on the secondary carbon atom of the epoxide, causing ring-opening and formation of an active chain end **(Scheme 3.8 (a)).**

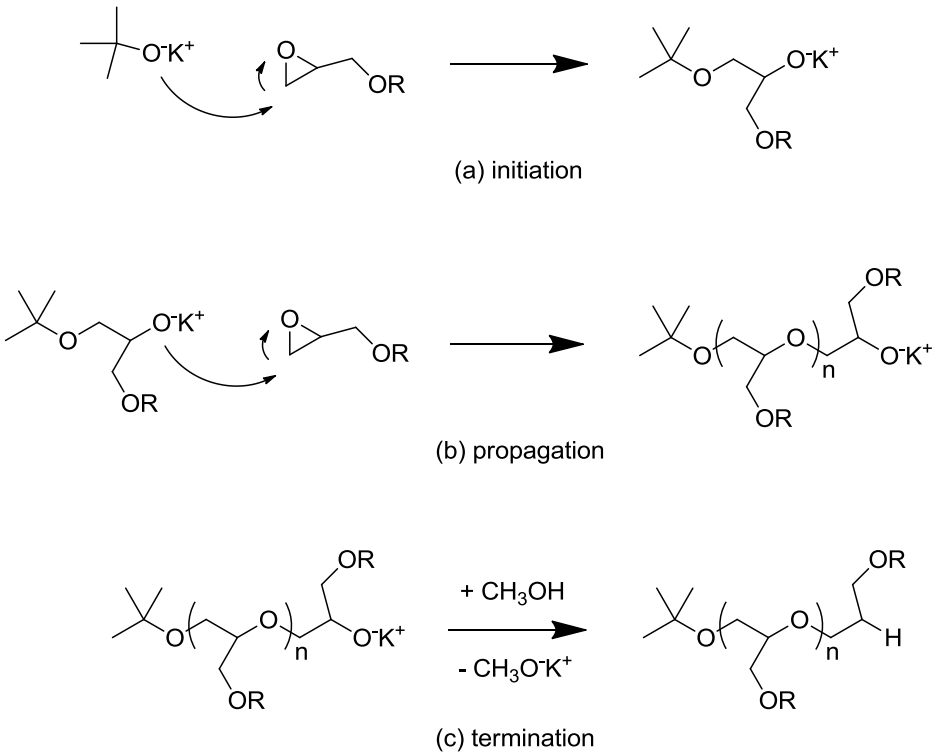

Scheme 3.8: Polymerization mechanism of living ring-opening anionic polymerization of ethoxy ethyl glycidyl ether

This propagates the reaction **(Scheme 3.8 (b)).** Termination of the polymerization can be achieved by deactivation of the active chain ends by a proton donors like water or methanol **(Scheme 3.8 (c)).** In this work as a protection method, the acid-catalysed reaction of glycidol with ethyl vinyl ether leading to *2,3*-epoxypropyl-*1*-ethoxy ethyl ether (EEGE) was chosen.[23] During this reaction, a big excess of vinyl ether was used where ethyl vinyl ether acted as a reagent as well as a solvent. The obtained protected monomer is stable under anionic polymerization conditions and more importantly, it can easily be polymerized via anionic polymerization under conditions close to the living to give linear polymer. Under these conditions, polymers with good control of the molar mass and narrow molar mass distribution can be obtained.[20]

Linear poly(glycidol acetal) polymer with degree of polymerization (DP) 60 was prepared. The polymerisation was carried out in a homogenous system, in dry THF as medium using potassium *t*-butylalcoholate (*t*-BuOK) as initiator. Important is also the

fact that the calculated DP values of polymers corresponded well to the targeted ones, indicating good control of polymerisation under chosen conditions. The polymer structure was confirmed by 1H NMR spectroscopy (**Figure 3.1)**

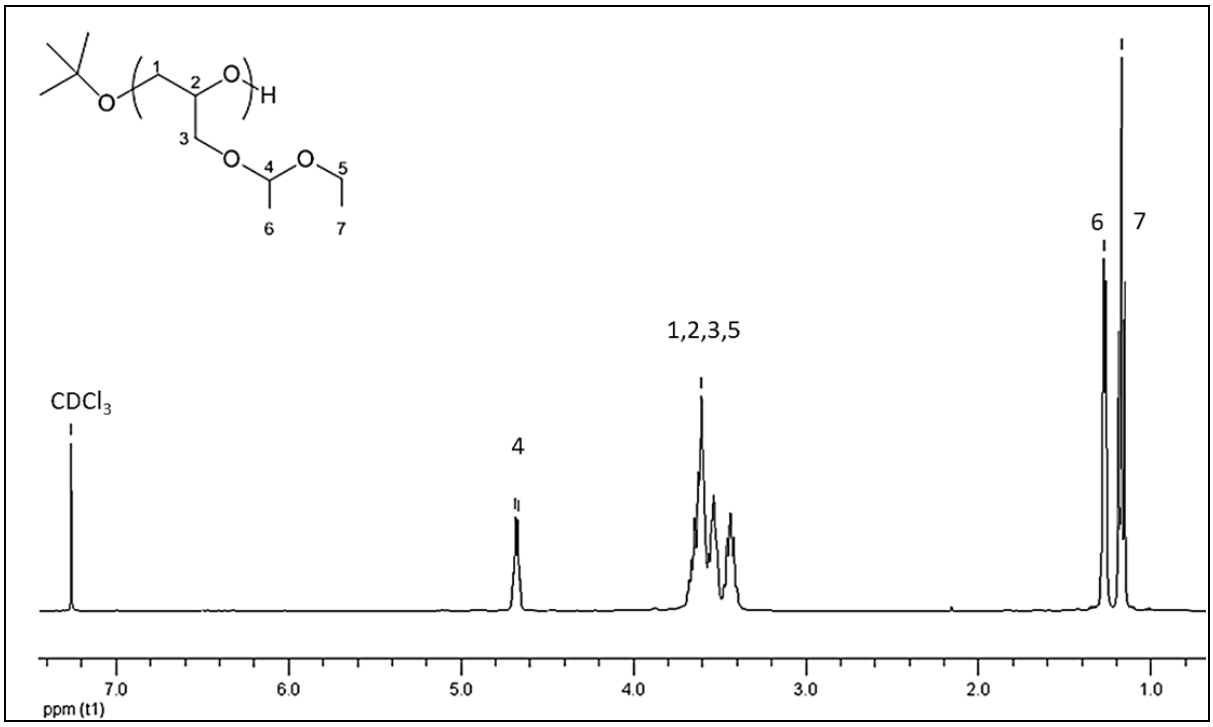

Figure 3.1: ^{1}H NMR spectrum of poly(glycidol acetal)

showing the presence of glycidol acetal repeating units. Three groups of signals were observed. However, exact calculation of molar masses of synthesized polymers based on the peak integration could not be performed using 1H NMR spectroscopy. The signals derived from the initiator methyl groups and methyl groups form acetal groups overlapped, making calculation impossible. From 1H NMR spectra (**Figure 3.2)**, it only can be concluded that upon this conditions monomer is stable and the protective groups remain unchanged. To de-protect poly(glycidol acetal) to poly(glycidol) different methods are already found and published.[20,24] Spassky *et al.* carried it out by acidic hydrolysis in two ways.[20] The first method was two step hydrolysis with concentrated formic acid to poly(formate), followed by saponification with KOH in dioxane/methanol mixture in order to regenerate the hydroxyl groups. The second one was the direct hydrolysis by aqueous hydrochloric acid in THF. However, in case of hydrolysis by HCl some polymer chain degradation was reported. The other published methods involved hydrolysis of acetal groups by oxalic acid in acetone/water mixture or in methanol using

$AlCl_3$ as de-protecting agent.[24] In this work de-protection of protected poly(glycidol acetal) was performed by hydrolysis in aqueous hydrochloric acid in THF.

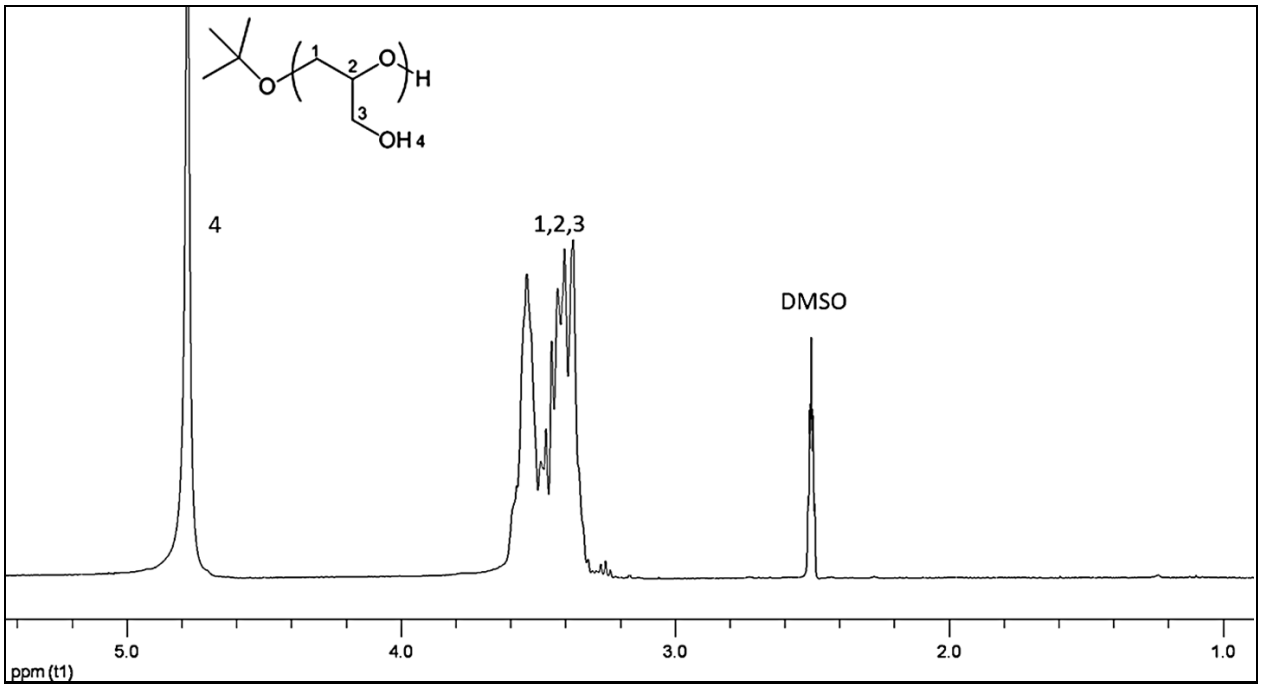

Figure 3.2: ^{1}H NMR spectrum of poly(glycidol)

3.3.2 Synthesis of Thiolated Polymers

sP(EO-*stat*-PO) is a six arm star shaped polymer with the average molecular weight of 12000g/mol. The backbone is a statistical copolymer of ethylene oxide and propylene oxide in the ratio 80 to 20 and the arms of the stars are terminated by –OH groups. The propylene oxide content prevents the crystallization of the ethylene oxide segment.

For the preparation of thiol functionalized polymers via Steglish esterfication branched prepolymers **sP(EO-*stat*-PO)** and linear **PG** were used. The thiol functionalized, hydrophilic polymers have been prepared in a two step synthesis. In the first step the –OH functionalized polymers, either **sP(EO-stat-PO)** or **PG**, have been crosslinked with disulfide crosslinker 3,3'-dithiopropionic acid (DTPA) followed by the reduction of disulfide bonds with tris(2-carboxyethy) phosphine (TCEP) to thiol groups in the second step. A general procedure for obtaining thiomers by this approach is presented in **Scheme 3.9**.

Step 1: Crosslinking of –OH functional polymers with DTPA

The crosslinking applied in this procedure is due to esterification reaction. Steglich esterification was used rather than Fisher esterification as it is a mild reaction which

allows the conversion of sterically demanding and acid labile substrates. The mechanism of Steglich esterifiction is as follows:

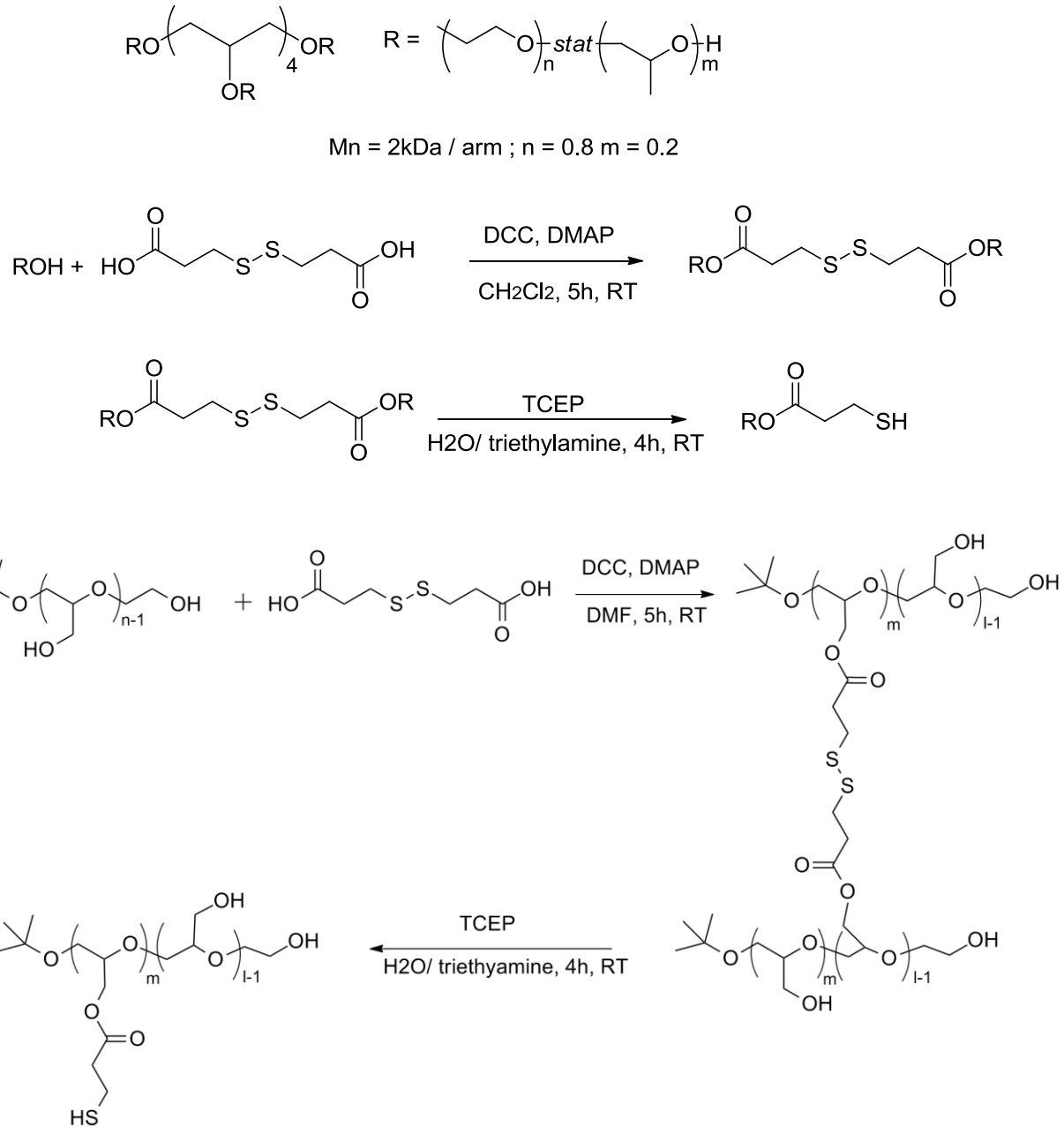

Scheme 3.9: Schematic representation of the –SH functionalised polymer synthesis.

DCC (dicyclohexylcarbodiimide) and the carboxylic acid are able to form an *O*-acylisourea intermediate, which offers reactivity similar to the corresponding carboxylic acid anhydride **(Scheme 3.10)**.

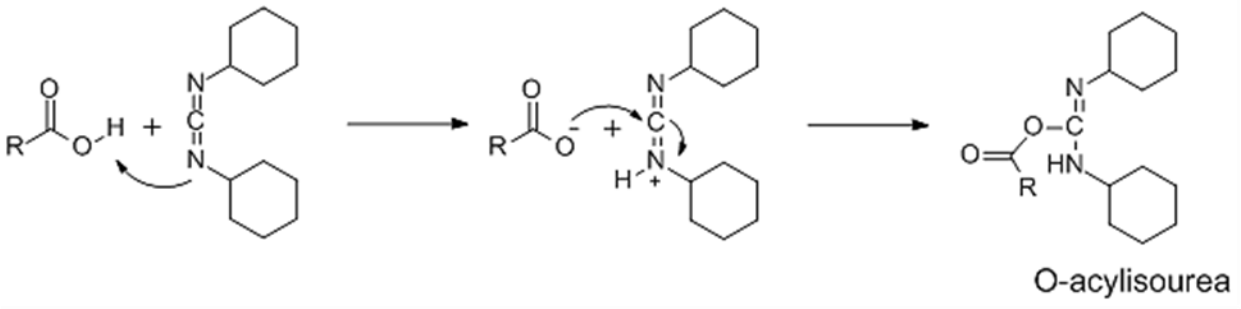

Scheme 3.10: Schematic representation of formation of O-acylisourea intermediate

The alcohol is then added to the activated carboxylic acid to form the stable dicyclohexylurea (DHU) and the ester **(Scheme 3.11).**

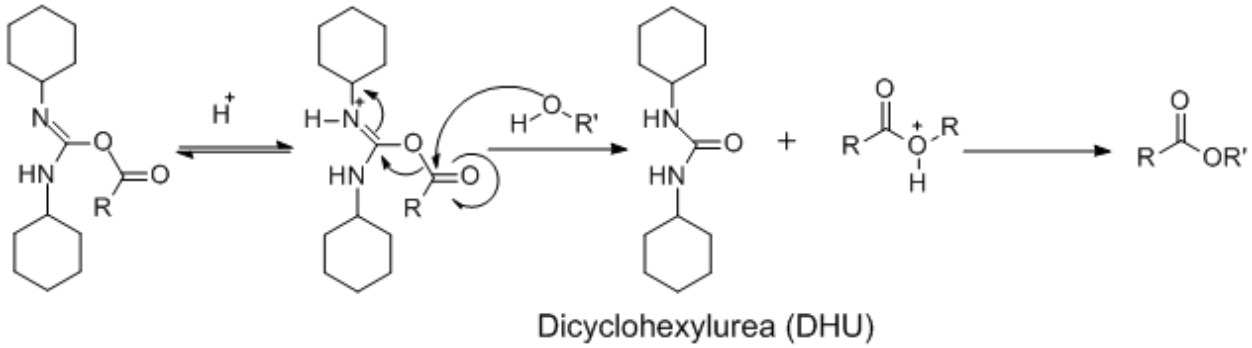

Scheme 3.11: Schematic representation of formation of stable dicyclohexylurea (DHU).

But the *O*-acylurea formed can undergo slow acyl migration to form *N*-acyl urea as a side product. In order to avoid this side reaction 4-*N,N'*-dimethylaminopyridine (DMAP) was used. DMAP, as a stronger nucleophile than the alcohol, reacts with the *O*-acylisourea leading to a reactive amide ("active ester"). This intermediate cannot form intermolecular side products but reacts rapidly with alcohols. Thus DMAP acts as an acyl transfer reagent in this way, and subsequent reaction with the alcohol gives the ester **(Scheme 3.12 and Scheme 3.13).**

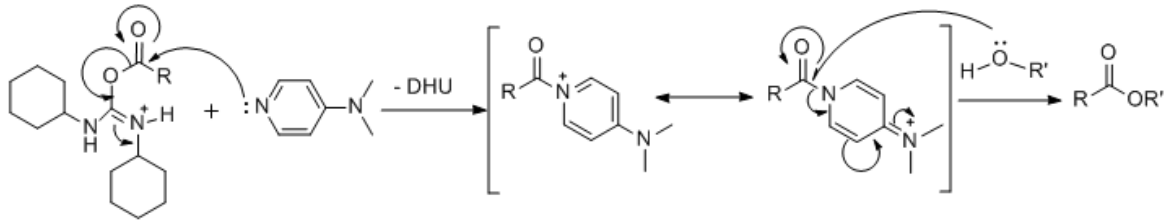

Scheme 3.12: Schematic representation of use of DMAP as an acyl transfer reagent.

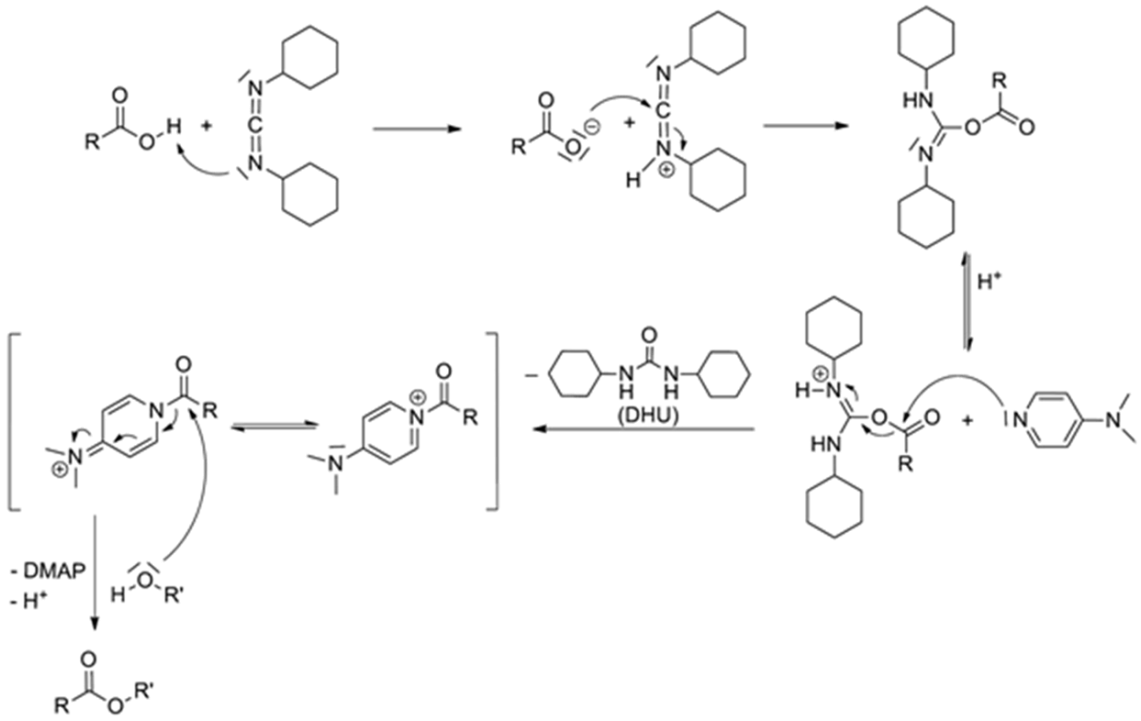

Scheme 3.13: Modified reaction scheme using DMAP as a catalyst for Steglish Esterification.

Step 2: Reduction of disulfide bonds

The water-soluble phosphine TCEP is widely employed as a reductant of disulfide bonds in a variety of peptide, protein, and cellular systems. Model studies show that reduction of disulfides by phosphines is initiated by rate-limiting formation of a thiophosphonium salt. Subsequent, rapid hydrolysis releases the second thiol fragment and the phosphine oxide **(Scheme 3.14).**

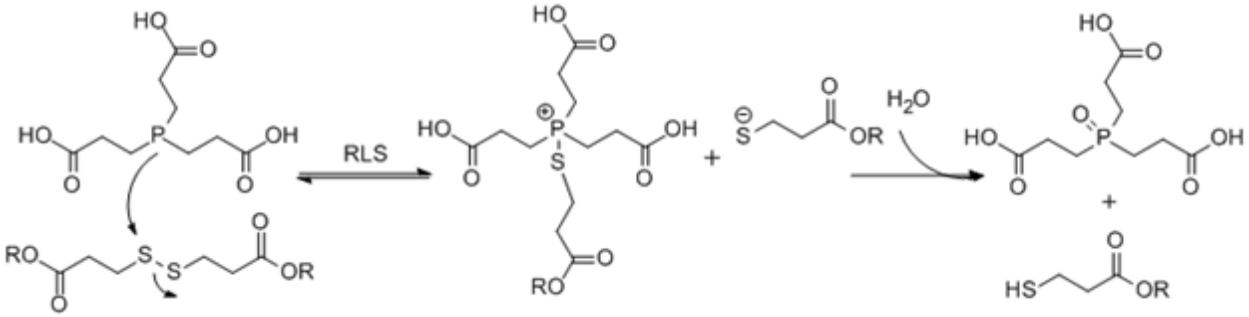

Scheme 3.14: Reduction of disulfide bonds with TCEP.

3.3.3 Characterization of Polymers

Both FT-IR and Raman spectroscopy are suitable tools to analyze structural and chemical properties of substances possessing sulfhydryl groups. The Raman S-H stretching band occurs in an interval of the vibrational spectrum (2500-2600 cm^{-1}) which is devoid of interference from any other fundamental mode of vibration of the macromolecule. Spectral interferences from water molecules and from possible overlap of bands are thus less problematic in Raman than in FT-IR spectroscopy.[25] Raman spectroscopy allows also a direct means of observing the disulfide group since the S-S stretching frequency normally appears as a sharp line near 500 cm^{-l}.

In this study both FT-IR and Raman spectroscopy have been used for the qualitative proof of the –SH bond formation in **sP(EO-*stat*-PO)** and **PG** polymers. FT-IR spectral analysis of the **HS-PG** clearly indicates the presence of the strong thiol bands at 2559 cm^{-1} and 917 cm^{-1}. In the **HS-sP(EO-*stat*-PO)** system however, it was not possible to detect the –SH characteristic band due to the overlap with the band in the 2560 cm^{-1} region. In contrast, in the Raman spectroscopy the S-H stretching mode can be clearly observed at 2578 cm^{-1} and at 2574 cm^{-1} for both **HS-sP(EO-*stat*-PO)** and **HS-PG**, respectively **(Figure 3.3)**. This is a clear indication for the thiol group presence.

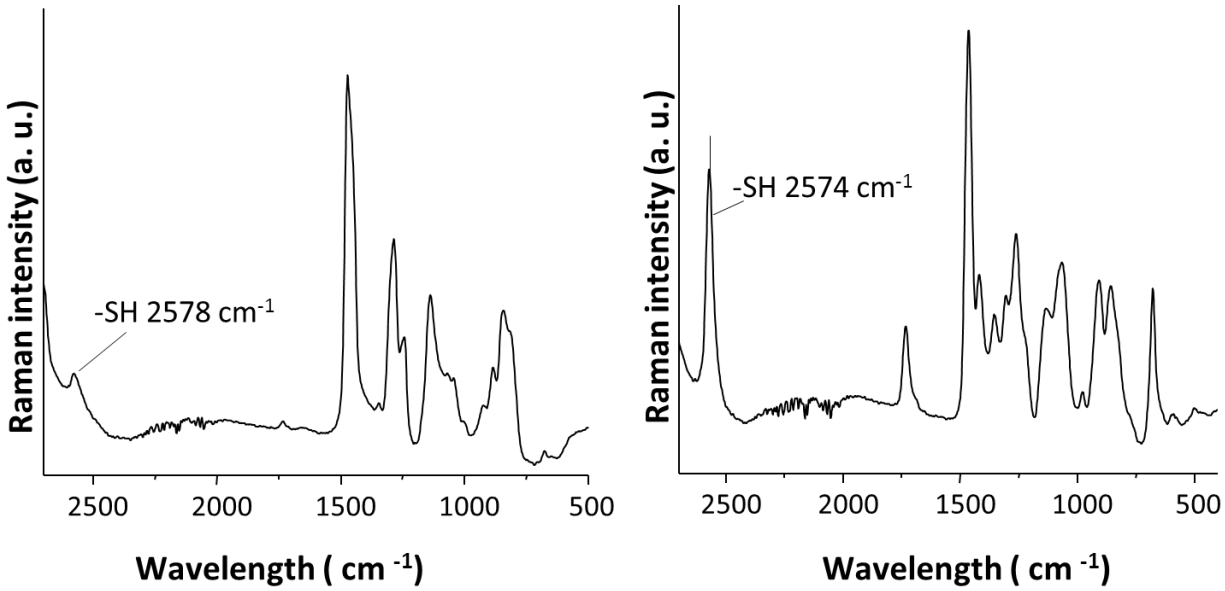

Figure 3.3: Raman spectra of **HS-sP(EO-*stat*-PO)** (left) and **HS-PG** (right) indicating the thiol signal ~ 2575 cm^{-1} and confirming the successful thiolation of the prepolymers.

In this work quantitative estimation of free thiol groups in **HS-sP(EO-*stat*-PO)** and **HS-PG** was determined from ^{1}H-NMR. Exact number of repeating units of the propylene oxide and ethylene oxide units in **HS-sP(EO-*stat*-PO)** was calculated according to Gasteier.[26] On calculation repeating propylene oxide units were found to be 36. Thus the number of proton from methyl group of propylene oxide comes to be 108 which were taken as reference at 1.21ppm. After thiol functionalization via Steglish esterification and subsequent reduction, the 4H (H-1/-2) proton shows a multiplet at 2.78 ppm. Integration of these protons comes out to be 12.11 and on division by 4 gives a value of 3.02, which indicates that out of 6 arm, 3 arm of the **sP(EO-*stat*-PO)** is thiol functionalised **(Figure 3.4)**.

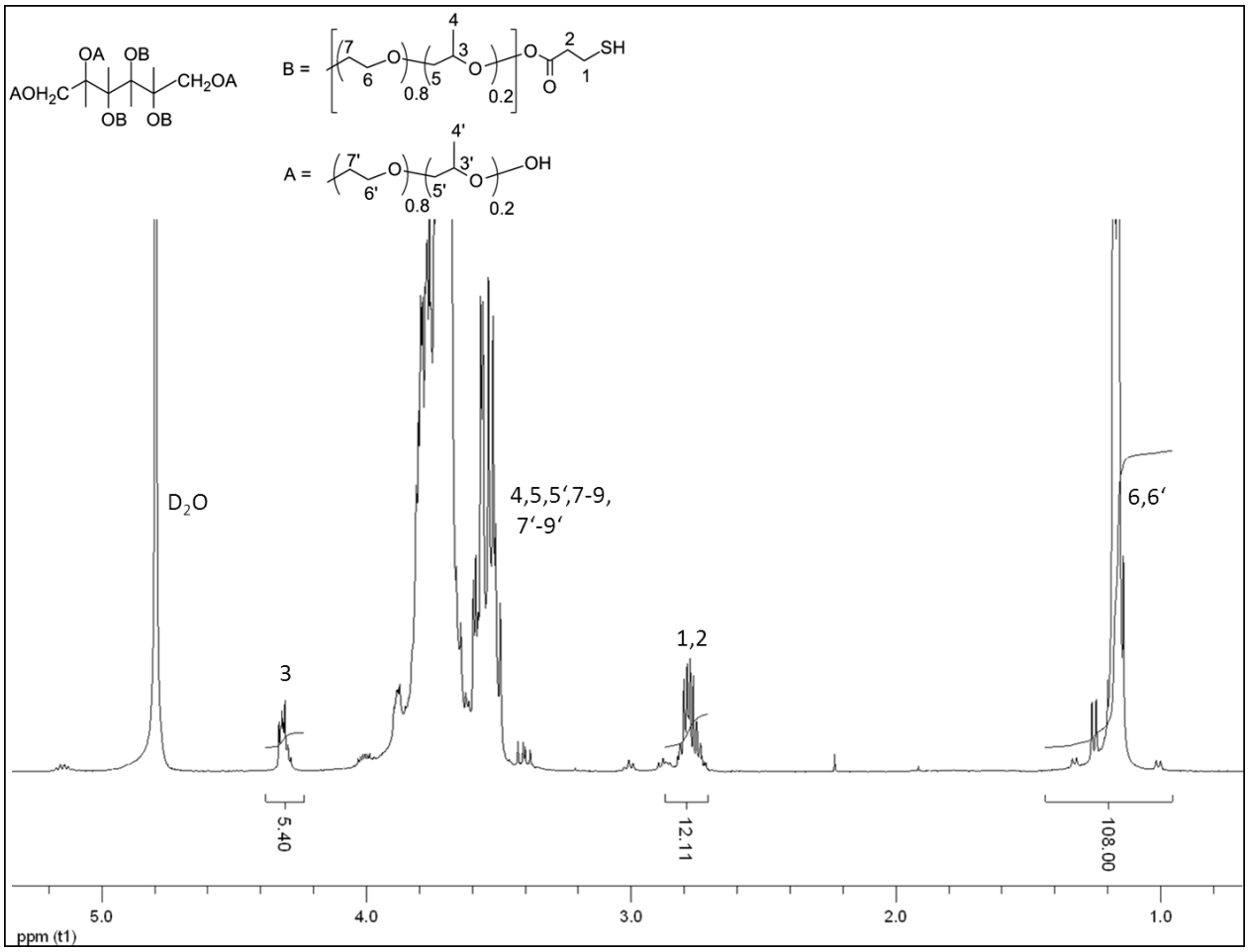

Figure 3.4: ^{1}H-NMR spectrum of thiol functionalized **sP(EO-*stat*-PO)**

The amount of free thiols as measured for **HS-sP(EO-*stat*-PO)** from several different synthesis was between 2.6 and 3.1 and did not change significantly from batch to batch.

For the determination of the thiol functionalization in **PG** comparison of backbone signal (H-2/-3/-7/-8/-9) with signals of the one methylene group (H-4) of thiol functionalised unit was done **(Figure 3.5)**. Signals at δ = 4.4 - 4.1 ppm belong to H-4. Signals at δ = 3.9 -3.4 ppm belong to H-2/-3/-7/-8/-9. The degree of functionalization was calculated from the ratio of these integrals. Setting the integral of the signals at δ = 4.4-4.1 ppm to 2, the integral of the signals at δ= 3.9-3.4 ppm acquire a value *x* specific for the degree of functionalization.

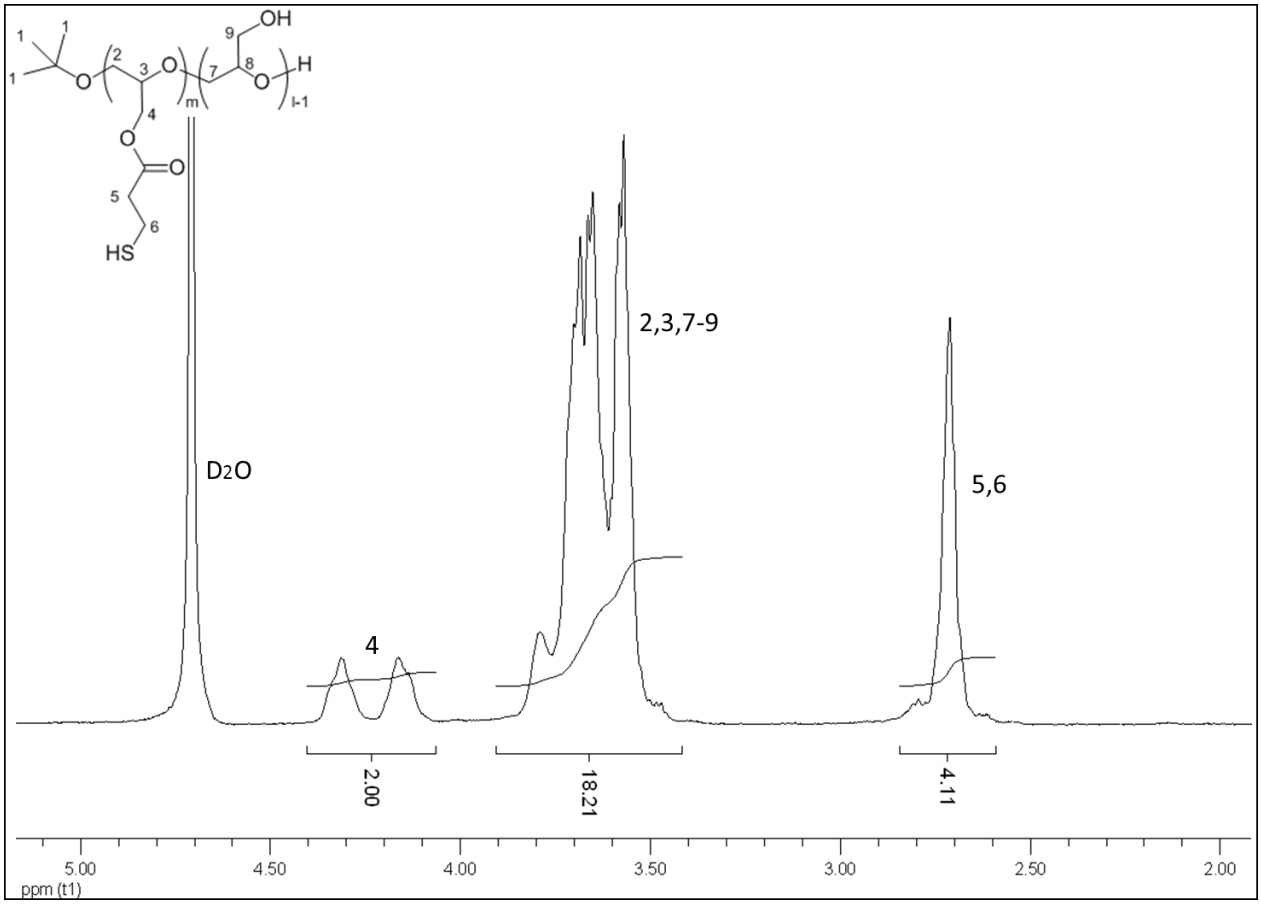

Figure 3.5: ^{1}H-NMR spectrum of thiol functionalized **PG**

If three protons, which belong to the thiopropionate repeating unit backbone, are subtracted from *x*, the integral value equals five protons belonging to the glycidol repeating units. From these values, the degree of functionalisation (DOF) can be calculated according to **Equation 3.3**.

$$DOF = 1/1+ ((x\text{-}3) /5) \times 100 \qquad \text{Eq.3.3}$$

In case of **Figure 2.5** DOF = 1/1+ ((18.21-3) /5) ×100, which comes out to be 24.74% and corresponds to 15 thiol group in **HS-PG**

3.3.4 Hydrogel Synthesis

The hydrogels were prepared from **HS-sP(EO-*stat*-PO)** as well as from **HS-PG** either by oxidation or Michael addition respectively. Regardless, the preparation procedure all gels were transparent and highly elastic.

One of the most characteristic reactions of the thiol groups is their oxidation to disulfide bonds **(Scheme 3.15)**. This reaction can be induced either by oxygen or by a variety of other chemical agents.

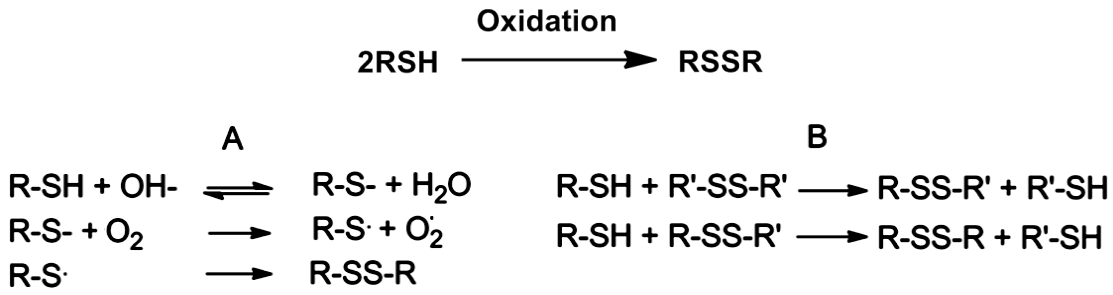

Scheme 3.15: Crosslinking mechanism of –SH groups to disulphide by oxidation.

Disulfide bonding is generally assumed to proceed through the deprotonated form of thiols. An effective reaction and a quick gelation can be obtained only at high values of pH. Oxidation of pendant thiol groups (R-SH) to disulfides (R-SS-R) can be achieved either by oxygen/oxidising catalyst (**Scheme 3.15, A**) or by a thiol-disulfide exchange reaction between the thiol (R-SH) and low-molecular weight disulfides (R'-SS-R', **Scheme 3.15, B**). The rate of air oxidation of the thiol group R-SH is determined by a one electron transfer from R-S- to oxygen. This reaction rate increases with increasing pH, because the concentration of ionized thiol groups increases in an alkaline environment.[27] During the oxidative gelation the formation of both intra- and inter-molecular disulfide bonds can be formed. Due to a higher degree of freedom of the molecule the intra-molecular reaction is likely to be thermo-dynamically favored. This is especially valid for the **HS-sP(EO-*stat*-PO)** system where due to the steric reasons the formation of inter- disulfide bonds is slightly improbable. However, from the relatively high fraction of thiol groups in linear **HS-PG** one can expect the formation of inter-molecular bonds in this polymer. But the oxidation in air normally takes several hours which in many cases is too slow in order to maintain stable miniemulsion for the production of nanogels described in the **Chapter 4**. Therefore in this work hydrogen peroxide is used

as an oxidizing agent. H_2O_2 is water soluble and after gelation, any excess of it can be removed easily by dialysis.

Gelation of **HS-sP(EO-*stat*-PO)** as well as **HS-PG** was initiated by addition of 3×10^{-3} mmol H_2O_2 at pH 7.4 on a 40% (w/v) polymer solution. The bulk gelation time of 5 and 3 min for **HS-sP(EO-*stat*-PO)** and **HS-PG** respectively at pH=7.4 was recorded. The crosslinking of the **HS-sP(EO-*stat*-PO)** and **HS-PG** was also performed with low molecular weight PEG-diacrylate through a Michael type addition reaction at pH = 7.4 **(Scheme 3.16).**

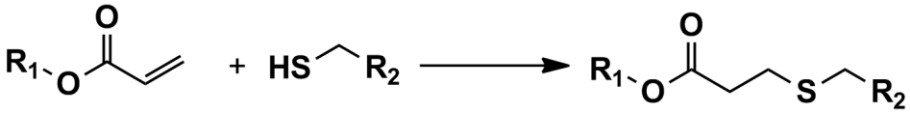

Scheme 3.16: Michael type addition reaction between acrylate and thiol group

Thiol to acrylate was taken in the ratio of 1:1 and it was observed that the gelation occurred within seconds.

Raman spectroscopy has been employed in order to prove the formation of disulfide bonds in the case of crosslinked hydrogels by oxidation as well as presence of –C-S- bond in the case of the hydrogels crosslinked both by oxidation and Michael addition.

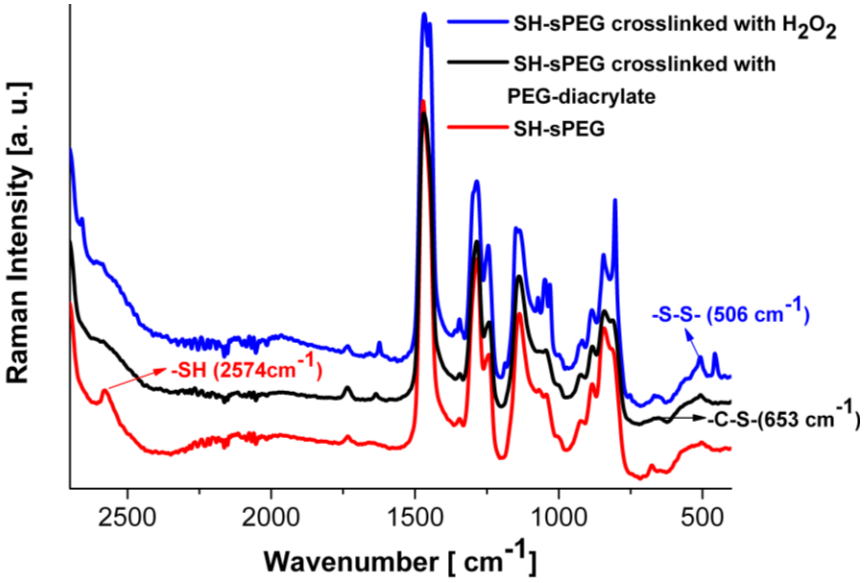

Figure 3.6: Raman spectrum showing characteristic peaks of **HS-sP(EO-*stat*-PO)** hydrogels crosslinked with H_2O_2 and PEG diacrylate.

From **Figure 3.6** and **3.7** presenting the Raman spectra of the hydrogels synthesized from **HS-sP(EO-*stat*-PO)** and **HS-PG** respectively one can clearly seen that the -SH band present in the polymers precursors strongly weakens upon crosslinking. In the case of hydrogels synthesized by oxidation two bands characteristic of -S-S- vibrations appear at 495 and 504-510 cm^{-1}. In addition, for all hydrogels the stretching vibrations of the C-S bonds is present at 671 and 652 cm^{-1} frequency.

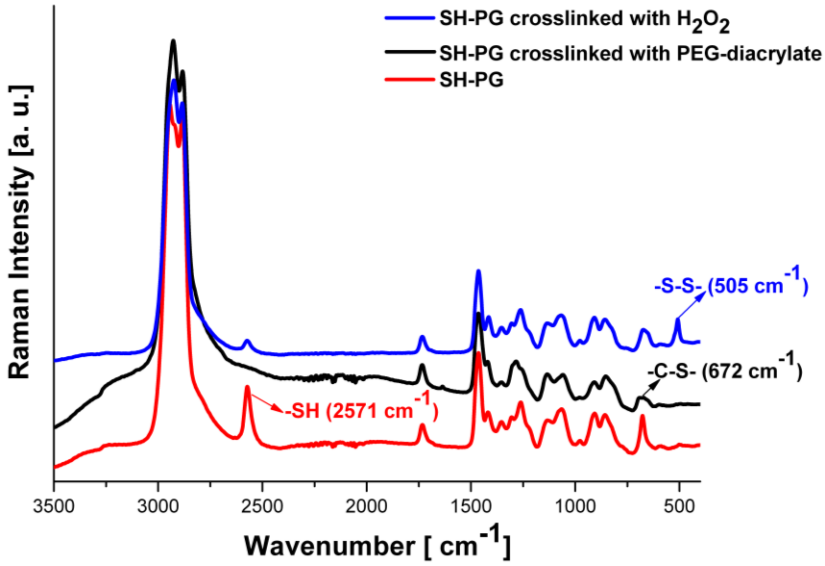

Figure 3.7: Raman spectrum showing characteristic peaks of **HS-PG** hydrogels crosslinked with H_2O_2 and PEG diacrylate

This confirms the presence of thioether linkages in the hydrogel synthesized by oxidation and especially in the gels synthesized by the Michael addition reaction between the thiol groups with the diacrylate.

3.3.5 HS-sP(EO-*stat*-PO) based Hydrogel for Chemokines Delivery.

3.3.5.1 Functional Analysis of Chemokines in HS-sP(EO-*stat*-PO) Hydrogels

Different biodegradable synthetic hydrogels were recently described to ensure the immobilization of the chemokines at the desired location as well as a continuous release over a predefined period.[28,29]

In this work selection of hydrogels for loading two different typed of chemokines was based on their degradation kinetics. A rapid degradable hydrogel assures a faster short release and action of a chemokine Met-CCL5 which blocks neutrophil infiltration in the first hours of MI. A second slower degradable hydrogel serves to ensure a long

release and action of another chemokine CXCL12 (S4V) to recruit hematopoietic stem cells over several weeks. It is well known that CXCL12 plays a very important role in driving chemotaxis of stem cells and progenitor cells to the infarcted myocardium and promotes neovascularization and tissue regeneration.[30,31] Due to the fast degradation of CXCL12 itself mutant CXCL12 resistant to matrix metalloproteinase-2 (MMP-2) and Dipeptidyl peptidase IV (DPPIV/CD26) cleavage was formulated in a synthetic, biodegradable hydrogel for a controlled long term release.

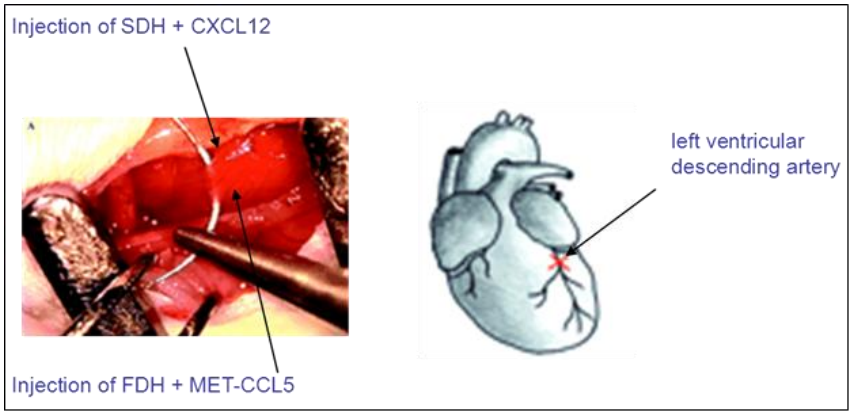

Figure 3.8: Showing the location of administration, for the two hydrogels in the heart.

The administration of this mixture of chemokine derivatives and synthetic biodegradable hydrogels manipulated the inflammatory reaction after MI and sustained the endogenous reparatory mechanisms. Therefore, this study describes a promising therapeutic strategy, which is a viable alternative to orthologous cell-based therapies, with important clinical significance.

In order to control the local release of the protease-resistant CXCL12 and Met-CCL5, two different hydrogels were utilized. **HS-sP(EO-*stat*-PO)** was chosen as precursors for both type of hydrogels, which were crosslinked in two ways, either by disulphide crosslinking or by thioether crosslinking resulting in fast degradable hydrogels or slow degradable hydrogels (FDH or SDH) respectively.

Fast degradable hydrogels are termed so due to fast reduction of disulphide bond in cytosolic environment while the slow degradable hydrogels degrade comparatively slowly due to slow hydrolysis of ester bonds.[32]

The FDH is used for the formulation with Met-CCL5 for a quick release to inhibit neutrophil infiltration within the first hour after MI. This fast release of Met-CCL5 from FDH was confirmed by incubation in PBS and 5mM glutathione, a tripeptide responsible for reduction of disulphide bonds in cytosol,[33] which led to complete

degradation of the gel after 24 h **(Figure 3.9A)**.The SDH was conceived for the formulation with the protease-resistant CXCL12 (S4V) for a gradual release in order to recruit hematopoietic stem cells from the circulating blood during a time period of 4 weeks after MI. To confirm the release rate, the CXCL12 (S4V)-SDH was incubated for 33 days in PBS for detection of local release over time. After 33 days the SDH was entirely degraded due to the hydrolytic cleavage of ester bonds in the backbone and release of chemokine was no longer detected (Figure 3.9B).

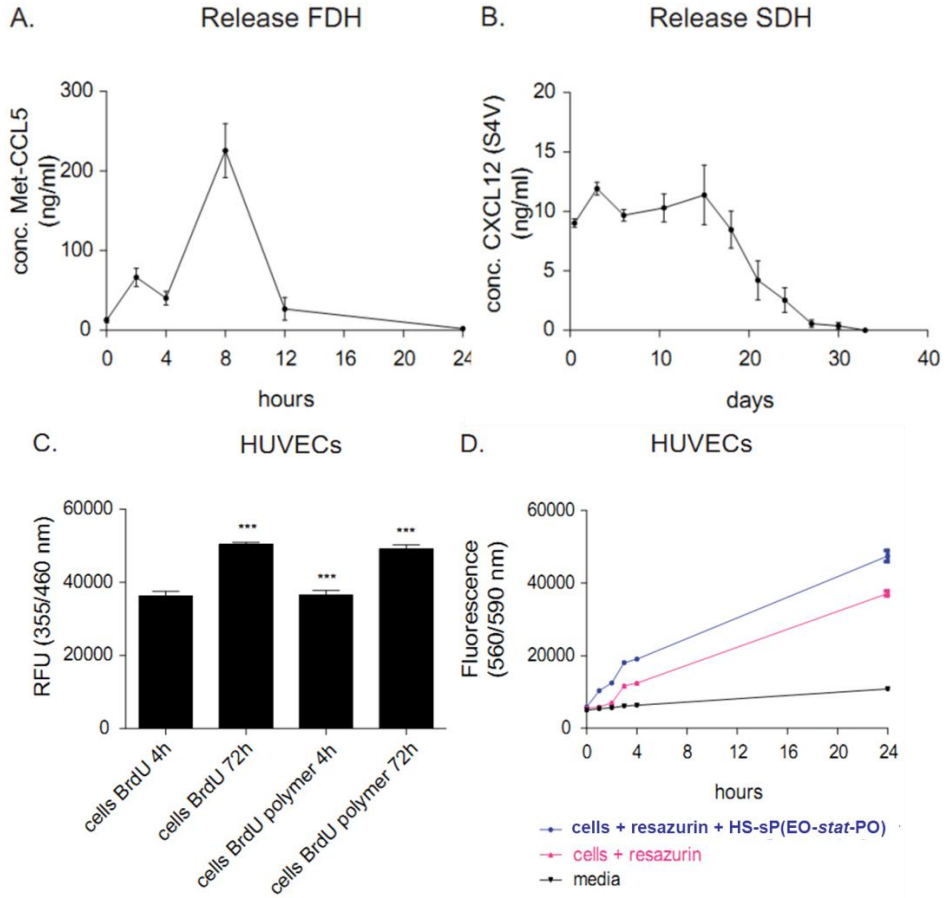

Figure 3.9: A. Release assay of the Met-CCL5 chemokine from the FDH over 24 hours. **B**. Release assay of the CXCL12 (S4V) chemokine from the SDH over 33 days. **C.** Proliferation assay of hydrogel-treated HUVECs compared with untreated cells. **D.** Cell viability assay of -treated HUVECs compared with untreated cells.

While proliferation and viability of HUVECs were not affected by culturing in the presence of the HS-sP(EO-*stat*-PO) (Figure 3.9C, D) proving it to be biocompatible.

Due to the fast degradation, CXCL12 quickly disappears after very short action. Therefore in this study, a mutant CXCL12, resistant to MMP-2 and DPPIV/CD26

cleavage was formulated in a synthetic, biodegradable hydrogel for a controlled long term release.

3.3.5.2 Improvement of Cardiac Function after MI in Mice by Combined Treatment with the Protease-Resistant CXCL12 and Met-CCL5

To investigate a possible beneficial role of a blocked short term neutrophil influx after cardiac ischemia combined with a longer term recruitment of hematopoietic cells, the chemokine-loaded hydrogels were applied in an experimental model of MI. In this strategy effect of combining the Met-CCL5 and protease-resistant CXCL12 was seen, for the simultaneous activation of two important mechanisms for preservation of heart function: inhibition of neutrophil infiltration and enhanced neovascularization by increasing recruitment of hematopoietic stem cells is shown. Met-CCL5 antagonizes CCR1 and CCR5 activation and function in response to its natural ligand CCL5, and is able to reduce inflammation in models of induced inflammatory and autoimmune diseases, but also after MI.[34]

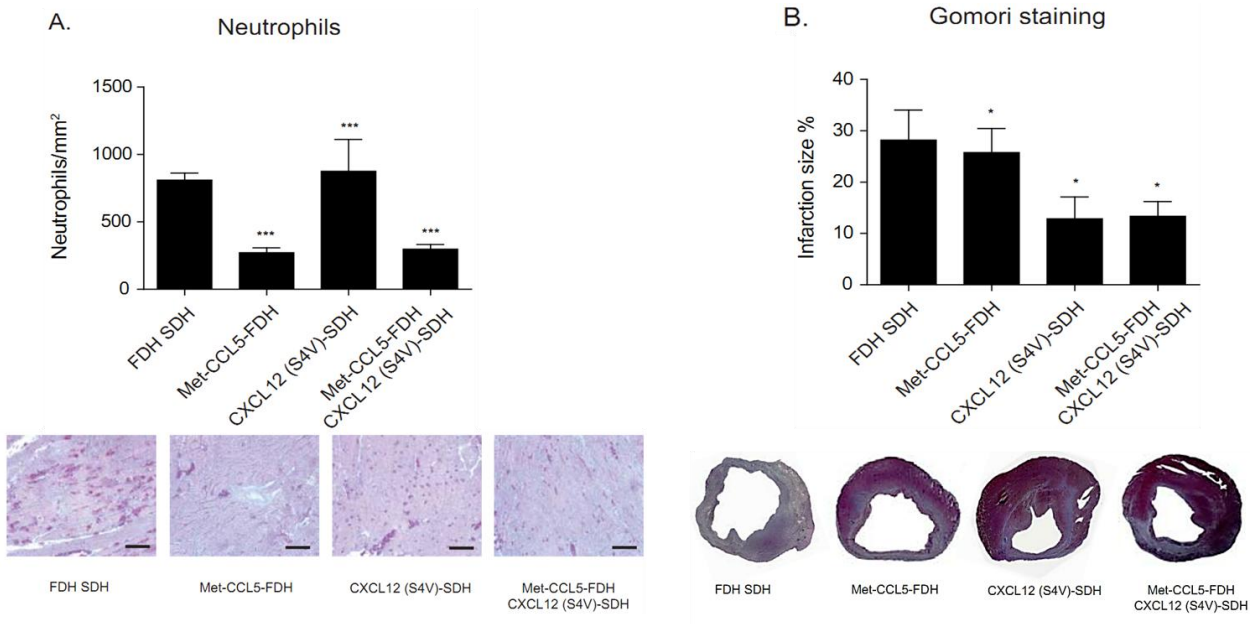

Figure 3.10: A. Neutrophil infiltration in the myocardium were reduced in Met-CCL5-FDH and in Met-CCL5-FDH+CXCL12 (S4V)-FDH, compared with FDH, SDH and CXCL12 (S4V)-FDH treated mice 1 day after MI. **B.** Compared with FDH SDH and Met-CCL5-FDH treated mice, the CXCL12 (S4V)-SDH and the combination Met-CCL5-FDH CXCL12 (S4V)-SDH displayed a significantly smaller infarct size after 4 weeks.

At day 1, infiltration of MI-induced neutrophils in the infarcted area was effectively reduced in both the Met-CCL5-FDH and the Met-CCL5-FDH+CXCL12 (S4V)-SDH

groups, but not in the control group that received only hydrogel or in only CXCL12 (S4V)-SDH group **(Figure 3.10, A)**. This confirmed the specificity of the administration of the CCR1 and CCR5 antagonist Met-CCL5 for the prevention of neutrophil recruitment. After 4 weeks, the infarcted area was reduced by 50% in the CXCL12 (S4V)-SDH and in the combined Met-CCL5-FDH+CXCL12 (S4V)-SDH group, compared to the groups that received hydrogel only and Met-CCL5-FDH **(Figure 3.10, B)**.

Since the infiltration of neutrophils occurs only for a short time period.[35] Met-CCL5 was combined with a very quickly biodegradable hydrogel, which assures the release of this antagonist only for several hours is essential to avoid the blocking of later functions of Met-CCL5 e.g. over CCR5, such as recruitment of reparatory monocytes or T regulatory cells,[36] which is necessary for a proper healing and scar formation.

3.3.5.3 Combined Treatment with the Protease-Resistant CXCL12 and Met-CCL5 after MI in Mice

Similarly, neovascularization after MI was also improved in both the CXCL12 (S4V)-SDH and Met-CCL5-FDH + CXCL12 (S4V)-SDH groups to a higher extent as the Met-CCL5-FDH, as quantified by CD31-staining (**Figure 3.11, A**). This indicates a CXCL12 (S4V)-mediated increase of angiogenesis in infarcted myocardium, supporting the hypothesis. Interestingly, these findings also suggest that recruitment of hematopoietic cells through CXCR4 would serve to reduce infarct size rather than the blockade of initial neutrophil infiltration. However, evaluation of the functional parameters of the heart revealed a significant improvement of cardiac function in the Met-CCL5-FDH + CXCL12 (S4V)-SDH group that received a combined treatment (**Figure 3.11, B**). The ejection fraction was increased in the group with Met-CCL5-FDH and CXCL12 (S4V)-SDH in comparison to the control group, but the combined treatment with Met-CCL5-FDH + CXCL12 (S4V)-SDH show the highest preservation of the heart function comparing to all other groups (**Figure 3.11, B**).

Remarkably, the combined treatment with Met-CCL5-FDH + CXCL12 (S4V)-SDH was also able to improve cardiac output compared with the hydrogel only and single chemokine-treated groups (**Figure 3.11, C**). Thus by the combined treatment with both recombinant chemokines formulated in a time-dependent degradable hydrogel, the heart function was significantly preserved and remodeling of the ventricle was improved.

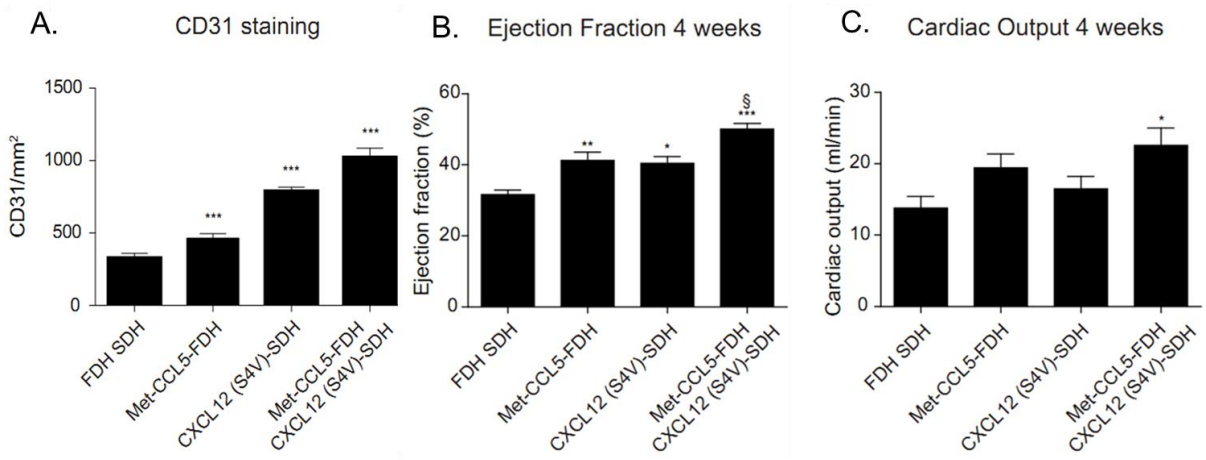

Figure 3.10: A. The neovascularization of CXCL12 (S4V)-SDH and the combination Met-CCL5-FDH CXCL12 (S4V)-SDH treated mice was higher compared with FDH, SDH and Met-CCL5-FDH treated mice, 4 weeks after MI. **B.** Ejection fraction (EF) was increased by the combined treatment with Met-CCL5-FDH+CXCL12 (S4V)-SDH compared with Met-CCL5-FDH, CXCL12 (S4V)-SDH and control, 4 weeks after MI. **C.** Cardiac output (CO) was increased by the combined treatment with Met-CCL5-FDH CXCL12 (S4V)-SDH compared with Met-CCL5-FDH and CXCL12 (S4V)-SDH and control, 4 weeks after MI.

3.4 Conclusion

Synthesis of linear **PG** via anionic polymerization as well as functionalization of **sP(EO-*stat*-PO)** and **PG** with thiol groups was acheived. In order to introduce thiol functionality, both polymers were crosslinked in the first step with the disulfide crosslinker, 3,3'-dithiopropionic acid. Subsequently, the disulfide bonds in the resulting hydrogel were reduced by tris(2-carboxyethyl) phosphine (TCEP). In this way thiol functional **HS-sP(EO-*stat*-PO)** and **HS-PG** could be obtained The prepolymers formed hydrogels by either oxidative or Micheal addition type crosslinking.

Further **HS-sP(EO-*stat*-PO)** prepolymer was used successfully for the synthesis of hydrogel for chemokine delivery. This study shows evidence that the combined therapy of the protease-resistant CXCL12-SDH and Met-CCL5-FDH in a time dependent manner preserves cardiac function, promotes angiogenesis and facilitates wound healing processes by recruitment of hematopoietic stem cells from the circulating blood and attenuating neutrophil-induced myocardial inflammation. This therapeutic strategy constitutes a promising and accessible option to optimize cardiac repair and remodeling

after myocardial injury, with significant clinical implications, offering a feasible and viable alternative to cell-based therapies.

3.5 References

[1] N. G. Frangogiannis, M. L. Entman, *Trends Cardiovascular Medicine* **2005**, 15, 163.

[2] G. Ren, O. Dewald, N. G. Frangogiannis, *Inflamm. Allergy* **2003**, 2, 242.

[3] D. Orlic, J. Kajstura, S. Chimenti, D. M. Bodine, A. Leri, P. Anversa, *Annals New York Acad. Sci.* **2001**, 938, 221.

[4] K. A. Jackson, S. M. Majka, H. Wang, J. Pocius, C. J. Hartley, M. W. Majesky, M. L. Entman, L. H. Michael, K. K. Hirschi, M. A. Goodell, *J. Clinical Investigation* **2001**, 107, 1395.

[5] A. Kawamoto, H. C. Gwon, H. Iwaguro, J. I. Yamaguchi, S. Uchida, H. Masuda, M. Silver, H. Ma, M. Kearney, J. M. Isner, T. Asahara, *Circulation* **2001**, 103, 634.

[6] B. E. Strauer, M. Brehm, T. Zeus, M. Kostering, A. Hernandez, R. V. Sorg, G. Kogler, P. Wernet, *Circulation* **2002**, 106, 1913.

[7] M. B. Britten, N. D. Abolmaali, B. Assmus, R. Lehmann, J. Honold, J. Schmitt, T. J. Vogl, H. Martin, V. Schachinger, S. Dimmeler, A. M. Zeiher, *Circulation* **2003**, 108, 2212.

[8] K. C. Wollert, G. P. Meyer, J. Lotz, S. Ringes-Lichtenberg, P. Lippolt, C. Breidenbach, S. Fichtner, T. Korte, B. Hornig, D. Messinger, L. Arseniev, B. Hertenstein, A. Ganser, H. Drexler, *Lancet.* **2004**, 364, 141.

[9] K. Lunde, S. Solheim, S. Aakhus, H. Arnesen, M. Abdelnoor, K. Forfang, *Scandinavian Cardiovascular J.* **2005**, 39, 150.

[10] A. Schuh, E. A. Liehn, A. Sasse, R. Schneider, S. Neuss, C. Weber, M. Kelm, M. W. Merx, *Basic Res. Cardiology* **2009**, 104, 403.

[11] E. A.Liehn, O. Postea, A. Curaj, N. Marx, *J. Am. College Cardiology* **2011**, 58, 2357.

[12] V. Braunersreuther, C. Pellieux, G. Pelli, F. Burger, S. Steffens, C. Montessuit, C. Weber, A. Proudfoot, F. Mach, C. Arnaud, *J. Mol. Cell. Cardiology* **2010**, 48, 789.

[13] E. A. Liehn, M. W. Merx, O. Postea, S. Becher, Y. Djalali-Talab, E. Shagdarsuren, M. Kelm, A. Zernecke, C. Weber, *J. Cell. Mol. Med.* **2008**, 12, 496.

[14] S. Baldus, T. Heitzer, J. P. Eiserich, D. Lau, H. Mollnau, M. Ortak, S. Petri, B. Goldmann, H. J. Duchstein, J. Berger, U. Helmchen, B. A. Freeman, T. Meinertz, T. Munzel, *Free Radical Bio. Medicine* **2004**, 37, 902.

[15] K. C. Koch, W. M. Schaefer, E. A. Liehn, C. Rammos, D. Mueller, J. Schroeder, T. Dimassi, T. Stopinski, C. Weber, *Basic Res. Cardiology* **2006**, 101, 69.

[16] A. Schuh, E. A. Liehn, A. Sasse, M. Hristov, R. Sobota, M. Kelm, M. W. Merx, C. Weber. *Basic Res. Cardiology* **2008**, 103, 69.

[17] A. Schuh, S. Breuer, R. Al Dashti, N. Sulemanjee, P. Hanrath, C. Weber, B. F. Uretsky, E. R. Schwarz, *J. Cardiovascular Pharmacol. Therapeutics* **2005**, 10, 55.

[18] V. F. Segers, T. Tokunou, L. J. Higgins, C. MacGillivray, J. Gannon, R. T. Lee, *Circulation* **2007**, 116, 1683.

[19] A. Fitton, J. Hill, D. Jane, R. Miller, *Synthesis* **1987**, 1140.

[20] A. Dworak, I. Panchev, B. Trzebicka, W. Wałach, *Macromol. Symp*. **2000**, 153, 233.

[21] E. A. Liehn, M. W. Merx, O. Postea, S. Becher, T. Y. Djalali, E. Shagdarsuren, M. Kelm, A. Zernecke,C. Weber, *J. Cell. Mol. Med.* **2008**, 12, 496.

[22] E. A Liehn, N. Tuchscheerer, I. Kanzler, M. Drechsler, L. Fraemohs, A. Schuh, R. R. Koenen, S. Zander, O. Soehnlein, M. Hristov,G. Grigorescu, A. O. Urs, M. Leabu, I. Bucur, M. W. Merx, A. Zernecke, J. Ehling, F. Gremse, T. Lammers, F. Kiessling, J. Bernhagen, A. Schober, C. Weber, *J. Cell. Mol. Med.* **2011**, 58, 2415.

[23] D. Taton, A. Le Borgne, M. Sepulchre, N. Spassky, *Macromol. Chem. Phys*. **1994**, 195, 139.

[24] W. Walach, B. Trzebicka, J. Justynska, A. Dworak, *Polymer* **2004**, 45, 1755.

[25] R.Tuma, S. Vohnik, H. Li, J. G. Thomas, *J. Biophysical Journal* **1993**, *65,* 1066.

[26] ((Highly functional star shaped prepolymers for ultrathin layer formation)) Peter Gasteier, PhD thesis, RWTH University ((Aachen)), October, **2009**.

[27] M. P. Lütolf, N. Tirelli, S. Cerritelli, L. Cavalli, J. A. Hubbell, *Bioconj. Chem*. **2001**, 12, 1051.

[28] L. Yu, J. Ding, *Chem. Soc. Rev.* **2008**, 37, 1473.

[29] D. Grafahrend, K. H. Heffels, M. V. Beer, P. Gasteier, M. Moeller, G. Boehm, P. D. Dalton, J. Groll, *Nature Mat.* **2011**,10,67.

[30] V. F.Segers, T. Tokunou, L. J. Higgins, C. MacGillivray, J. Gannon, R. T. Lee, *Circulation* **2007**, 116, 1683.

[31] A. T. Askari, S. Unzek, Z. B. Popovic, C. K. Goldman, F. Forudi, M. Kiedrowski, A. Rovner, S. G. Ellis, J. D. Thomas, P. E. DiCorleto, E. J. Topol, M. S. Penn, *Lancet.* **2003**, 362, 697.

[32] R. J. Linhardt, Biodegradable Polymers in Controlled Release of Drugs, M. Rosoff (Ed.), VCH Publishers Inc. New York, **1988**.

[33] F. Meng, W. E. Hennink, Z. Zhong, *Biomaterials* **2009**, 30, 2180.

[34] V. Braunersreuther, C. Pellieux, G. Pelli, F. Burger, S. Steffens, C. Montessuit, C. Weber, A. Proudfoot, F. Mach, C. Arnaud, *J. Molecular Cellular Cardiology* **2010**, 48, 789.

[35] L. Yu, J. Ding, *Chem. Society Rev*. **2008**, 37, 1473.

[36] E. A. Liehn, O. Postea, A. Curaj, N. Marx, *J. Am. College Cardiology* **2011**, 8, 2357.

[37] M. Dobaczewski, Y. Xia, M. Bujak, C. Gonzalez-Quesada, N. G. Frangogiannis, *Am. J. Patol.* **2010***,* 176, 2177.

CHAPTER 4

Biocompatable and Degradable Nanogels via Oxidation and Addition Reactions of Synthetic Thiomers in Inverse Miniemulsion

Part of the work dealing with hemocompatibility studies of nanogel was performed in the work group of Prof. Christian Grandfils CEIB, University of Liège, Allee de la Chimie, 3, B6c, B-4000 Liege, Belgium.

Part of this work is published in Journal of Polymer Science Part A: Polymer Chemistry 2009, 47, 5543.

4.1 Introduction

Hydrogel nanoparticles, so called nanogels, are hydrophilic cross-linked polymeric particles with sub-micrometer size. They combine characteristics of hydrogels like biocompatibility, high water content, as well as tunable chemical and mechanical properties with the features of nanoparticles such as high surface area and overall sizes in the range of cellular compartments. These properties make them intriguing candidates for entrapment of hydrophilic bioactive molecules such as DNA or proteins to provide a hydrophilic, protective environment and thus prevent degradation.[1,2] So far, little attention has been paid to the size-dependence on the cellular uptake and pharmacokinetics. A prerequisite for this is however, synthetic access to well defined particles.

Several techniques have been used for the preparation of nanogels such as precipitation polymerization, photolithography, micromolding, microfluidics and inverse emulsion techniques.[3] Polymerization in inverse miniemulsion is one way that allows preparation of gel particles with controlled size in the submicron range. Yet, syntheses of nanogels in inverse emulsions are mostly done by radical polymerization[4-7] and only little work has been reported on cross-linking of well defined prepolymers.[8,9] Such a prepolymer condensation concept based on hydrophilic, multi-thiolfunctionalized oligomers and polymers will be particularly suitable for incorporating peptides and proteins in particles that are stable in extracellular physiological conditions but degrade

after uptake by cells within the reductive environment of the cytosol where, for example, glutathione, a tripeptide with a free thiol group, readily cleaves disulfides to thiols.[10] In contrast to radical polymerisation techniques, oxidative coupling of thio-functional macromers in inverse miniemulsion allows the attachment of cystein-terminated peptide sequences as the free thiol groups do not interfere with the polymerization. As a best example so far, high molecular weight, thiol-functionalized hyaluronic acid has been cross-linked in inverse miniemulsion by oxidation.[11] However, variation of functionality or molecular architecture of the gel precursor could not be achieved.

In this chapter synthesis and characterization of biocompatible and degradable nanogel carriers composed of thiol-functionalized polymers based on **sP(EO-*stat*-PO)** and **PG** is presented. Nanogel particles are prepared by cross-linking the polymers in inverse miniemulsion via oxidation of thiol groups to disulfide bonds. Synthesis and characterization of the gel-precursors, preparation of the nanogels and their characterization regarding particle size distribution in solution and in the dried state, chemical composition, degradation behaviour as well as in vitro biocompatibility and hemocompatibility studies are presented and discussed.

4.2 Experimental

4.2.1 Materials and Methods

For preparation of nanogels thiol-functionalized **sP(EO-*stat*-PO)** and **PG** were synthesized as described in **Chapter 3.** n-hexane (HPLC) (Sigma), THF (p.A.) (VWR), Span 80 (Sorbitan monooleate) (Sigma), Tween 80 (polyoxyethylene (20) sorbitan monooleate) (KMF), Hydrogen peroxide 30% (p.a.,VWR), PEG diacrylate (M_n=700 g/mol Sigma), Glutathione (99%, Aldrich) were used as received. Phosphate buffered saline (PBS) from Sigma has been dissolved in water to 0.04 M concentration (pH=7.4). Dialysis membrane (MWCO = 3500 Dalton), has been purchased from Spectrum Laboratories, Inc. Demineralised water was used throughout the work.

Scanning Force Microscopy (SFM) studies were conducted using a Nanoscope IIIa from Digital Instruments operating in the tapping mode. Standard silicon cantilevers were used (PPP-NCH from Nanosensors) with a spring constant $k \approx 42$ N/m and an oscillation frequency $f_o \approx 70$ kHz. For the SFM measurements samples were cast onto

freshly cleaved mica by spin coating at the rotation speed of 2000 rpm. The samples were dried in vacuum for 2 h prior to measurements.

Scanning electron microscopy (SEM*)* was performed with a HITACHI S- 4800 instrument in a cryo mode with secondary electron image resolution of 1.0 nm at 15 kV, 2.0 nm at 1 kV and 1.4 nm at 1 kV with beam. The material is fixed on a holder and was rapidly frozen with boiling liquid nitrogen. It was then transferred to the high vacuum cryo-unit, the Balzers BF type freeze etching chamber. The cryo-chamber equipped with a knife can be handled from outside by means of a level to fracture the sample for applications in which imaging of the surface of inner structures is aimed. In order to remove humidity the sample is sublimated from 5 to 15 min then the entire material is further inserted into the observation chamber.

Dynamic Light Scattering (DLS). The particle sizes were measured by photo correlation spectroscopy using a Malvern Zetasizer Nano ZS at a fixed scattering angle of 173°. Non-invasive back scatter (NIBS) technology takes particle sizing to sensitivity in the 0.6 nm to 6 μm range. Disposable poly(styrene) cuvettes were used for measurement in water. 'Expert System' software was used for data interpretation. The presented data is the average value from five measurements. The DLS measurements give a *z*-average size (or cumulant mean) value, which is an intensity mean and the polydispersity index (PDI). The cumulant analysis has the following form:

$$ln(g^{(1)}(t)) = -\bar{\Gamma}t + \mu_2 t^2 + ...$$

where $g^{(1)}$ is the first order correlation function; $\bar{\Gamma}$ is the average decay rate and first cumulant; μ_2 is the second cumulant. The value of $\mu_2/\bar{\Gamma}^2$ is known as polydispersity index (PDI).

4.2.2 Preparation of Nanogels in Inverse Miniemulsion

For preparation of the miniemulsion, 5 mL of n-hexane containing 150 mg of a 3:1 weight ratio of Span 80 and Tween 80 were used as organic phase, while the aqueous phase consisted of 220 mg polymer dissolved in 0.5 mL 0.04 M PBS buffer (pH = 7.4). The two phases were combined and pre-emulsified by magnetic stirring for 10 min followed by miniemulsification by ultrasonication for 60 s with a Branson sonifier (W450

Digital at duty cycle of 30% and output control of 90%). During the sonication, the reaction vessel was cooled with an ice-bath. Subsequently, 20 μL of 0.1 M H_2O_2 was added and the mixture was sonicated again for 60 s. The reaction was allowed to proceed for 15 min at room temperature followed by quenching of the oxidation by addition of 4 mL of acidic water (pH = 3). For synthesis of nanogels cross-linked via Micheal addition similar procedure as stated above was followed with addition of PEG diacrylate 129 mg (for **HS-PG** nanogels) or 13.0 mg (for **HS-sP(EO-*stat*-PO)** nanogels**)**. Separation of the nanogels was achieved by centrifugation at 10000 rpm for 30 min followed by decantation of the supernatant. Nanogels present in the aqueous layer were carefully washed twice with hexane (10 mL) and four times with THF (20 mL) in order to remove the surfactants and unreacted polymer. The remaining organic solvents and acid were removed by dialysis. Purified nanogels were stored in millipore water at 4 °C for further use.

4.2.3 Degradation of Nanogels

Reductive degradation of the nanogels to the corresponding thiol-containing **sP(EO-*stat*-PO)** and **PG** fragments was conducted in the presence of 10 mM glutathione in PBS buffer (pH=7.4) at 37 °C (mass ratio glutathione/nanogel = 0.4). After 6 h, the solution was dialysed, freeze-dried followed by analysis with Raman-spectroscopy. A part of the solid was dissolved in water, spin casted onto mica and the resulting polymer film was analysed by SFM.

4.2.4 Cytotoxicity of Nanogels

Standard indirect cytotoxicity tests were carried out based on the recommendation of the International Standardization Organization (ISO) described in DIN EN ISO 10993-5. For cytotoxicity testing L929 mouse connective tissue fibroblasts were purchased from DSMZ GmbH (Germany). L929 cells were seeded on tissue culture polystyrene (TCPS) and were maintained in RPMI supplemented with L-glutamine, 10 % fetal calf serum and 1% penicillin-streptomycin (PAA, Germany) at 37°C and humidified atmosphere containing 5% CO_2. All experiments were conducted on subconfluent cell layers. To detect cytotoxic effects, the cells were incubated with 0.5 mg/mL concentration of the nanogel particles. The LIVE/DEAD® Viability/Cytotoxicity Assay Kit from Molecular Probes (MoBiTec GmbH, Germany) was applied 24 and 72 h after addition of the nanogel particles to the cultivated L929 fibroblasts. This test provides a two-color

fluorescence cell viability assay that is based on the simultaneous determination of live (green colored) and dead (red colored) cells with two probes that measure recognized parameters of cell viability – intracellular esterase activity and plasma membrane integrity.

4.2.5 Hemocompatibility Tests were performed according to 1SO 10993-4 adopting the general conditions of interaction of nanoparticles with blood). The tests are summarised below.

The hemocompatibility of the nanogels has been assessed analysing the following standard parameters

1. Microscopic pictures of the whole blood after material exposure (smear)
2. Haemolysis test according to ASTM (Standard practice for assessment of haemolytic properties of materials, American Society for Testing and Materials Designation: ASTM: F 756-00).
3. Platelets and Red blood cell counting.
4. Analysis of the activation of the coagulation cascade either by the intrinsic (TCA test) or the extrinsic (Quick) pathways.
5. Complement activation by determination of the C3a concentration (ELISA kit).

4.2.5.1 Blood Sample Collection

Human blood was obtained from The Red Cross Transfusion at Central Hospital of the University of Liège. Blood was collected from healthy donors in 4.5 mL tubes containing 3.2% sodium citrate (anticoagulant). Experiments were performed within 2 hours after collection. This study received the approval of the Ethical Committee of the Medical Faculty of Liège.

4.2.5.2 Sample Preparation

Briefly, in micro Eppendorf tubes (200 μL) one volume of nanogel solution (10 mg/mL) was diluted in nine volumes of whole blood. In all the experiments a rapid homogenization of the nanoparticle suspension with the whole blood was performed in order to avoid any high local concentration of NP's. Samples were incubated for 15 minutes at 37°C under horizontal roller mixing (35 rpm). For all the tests, pyrogen free water which was used to disperse the nanogel was also measured as a control.

4.2.5.3 Realization of Blood Smears for Control of RBC's morphology

Just after blood incubation, 5 μL of the blood / NP mixtures were withdrawn and spread immediately on microscopy glass slide. Blood cells were observed with Olympus Provis microscope at 50x magnification in transmission mode. At least two representative pictures were taken per sample.

4.2.5.4 Hemolysis test

Hemolysis test was adapted from Standard Practice for Assessment of Hemolytic Properties of Materials (ASTM designation: F 756-00).[12] NP and blood were prepared and incubated as described above. After incubation samples were centrifuged for 5 minutes at 600 g at room temperature (RT). Supernatants were collected and mixed with cyanmethemoglobin reagent. Hemoglobin released was measured at 540 nm in a microplate reader (Anthos HT III, type 12600). A calibration curve was established with bovine hemoglobin standard over a range of hemoglobin concentrations from 0.025 μg/mL to 3700 μg/mL. Saponine (0.8 mg/mL) and PBS were used as positive and negative control respectively. Total hemoglobin released from whole blood diluted in cyanmethemoglobin reagent was determined as 100% hemoglobin release. Hemolysis was expressed as the percentage of hemoglobin released (% rHb) to total content. Tests were done in triplicate.

4.2.5.5 Counting of Platelets and Red blood cells (Emerald)

Red blood cells (RBC) and platelets count was determined with a Coulter Multisizer IIS after blood dilution in Isoton II. For RBC's analysis the whole blood was diluted (20x) in isotonic medium. Platelets were analysed starting from a platelet rich fraction obtained by centrifugation blood samples diluted (24x) in isotonic solution performed at 850*g* for 90s at RT. 1 mL aliquots of the supernatants were added to 40 mL isotonic solution. Counting was performed on a Coulter Multisizer II equipped with an orifice tube of 70 μm. RBC's were counted between 3.7 and 8 μm and platelets between 1.0 and 3.7 μm. Samples incubated with PBS (pH 7.4) were used as negative control. Tests were done in duplicate.

4.2.5.6 Evaluation of Blood Coagulation: Intrinsic and Extrinsic pathways

TCA assays and Quick test were performed on a Dade Behring instrument (Behring Coagulation Timer, or **BCT**) with commercial reagents (a C.K. PREST kit (Roche Diagnostic) for TCA and Tromborel S (Dade Behring/Siemens for Quick test).

Whole blood and NP suspensions were mixed and incubated as described above. Samples were centrifuged during 5 minutes at 2000 g (RT). After supernatant collection prothrombin time (PT) and activated partial thromboplastin time (APTT) were measured directly with a Behring Coagulation Timer analyzer (BCT) (Dade Behring). Kaolin (0.5 mg/mL final blood concentration) was used as a positive control in TCA and PBS as negative control. Measurements were conducted in duplicate.

4.2.5.7 Complement Activation

After incubation of NP with blood, EDTA (1 mM final) was added in order to stop any complement activation. Zymozan (final blood concentration: 2 mg/mL) was used as positive control, and PBS, as negative control. Non-incubated blood was added as additional negative control. Samples were centrifuged for 5 minutes at 2000 g at RT. Supernatants were stored at –80°C until the analysis. Complement activation was estimated adopting the Human C3a ELISA kit for quantification of Human C3a-desArg (Beckton Dickinson). Absorbance was measured at 450 nm with a microplate reader (Anthos HT III, type 12600). Concentration of C3a was expressed in ng/mL and as percentage of activation. Measurements were conducted in duplicate.

4.3 Results and Discussion

Linear poly(glycidol) (M_n = 4500 g/mol, **PG**) and six arm, star shaped polymers with copolymerized ethylene oxide and propylene oxide in the ratio 4 to 1 (M_n = 12000 g/mol, **sP(EO-*stat*-PO)**) were chosen as precursors for the nanogels. Both polymers are hydrophilic and biocompatible, and the molecular weights are well below 30000 g/mol, which are set as limit that allows renal clearance for linear PEO.[13]

It is known that inverse emulsions are generally less stable than regular oil-in-water emulsions due to lack of electrostatic stabilization.[8] Based upon numerous experiments with different surfactants and co-surfactants which could form stable emulsions, FDA approved Span 80 and mixture of Span 80 and Tween 80 surfactants were selected for the particle synthesis since they showed most efficient stabilization of the miniemulsion

droplets with the given experimental setup and procedure. Besides checking for different surfactants, optimization of bulk cross-linking kinetics of **HS-sP(EO-*stat*-PO)** and **HS-PG** with H_2O_2 and PEG-diacrylate was also done. **Scheme 4.1** schematically shows the synthesis of nanogels via inverse miniemulsion.

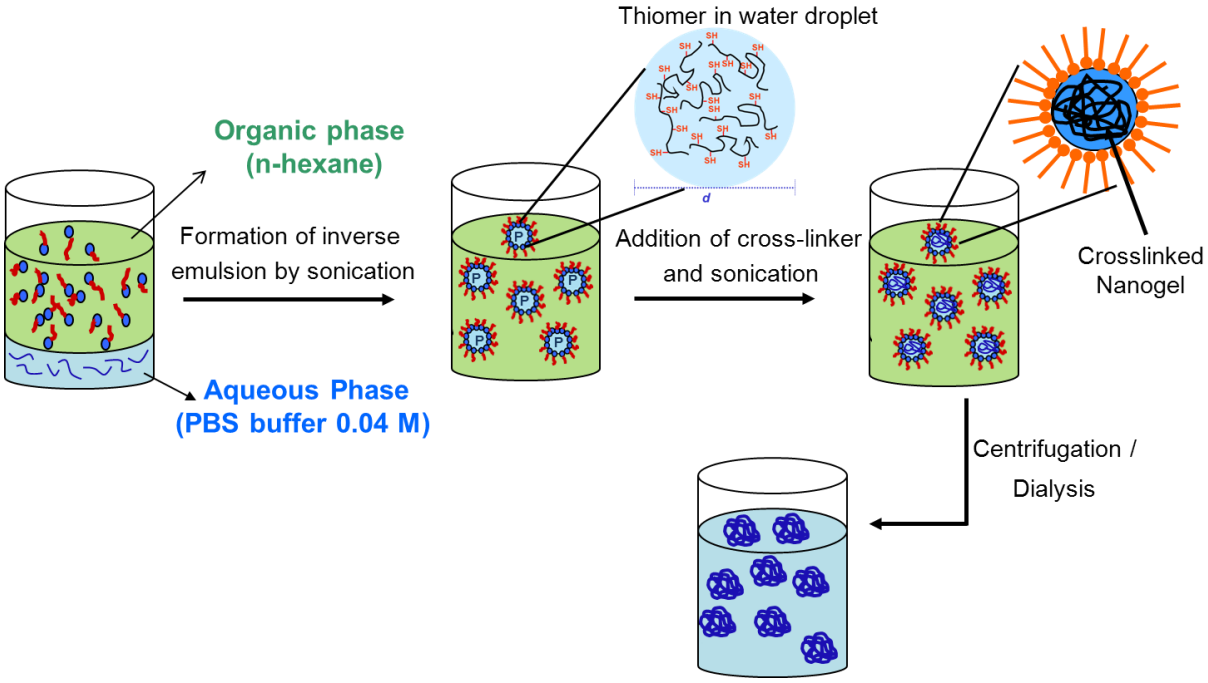

Scheme 4.1: Schematic representation of cross linking in inverse miniemulsion

Nanogels were obtained both by using only Span 80 and a mixture of Span 80 and Tween 80 (3:1 ratio) as surfactants. However, the SFM and DLS analysis revealed that when only Span 80 was used as a surfactant poorly defined particles with high polydispersed were obtained **(Figure 4.1 left)**. In contrast, when the mixture of Span 80/Tween 80 was used as surfactant well-defined, and relatively monodisperse particles were formed **(Figure 4.1 right)**. This can be explained as for maximum stability, the interfacial film resulting from the absorbed surfactant should be condensed, with strong lateral intermolecular forces and should exhibit high film elasticity. Since highly purified surfactants generally produce interfacial films that are not closed packed and hence not mechanically strong, good emulsifying agents are usually a mixture of two or more surfactants rather than an individual surfactant.[14]

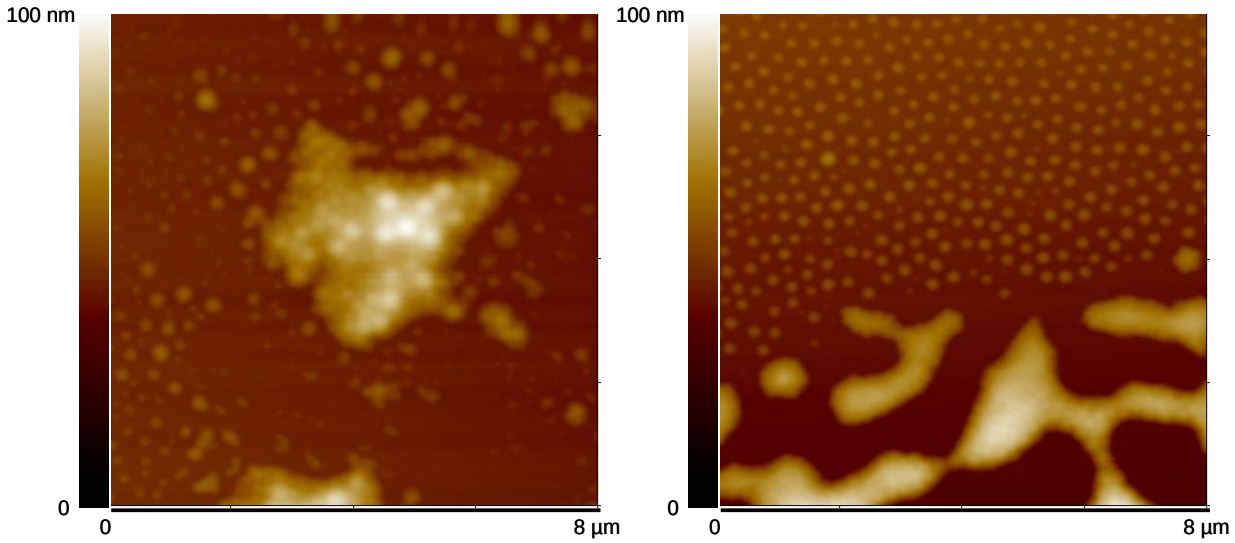

Figure 4.1: SFM topography images of nanogels prepared in the inverse miniemulsion with Span 80 only (left) and mixture of Span 80/Tween 80 (right).

For surface activity, all surfactants must have a hydrophobic and hydrophilic portion and the ratio of hydrophobic to the hydrophilic portion is what is called as its balance i.e. “HLB” which stands for HYDROPHILE/LIPOPHILE/BALANCE. It was invented for use with NONIONIC surfactants in particular. The hydrophilic portion is usually a polyhydric alcohol or ethylene oxide, while the lipophilic group is usually a fatty acid or a fatty alcohol in most cases. HLB of a surfactant is thus an indication of the solubility of the surfactant, the lower the HLB value, the more lipophilic or oil soluble the surfactant, the higher the HLB value the more water soluble or hydrophilic the surfactant is. The hydrophilic-lipophilic balance of a surfactant is thus a measure of the degree to which it is hydrophilic or lipophilic. Generally, HLB values can be used as rough guide for surfactant selection and to predict the surfactant properties of a molecule. For W/O emulsions, HLB values from 4 to 7 are best suited, while HLB values in the range of 8-16 are considered for O/W systems. Therefore the correct selection of surfactants and thus HLB is important so as to ensure colloidal stability of aqueous droplets and the resulting polymeric particles.[15] Moreover Poly(ethylene glycol) part of Tween 80 shows strong interaction with aqueous phase providing better interfacial tension and hence barrier to coalescence,[14] and hence co-surfactant systems containing Span 80 (sorbitan monooleate) with a low HLB (4.3) and Tween 80 (polyethyleneglycol-sorbitan monooleate) **(Scheme 4.2)** with a higher HLB (15) were

thus used to keep the HLB value in the range for W/O emulsion and optimize the emulsion stability.

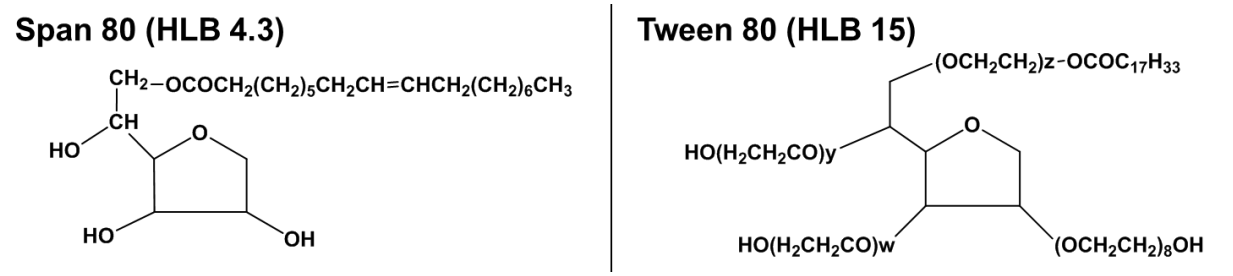

Scheme 4.2: Schematic representation of the surfactant Span 80 and Tween 80.

Using this surfactant system first, preparation of disulfide crosslinked particles from **HS-sP(EO-*stat*-PO)** polymers by oxidation in inverse miniemulsion is discussed. Generally, disulfide formation proceeds through the deprotonated form of thiol groups. Thus, in order to maintain slightly basic reaction conditions PBS buffer (pH=7.4) is used as a dispersed phase. Furthermore, the ionic strength of PBS serves as osmotic agent in the droplets to stabilize them against Ostwald ripening. Bulk experiments with **HS-sP(EO-*stat*-PO)** showed that simple oxygen mediated gelation takes more than six hours at physiological pH = 7.4, thus too long with respect to inverse miniemulsion stability. Upon addition of H_2O_2 as an oxidation promoter, the bulk cross-linking reaction could be shortened to 5 min. Therefore it can be concluded that presence of H_2O_2 is indispensable for the formation of disulfide cross-linked nanogels in the inverse miniemulsion. Cryo-scanning electron microscopy (cryo-FESEM) and dynamic light scattering (DLS) were applied to characterize the nanogel particle size in water, and thus in the swollen state, and scanning force microscopy (SFM) has been used as a characterization technique for dry particles. **Figure 4.2** shows the cryo-FESEM and DLS analysis of **HS-sP(EO-*stat*-PO)** nanogels. Particle size analysis with DLS gives the z-average particle diameter of 380 nm with a PDI of 0.24. Cryo-SEM images clearly show that the particles have a well-defined spherical shape, as expected for particles synthesized by miniemulsion techniques, with particle diameters d in the range of 230 nm < d < 350 nm. Taking into account the freezing-step that may lead to partial volume loss of the nanogels during cryo-FESEM, these two techniques correlate well with respect to size analysis of the nanogels in the hydrated state.

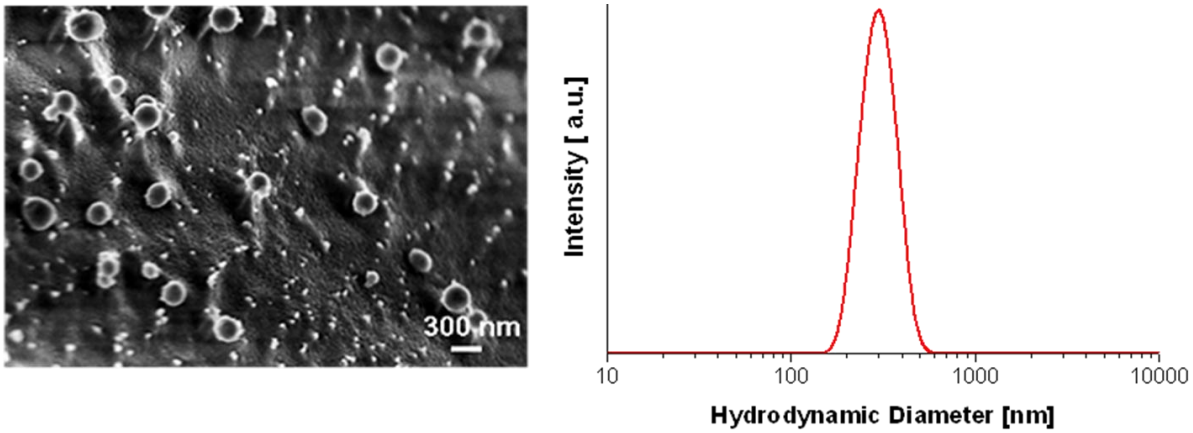

Figure 4.2: Characterization of **HS-sP(EO-*stat*-PO)** nanogels prepared by oxidative crosslinking in water (swollen state): by cryo-FESEM (left) and by DLS (right).

Size determination of such disulfide cross-linked **HS-sP(EO-*stat*-PO)** nanogels in the dry state has been achieved by scanning force microscopy. Samples were prepared by spin-coating from aqueous solution onto mica followed by drying in vacuum. By the spin-coating process a dense monolayer of single particles is formed initially. Upon drying, the nanogels decrease their volume and a regular pattern of separated, single nanogel particles results. From the SFM topography image showing isolated nanogels **(Figure 4.3)** an average diameter d_{av} = 110 ± 10 nm and an average height h_{av} = 28 ± 2 nm could be determined as adsorbed on mica. The large anisotropy demonstrates that on mica, the soft and deformable nanogels adopt a flattened, oblate spheroidal shape. This flattening can be contributed to a strong affinity of the hydrophilic particles towards the polar mica surface in air as well as to indentation by the SFM tip. Regardless of the reason for flattening, the volume (V) of the adsorbed particles can be calculated form the formula for spheroids: $V = 4/3\pi\ abh_{av}$ (where $a = b$ = average diameter (d_{av}) = 110 ± 10 nm; average height h_{av} = 28 ± 2 nm). With the equation for a perfect sphere $V = 4/3\pi R^3$, the radius R and thus, also the d_{av} of perfectly spherical nanogels in the dry state could be calculated to be d_{av} = 70 ± 5 nm. Hence, by comparing this value with the size in aqueous environment determined from cryo-FESEM and DLS, a strong swelling ability of the nanogels is obvious and the swelling ratio can be estimated in between 3.5 and 5 **(Figure 4.3)**.

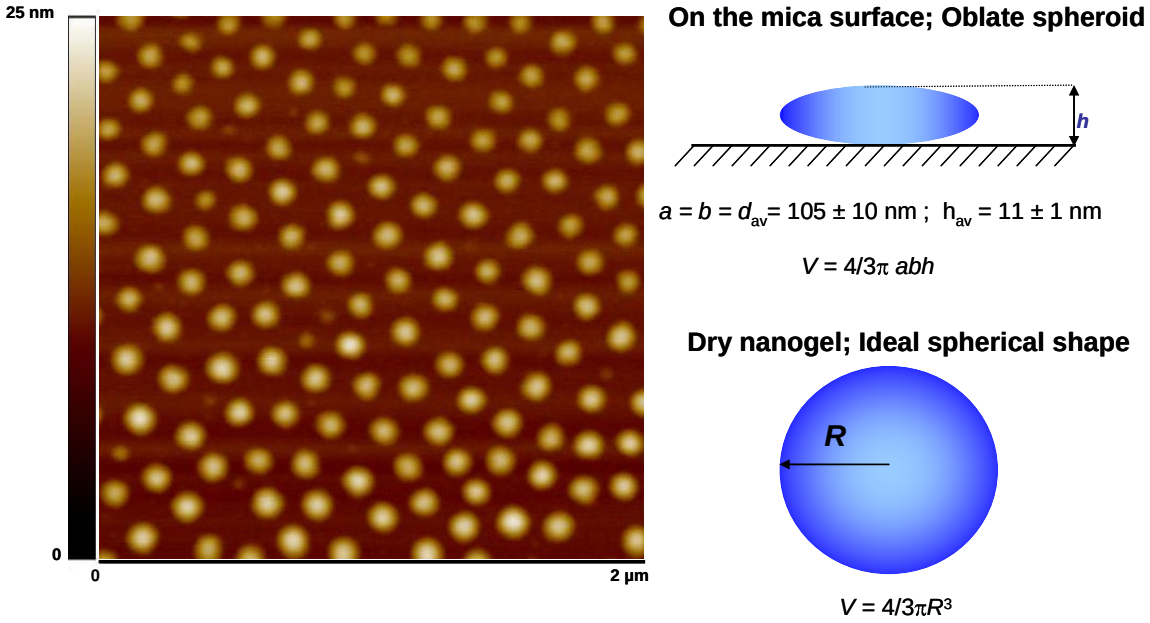

Figure 4.3*:* Left: SFM topography image of the **HS-sP(EO-*stat*-PO)** nanogels prepared by oxidation crosslinking. Scan size is 2 × 2 μm and z-range is 40 nm. Right: Schematical representation of the nanogel adsorbed on to mica surface and a nanogel adopting ideal spherical shape.

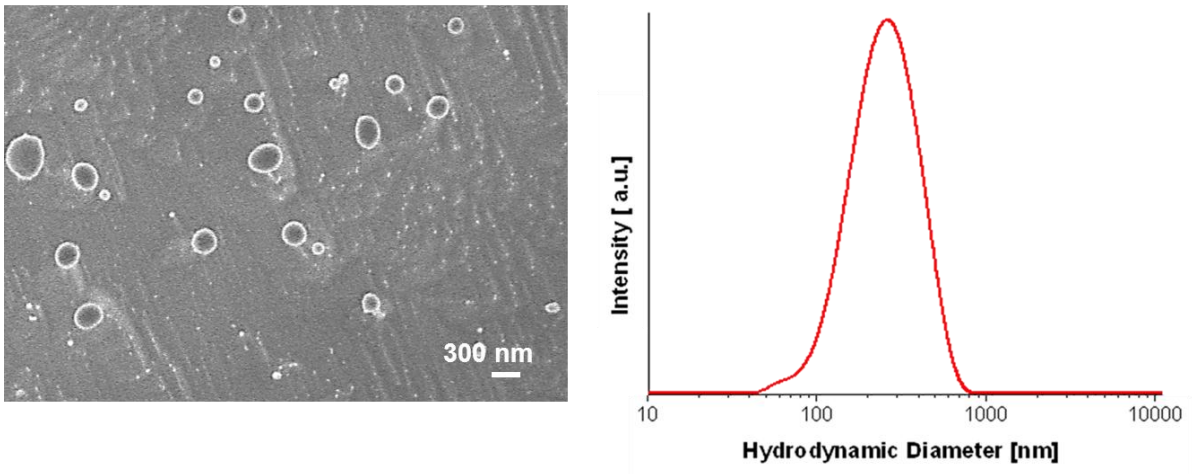

Figure 4.4: Characterization of **HS-sP(EO-*stat*-PO)** nanogels in water (swollen state) prepared via Michael addition reaction: by cryo-FESEM (left) and by DLS (right).

Figure 4.4 presents the cryo-SEM and DLS of the **HS-sP(EO-*stat*-PO)** nanogels prepared by the crosslinking via Michael addition. Similar to the disulphide crosslinked particles nanogels prepared via Michael adddition have spherical shape. The size of the particles determined from cryo-FESEM image analysis is 250 nm < d_{av} < 400 nm

and from DLS d_{av} = 220 nm. The nanogels however have broader size distribution in comparison to the particles shown in **Figure 4.2**.

It is known that PEO based polymers show a tendency to form aggregates in water that may be easily confused with real cross-linked particles in the DLS analysis.[16] Also the regular pattern formation on mica is not an unequivocal proof for the formation of nanogels since in some cases, dewetting of polymer films may result in similar patterns.[17] Thus optimization of spin-coating parameter was done and areas of the sample where the transition between nanogel aggregates and the monolayer occurs were analysed. The clear detection of individual nanogels in the larger aggregates that were formed during the spin-coating process undoubtedly proves the successful cross-linking of the prepolymers to nanogel particles **(Figure 4.5)**.

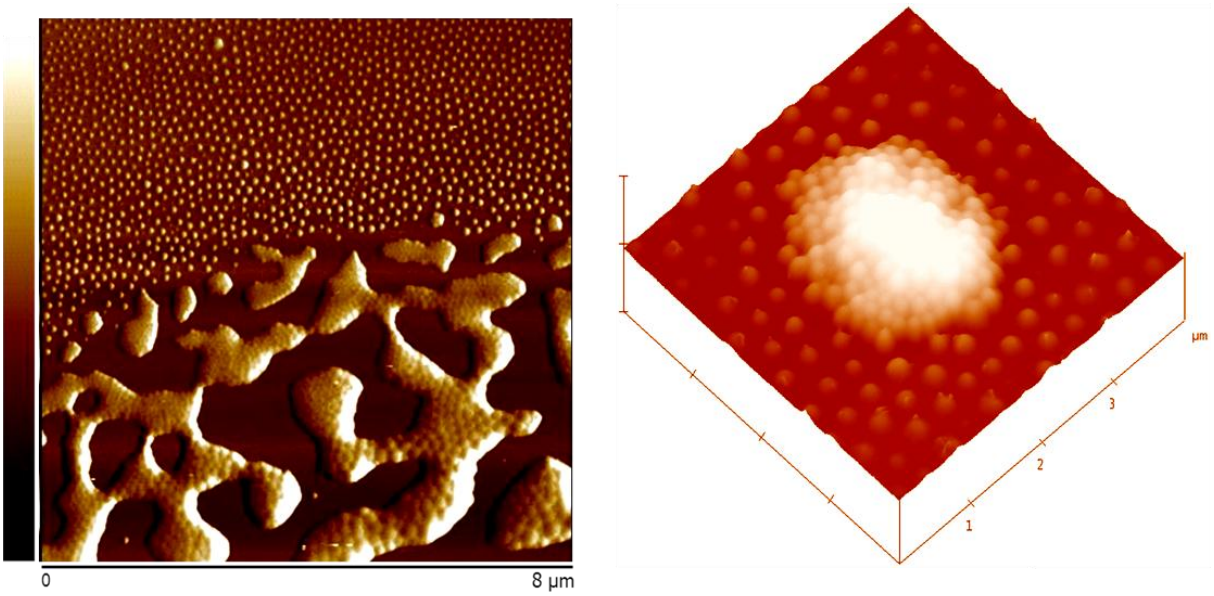

Figure 4.5: SFM topography image depicting the transition between the aggregated and isolated **HS-sP(EO-*stat*-PO)** nanogels. The formation of aggregates is due to the spin coating process and does not reflect the situation in the water. Scan size is 4 × 4 μm and z-range is 150 nm.

Generally, particles prepared by oxidation of **HS-PG** showed very similar behaviour to **HS-sP(EO-*stat*-PO)** nanogels regarding their dispersion stability. However, in water these nanogels possess broader size distributions with a z-average particle diameter of 330 nm and PDI = 0.54 as measured by the DLS and particle diameters d in the range of 100 nm < d < 350 nm determined by cryo-FESEM. For nanogels prepared by Michael addition particle diameters d was in the range of 250 nm < d < 550 nm **(Figure**

4.6, left) by cryo-FESEM while with DLS they showed a diameter of 450 nm and PDI = 0.65.

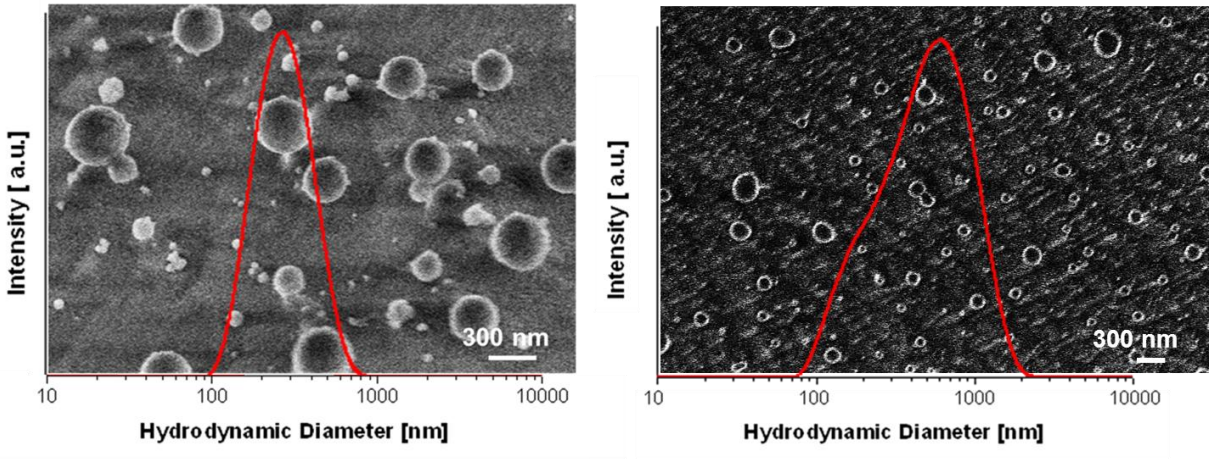

Figure 4.6: Characterization of **HS-PG** nanogels in water (swollen state): by cryo-FESEM and DLS technique for nanogels prepared by oxidative crosslinking (left) and by Micheal addition (right).

The SFM of the dry **HS-PG** nanogels prepared both by oxidation crosslinking as well as by Michael addition is presented in **Figure 4.7**. It can be seen that in the size distribution of the particles crosslinked via oxidation is large in comparison with the nanogels crosslinked with PEG-diacrylate. SFM measurements of nanogels on mica performed in the dry state confirm the DLS results and show polydisperse disulfide crosslinked **HS-PG** particles **(Figure 4.7).**

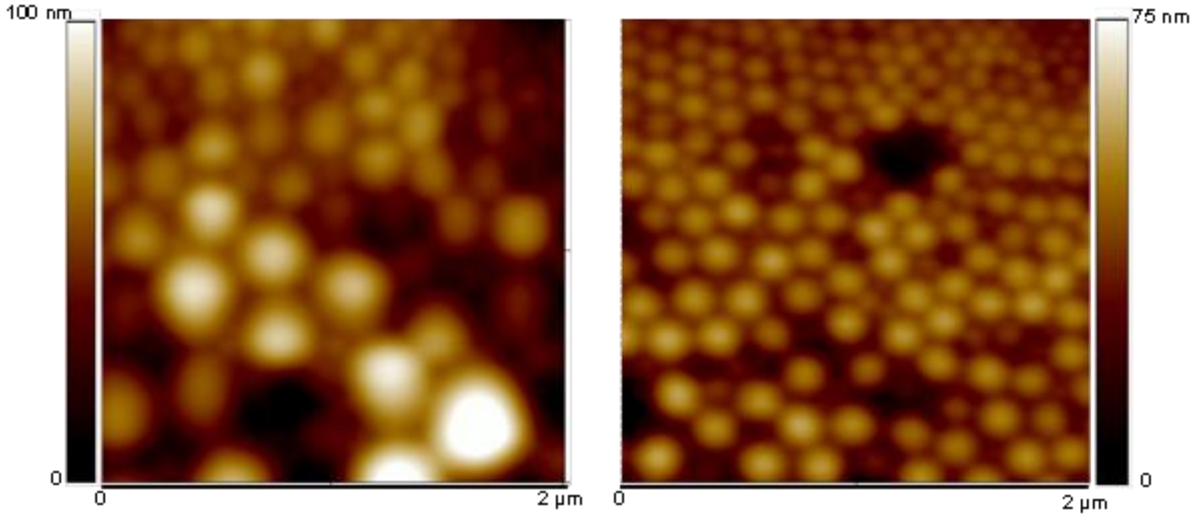

Figure 4.7: SFM characterization of dry SH-PG nanogels crosslinked by oxidation (left) and via Michael addition (right).Scan size is 2 × 2 μm and z-range is 100 nm.

In order to prove the degradability the disulfide cross-linked nanogels were incubated with a glutathione (GSH) solution. **Figure 4.8a** illustrates the 2000 - 3500 cm^{-1} Raman spectra range of **HS-sP(EO-*stat*-PO)** nanogels before and after incubation with 10 mM GSH for 6 h. The noteworthy feature is the band at about 2580 cm^{-1} which corresponds to stretching modes of thiol groups in the reduced particles. This band is not detectable in the crosslinked nanogels and appears upon incubation with GSH. In addition, spin-coating the nanogel-solution after reduction onto mica resulted in a dewetted polymer film where no nanogels could be detected **(Figure 4.8b)**. These results evidence that the nanogel disulfide cross-linkages can be cleaved with GSH what confirms degradability of the particles under cytosolic conditions.

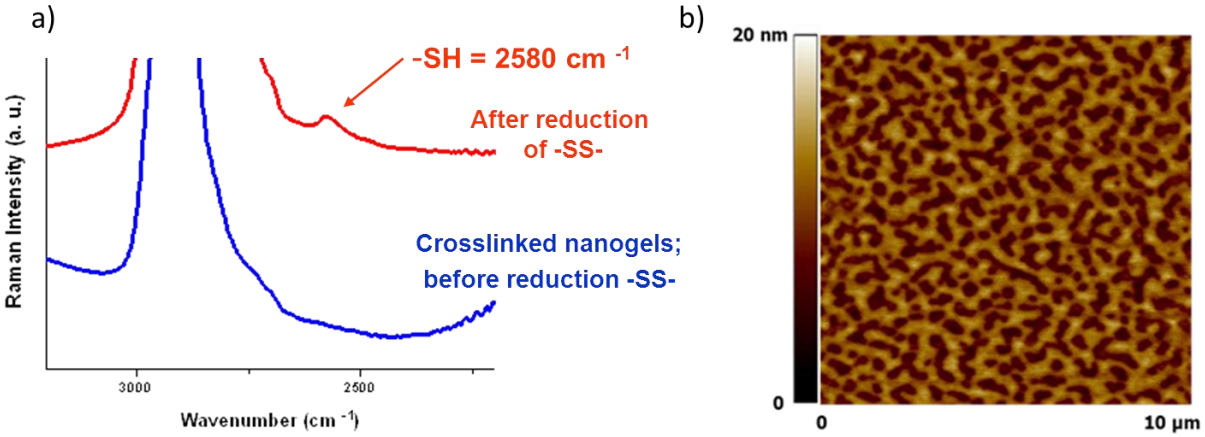

Figure 4.8: Characterization of reduced **SH-sP(EO-*stat*-PO)** nanogels: (a) by Raman spectroscopy of reduced nanogels (upper spectra) and nanogels before the reduction (lower spectra); (b) SFM topography image. Scan size is 10 × 10 μm and z-range is 20 nm.

4.3.1 Cytocompatibility

A live/dead cell viability assay was used to investigate the cytotoxicity of all prepared nanogels. After 24 and 72 h incubation of L929 cells with nanogels (c = 0.5 mg/mL), differential interference contrast (DIC) microscopy and fluorescence microscopy were used to assess cell morphology and visualize live and dead cells.

Live cells with intact membranes are stained with green fluorescence, while dead cells were stained with red fluorescence. **Figure 4.9** shows fluorescence images of cells incubated with **HS-sP(EO-*stat*-PO)** nanogels after live/dead staining.

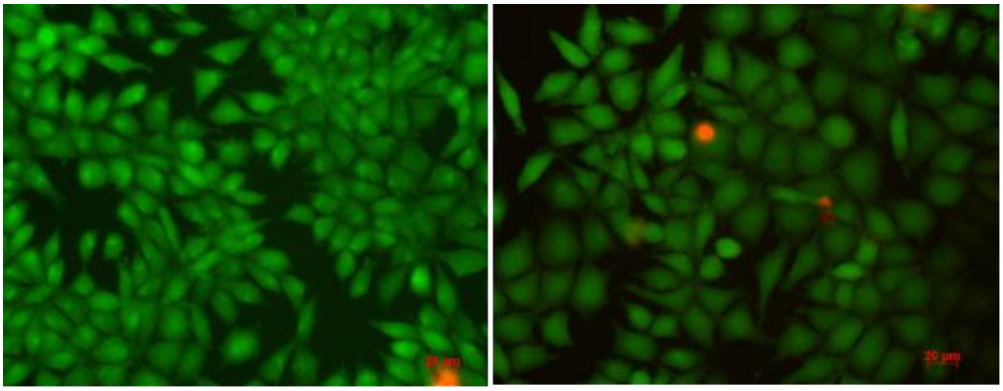

Figure 4.9: Fluorescent image of live (green) and dead (red) L929 cells after 72 h incubation with nanogels (c = 0.5 mg/mL). Counting of live and dead cells indicated 94 ± 2% viability

Careful counting of live and dead cells indicated 94 ± 2% viability of L929 cells in the presence of **HS-sP(EO-*stat*-PO)** nanogels, as compared to 96 ± 2% cell viability in the absence of nanogels as a control experiment. Comparable results have been achieved with **HS-PG** nanogels. This clearly shows the cytocompatibility of nanogels prepared from **HS-sP(EO-*stat*-PO)** and **HS-PG.**

4.3.2 Hemocompatibility

Estimation of hemocompatiblity of the nanoparticles is required to elicit several toxicological reactions, in particular embolisation, hemolysis, cellular activation, and several well-known biological cascades such as coagulation, complement activation, kinin/kininogen, and fibrinolysis. When using nanoparticles as carriers the first barrier that they meet is the blood itself and the Reticulo-Endothelial System (RES) which is directly connected to the liver/spleen. The efficiency of this clearance system at eliminating foreign bodies from the blood circulation is so effective that the blood life-time of nanoparticles typically does not exceed some part of minutes. This efficiency in elimination has been demonstrated as the result of non-specific[18] or immune-specific immunogenic response.[19] Therefore, to verify the hemocompatibility of nanogels both for toxicological reasons and efficiency of targeting is required. The nanoscale of nanogels amplifies the total surface exposed to the human body, as compared to the same amount of bulk material. As a rough calculation 10 mg of spherical nanogels with a mean diameter of 100 nm and of a density of 1 will develop a total area of 0.6 m^2. In regards to that, when the nanogels are diluted with 1 mL of human blood, they will be

exposed to 4.5 billion of RBC's, 400 million of platelets, ~ 5 million of white blood cells and about 70 mg of plasma proteins. Therefore nanogels may significantly interact with humoral and cellular blood components and could significantly modify the well-known biological cascades involved in blood reactivity. It is also important to stress the need to evaluate the hemo-reactivity of nanogels tailored for external applications like oral and nasal administration. Indeed, in the present status of knowledge of the final outcome / biodistribution of these nanoparticles, it cannot be excluded that the particles could finally be transferred within the blood circulation. It has, for example already been reported that the nasal epithelium displays a relatively high permeability to drugs due to the presence of a dense blood vessel network.[20] Recently, several studies have indicated that hydrophilic or relatively large molecules such as proteins, viruses or dextrans with a molecular weight up to 20 kDa can be directly transported from the nasal cavity to the Cerebro Spinal Fluid (CSF) using neuronal anterograde and retrograde transport in a molecular weight dependent manner.[21, 22] Thus a drug administered by the nasal route may enter either the blood of the general circulation or into CSF via choroids plexus blood-brain. Thus for potential use of nanoparticles as drug carriers, screening them for hemocompatibility becomes a requisite criterion.

In order to detail the hemoreactivity of disulphide crosslinked **sP(EO-*stat*-PO)** and **PG** nanogels following panel of tests as given below were performed adopting the ISO 10993-4. It is worthwhile to mention that the hemocompatibility assessment were performed only when following key criteria like chemical purity, size (at least below 1 *µ*m), batch reproducibility, NP *in vitro* stability, *in vitro* safety verified on at least one animal cell type, were satisfied.

4.3.2.1. Realization of Blood Smears for Control of the RBC's Morphology

In this study the interaction of nanogels on the morphology of red blood cells (RBC) was investigated. The microscopic analyses of RBC incubated with nanogels showed no change in morphology for the concentrations evaluated.

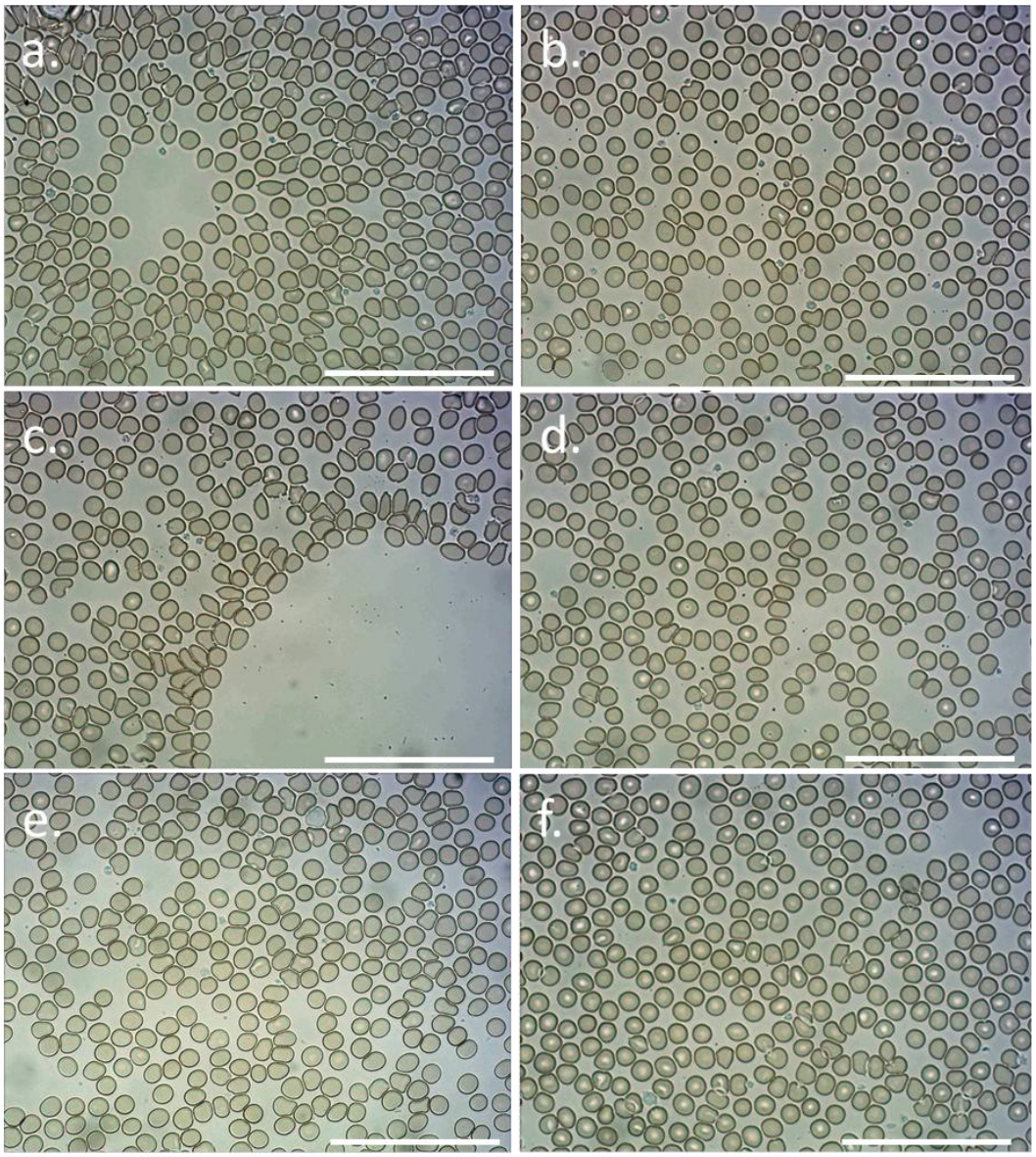

Figure 4.10: Microscopic pictures of the whole blood smear after exposure to a.) sP(EO-*stat*-PO) nanogel (1/20 dilution), b) sP(EO-*stat*-PO) nanogel (1/200 dilution), c). PG nanogel (1/20 dilution), d.) PG nanogel (1/200 dilution), as a control e.) PBS buffer non-incubated and f.) PBS buffer incubated was used. Maginfication 50x, scale 100µm.

On visualising the smear after its interaction with nanogels, no significant change or alternation in the morphology of RBS's was observed. There was small patch like area seen when higher concentration of **PG** nanogels were used, which could be attributed to change in wetting properties of the glass substrate when in contact with the nanogels. As a consequence adhesion of the blood cells alters and this alteration occurs in "a patch way" producing macro-irregularities in the deposition of the blood cells.

4.3.2.2 Hemolysis Test

This assay is based on colorimetric detection of cyanmethemoglobin in solution. The cyanmethemoglobin reagent which is used in this assay is a mixture of potassium ferricyanide, potassium cyanide and sodium bicarbonate. Nanogels were incubated in blood, and hemoglobin released by damaged cells due to nanogels interaction was measured. Ferrous ions from the released hemoglobin get oxidized to methemoglobin in by ferricyanide in presence of bicarbonate and subsequent step cyanide converts the methemoglobin to cyanmethemoglobin. The undamaged erythrocytes from the sample were removed by centrifugation and the amount of cyanmethemoglobin in the supernatant was measured spectrophotometrically via the absorbance at 540 nm **(Figure 4.11)**.

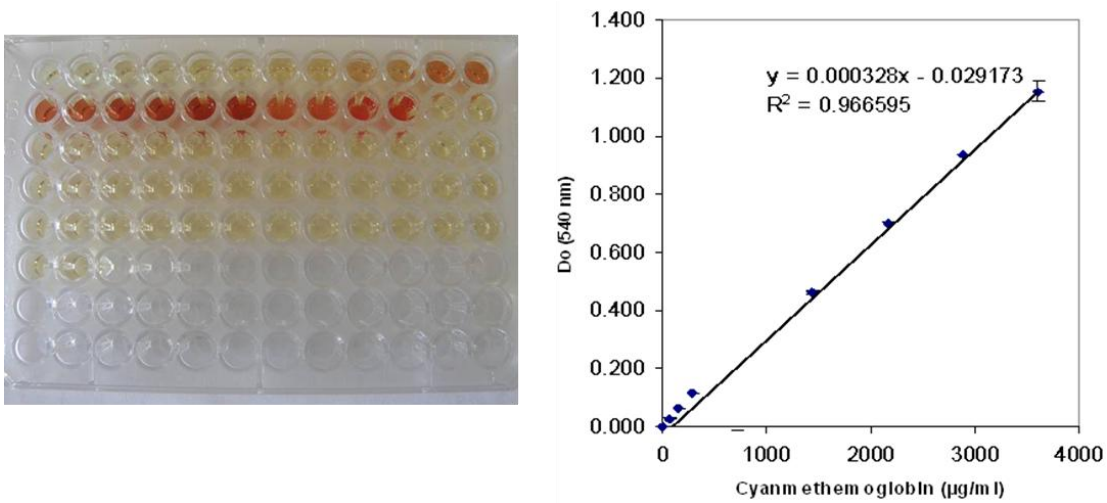

Figure 4.11: Multiplate of the haemolytic test and calibration curve of the cyanmethemoglobin test**.**

This measured absorbance was compared to the standard curve in order to determine the concentration of hemoglobin in the supernatant and this hemoglobin concentration was compared to the value obtained from the supernatant of the blood sample untreated with nanogels to obtain the percentage of particle induced hemolysis referred to as percentage hemolysis.

The results highlighted in **Table 4.1** show that both type of nanogels were not haemolytic (< 2 %) according to ASTM standard (F 756-00) for the concentrations measured.

Table 4.1 Counting of Platelets and red blood cell after interaction of nanogels to blood

Sample ID	% Hb		± SD	
C+	14.91		0.62	
C-	1.34		0.10	
Plasma	0.60		0.03	
	Mean	± SD	Mean	± SD
	1/20		1/200	
sP(EO-*stat*-PO)nanogels	1.05	0.11	0.84	0.05
PG nanogels	1.19	0.11	1.11	0.05
Water	1.19	0.11	1.11	0.05

4.3.2.3 Platelet and Red Blood Cell Counting

The counts of Platelet and RBC in blood were measured after there interaction with nanogels **(Table 4.2)**.

Table 4.2 Counting of Platelets and red blood cell after interaction of nanogels to blood

Sample ID	Mean	± SD	Mean	± SD
Platelets, N/μL	Ctrl n/inc		Ctrl inc	
	222000	6557	210667	22502
	1/20		1/200	
sP(EO-*stat*-PO) nanogel	214000	9849	211667	10408
PG nanogel	271667	5132	217667	6506
water	195667	19732	190000	26153
RBC's, N/μL	Ctrl n/inc		Ctrl inc	
	4063333	57735	4110000	160000
	1/20		1/200	
sP(EO-*stat*-PO) nanogel	4083333	210079	4116667	160416
PG nanogel	3876667	51316	3946667	73711
water	4286667	411866	3976667	55076

* Ctrl n/inc : blood control non incubated ** Ctrl inc: blood control incubated

N/μL = number of cells counted per μL ; SD : Standard Deviation

No significant changes were observed in platelet and RBC's counting for the concentrations of nanogels evaluated.

4.3.2.4. Coagulation Cascade Activation through Intrinsic and Extrinsic Pathways

4.3.2.4.1 TCA I normal: This analysis of the coagulation through the intrinsic pathway is realized in standard conditions of operation in clinical biology, i.e. with the addition of kaolin, as activator of this biological cascade. It allows to verify if the factors associated with this cascade are adsorbed or denaturated by the foreign material (i.e. the NP). A reduction of the percentage corresponds to an inactivation of this coagulation pathway.

Table 4.3 Hemostasis control test for nanogels

Sample ID	TCA I normal (%)		Quick (%)	
Positive Ctrl+Kaolin	40.6		>130	
	1/20	1/200	1/20	1/200
sP(EO-*stat*-PO) nanogel	>100	>100	103.3	100
PG nanogel	>100	>100	105.0	100
water	>100	>100	103.3	98.4
Ctrl n/inc	>100	>100	103.3	101.6

* Ctrl n/inc : blood control non incubated

In order to activate this pathway, phospholipid suspension, an activator (kaolin), and calcium (to reverse the anticoagulant effect of citrate) were mixed into the plasma sample and the time of clot formation was measured.

4.3.2.4.2 Quick Test: The Quick test was performed to explore the extrinsic coagulation system. Calcium thromboplastin and excess calcium were added to citrated plasma to induce coagulation and the time of fibrin clot formation was measured. This analysis of the coagulation through the extrinsic pathway is realized in standard conditions of operation in clinical biology, with the addition of thromboplastin, as activator of this biological cascade. It allows to verify if the factors associated with this cascade are adsorbed or denaturated by the foreign material (i.e. the NP). A reduction of the percentage corresponds to an inactivation of this coagulation pathway. As the results in **Table 4.3** shows neither extrinsic, nor intrinsic pathways of the coagulation are affected by the presence of the nanogels at the concentration considered.

4.3.2.5 Compliment Activation

Complement system represents a major mechanism of our immune response. It depends upon a biochemical cascades that recognizes foreign antigens. It occurs via three different pathways: the classical pathway, the alternative pathway, and the mannose-binding lectin pathway.[23] Although the triggers and the initial steps in the activation of each of these pathways differ, they all converge at the formation of C3 convertase. C3 convertase cleaves C3; this is the most important step in the activation pathway. Large numbers of opsonizing proteins, primarily C3a and C3b are generated on C3 hydrolysis, which coat the pathogens surfaces to facilitate their uptake and destruction by phagocytic cells.[24]

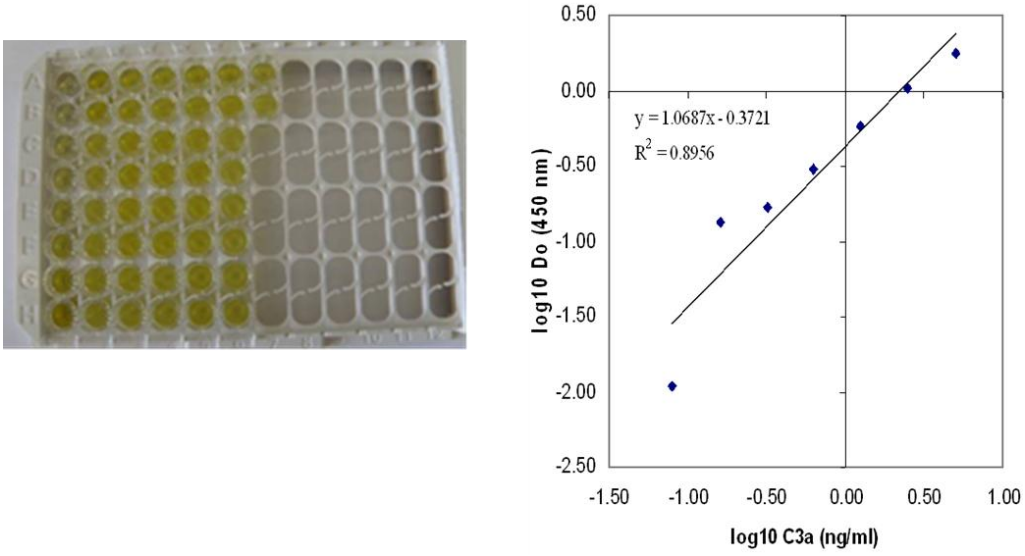

Figure 4.12: Multiplate of Compliment activation test and calibration curve for C3a assay

Table 4.6 Compliment Activation assay for nanogels

Sample ID	C3a (ng/mL)	± SD (ng/mL)	C3a (ng/mL)	± SD (ng/mL)
Ctrl Non-Inc*	2666.3	120.1	-	-
Ctrl Inc**	2727.9	259.3	-	-
Ctrl +	6438.1	663.0	-	-
	1/20		1/200	
sP(EO-*stat*-PO) nanogel	3075.0	212.2	4087.5	113.5
PG nanogel	4123.1	132.3	3826.2	110.8
water	3776.7	193.3	3938.0	15.8

Nanoparticles can be cleared from the blood circulation as a consequence of complement activation in particular via a pathway which arises from the proteolytical cleavage of C3 into anaphylatoxic peptide C3a. Due to the large surface exposed, nanoparticles in suspensions within the blood could enhance the activation of the complement.

The assay is based on the detection of C3a, when nanoparticle comes in contact with blood. C3a is a small polypeptide consisting of 74 amino acids and in itself is very short-lived. In serum, it is cleaved rapidly into the more stable C3a-desArg (also called acylation stimulating protein, ASP). Therefore, measurement of C3a-desArg allows reliable conclusion about the level of complement activation in the samples. For convenience, both forms will be referred as C3a. From **Table 4.6** it could be seen that no significant activation of the complement was observed in the presence of the nanogels.

4.4 Conclusion

Formation of nanogels by cross-linking of thiol-functional hydrophilic prepolymers in inverse miniemulsion was demonstrated and unequivocally proven by a combination of DLS, cryo-SEM and SFM characterization. Oxidative coupling resulted in particles that are stable in PBS buffer at pH 7.4 but decompose in reductive conditions. Cell viability test according to ISO 10993-5, showed that the nanogels were non cytotoxic towards L929 fibroblasts. Hemocompatibility studies showed that the nanogels were hemocompatible according to ISO 10993-4 adopting general conditions of interaction of nanoparticles with blood. Biocompatibility, intracellular degradability, fully synthetic polymeric building blocks with molecular weights that allow renal clearance and the possibility to tailor the synthetic precursors regarding structure and functionality make this system a versatile platform for drug delivery.

4.5 References

1. J. K. Oh, R. Drumright, D. J. Siegwart, K. Matyjaszewski, *Prog. Polym. Sci.* **2008**, 33, 448.
2. M. Hamidi, A. Azadi, P. Rafiei, *Adv. Drug Del. Rev.* **2008**, 60, 1638.
3. D. Crespy, K. Landfester, *Macromol. Chem. Phys.* **2007**, 208, 457.

4. K. McAllister, P. Sazani, M. Adam, M. J. Cho, M. Rubinstein, R. J. Samulski, J. M DeSimone, *J. Am. Chem. Soc.* **2002**, 124, 15199.
5. J. K Oh, C. Tang, H. Gao, N. V. Tsarevsky, K. Matyjaszewski, *J. Am. Chem. Soc*. **2006**, 128, 5578.
6. J. K. Oh, D. J. Siegwart, H. I. Lee, G. Sherwood, L. Peteanu, J. O. Hollinger, K. Kataoka, K. Matyjaszewski, *J. Am. Chem. Soc*. **2007**, 129, 5939.
7. N. Murthy, M. Xu, S. Schuck, J. Kunisawa, N. Shastri, J. M. Fréchet, *J. Proc. Natl. Acad. Sci.* **2003**, 100, 4995.
8. D. Missirlis, N. Tirelli, J. A. Hubbell, *Langmuir* **2005**, 21, 2605.
9. A. Ethirajan, K. Schoeller, A. Musyanovych, U. Ziener, K. Landfester, *Biomacromolecules* **2008**, 9, 2383.
10. A. Meister, M. E. Anderson, *Ann. Rev. Biochem.* **1983**, 52, 711.
11. H. Lee, H. Mok, S. Lee, Y. K. Oh, T. G. Park, *J. Control. Rel.* **2007**, 119, 245.
12. Standard Practice for Assessment of Hemolytic Properties of Materials (ASTM designation F 756-00)
13. T. Yamaoka, Y Tabata, Ikada, *J. Pharm. Sci.* **1994**, 83, 601.
14. J. Boyd, C. Parkinson, P. Sherman, *J. Colloid Interface Sci*. **1972**, 41, 359.
15. D. Y. Luo, A. C. Dai, Y. W. Chiu, *J. Colloid Interface Sci*. **2009**, 330, 170.
16. T. Sakai, T. Matsunaga, Y. Yamamoto, C. Ito, R. Yoshida, S. Suzuki, N. Sasaki, M Shibayama, U. Chung, *Macromolecules* **2008**, 41, 5379.
17. P. Müller-Buschbaum, M. Wolkenhauer, O. Wunnicke, M. Stamm, R. Cubitt, W. Petry, *Langmuir* **2001**, 17, 5567.
18. S. M. Moghimi, *Adv. Drug Del. Rev.* **1995**, 17, 103.
19. T. Ishida, K. Atobe, X. Yu Wang, H. Kiwada, *J. Control. Rel.* **2006**, 115, 251.
20. P. Arora, S. Sharma, S. Garg, *Drug Discovery Today* **2002**, 7, 967.
21. E. Garcia-Garcia, K. Andrieux, S. Gil, *Int. J. Pharmaceutics* **2005**, 298, 274.
22. M. Dahlin, E. Björk, *Int. J. Pharmaceutics* **2000**, 195, 197.
23. M. Carroll, *Nature* **2006**, 444, 159.
24. C. A. Janeway, P. Travers, M. Walport, J. D. Capra, Immunobiology: The Immune system in Health and Disease 6th ed. Garland Science Publishing **2005**.

CHAPTER 5

Mild Oxidation of Thiofunctional Polymers to Cytocompatible and Stimuli-Sensitive Hydrogels and Nanogels

Part of this work is published in Macromolecule Bioscience DOI: 10.1002/mabi.201200389

5.1 Introduction

Aside of functionalization with bioactive ligands, nanoparticle size control is one key aspect in nanotechnology, as many *in-vivo* functions and effects of Nanoparticles depend on their size including internalization pathways, complement activation, immunogenicity, intracellular trafficking, circulation times, targeting and clearance.[1] Rejman *et al.* demonstrated that nanoparticles with a diameter < 200 nm are internalized via clathrin-coated pits while the internalization of 500nm sized particles were caveolae mediated. In addition, the larger particles were not delivered to the lysosomes, which could be one of the reasons why larger nanoparticles result in higher transfection efficiencies even with smaller ones being internalized better.[2] Porter *et al.* found that PEGylated nanoparticles smaller than 150 nm in diameter accumulated in the bone marrow of rabbits whereas larger particles were mostly sequestered by the liver and spleen and only a small fraction reached the bone marrow.[3] In recent studies it was also illustrated that nanoparticles with size around 100 nm had a greater uptake than microparticles of 1 μm and much greater uptakes than 10 μm microparticles. A similar study conducted in rat's *in situ* intestinal loop model, exhibited widespread penetration of nanoparticles in submucosal layer, while microparticles were localized mainly in the epithelial lining.[4, 5]

These few examples underline the importance of the precise case-sensitive size selection and size control of nanoparticles for a demanded application. Drug release at the site is also influenced by particle size. Faster discharge of drug is accomplished by

use of smaller particles with larger surface area to volume ratio as they lead to conjunction of the drug near the particle surface. On the contrary, drug release is slower with particles with larger core size, even though they encapsulate higher amounts of the drug.[6] While smaller particles show advantage with respect to drug discharge they also run a higher risk of aggregation during storage and transportation. Thus to develop nanoparticles with smallest possible size and maximum stability at the same time is a challenging task.

Therefore nanoparticle size control is the key to optimize nanoparticle delivery vehicles for controlled release and thereby making them applicable in various clinical fields. Also the influence of size on nanoparticle bio-distribution has been established as organ specific and non-linear.[7] This is in part attributed to organ-specific physical and physiological barriers that systematically administered nanoparticles come across.[8] Therefore the significance of tuning nanoparticle size for each distinct *in vivo* application is emphasized by non-linear influence of nanoparticle size on bio-distribution, which varies from organ to organ.

As discussed earlier disulfide cross-links can be introduced either by using reactive disulfide cross-linkers[9] or by oxidation of thiol functional precursors.[10] The latter method allows covalent coupling of cysteine-terminated drugs (for example peptides) to the particle matrix through disulfide bonds during or after particle preparation. Thus, in the extracellular milieu, the bioactive molecules are protected against degradation and will be released upon entering the targeted cell. Oxidation of thiol bearing matrix molecules can be performed upon exposure to air.[11] This process is, however, relatively slow and not useful for most nanogel preparation techniques. Thus, oxidizing catalysts such as diamide, peroxides, and sodium tetrathionate, or a catalyst based on Fenton chemistry, are often applied in order to shorten the oxidation time.[12] Those catalysts possess strong oxidation potential which is favorable for fast gelation but on the other side also results in oxidation of thiols to higher oxidation numbers and restricts the possibility to embed oxidation sensitive molecules into the hydrogels.

In **Chapter 4** formation of redox-sensitive and biodegradable nanogels with hydrodynamic diameter of 350 ± 50 nm using hydrophilic thiol-functionalized prepolymers based on star shaped poly(ethylene oxide-*stat*-propylene oxide) (**sP(EO-*stat*-PO)**) and linear poly(glycidol) (**PG**) was reported. Nanogels were prepared by oxidative cross-linking of thiol groups to disulfide bonds in inverse miniemulsion using hydrogen peroxide.[13] While this proof-of concept study has shown that this preparation

route is feasible, only poor control over nanogel size could be achieved. More importantly, the use of hydrogen peroxide as oxidation catalyst is unfavourable for the embedding of peptides and proteins, as under certain conditions, disulphides are not the sole reaction products.[14]

In this chapter a comparative investigation of alloxan, a mild oxidation catalyst, and hydrogen peroxide as oxidation catalyst for the formation of disulphide crosslinked hydrogels and nanogels is made. Further formulation strategies to control the size of the disulphide crosslinked **PG** nanogel prepared via inverse miniemulsion for both catalyst systems is presented and the differences are discussed. Finally, investigations on nanogel stability and degradation behaviour in presence of GSH as well as *in vitro* cytocompatibility are shown.

5.2 Experimental

5.2.1 Materials and Methods

Thiol functionalized linear poly(glycidol) (**HS-PG**) (M_n = 6100 g/mol, M_w/M_n = 1.17, 15 thiol groups) was prepared as described in literature.[13] n-hexane (≥ 95%, Sigma), THF (99%, VWR), hydrogen peroxide (30%, VWR), Span 80 (Sigma), and Tween 80 (Sigma-Aldrich), Brij 30 (Sigma), Laureth-3 (Fluka), Span 60 (Sigma), 2-hydroxyacrylate (96%, Sigma), glutathione (GSH) (99%, Sigma), alloxan monohydrate (Sigma) and Alexa Fluor 488 maleimide dye (720.88 g/mol) (Invitrogen), WST reagent (Roche Diagnostics) Accutase (PAA), Isoton III (Beckmann Coulter) were used as received. DMEM, 10 % Fetal Calf Serum (FCS), 1 % penicillin/streptomycin and 1 % HEPES buffer were purchased from Invitrogen. Phosphate buffer saline (PBS) from Sigma has been dissolved in water to 0.04 M concentration (pH = 7.4). Minisart syringe filters (5 μm) were purchased from Sartorius and dialysis membrane (MWCO = 3500 Da) was purchased from Spectrum Laboratories, Inc.

UV/Vis- Spectrophotometry UV/Vis transmission spectra were determined using a Varian Cary 100 Bio-UV-Visible split-beam spectrophotometer running with Cary WinUV scan application with a capacity of measuring 6 samples at a time. Samples were scanned at 500 nm. A high-intensity Xe flash lamp was used as the source for UV light, which permits taking 80 data per second.

Fluorescence Microscopy Zeiss Axioplan 2 upright digital imaging microscope was used for fluorescent imaging. It was equipped with a high resolution digital camera (Zeiss Axiocam HRc) and image processing software (AxioVision Release 4.7) with 100 W tungsten and mercury light sources. Axiovision software controls the stage, filter sets, and AxioCam camera provides Z-stack and multi-channel digital image capture capabilities with a resolution of 1300 × 1030 (native) up to 3900 × 3090 pixels. Microscope objectives available were 10X, 20X and 50X.

5.2.2 Bulk gelation kinetics

In order to determine the kinetics of bulk hydrogel formation 50 mg of **HS-PG** (8.20×10^{-3} mmol) was dissolved in 125 μL PBS buffer at pH 6.0 and 7.4 or borate buffer at pH 8.0. The solutions were homogeneously mixed followed by the addition of the oxidation catalyst. The amounts of the added catalyst are listed in **Table 5.2**. Gelation time was qualitatively determined by the vial inversion method.

5.2.3 HS-PG Labelling with Alexa Fluor 488

Fluorescently labelled **HS-PG** was synthesized by the Michael addition type reaction between maleimide group present in the Alexa Fluor dye and the thiol functionalities of **HS-PG**. In this reaction 1 g of **HS-PG** (1.64×10^{-1} mmol) was dissolved in 5 mL of PBS buffer at pH = 7 followed by the addition of 0.3545 g Alexa Fluor maleimide (4.91×10^{-1} mmol). The mixture was stirred in dark for 12 h under argon atmosphere followed by dialysis and lyophilisation.

5.2.4 Nanogel Preparation

Nanogels were prepared via inverse miniemulsion method. For the preparation of the miniemulsion, surfactant (37.5 mg of 3:1 weight ratio of Span 80 and Tween 80, if not stated otherwise) dissolved in 1.25 mL of n-hexane was used as organic phase. The aqueous phase consisted of 50 mg (8.20×10^{-3} mmol) of **HS-PG** dissolved in 125 μL of 0.04 M PBS buffer (pH = 7.4). The organic and the aqueous phases were pre-emulsified by magnetic stirring for 10min. After stirring the system was ultrasonicated using a Branson sonifier W450 with a ¼ ″ horn at duty cycle of 30% and output control of 90% under ice cooling. Glass vials of 18 mm in diameter were used for all nanogel synthesis. It was found that the geometry of the vessel and location of sonication probe in the vessel was very important for the efficiency of sonication. Thus, each run used

the same type of vessel with the horn immersed to the same depth each time. Cross-linking was initiated by subsequent addition of H_2O_2 or alloxan catalyst followed by a further sonication step. If not stated otherwise, 30 μL of 0.1 M H_2O_2 or 0.1 M alloxan (3×10^{-3} mmol) was used. The sonication times before and after the addition of catalyst are specified in the following sections. The reaction was allowed to proceed for 20 min at room temperature with constant stirring followed by quenching of free thiol groups by 2-hydroxy acrylate at pH = 7.4. Any further oxidation was stopped by addition of 1.5 mL of acidic water (pH = 3). Separation of the nanogels was achieved by centrifugation at 10000 rpm for 30 min followed by decantation of the supernatant. Nanogels present in the aqueous layer were carefully washed with n-hexane (2 × 1.5 mL) and THF (4 × 2.5 mL) in order to remove the surfactants and unreacted polymer. The remaining organic solvents and acid were removed by dialysis. Purified nanogels were stored in Millipore water at 4 °C for further use. This standard procedure for the synthesis of nanogels could be easily scaled for higher or lower amounts as long as the ratio of the reactants used is maintained.

5.2.5 Influence of Preparation Parameters

Sonication Time. To assess the effect of sonication time variation before and after addition of the catalyst, in two sets of experiments were performed where either one of the two times was kept constant at 60s, while to other was varied between 60s and 1500s. For clarity of sample nomenclature, nanogels prepared with sonication time of 60s before and 120s after addition of the catalyst are named as 60s/120 s. The following combination of parameters was examined for both catalysts: 60s/60s, 120s/60s, 180s/60s, 240s/60s, 300s/60s, 360s/60s 420s/60s, 600s/60s, 1500s/60s, 60s/120s, 60s/180s, 60s/240s, 60s/300s, 60s/360s, 60s/420s, 60s/600s, 60s/1500s.

Influence of Hydrophilic-Lipophilic Balance (HLB) of the Surfactant

The HLB value was tuned by the variation of the ratio of the surfactants Span 80 and Tween 80 **(Table 5.1)**. The dependence on nanogel diameter was investigated for four HLB values: 5, 6, 7 and 8. The experiments were performed at three different sonication times: 60s/60s, 300s/60s, 360s/60s.

Table 5.1 Span 80/Tween 80 composition at different HLB values

HLB	Span 80 [mg]	Tween 80 [mg]
5	35.05	2.45
6	31.54	5.96
7	28.04	9.46
8	24.53	12.97

Influence of Type of Surfactant at HLB 7

The dependence on nanogel diameter was investigated for four HLB values: 5, 6, 7 and 8. As HLB 7 was found to be most suited value, different combination of surfactants and co-surfactants were further investigated at this HLB value for the nanogel preparation by inverse miniemulsion at three different sonication times: 60s/60s, 300s/60s, 360s/60s.

Table 5.2 Different surfactant composition at HLB 7

HLB	Surfactant 1	Surfactant 2
7	Span 60 (29.12 mg)	Tween 80 (8.38 mg)
7	Span 80 (15.94 mg)	Brij 30 (31.56 mg)
7	Span 80 (17.25 mg)	Laureth 3 (20.25 mg)
7	Span 80 (24.53 mg)	Tween 80 (12.97 mg)

Influence of Polymer Concentration. To determine the effect of polymer concentration on the size of nanogels, nanogels were prepared as described with varying polymer concentrations of 40, 28 and 12 w/v % with respect to the aqueous phase (PBS buffer) at sonication time of 60s/60s, 300s/60s and 360s/60s.

5.2.6 Nanogel Dispersion Stability in PBS at 37 °C and Reductive Degradation.

Stability of the nanogel dispersions at 37 °C in PBS buffer, with respect to aggregation and particle diameter was checked for standard alloxan and H_2O_2 crosslinked nanogels at 0 h, 0.25 h, 1 h, 6 h, 12 h, 24 h and 60 h by DLS and cryo-FESEM measurements.

Degradation of unlabelled as well as Alexa Flour 488 labelled nanogels was performed in 10 mM GSH solution in PBS (pH = 7.4) at 37 °C. Fluorescence microscopy images of particle dispersions before and after reduction were taken to check whether the fluorescence is localized in the nanogels before reduction and homogeneously distributed in the solution after reduction. Assessment of reduction kinetics in the presence of 1, 5 and 10 mM GSH was followed by measuring the solution transmittance by means of UV-Vis spectrometry in PBS buffer at 37 °C with different ratios of GSH to nanogels. For the concentration 1 mM GSH, degradation kinetics were also evaluated by multiple GSH addition. In this experiment, 0.768 mg GSH was added into 2.5 mL nanogel solutions every 200 min so that at the beginning of each step the GSH total concentration was 1 mM.

5.2.7 Cytocompatibility

L929 mouse fibroblasts were seeded in a 48 well tissue culture plate (20000 cells per well in 500μL DMEM containing 10% FCS, 1% penicillin/streptomycin and 1% HEPES buffer) a total of 24 wells were seeded. The cells were incubated for 24h at 37°C in a 5% CO_2 humidified atmosphere. The nanogel sample was dialysed against DMEM without additives for 24 h. Afterwards the FCS, penicillin/streptomycin, and HEPES were added in the adequate quantity. The culture medium was aspirated from the cells and 500 μL of the dialysed nanogels were added to two wells each. 1mL of the remaining microgel solution was diluted in DMEM at a ratio of 1:1 and 500 μL of this solution was added to three wells each, the remaining 500 μL were diluted 1:2 and dispensed to three wells each. The cells were incubated for 48h at 37 C in a 5% CO_2 humidified atmosphere.

Cytocompatibility of the nanogels with concentrations of 10mg/mL, 5mg/mL and 1.7mg/mL was evaluated by means of visual examination of cell morphology in a light microscope, cell counting and determination of cell activity using the WST reagent according to DIN EN ISO 10993-5 was performed. In detail, after incubating the cells with the WST reagent at a ratio of 1:10 in supplemented DMEM for 30min at 37°C, the adsorption of the supernatant was quantified in a Tecan spectra fluor plus photometer (Tecan, Crailsheim, Germany). The cells were rinsed twice with PBS and were detached from the surface by incubation with Accutase and diluted 1:100 in 10 mL Isoton III. Cells were counted using a CASY 1 TTC cell analyzer (Schärfe System, Reutlingen, Germany). Cell number was calculated automatically by the Casy-stat

software (Schärfe System). The average and standard deviation were calculated using Microsoft Excel.

5.3 Results and Discussion

This study was conducted with two major goals, the first being identification of preparation conditions for redox-sensitive nanogels from thiofunctional prepolymers with precise control over particle size in the range of 150 to 500 nm, the second, being the establishment of an alternative and milder oxidation catalyst than the often used, hydrogen peroxide, so as to enable the encapsulation of oxidation sensitive drugs within the hydrogels and nanogels.

Hydrogen peroxide can oxidize thiols to higher oxidation states. Diverse studies describe the products of thiol oxidation with hydrogen peroxide; however there is no consensus concerning the reaction products obtained at different reaction conditions as well as the possible mechanisms. Based on the experiments performed with small molecular thiol containing compounds, several groups proposed a two-step nucleophilic reaction mechanism involving the rate-determining nucleophilic attack of the thiolate anion on the unionized H_2O_2 to generate cysteine sulfenic acid (CSOH) as an intermediate in a first step. In the case of peroxide excess, this intermediate can undergo a condensation reaction to thiosulfinate or it can further react with H_2O_2 forming sulfinic acid (RSO_2H) and sulfonic acid (RSO_3H) in a subsequent step. This reaction strongly depends on the molar ratio between peroxide and thiol. At molar ratios of H_2O_2: HS ≤ 1, disulfides are the sole reaction product.[14] However, local concentration differences could result in unfavorable side reactions even if the overall stoichiometry is correct, and the high global concentration of hydrogen peroxide generates a strong oxidizing environment.

Alloxan (2, 4, 5, 6-tetraoxypyrimidine) was chosen as an alternative to the direct use of hydrogen peroxide as it provides a slow, homogeneous and molecularly stoichiometric in-situ generation of hydrogen peroxide.[15] Thiols reduce alloxan to dialuric acid, in a exact molar stoichiometry of 1:1. Dialuric acid readily auto-oxidizes back to alloxan by consumption of oxygen. In this process the oxygen is reduced and H_2O_2 is generated which converts the thiols to disulfides. This redox cycling of alloxan is considered to be a slow process with the presence of thiols as driving force of the reaction.[16] Thus it is a step by step in-situ generation and consumption of peroxide at low concentration with

direct formation of disulfide contrary to the use of H_2O_2 as oxidation catalyst where much higher concentrations have to be applied and a stronger oxidizing environment is generated.

As a nanogel precursor, linear poly(glycidol) (**PG**) with a molecular weight of M_w = 4500 g/mol was used. Linear **PG** is a hydrophilic polyether with structural analogy to poly(ethylene oxide) (PEG) and additional hydroxymethylene groups attached to each repeating unit. It is a biocompatible polymer[17] and the molecular weight chosen here is well below the limit for renal clearance of linear PEG (30,000 g/mol).[18] Thiofunctionalization of linear **PG** has been achieved through carbodiimide mediated Steglich esterification between the free hydroxyl groups of the polymers and 3, 3'-dithiodipropionic acid. This reaction yielded hydrogels that were subsequently reduced by cleaving the disulfide cross-linkages to thiol groups. NMR analysis showed that the thiofunctional **PG** (**HS-PG**) contains an average of 15 thiol groups per chain with an overall molecular weight of M_w = 6100 g/mol.

5.3.1 Bulk Gelation Kinetics

Gelation kinetics of bulk hydrogels as a function of pH and time were investigated at first to identify parameter ranges suitable for nanogel preparation. This was particularly important in the case of alloxan as there was no experience with this system in the setup. Generally, the formation of disulfide linkages proceeds through the deprotonated form of thiol groups, so that the reaction only occurs at neutral or basic pH, hence control over the pH value is of critical importance. Thus, in order to maintain slightly basic reaction conditions and to keep the pH value constant, the oxidation reactions were performed in buffer solutions. Bulk experiments showed that simple oxygen mediated gelation took more than 6 h in air at physiological pH (PBS buffer, pH = 7.4). This is too long with respect to inverse miniemulsion stability, so that the use of an oxidation catalyst is indispensable for nanogel formation. Therefore, as described above, hydrogen peroxide and alloxan were used as oxidation catalysts. Both substances are water soluble and any remaining excess can be removed easily by dialysis after gelation. Regardless of the catalyst, the obtained gels were transparent and highly elastic. As expected, for both catalysts the gelation kinetics increases with increasing pH value due to the higher concentration of thiolate anions **(Table 5.3).** However, at the same pH the gelation time differs dramatically when comparing the two catalysts. The hydrogel formation using peroxide was 15, 19 and 17 times faster for pH

6.0, 7.4 and 8.0, respectively, in comparison to the gel formation with alloxan. This observation can be explained by the slow redoxcycle of alloxan and the *in-situ* generation of low amounts of peroxide as compared to the fast oxidation of thiols in the presence of higher concentration of peroxide that is directly added for gelation.

Table 5.3. Bulk gelation kinetics at different pH with H_2O_2 and alloxan

Oxidation catalyst	Gelation time [min]		
[3×10^{-3} mmol]	pH = 6.0	pH = 7.4	pH = 8.0
H_2O_2	8	3	1
Alloxan	125	59	17

Also the influence of the amount of catalyst was investigated at different pH values. **Table 5.4** presents the representative data for the set of experiments performed at pH=7.4 and pH=8.0 for hydrogen peroxide and alloxan, respectively. For alloxan, pH = 8 was chosen so that the reaction is fast, whereas pH = 7.4 was chosen for peroxide so that the reaction was slow enough to allow determination of the gelation time.

Table 5.4. Dependency of catalyst concentration on bulk gelation kinetics.

Amount of Catalyst [mmol]	HS / catalyst ratio	Gelation time [min]	
		H_2O_2 (pH = 7.4)	Alloxan (pH = 8.0)
1×10^{-3}	123	5	32
3×10^{-3}	41	3	17
5×10^{-3}	25	2	16
7×10^{-3}	18	1	15
9×10^{-3}	14	0.7	10
1.1×10^{-2}	12	0.7	10
1.5×10^{-2}	8	0.7	precipitation

It is remarkable that even at the lowest amount of catalyst, where the ratio between SH groups and catalyst was ~120:1, stable and elastic hydrogels were obtained. Up to the value of 7×10^{-3} mmol of added catalyst the reaction kinetics are proportional to the amount of H_2O_2 or alloxan added, however for all catalyst concentrations the reaction is slower in the case of alloxan. For the amounts $\geq 9 \times 10^{-3}$ mmol the gelation time stays constant in both cases. For alloxan, precipitation occurred at 1.5×10^{-2} mmol. This can be attributed to the plateau in cross-linking kinetics in the case of alloxan to its solubility in the reaction mixture, which results in a constant maximum alloxan concentration of around 10^{-2} mmol. In the case of peroxide, accelerated cross-linking upon addition of higher catalyst amount results in rapid and little controlled network formation. At a cross-linking time of 0.7 min, a maximum in the kinetics for the given polymer concentration is reached, so that higher peroxide concentration does not result in faster gelation.

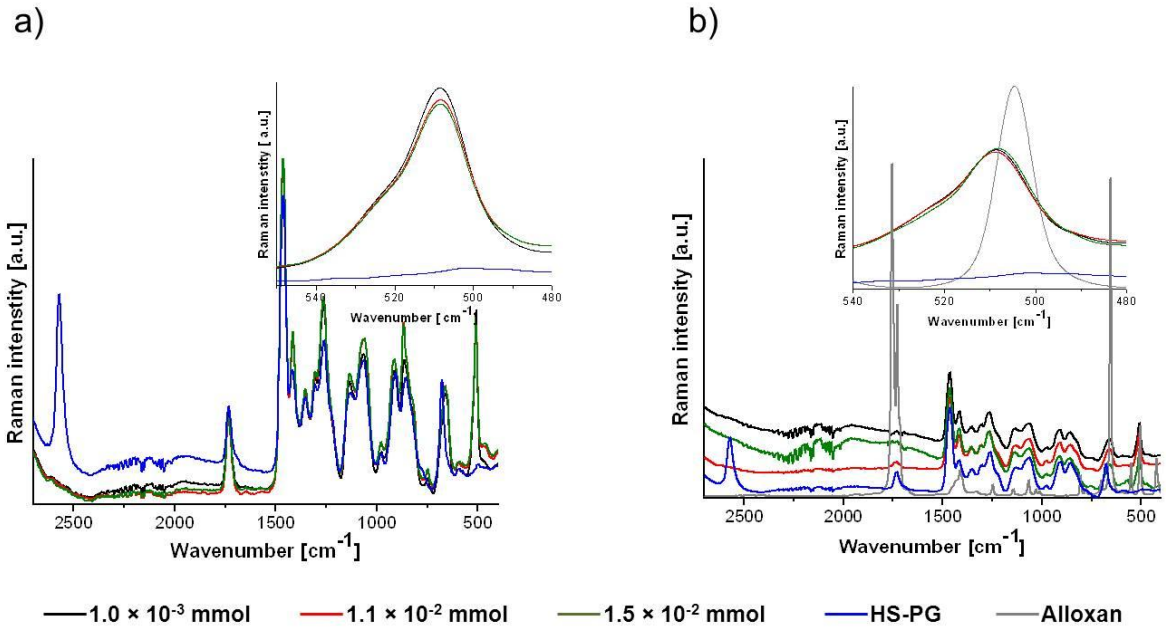

Figure 5.1: Normalized Raman spectra of hydrogels prepared with three different concentrations of (a) H_2O_2 and (b) alloxan. Inset depicts the S-S stretching frequency appearing as a sharp band near 500 cm^{-l}. As control non cross-linked **HS-PG** prepolymer as well as alloxan were measured.

In order to determine and compare the reaction products in the hydrogels prepared with peroxide as well as alloxan, Raman spectroscopy was performed for the different

hydrogels **(Figure 5.1).** Raman spectroscopy is a qualitative tool which gives a clear evidence of the disulfide group since the S-S stretching frequency appears as a sharp band near 500 cm^{-1}.[19]

For the hydrogels prepared with peroxide, increasing the catalyst amount results in a reduction of the S-S band intensity even though in all experiments, the ratio between peroxide and thiol groups was H_2O_2 / HS < 1. This effect supports the hypothesis that a more rapid network formation results in a higher number of free thiol groups that are, due to steric constraints, not able to take part in further network formation. Most probably, the higher amount of free peroxide with increasing amount of added catalyst and the higher amount of remaining free thiols results in formation of oxidation products other than disulfides such as sulfinic and sulfonic acid as reported before by others.[14] These, however, could not be directly detected here due to the overlap of their characteristic bands between 1090 - 990 cm^{-1} and 1070 - 1040 cm^{-1} respectively, with the polymer backbone.

Gels prepared with increasing amount of alloxan did not show any remarkable change in disulfide intensity. This can be attributed to the slower mechanism of thiol oxidation by alloxan in combination with the observed solubility effects. At the fastest gelation time of 10 min, the flexibility of the polymer chains is sufficiently high during cross-linking to result in a constant cross-linking density and thus disulfide content at all alloxan concentrations.

5.3.2 Nanogel Preparation

Based on the data from bulk gelation kinetics, disulfide cross-linked **HS-PG** nanogels were prepared by inverse miniemulsion. One of the crucial steps in creating a stable miniemulsion with well-defined small droplets is the homogenization. Sonication is a widely used homogenization method in a lab-scale batch process in which through constant fusion and fission processes induced by high shear, both the size and polydispersity decrease until the miniemulsion reaches a steady state. The non-ionic surfactants used for stabilizing inverse miniemulsions allow droplets preparation in the size range from 100 to 800 nm. The stability of these droplets is limited, however, due to coalescence and Ostwald ripening. Suppression of these two processes is required for the formation of a stable miniemulsion.[20] While coalescence can be controlled by choosing the appropriate surfactant or surfactant mixture, Ostwald ripening can be controlled by the addition of hydrophilic agents into the dispersed phase.[21] In this

system the aqueous phase was composed of PBS buffer which did not only serve as stabilizing agent preventing the Ostwald ripening, but also provided a basic medium for the deprotonation of thiols as first and rate limiting step for oxidation to disulfides. A PBS concentration of 0.04 M yielded most well defined particles. At lower PBS concentrations the stability of the miniemulsion was not sufficient for the cross-linking reaction so that polydisperse particles were produced, while higher concentrations caused poor polymer solubility. In all experiments the water to oil ratio was kept constant at 1:10.

With these core settings, the dependence of different parameters on particle size and size distribution including sonication time, surfactant and surfactant combination, catalyst and polymer concentration have been assessed through systematic variation of concentrations and ratios. As standard surfactant mixture, Span 80 / Tween 80 = 3 / 1 (weight ratio) were used for initial examination of the influence of sonication time, while a detailed study of different surfactant combinations were performed subsequently.

5.3.2.1 Sonication Time before Catalyst Addition

It was observed that variation of the sonication time before catalyst addition strongly affects size and size distribution of the nanogels. **Table 5.5** presents and compares the diameter z-average as well as polydispersity index (PDI) values obtained from dynamic light scattering (DLS) analysis for sonication times ranging from 60 to 1500 s before catalyst addition with a constant sonication of 60 s after catalyst addition. In the case of peroxide as oxidation catalyst, up to 240 s only marginal changes in the average nanogel size were observed. Increase of the sonication time to 300 s results in a drastic z-average decrease and to considerable lower PDI values in comparison to the values obtained with shorter sonication times. Also, at 300 s, nanogels smaller than at sonication times below 360 s with a relatively low PDI of 0.245 were obtained, while further increase of the sonication time leads to a strong increase in nanogel size and PDI up to micrometer range for 600 s followed by precipitation of larger aggregates at even longer sonication times.

In contrast, the diameter of the nanogels prepared with the alloxan changes only slightly as a function of sonication time. The z-average remains at ~ 270 nm for sonication times up to the 240 s. Similarly to nanogels prepared with peroxide, the particle diameter as well as PDI decreases at a sonication time of 300 s to the smallest

particles (diameter 200 nm) with lowest PDI (0.174). Further increase of the sonication time results in a slight increase of the particle size as well as the PDI. However, in contrast to the particles prepared by peroxide, no formation of micrometer sized particles or aggregation was observed.

Table 5.5. Influence of sonication time before addition of catalyst on nanogel size

Sonication time before addition of catalyst [s]	H_2O_2		Alloxan	
	Z-average	PDI	Z-average	PDI
60	350±13	0.410±0.010	260±10	0.151±0.002
120	350±10	0.231±0.008	270±10	0.210±0.002
180	350±09	0.320±0.012	270±10	0.210±0.001
240	400±15	0.420±0.021	270±13	0.340±0.005
300	150±11	0.175±0.013	200±12	0.174±0.010
360	250±11	0.245±0.021	250±10	0.230±0.006
420	450±10	0.350±0.012	250±12	0.310±0.007
600	1050±17	1.000±0.012	330±12	0.330±0.006
1500	-[a)]	-[a)]	350±10	0.350±0.008

[a)] Precipitation of large aggregates

The formation of large particles and the precipitation with longer sonication times in the case of peroxide can be thus attributed to instabilities in the miniemulsion caused by long sonication times. Due to the strong oxidation potential of peroxide and the high specific surface of the particles in comparison to bulk gels, the cross-linking times are much shorter so that the larger aggregates are immediately fixed through rapid cross-linking by addition of peroxide. For alloxan, the cross-linking is still sufficiently slow to allow homogenization of the dispersion with the second sonication step. This significantly reduces the effects of the first sonication step before addition of the catalyst on nanogel size and PDI.

Cryo-FESEM images were taken of nanogel samples prepared with 60s/60s, 300s/60s and 360s/60s sonication time for direct visualization of the nanogels in the quasi-swollen state. Nanogel size was determined for 300 nanogel particles for each sample with the help of Quartz PCI software and a Gaussian curve was drawn and average nanogel size was determined. In all cases, cryo-FESEM images of the samples show that the particles have well-defined spherical shapes, as expected for particles synthesized by miniemulsion techniques (**Figure 5.2 and 5.3**)

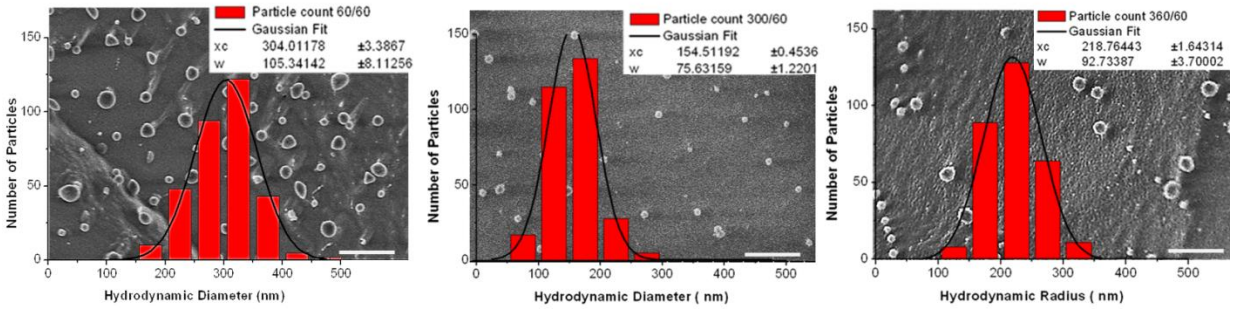

Figure 5.2: Cryo-FESEM images, particle size Gaussian curve from size distribution histograms show the difference in nanogel diameter at sonication time of 60s/ 60s , 300s/60s, 360s/60s prepared by oxidation with H_2O_2. Scale bar in the cryo-FESEM images corresponds to 1 μm.

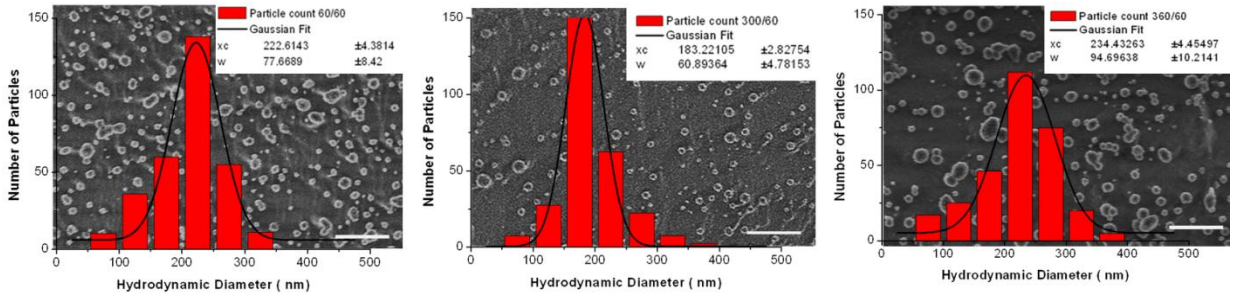

Figure 5.3: Cryo-FESEM images, particle size Gaussian curve from size distribution histograms show the difference in nanogel diameter at sonication time of 60s/ 60s, 300s/60s, 360s/60s prepared by oxidation with alloxan. Scale bar in the cryo-FESEM images corresponds to 1 μm.

The size evaluation by DLS measurement was in very good accordance with cryo-FESEM and the particle size trends with changing sonication time before addition of the catalyst were confirmed, showing that both methods correlate well to each other with respect to size analysis of the nanogels in the hydrated state. These results show that

by proper choice of the sonication time before catalyst addition, size of the nanogels can be tailored in the range between 150 and 450 nm.

5.3.2.2 Sonication Time after Catalyst Addition

While a variation of sonication time before addition of the catalyst showed strong influence on particle size, variation of sonication time after catalyst addition did not show significant effect on particle size. In a first series of experiments, the sonication time before the addition of catalyst was kept constant at 60 s and the sonication time after the catalyst addition was varied from 60 s up to 1200 s. **Table 5.6** presents and compares the diameter z-average as well as polydispersity index (PDI) values obtained from dynamic light scattering (DLS) analysis.

Table 5.6. Influence of sonication time after addition of catalyst on nanogel size

Sonication time after addition of catalyst [s]	H_2O_2		Alloxan	
	Z-average	PDI	Z-average	PDI
60	350±13	0.410±0.010	260±12	0.151±0.001
120	400±20	0.334±0.012	260±15	0.220±0.020
180	400±15	0.392±0.012	260±10	0.220±0.013
240	400±22	0.318±0.014	300±15	0.250±0.001
300	420±20	0.301±0.002	300±14	0.248±0.018
360	420±16	0.344±0.004	300±15	0.290±0.017
420	500±23	0.375±0.006	220±15	0.208±0.003
600	-[b]	-[b]	220±17	0.250±0.004
1000	-[b]	-[b]	300±11	0.250±0.003
1200	-[b]	-[b]	1060±20	0.551±0.005

[b)] Precipitation of large aggregates

In the case of the peroxide, the diameter z-average increased gradually up to the value of 500 nm for 420 s. Further increase of the sonication time led to the formation of visible large aggregates. When alloxan is used as a catalyst the diameter of particles first increases slightly up to 300 nm at sonication time of 360 s, then it decreases to

220 nm at 420 s and 600 s, followed by a dramatic z-average increase to 1060 nm for the sonication time of 1200 s.

These results suggest that long sonication times lead to destabilization of the emulsion which favours particle aggregation. In addition, despite of ice cooling, longer sonication can cause a certain bulk thermal heating caused by longer shear times. Since in the system there is still a small fraction of highly reactive peroxide present longer sonication time could lead to formation of free radicals. These can further interact with the polymer network and support inter-particle aggregation. As the amount of peroxide is much lower in the case of alloxan, this mechanism is not of major importance for the nanogels prepared with alloxan, so that much longer sonication times can be used for the generation of nanogels.

From the obtained results it can be concluded that after cross-linking nanogel size was relatively unaffected by sonication time. For the nanogels prepared with the peroxide, the slight change of the z-average is proportional to the sonication time while for alloxan nanogels the change is rather random. Only at long sonication times, regardless of the catalyst used, over sonication led to the formation of large aggregates. Based on these results all further experiments were performed by the sonication for 60 s after the catalyst addition

5.3.2.3 Influence of the Surfactants and the Hydrophilic-Lipophilic Balance (HLB)

The choice of appropriate surfactant and surfactant combination is a key to reducing the rate of the coalescence of the dispersed droplets and thus increasing the miniemulsion stability. Generally, the application of one component surfactant system results in poorly packed interfacial films leading to low emulsion stability. Often, a combination of surfactants is used with one water-soluble and one oil-soluble surfactant. Correlation between the chemical structure of the surfactant and its ability to form stable interfacial film is trivial and is unique for each miniemulsion system.[22] A frequently used indicative approach for predicting the surfactant emulsification behaviour is a so called HLB method which shows the relationship between hydrophilic and hydrophobic fraction of the molecule as discussed in **Chapter 4**.

Particle size dependence at different HLB's in the range of 5 to 8 was investigated with three different sonication time parameters 60s/60s, 300s/60s and 360s/60s **(Table 5.7)**. A desired HLB value was obtained by changing the weight ratio of two surfactants

according to **Equation 5.1**. The weight ratios of emulsifiers to reaction ingredients was always kept constant at 5 wt. %.

$$HLB = [4.3 \times x] + [15.0 \times (1-x)] \quad \text{Eq.5.1}$$

Where x is the weight fraction of Span 80. Values of 4.3 and 15 denote the HLB of Span 80 and Tween 80, respectively.

Table 5.7 Influence of HLB in Span80/Tween 80 blend on nanogel size

Sonication time before catalyst addition [s]	HLB	H_2O_2		Alloxan	
		Z-average [nm]	PDI	Z-average [nm]	PDI
60	5	350±12	0.230±0.010	350±12	0.201±0.004
60	6	450±15	0.439±0.012	300±15	0.210±0.002
60	7	350±13	0.410±0.010	260±10	0.151±0.002
60	8	650±18	0.446±0.006	380±21	0.251±0.004
300	5	300±20	0.199±0.007	210±15	0.230±0.010
300	6	300±13	0.262±0.006	200±17	0.200±0.008
300	7	150±11	0.175±0.013	200±12	0.174±0.010
300	8	350±13	0.387±0.010	300±18	0.190±0.007
360	5	300±11	0.230±0.012	280±13	0.250±0.010
360	6	275±21	0.310±0.008	280±14	0.210±0.010
360	7	250±11	0.245±0.021	250±10	0.230±0.006
360	8	400±14	0.275±0.014	300±11	0.245±0.009

From the results presented in **Table 5.7** one can see that in almost all cases, at each sonication time applied and regardless of the catalyst used the nanogel diameter changes only slightly for HLB 5 and 6 followed by size and PDI decrease at HLB = 7.

Subsequently, at HLB = 8 size as well as size distribution increase is observed. According to the Bancroft rule the phase in which the surfactant is most soluble forms the continuous phase. In case of HLB = 8 the surfactant serves rather as wetting agent than as a emulsifier since, showing more solubility in the aqueous phase, the interfacial gradient cannot develop and the droplets start to coalesce yielding broader distribution of nanogel size. Summarizing, regardless of the oxidation agent and sonication time applied, nanogels with the lowest z-average diameter and PDI were obtained at HLB = 7.

Based on the results presented in the previous section, the influence of different combinations of commercially available nonionic surfactants and co-surfactants at constant HLB = 7 was investigated. As oil soluble surfactants, Span 80 as well as Span 60 (HLB = 4.7) were used. Next to Tween 80 both Brij 30 (Laureth 4) (HLB = 9.7) as well as Laureth 3 (HLB = 8.0) were applied as water soluble co-surfactants. As seen from **Table 5.8**, nanogels prepared with surfactant/co-surfactant combination of Span 60 / Tween 80 and Span 80 / Tween 80 showed narrow PDI with small particle size at sonication time of 300s/60s whereas nanogels prepared with other surfactant combinations at this sonication time exhibited broader size distribution.

This difference, especially profound in the case of Span80/Brij 30 system, is not immense; however, it demonstrates that a careful selection of the appropriate emulsifying system has an impact on the size and polydispersity of the particles. A possible explanation for this behavior is a lower HLB of the co-surfactants Brij 30 and Laureth3, making the interfacial film not closely-packed and thus mechanically weak and less stable in comparison to a better water soluble Tween 80. Comparable results obtained with Span 60 and Span 80 is due to similarity in their molecular structure with only difference in the presence of a one double bond in a hydrophobic tail leading to a slightly better solubility of Span 80 in the oil phase. The yield of nanogels in all cases was between 85-90% with respect to the amount of polymer used was calculated by the dry mass of the nanogels after dialysis.

Table 5.8 Influence of type of surfactant at HLB 7 on nanogel size

		H_2O_2		Alloxan	
Surfactants	Sonication [s]	Z-average [nm]	PDI	Z-average [nm]	PDI
Span 60 : Tween 80	60/60	300±15	0.308±0.008	300±12	0.268±0.001
	180/60	200±20	0.267±0.010	275±14	0.275±0.005
	300/60	200±21	0.211±0.010	250±20	0.242±0.004
	360/60	250±23	0.240±0.011	275±12	0.215±0.005
Span 80 : Brij 30	60/60	450±12	0.433±0.012	375±14	0.310±0.006
	180/60	400±18	0.365±0.012	350±16	0.250±0.010
	300/60	350±13	0.417±0.011	300±19	0.301±0.006
	360/60	375±16	0.350±0.010	300±20	0.285±0.010
Span 80 : Laureth 3	60/60	250±17	0.232±0.008	200±21	0.250±0.010
	180/60	250±15	0.318±0.002	250±15	0.351±0.007
	300/60	200±15	0.390±0.003	250±18	0.210±0.006
	360/60	250±16	0.351±0.006	270±20	0.250±0.010
Span80 : Tween 80	60/60	350±13	0.410±0.010	260±10	0.151±0.002
	180/60	350±09	0.320±0.012	270±10	0.210±0.001
	300/60	150±11	0.175±0.013	200±12	0.174±0.010
	360/60	250±11	0.245±0.021	250±10	0.230±0.006

5.3.2.4 Influence of the Catalyst Amount

With decreasing amount of the oxidation catalyst one would expect an increase in nanogel size due to pronounced swelling as a result of low cross-linking in comparison to a high amount of catalyst employed where the nanogel size is expected to shrink as a result of high cross-linking density. However, remarkable changes in the nanogel size were not observed showing that cross-linking was very efficient with respect to the amount of catalyst used **(Table 5.9).**

Table 5.9. Influence on nanogel size with varying catalyst amount

Amount of Catalyst	H_2O_2		Alloxan	
[mmol]	Z-average	PDI	Z-average	PDI
1×10^{-3}	300±13	0.216±0.010	270±12	0.176±0.001
3×10^{-3}	350±21	0.410±0.010	260±12	0.151±0.005
5×10^{-3}	250±20	0.406±0.011	250±13	0.210±0.004
7×10^{-3}	250±22	0.495±0.008	250±12	0.340±0.007
9×10^{-3}	250±21	0.372±0.009	250±11	0.215±0.010
1.1×10^{-2}	275±19	0.401±0.010	240±10	0.210±0.010

This is in accordance to the results obtained with the bulk hydrogels. In addition, higher cross-linking density of the nanogels is not possible most likely due to the constrained confinement of polymer chains in the small miniemulsion droplets, even when a very high shear force produced by sonication allows the catalyst to be homogeneously distributed within the aqueous droplet.

5.3.2.5 Influence of Polymer Amount

In all experiments described so far the prepolymer concentration was 40 w/v %. In this section, the influence of the amount of prepolymer on the particle size at two additional concentrations: 28 and 12 w/v % and at different sonication times is shown. From the data presented in **Table 5.10** it can be clearly seen that a decrease in polymer concentration leads to an increase of nanogel size.

Table 5.10 Influence of polymer amount

Sonication time [s]	Polymer concentration [w/v %]	H_2O_2		Alloxan	
		Z-average [nm]	PDI	Z-average [nm]	PDI
60/60	40	350±13	0.410±0.010	260±10	0.151±0.002
60/60	28	450±13	0.400±0.009	300±13	0.175±0.002
60/60	12	480±14	0.375±0.006	350±12	0.180±0.008
300/60	40	150±11	0.175±0.013	200±12	0.174±0.010
300/60	28	250±14	0.125±0.008	250±15	0.220±0.008
300/60	12	275±15	0.123±0.018	250±18	0.250±0.006
360/60	40	250±11	0.245±0.021	250±10	0.230±0.006
360/60	28	300±16	0.290±0.011	300±11	0.250±0.010
360/60	12	375±16	0.310±0.008	325±12	0.275±0.010

This tendency is apparent for both catalysts to the comparable extent. Since the sonication time, water oil ratio and the surfactant amount are kept constant, the size of the water droplets is most likely not affected by the polymer mass. However, by increasing the polymer amount the molar concentration of thiols in each water droplet increases. Thus, a higher concentration of the polymer results in increased cross-linking density which decreases the relative swelling of nanogels and hence also the hydrodynamic radius in comparison with nanogels prepared using lower thiol-polymer concentration.

5.3.3 Stability of Nanogels and Nanogel dispersions

A prerequisite for nanoparticles that are intended for biomedical applications is their maintained integrity under physiological conditions for at least the time they need to actively or passively accumulate in or close to the target cells. For intravenous administration this usually occurs rapidly within minutes and hours so that particle stability under physiological conditions for 48h is sufficient. Nanogel dispersions were incubated in PBS buffer at 37 °C for 60 h and samples were taken at 0 h, 0.25 h, 1 h, 6 h, 12 h, 24 h and 60 h to assess NP size and aggregation by DLS and cryo-FESEM **(Figure 5.4)**. No significant changes in size and polydispersity could be determined by

DLS and cryo-FESEM performed with nanogels incubated for 0 h and for 60 h demonstrating no conspicuous difference in morphology of both samples after incubation at 37°C for 60h. These results show that nanogels remain stable in physiological conditions making them appropriate candidates for *in-vitro* applications.

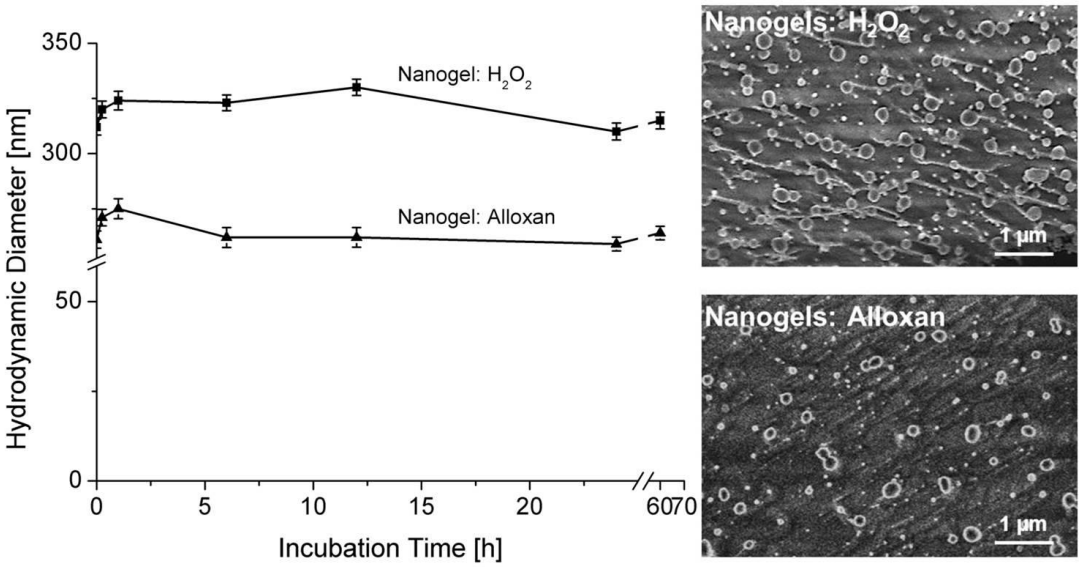

Figure 5.4: Nanogel stability at pH = 7.4 and 37 °C. Left: hydrodynamic diameter determined from DLS after 0 h, 0.25 h, 1 h, 6 h, 12 h, 24 h and 60 h; right: cryo-FESEM of nanogels after 60 h incubation.

5.3.4 Biodegradation of Nanogels

Nanogels degradation was investigated in the presence of GSH, a tripeptide with a free thiol group, which readily cleaves disulfides to thiols. It is present in the cytosol of mammalian cells with a concentration in the range of 0.5–10 mM and acts as major protection against oxidants such as reactive oxygen species. When reacting with oxidants, GSH itself is oxidized and forms disulfides (GSSG). In a healthy cell, 90% of GSH is present in the reduced form. In contrast to the fluid inside cells, the concentration of GSH in blood and the extracellular matrix (ECM) is lower than 20 μM.[23] This high redox potential difference between the neutral or oxidizing extracellular space and the reducing intracellular space makes disulfide cross-linked particles especially attractive as drug delivery systems due to the possibility of controlled biodegradation of the cross-linked network, and thus quantitative drug release in the cytosol.[7, 8]

As shown in **(Figure 5.5 a, left vial)** purified nanogels dispersed in water had a turbid appearance. Upon addition of water-soluble GSH as a reducing agent (total GSH concentration was 10 mM), the nanogel dispersion turned into a transparent solution caused by nanogel degradation into individual polymeric chains **(Figure 5.5 a, right vial)**. The nanogel degradation was also further confirmed by optical fluorescence microscopy with Alexa Fluor 488 labelled particles. Before the degradation, particle aggregates appear as individual bright green spots on the dark background **(Figure 5.5 c)**.

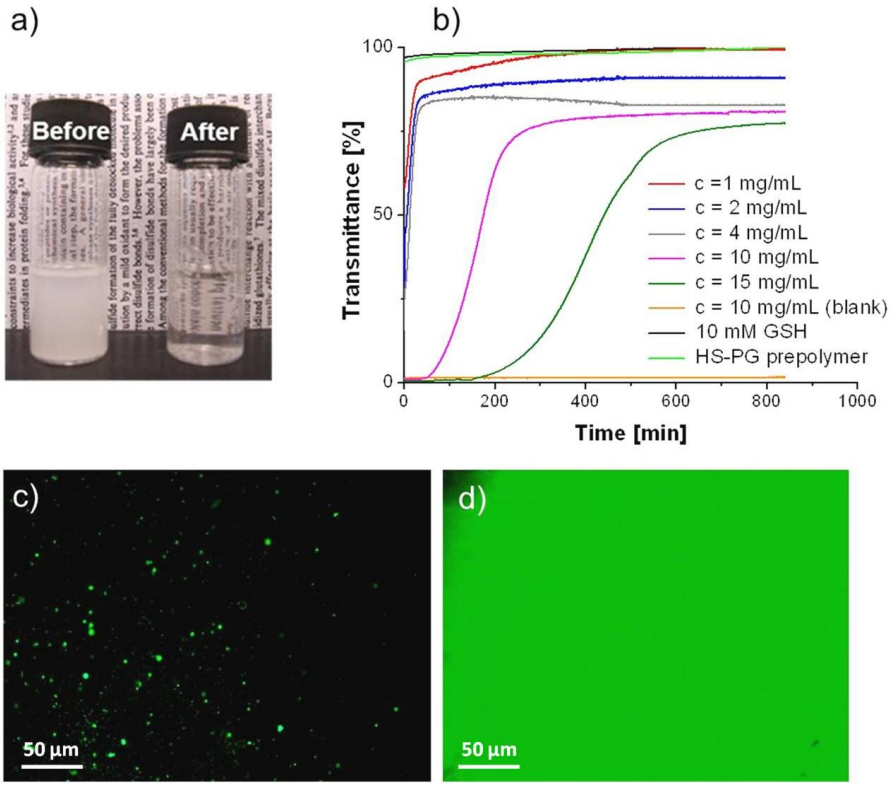

Figure 5.5: Reductive degradation of the nanogels by 10 mM GSH: (a) vials containing PBS nanogel solutions before and after reduction; (b) Transmittance study performed by UV-Vis method with different concentrations of nanogel solution. Optical fluorescence microscopy images of Alexa Fluor 488 conjugated nanogels (c) before and (d) after degradation.

This implies that the dye is conjugated to the particles since the non-bound dye was successfully removed by the dialysis. Upon GSH addition, the fluorescent signal is spread as shown in **Figure 5.5 d,** depicting a completely green background, which proves disulphide reduction and thus nanogel degradation. Assessment of reduction kinetics in the presence of 10 mM GSH was followed by transmission measurements in

PBS buffer at 37 °C **(Figure 5.5 b).** In this experiment the milky nanogel solutions turn transparent upon reduction resulting in an increase in the transmittance. Five different nanogel concentrations were studied while the GSH concentration remained constant. As a control, nanogels without addition of GSH (blank), 10 mM GSH solution as well as **HS-PG** prepolymer solution (c = 15 mg/mL) were used. The transmission of blank solutions (without GSH) remained constant, showing no degradation while the transmittance of GSH and **HS-PG** was 100 % throughout the measurement. For the 1, 2 and 4 mg/mL concentrated solutions the burst reduction was observed within first 40 min, followed by a plateau, where no further increase in transmittance was monitored. The transmittance of higher concentrated 10 mg/mL and 15 mg/mL solutions showed an induction period of 50 and 150 min and then reached a plateau after 260 and 600 min, respectively. The induction period observed in both samples with high concentration indicates a mechanism of reduction via surface erosion. The 100 % transmittance was observed only for 1 mg/mL solutions, while for more concentrated solutions it was below 100 % showing incomplete reduction of the particles. The experiments were also performed at lower GSH (1 and 5 mM) concentrations. For three different concentration of nanogels (4, 8 and 12 mg/mL) at pH = 7.4 and 37 °C.

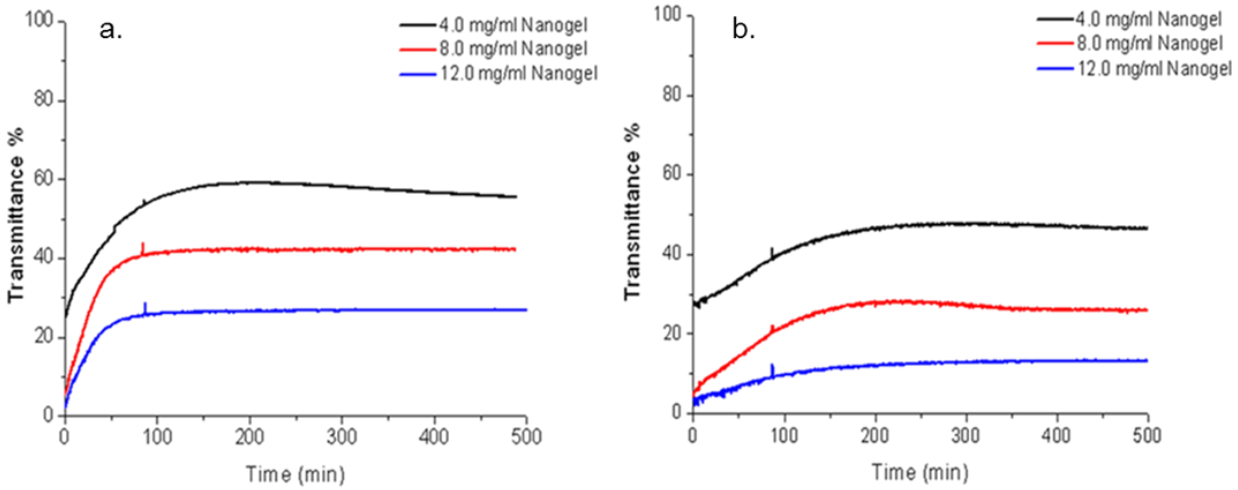

Figure 5.6: UV-Vis spectra showing nanogel reduction kinetics in PBS buffer at 37 °C with a) 5 mM GSH and b) 1 mM GSH.

Transmission measurements performed by UV-Vis spectroscopy at 500 nm for 1000 min were used to monitor the kinetics. It was observed that the increase in transmittance was in the range of 25-30 % and 10-20 % for 5 mM GSH and 1 mM reduced solutions, respectively **(Figure 5.6).** The plateau, where no further

transmittance increase was observed was reached within 100 min for 5 mM and 150 min for 1 mM solutions, showing incomplete nanogel reduction at such low GSH concentrations.

Subsequently, following the procedure described by Cerritelli *et al*.[24] another test of reductive sensitivity was carried out by multiple additions of the same total amount of GSH to the nanogels dispersions in the cuvette **(Figure 5.7).** Thus, in this experiment, a stronger reduction effect could be obtained in the presence of a more constant level of reduction potential, simulating the situation inside a living cell where the redox-potential is actively kept constant. The transmission of blank solutions (without GSH) remained constant throughout the measurement showing no degradation

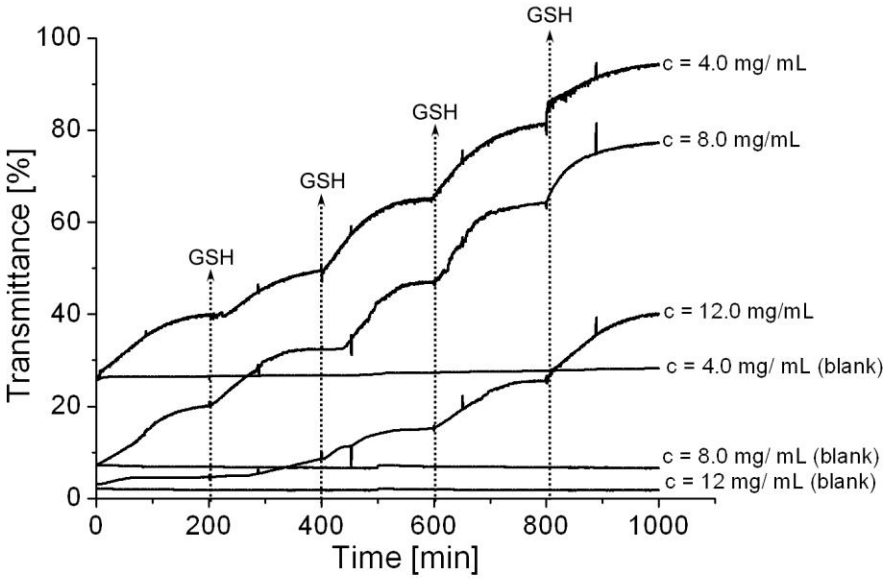

Figure 5.7: Transmittance measurement of nanogel solutions performed after multiple additions of GSH. The final GSH concentration was 1 mM at the beginning of each step.

Indeed, addition of 1 mM GSH solution in 200 min steps led eventually to transparent solutions within 1000 min in the case of 4 mg /mL concentrated samples **(Figure 5.7).** It is however to be noted that all reduction experiments described in this section are qualitative and are only indicative with respect to the *in-vivo* case, where the total particle concentration in the cell will be much smaller then presented in this study.

5.3.5 Cytocompatibility of the Nanogels

Both types of nanogels were assessed for cytocompatibility according to DIN EN ISO 10993-5 at concentrations of 10 mg/mL, 5 mg/mL and 1.5 mg/mL. After incubating L929 cells with nanogels for 48h, light microscopy was used to assess cell morphology. There was no difference in cell morphology comparing control cells to nanogel treated cells. Counting of live cells indicated more than 90 % viable L929 mouse fibroblasts when compared to the untreated control. The viability of L929 mouse fibroblasts cells in the presence of nanogels as assessed by the WST test was the same as the cell viability of control cells on TCPS in DMEM without nanogels.

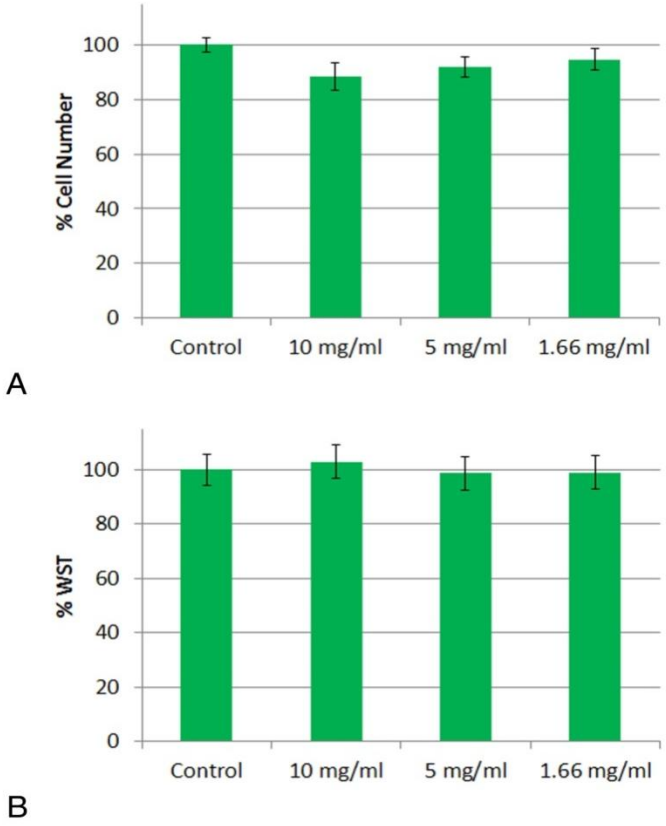

Figure 5.8: Nanogel cytocompatibility at three different concentrations after 24 h incubation with L929 mouse fibroblasts cells demonstrated through cell numbers (a) and cell vitality (b) in comparison to control experiments on TCPS, respectively.

Cells grown in nanogel medium were healthy and not optically different to the control cells. No significant difference was observed for nanogels prepared by peroxide or alloxan. These results show that during the course of incubation, no endotoxins or other cytotoxic compounds were released and that the nanogels as such are cytocompatible even at a high concentration of 10 mg/mL **(Figure 5.8).**

5.4 Conclusion

This study is concerned with the preparation of redox-sensitive nanogels through oxidative coupling of thiofunctional polymers in inverse miniemulsion. Comparison of hydrogen peroxide and alloxan, a milder oxidation catalyst, with respect to their applicability for the preparation of nanogels from thiofunctional poly(glycidols) and especially their suitability for precise control over nanogel size and size distribution was performed. Multiple parameters such as the sonication time, the amount of catalyst, the amount of polymer and the HLB value were systematically changed, and the conditions were identified that allow the preparation of nanogels with sizes between 150 and 350 nm and good size distributions. *In vitro* degradation of the nanogels under cytosolic conditions using glutathione (GSH) as reducing agent as well as cytocompatibility of the nanogels with concentrations up to 10 mg/mL using L929 fibroblasts was demonstrated. These results demonstrate that also mild oxidation catalysts such as alloxan can be used for the preparation of redox-sensitive nanogels that specifically degrade in cytosolic conditions, thus broadening the range of possible payloads. Current and ongoing studies concern the loading of and release from such nanogels with protein drugs as well as studies on cellular uptake and subsequent particle degradation and payload release.

5.5 References

[1] S. Mitragotri, J. Lahann, *Nat. Mater.* **2009**, 8, 15.

[2] J. Rejman, V. Oberel, I. S. Zuhorn, D. Hoekstra, *Biochem. J.* **2004**, 377, 159.

[3] A. Prokop, M. J. Davidson, *J. Pharm. Sci.* **2008**, 97, 3518.

[4] V. J. Mohanraj, Y. Chen, *Tropical J. Pharm. Res.* **2006**, 5, 561.

[5] M. P. Desai, V. Labhasetwar, G. L. Amidon, R. J. Levy, *Pharm. Res.* **1996**, 13, 1838.

[6] H. M. Redhead, S. S. Davis, L. Illum, *J. Control. Rel.* **2001**, 70, 353.

[7] J. Cheng, B. A. Teply, I. Sherifi, J. Sung, G. Luther, F. X. Gu, E. L. Nissenbaum, A. F. R. Moreno, R. Langer, O. C. Farokhzad, *Biomaterials* **2007**, 28, 869.

[8] S. M. Moghimi, C. J. H. Porter, I. S. Muir, L. Illum, S. S. Davis, *Biochem. Biophy. Res. Comm.* **1991**, 177, 861.

[9] K. J. Oh, J. D. Siegwart, H. Lee, G. Sherwood, L. Peteanu, O. J. Hollinger, K. Kataoka, K. Matyjaszewski, *J. Am. Chem. Soc.* **2007**, 129, 5939.

[10] A. Bernkop-Schnürch, A. Heinrich, A. Greimel, *Eur. J. Pharm. Biopharm.* **2006**, 63, 166.

[11] H. Lee, H. Mok, S. Lee, K. Y. Oh, G. T. Park, *J. Control. Rel.* **2007**, 119, 245.

[12] K. Albrecht, M. Moeller, J. Groll, *Adv. Polym. Sci.* **2011**, 234, 65.

[13] J. Groll, S. Singh, K. Albrecht, M. Moeller, *J. Polym. Sci. Part A: Polym. Chem*. **2009**, 47, 5543.

[14] D. Luo, W. S. Smith, D. B. Anderson, *J. Pharm. Sci.* **2005**, 94, 304.

[15] AplaGen, Process for Forming Disulphide Bridges US Patent Application 20100203001, August 12, **2010**.

[16] (A) I. Miwa, J. Okuda, *Biochem. Pharmacol.* **1982**, 31, 921. (B) S. Lenzen, R. Munday, *Biochem. Pharmacol*. **1991**, 42, 1385. (C) H. J. Broemmel, R. Weinandy, D. Peschke, E. Peschke, *Horm. Metab. Res*. **2001**, 33, 106.

[17] K. R. Kainthan, J. Janzen, E. Levin, V. D. Devine, E. D. Brooks, *Biomacromolecules* **2006**, 3, 703.

[18] T. Yamaoka, Y. Tabata, Y. Ikada, *J. Pharm. Sci.* **1994**, 83, 601.

[19] R. Tuma, S. Vohnik, H. Li, G. J. Thomas, *Jr. Biophysical Journal* **1993**, 65, 1066.

[20] Z. B. Putlitz, K. Landfester, H. Fischer, M. Antonietti, *Adv. Mater*. **2001**, 13, 500.

[21] T. Tadros, P. Izquierdo, J. Esquena, C. Solans, *Adv. Colloid. Interface Sci.* **2004,** 108, 303.

[22] Milton J. Rosen: Surfactants and Interfacial Phenomena 3rd Edition, Wiley-Interscience, **2004**.

[23] (A) A. Meister, E. M. Anderson, *Annu. Rev. Biochem.* **1983**, 52, 711. (B) G. Wu, Z. Y. Fang, S. Yang, R. J. Lupton, D. N. Turner, *J. Nutr.* **2004**, 134, 489.

[24] S. Cerritelli, D. Velluto, J. A. Hubbell, *Biomacromolecules* **2007**, 8, 1966.

CHAPTER 6

Embedding of Active Proteins and Living Cells in Redox-Sensitive Hydrogels and Nanogels through Enzymatic Cross-Linking

Part of this work is published in Angewandte Chemi DOI: 10.1002/anie.201206266

6.1 Introduction

Redox-sensitive materials have gained interest significantly over the last few years.[1] Disulfide cross-linked networks are particularly appealing, as disulfides are structure-forming groups in proteins as well as in natural processes and conditions in cells exists which allows reductive scission of these covalent links. Hence, such materials are predetermined for drug delivery, as disulfides are rapidly reduced to thiols under the reductive environment inside cells allowing quantitative release of the payload incorporated within the particles.[2] Disulfide cross-links can be introduced by using disulfide containing cross-linkers during particle preparation by polymerization,[3] or by the coupling of thiol functional precursors [4] which allows covalent binding of cysteine-terminated drugs (for example peptides) to the particle matrix by the disulfide bonds. Oxidation of thiol bearing matrix molecules is possible solely upon exposure to air[5] but is relatively slow and not useful for many nanoparticle preparation techniques. Therefore, different oxidizing catalyst may be applied in order to shorten oxidation times.[6] Hydrogen peroxide is the one often used but is cytotoxic and due to its strong oxidation potential, disulfides are not its sole reaction products with thiols[7] as discussed in **Chapter 5**, therefore the number of possible payloads is restricted. Enzymes as biological catalysts can be used to mediate hydrogel formation with the advantages of i) cross-linking under mild conditions, ii) unique chemo-, regio, enantioselectivity, iii) no need for toxic cross-linkers, and iv) biologically controlled gelation. A number of studies have thus been reported on enzyme-mediated hydrogelation.[8-10] Inspired by the natural

gelation process of fibrin, Lutolf *et al.* have used used transglutaminase to cross-link polymers to form hydrogels. They used this process to generate cell adhesion peptide functionalized hydrogels that are also degradable by matrix metalloproteases.[11]

Approaches for the enzymatic cross-linking of hydrogels especially for biomedical applications have most recently been reviewed.[12] This overview shows that enzymatic cross-linking has so far always resulted in networks for which degradation is either possible through enzymatically catalyzed cleavage of covalent bonds or rather harsh and not cytocompatible chemical conditions like drastic pH changes. Horseradish peroxidase (HRP) is one of the most studied oxidation-catalyzing enzyme due to its catalytic role on a wide range of substances.[13] However, the conventional HRP cycle involves its reaction with H_2O_2 resulting in formation of reactive intermediates, so that addition of hydrogen peroxide is necessary for HRP mediated cross-linking.[14-16] Herein the HRP-mediated preparation of functional, redox-sensitive disulfide-cross-linked hydrogels and nanogels through the gelation of thiomers without the requirement of H_2O_2 is described.

.

6.2 Experimental

6.2.1 Materials and Methods

Linear poly(glycidol) (**PG**) (M_n = 4500 g/mol, M_w/M_n = 1.17) was synthesized as mentioned in Chapter 3. N,N-dicyclohexyl-carbodiimide (DCC, Acros, 99%), 4-(dimethylamino) pyridine (DMAP, Aldrich, 99%), 3,3'-dithiodipropionic acid (DTPA, Aldrich, 99%), tris(2-carboxyethyl) phosphine (TCEP, Aldrich, 99%), dichloromethane (HPLC grade, Aldrich), cysteamine (2-mercaptoethylamine, Biochemica), 5,5'-dithio-bis(2-nitrobenzoic acid) (DTNB, Merck), anhydrous N,N-dimethylformamide (DMF, Sigma-Aldrich, 99.8%), Span 80 (Sigma), and Tween 80 (Sigma-Aldrich), pyragallol (≥ 98%, Sigma), immobilised TCEP (Thermo Scientific), AGBBB015F peptide (3230 g/mol, AplaGen), glutathione (≥ 98%, Sigma), Caffeine (Sigma) were used as received. THF was dried over $LiAlH_4$. Horseradish peroxidase with an initial enzymatic activity of 320 U/mg was purchased from CalBioChem. Dialysis membranes (MWCO: 3500 Da, 20,000 and 100,000 Da) were purchased from Spectrum Laboratories.

6.2.2 Bulk Hydrogel Synthesis.

(0.150 g, 3.33 × 10^{-2} mmol) was dissolved in 350 μL buffer at pH 7.4, 8.0, 8.5 and was mixed thoroughly. To this solution HRP was added in different molar ratios. The bulk gelation of **HS-PG** was induced by addition of four different equivalents of HRP with respect to thiol functionalities present in the polymer backbone as –SH : HRP: 1:0.01, 1:0.02, 1:0.04, 1:0.08. In order to test the role of HRP in gelation, samples with PG was also monitored for 24 h without addition of HRP.

6.2.3 Rheological Analysis of Bulk Hydrogels

Dynamic oscillatory deformation measurements were performed with a Bohlin CVR-50 (Malvern Instruments Ltd, England) in a cone-plate configuration. The upper plate (cone plate 1^{o}, 20 mm) was set at a distance of 150 μm before the onset of the reactions. During all the rheological measurements, a thin film of low-viscosity silicone oil covering the sample perimeter was used to prevent solvent evaporation. Measurements were carried out at a frequency of ω = 1 Hz and a deformation amplitude γ^{o} = 0.01 to ensure that the oscillatory deformation is within the linear viscoelastic regime.

6.2.4 Reduction of Bulk Hydrogels with GSH

The degradation behaviour of **HS-PG** hydrogel was investigated in presence of water-soluble reducing agent glutathione (GSH). Prior to reduction, the hydrogels were allowed to swelling in a PBS (pH 7.4), followed by addition of 10 mM GSH and incubated at 37 °C. The reduction was allowed until the transition of gel to sol was observed.

6.2.5 Nanogels Synthesis

Nanogels were synthesised via inverse miniemulsion method. For the preparation of the miniemulsion, surfactant (100 mg of 3:1 weight ratio of Span 80 and Tween 80) dissolved in 3.74 mL of n-hexane was used as organic phase. The aqueous phase consisted of 150 mg (3.68 × 10^{-1} mM) of **HS-PG** dissolved in 300 μL of 0.04 M PBS buffer (pH = 8.5). The organic and the aqueous phases were pre-emulsified by magnetic stirring for 10 min. After stirring the system was ultrasonicated using a Branson sonifier W450 with a ¼ ″ horn at duty cycle of 30% and output control of 90%

under ice cooling. Cross-linking was initiated by subsequent addition of HRP (0.0128 g, 3.2 x 10^{-6} mmol) dissolved in 30 μL of PBS buffer (pH = 8.5) and the mixture was sonicated for another 60 s. The reaction was allowed to proceed for 50 min at room temperature with constant stirring followed by quenching of the free thiol groups by 2-hydroxy acrylate at pH = 8. Any further oxidation was stopped by addition of 1.5 mL of acidic water (pH = 3). Separation of the nanogels was achieved by centrifugation at 10000 rpm for 30 min followed by decantation of the supernatant. Nanogels present in the aqueous layer were carefully washed with hexane (2 × 1.5 mL) and THF (4 × 2.5 mL) in order to remove the surfactants and unreacted polymer. The remaining organic solvents and acid were removed by dialysis. Purified nanogels were stored in Millipore water at 4 °C for further use.

6.2.6 Peptide Conjugation to HS-PG Nanogels

Carboxyfluorescein labelled, cysteine terminated CGGKTFFYGGSRGKRNNFKTEEY peptide was used as a model peptide for HRP mediated covalent attaching to **HS-PG** nanogels. Prior to conjugation the peptide was reduced using immobilised TCEP. For coupling, 1 mg of peptide (3.096 × 10^{-4} mmol) was dissolved in miniemulsion aqueous phase during nanogel formation keeping the rest of the parameters as described above. After nanogel purification the amount of conjugated peptide was quantified by means of UV-Vis method. The absorption spectra were recorded between 300-600 nm with λ_{max} at 475 nm by making a standard curve for increasing peptide concentration. Total amount of the conjugated peptide was determined by measuring the absorbance of the non-conjugated peptide present in the supernatant and subtracting this value from the total amount used for coupling.

6.2.7 Nanogels Degradation

Peptide labelled nanogels (100 mg) were degraded in the presence of water soluble reducing agent GSH (10 mM) in PBS buffer (10 mL pH = 7.4) at 37 °C imitating the biological conditions. Optical fluorescence microscopy was used for imaging of peptide conjugated particles before and after reduction. Images were recorded at 20-fold magnification and 50 ms exposure time.

6.2.8 HRP Activity Assay

The enzyme activity assays of the released HRP from the cross-linked networks were performed by means of the well-established procedure of HRP mediated pyrogallol oxidation to purpurogallin. The purpurogallin which is yellow in color can be readily detected spectrophotometrically at 420 nm. One unit of peroxidase is defined as the amount of enzyme required to catalyse the production of 1 mg of purpurogallin from pyrogallol in 20 seconds at 20°C under the assay conditions described. Prior to measurements the release of the HRP from hydro- and nanogels was performed as followed. Hydrogel samples were immersed at 25°C in 10 mL of PBS buffer at pH = 6. Subsequently after 1, 4, 8, 12, 24 h the buffer solution was carefully replaced by same amount of fresh solution. Followed washing steps, nanogel particles were re-suspended in 10 mL PBS buffer at pH = 6 at 25 °C and were centrifuged. At an interval time of 1, 4, 8, 12, 24, 36, 48, 52 and 72 h nanogels were centrifuged and then re-suspended in fresh buffer solution. The extracted amount of HRP during the washing was subtracted from the final value. The release was monitored spectrophotometrically for all the supernatants obtained from hydro- and nanogel samples. Since the activity of enzyme is proportional to the concentration of active enzyme, this method was also used to determine the amount of active enzyme which was not released from the hydrogel and nanogels. For measurements, in 3.0 mL of reaction mixture for each blank and sample, the final concentration of 14 mM PBS buffer, 0.027 wt% hydrogen peroxide and 0.5 wt% pyrogallol was present. To achieve a temperature control both mixture in cuvettes were incubated in spectrophotometer at 20 °C for 4 min. Then 100 μL of PBS and 100 μL diluted HRP were added respectively. The change in the absorbance was continuously recorded against the corresponding control containing all of the reagents, except peroxidase, at 20 °C. The initial velocity was recorded by the absorbance-time curve. The concentration of HRP was kept so dilute that a ΔA/min was in the range of 0.02 to 0.04. The measurements were started immediately and colour densities of product solution were measured at 420 nm for 3-4 min. The values obtained in the blank reactions performed in the absence of enzyme were subtracted from all the readings.

6.2.9 Unfolding and Refolding of HRP

Nanogels (100mg) with remaining 20% of HRP after 72h of its release were reduced in presence of 10mM GSH with incubation in PBS buffer for 24h at 37°C. After reduction

they were dialysed through dialysis membrane (MWCO 20 kDa) against deionised water for 24h under argon. The dialysed sample was divided into two parts, one part was directly used to measure the activity of reduced HRP, while the other part was again dialysed against PBS buffer pH 7.4 with 1 mM dissolved caffeine to facilitate the refolding of HRP for 24h and further dialysed against deionised water under argon prior to activity measurement.

6.2.10 β-Galactosidase Loading

Encapsulation of β-Galactosidase (β-Gal) in the nanogel was performed during the formation of the nanogel. The procedure was essentially the same as the preparation of unloaded nanogels except that 5wt% and 10wt% of the enzyme with respect to the polymer weight were dissolved in the initial aqueous phase while synthesising nanogels. The enzyme encapsulation and activity was determined by using o-nitrophenyl- β-D-galactopyranoside (ONPG) assay for β-Gal.[23]

6.2.11 o-nitrophenyl- β-D-galactopyranoside (ONPG) Assay

The enzyme β-Gal plays an important role in cellular metabolism by breaking down lactose into glucose and galactose. Enzymatic activity of β-Gal can be indirectly measured using a lactose analog, ONPG which is cleaved by β-Gal to o-nitrophenyl (ONP) which has a yellow color. The absorbance of ONP can be measured at a wavelength of 420nm spectrophotometrically. 1 unit of β-galactosidase is defined as the amount which hydrolyzes 1 µmol of ONPG to o-nitrophenol and D-galactose.The assay was performed in a Z-buffer at pH 7.0. For making 500 mL Z buffer: 150 mL 0.2 M Na_2HPO_4, 100 mL 0.2 M NaH_2PO_4, 5 mL 1 M KCl, 5 mL 0.1 M $MgSO_4$ were added in 240 mL of distilled water. Just before using, β-mercaptoethanol (35 μL per 10 mL Z buffer) was added. ONPG concentration was kept at 4mg/mL while 1M Na_2CO_3 was prepared to stop the reaction.

A calibration curve was obtained for 0.5, 1.0, 1.5, 2.0, 2.5, 3.0, 3.5, 4.0, 4.5, and 5.0 mg/mL of β-Gal with the ONPG assay. 200 μL of β-Gal was added to 1000 μL of Z-buffer and incubated for 2 min at 37°C following which 200 μL of ONPG was added and the mixture was again incubated at 37°C. The reaction was allowed to proceed for 3 min and then was stopped with the addition of 500 μL of 1M Na_2CO_3. Immediately the absorbance was measured at 420 nm. Blank measurements were made in a similar way without addition of the enzyme and values were subtracted from all the readings.

For estimation of β-Gal loading in the nanogels, supernatant from the washing of 5wt% and 10wt% of β-Gal loaded nanogel was taken and analysed in similar way as stated above. The unloaded amount calculated from the supernatant was subtracted from the amount of β-Gal used for loading and actual loading in the nanogels was estimated. All the measurements were performed in triplicate. For activity estimation of loaded β-Gal in the nanogel, loaded and unloaded nanogels were reduced as stated before. Reduced nanogels solution was dialysed for 12h through a 10,000 MWCO membrane. The ONPG assay was performed and absorbance was measured at 420nm. As a blank correction, measurements made with unloaded nanogels, were subtracted from the loaded once. The activity of the enzyme was calculated by the following equation.

Activity = $(OD_{420} \times 1.9 \times 1nmol) / (t \times V \times 0.0045\ mL\ cm)$

Were 1.9 = total volume in cuvette, t = time of reaction, V = volume of β-Gal used for analysis, 0.0045 OD 420/nmol = ε_{420} ONP, path length = 1 cm

6.2.12 Cytocompatibility Assessment

Human fibroblast cell line 84-9 derived from a haemophilia patient was seeded in 48 well tissue culture plates (25000 cells per well in 500 µL DMEM with 10 % FCS, 1 % penicillin/streptomycin, 1 % HEPES buffer, all from Invitrogen Life Technologies, Karlsruhe, Germany). The cells were incubated for 24 h at 37 °C in a 5 % CO_2 humidified atmosphere. Three different nanogel samples were tested for their cytocompatibility: Crosslinking mediated by HRP, as prepared (HRPap), crosslinking with HRP catalysis followed by dialysis against distilled water (HRPdia) as well as crosslinking with H_2O_2 as prepared (H_2O_2ap). All nanogel samples were dialysed against DMEM without additives for 24 h. After that FCS, pen/strep, and HEPES were added in adequate amount and the samples were diluted 1:10 and 1:100 to reach solutions with 1 mg/mL and 0.1 mg/mL of nanogel. In addition, cytocompatibility of HRP (0.85 mg/mL solution diluted 1:10 and 1:100 respectively, HRPsol) was determined. The culture medium was aspirated from the cells and 500 µL of the dialysed nanogel and the HRP solutions respectively were added per well and incubated for 24 and 48 h at 37 °C in a 5 % CO_2 humidified atmosphere. Cells cultured in DMEM without any nanogel or HRP served as control. Cytocompatibility of nanogels with 1 mg/mL and 0.1 mg/mL concentration was evaluated by means of LIVE/DEAD staining kit (L3224, Invitrogen Life Technologies, Karlsruhe, Germany), determination of cell activity using the WST reagent (Roche Diagnostics, Mannheim, Germany) according to DIN EN ISO

10993-5 as well as cell counting. For LIVE/DEAD staining, cells were washed two times with BPS and incubated with 200 μL per well of the staining solution (2 μmol calcein and 1 μmol ethidium-homodimer in PBS) for 30 min. Afterwards, the cells were analyzed by means of fluorescence microscopy (Axioimager M1, Zeiss, Germany). For WS cell activity test, the cells were incubated with the WST reagent 1:10 in supplemented DMEM for 30 min at 37°C. The absorption of the supernatant was quantified in a Tecan spectra fluor plus photometer (Tecan, Crailsheim, Germany) at a wavelength of 450 nm. Cell counting was performed using a CASY cell counter (Roche, Diagnostics, Mannheim, Germany). Samples for cell activity and cell counting were measured in quadruplicate. The average and standard deviation were calculated using Microsoft Excel.

6.2.13 Cell Encapsulation in the Hydrogel

Cell Encapsulation in the hydrogel was done layer by layer. First SH-PG (0.025 g, 5.55 × 10^{-3} mmol) was dissolved in 70 μL buffer at pH 8.5. To this solution HRP (0.0003 g, 7.5 × 10^{-7} mmol) was added. The mixture was mixed thoroughly and was poured into the well plate. After 1h of incubation of the hydrogel, SH-PG (0.015 g, 3.34 × 10^{-3} mmol) dissolved in 40 μL buffer at pH 7.4 mixed with HRP (0.00018 g, 4.5 × 10^{-7} mmol) and 300,000 L929 mouse fibroblasts (ATCC CCL-1) were added on top of the pre-gelling hydrogel. Complete gelation of hydrogel with encapsulated cells took place within 2h. Afterwards the gel was swelled in 1mL DMEM plus 10 % FCS, 1 % penicillin/streptomycin, 1 % HEPES buffer, (Invitrogen Life Technologies, Karlsruhe, Germany) and live dead viability staining (LIVE/DEAD staining kit, Invitrogen, Karlsruhe, Germany) of the cells was performed according to manufacturers protocol after 1h and 18h.

6.3 Results and Discussion

Herein, HRP-mediated preparation of functional, redox-sensitive disulfide cross-linked hydrogels and nanogels through gelation of thiomers without the requirement of H_2O_2 is presented. Thiol functionalised linear poly(glycidol) (Mn = 6100 g/mol; **HS-PG**) was chosen as hydrophilic and cytocompatible gel precursor.[17] Homogeneous thiofunctional prepolymer solutions in PBS (30 wt%, pH=7.4, 8.0, 8.5) did not yield hydrogels within 24 h at ambient conditions in the absence of HRP. Upon HRP

addition, gel formation was observed after 4 h only at pH = 8.5, suggesting the occurrence of enzyme-triggered hydrogelation **(Figure 1)**. Hydrogel formation was confirmed *in situ* during the network evolution by rheological analysis using oscillatory deformation tests. A typical gelation profile is characterized by two-phases **(Figure 1)**. An initial lag phase of about 2 h, during which both moduli (elastic (*G´*) and viscous (*G´´*)) remain almost unchanged, may be related to the formation of prepolymer aggregates in the reaction system. The lag phase is followed by a log phase at which rapid increase of *G´* is observed, suggesting the occurrence of cross-linking reactions in the prepolymer aggregates. The gel point can be assumed at the crossover point of *G´* and *G´´* in the case of low entangled networks and was observed at about 150 min. The assessment of gelation kinetics reveals a marked dependence of gelation time on HRP content. The gelation time decreased with increasing amount of HRP and reached a plateau at 110 min for a molar ratio of -HS : HRP = 0.08. A further increase of the HRP amount did not affect the gelation time.

The conventional HRP cycle involves its reaction with H_2O_2 resulting in formation of highly reactive intermediates acting as powerful oxidants. In the presence of thiol groups these intermediate compounds generate active thiyl radicals that may then dimerize to disulfide bonds or react with thiolates forming the disulphide radical which can transform to a disulphide bond after the reaction with oxygen. Under aerobic conditions however, there is no need for H_2O_2 addition as H_2O_2 is formed during auto-oxidation of thiol in stoichiometric ratios.[18] It can then act according to the mechanism described above as catalyst for disulphide formation, without the need for further addition of peroxide. Due to the strictly stoichiometric molar ratio between the generated peroxides and thiols, no further oxidation of the forming disulphide groups occurs. Strong pH dependence on the gel formation indicates that in this system reaction between thiyl radicals and thiolates is a dominating process.

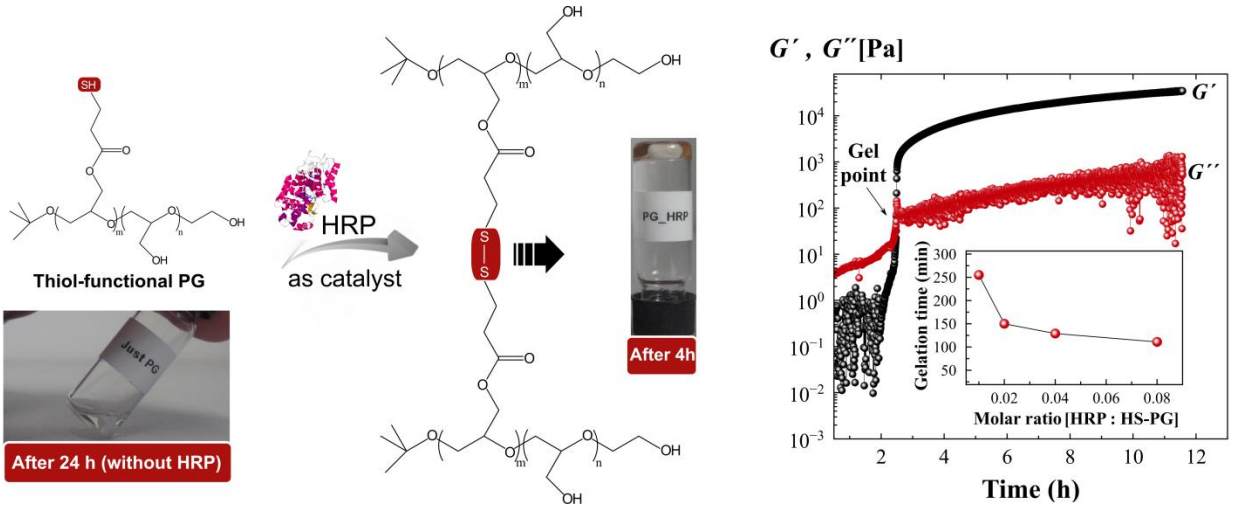

Figure 6.1: Hydrogel formation from thiofunctional prepolymers upon HRP addition with corresponding pictures of hydrogels. (Right) Changes in elastic *G´*, and viscous modulus *G´´* measured at 1 Hz during the cross-linking reactions. **(Inset figure)** Dependency of gelation time on molar ratio of HS-PG to HRP.

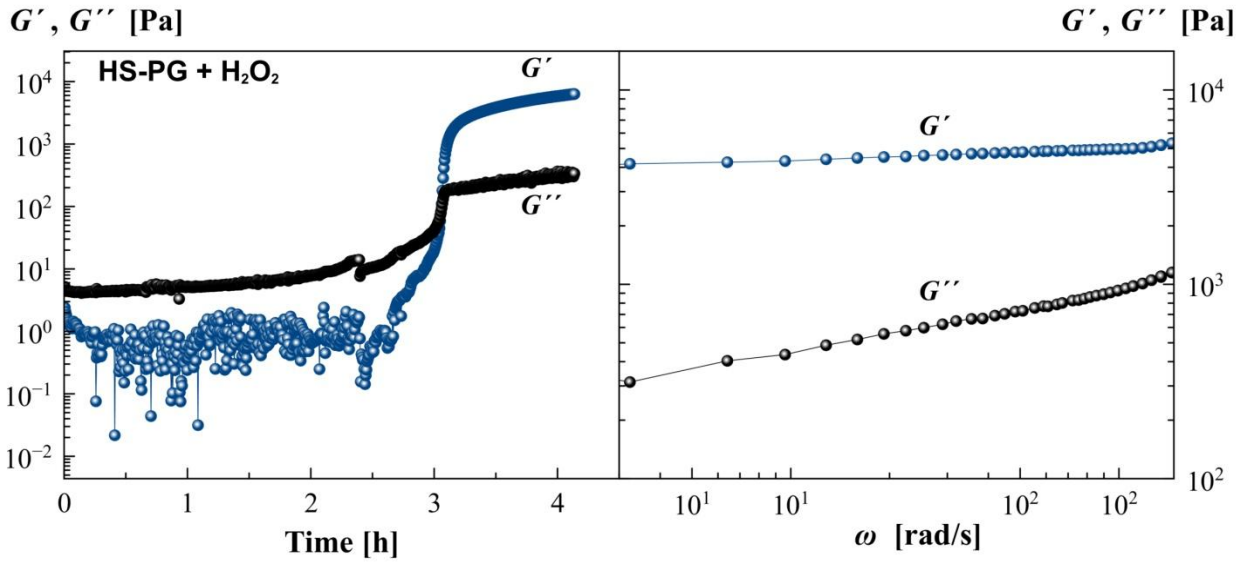

Figure 6.2: (Left) Elastic (G´) and viscous (G´´) modulus during the gelation of HS-PG in the presence of H_2O_2. (Right) the changes in G´ and G´´ of the same sample after time sweep test as a function of frequency.

For comparison, an oscillatory rheological analysis with H_2O_2 instead of HRP as oxidizing agent was performed **(Figure 6.2).** Gelation of HS-PG precursors in the presence of H_2O_2 is slower than the HRP-mediated process, but the frequency sweep tests show that both processes yield elastic network formation.

Raman Spectroscopy was performed to qualitatively determine and compare the reaction products obtained by the thiomer gelation mediated with HRP and H_2O_2 **(Figure 6.3).** The Raman spectra of HS-PG cross-linked with H_2O_2 showed considerable amount of free thiol (2075 cm^{-1}) in the stipulated time of 4 h in comparison of hydrogels formed by HRP cross-linking where almost all the thiol functionalities are converted into disulfide (507 cm^{-1}). These results correlate well with rheological tests indicating that HRP is more effective catalyst in disulfide bond formation in comparison to H_2O_2.

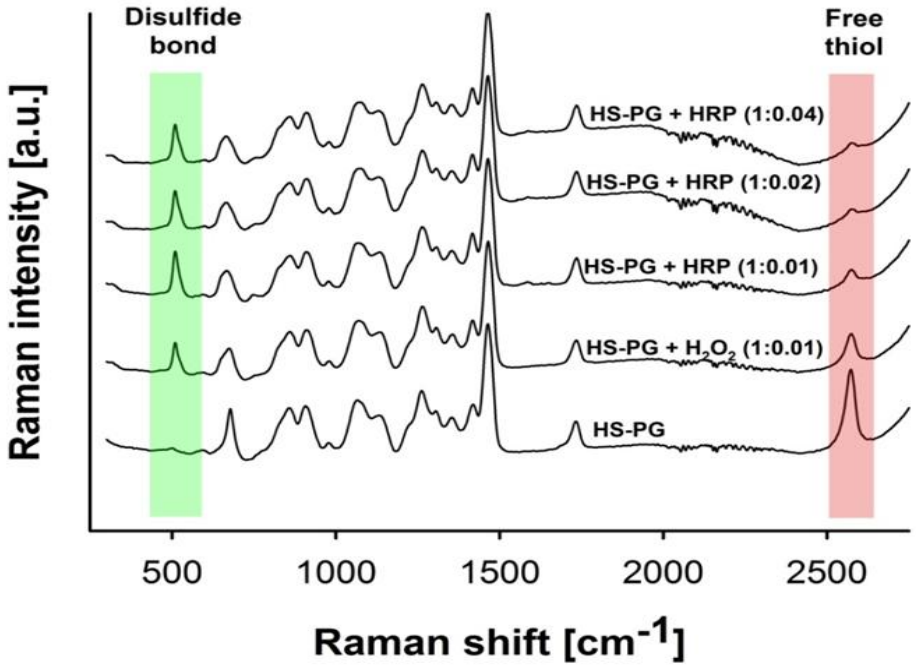

Figure 6.3: Raman spectra of HS-PG hydrogels cross-linked with H_2O_2 (0.01 ratio of HS-PG) and HRP at different molar ratios, as indicated.

In order to prove the versatility of the HRP mediated thiomer oxidation nanogel particles were prepared by inverse miniemulsion technique.[17]

Cryo-scanning electron microscopy (cryo-SEM) and dynamic light scattering (DLS) techniques were applied to characterize the nanogel particle diameter in the swollen state **(Figure 6.4)**. Particle size analysis with DLS yields a z-average particle diameter of 250 nm with a PDI of 0.24. Cryo-SEM images demonstrate that the particles have well-defined spherical shapes with particle diameters *d* in the range of 200 nm < *d* < 350 nm. These results show that both techniques correlate well to each other with respect to size analysis of the nanogels in the hydrated state

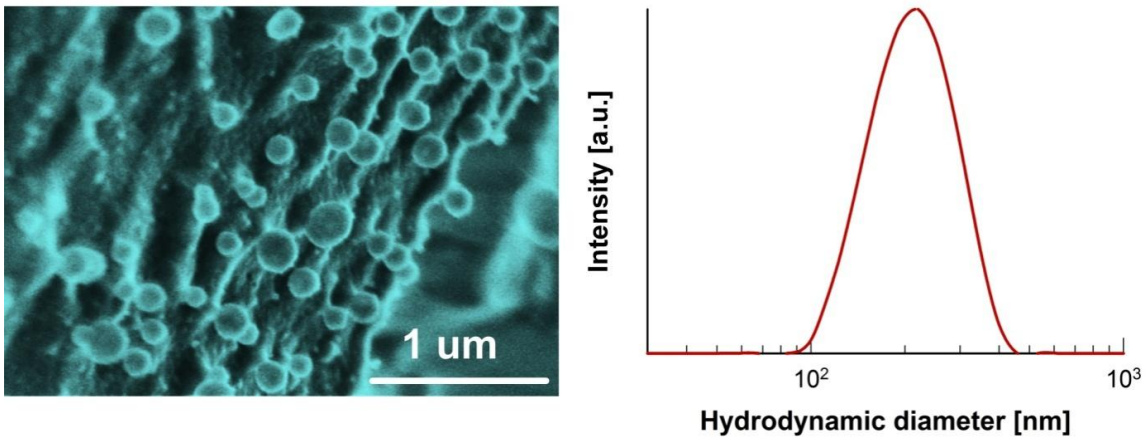

Figure 6.4: Cryo-SEM and DLS of HS-PG nanogels in water.

HRP mediated cross-linking of thiofunctional polymers can also be used to generate functionalized nanogels in a one step-procedure. It was demonstrated by adding the carboxyflourescein (FAM) labeled model peptide sequence CGGKTFFYGGSRGKRNNFKTEEY to the nanogel preparation.

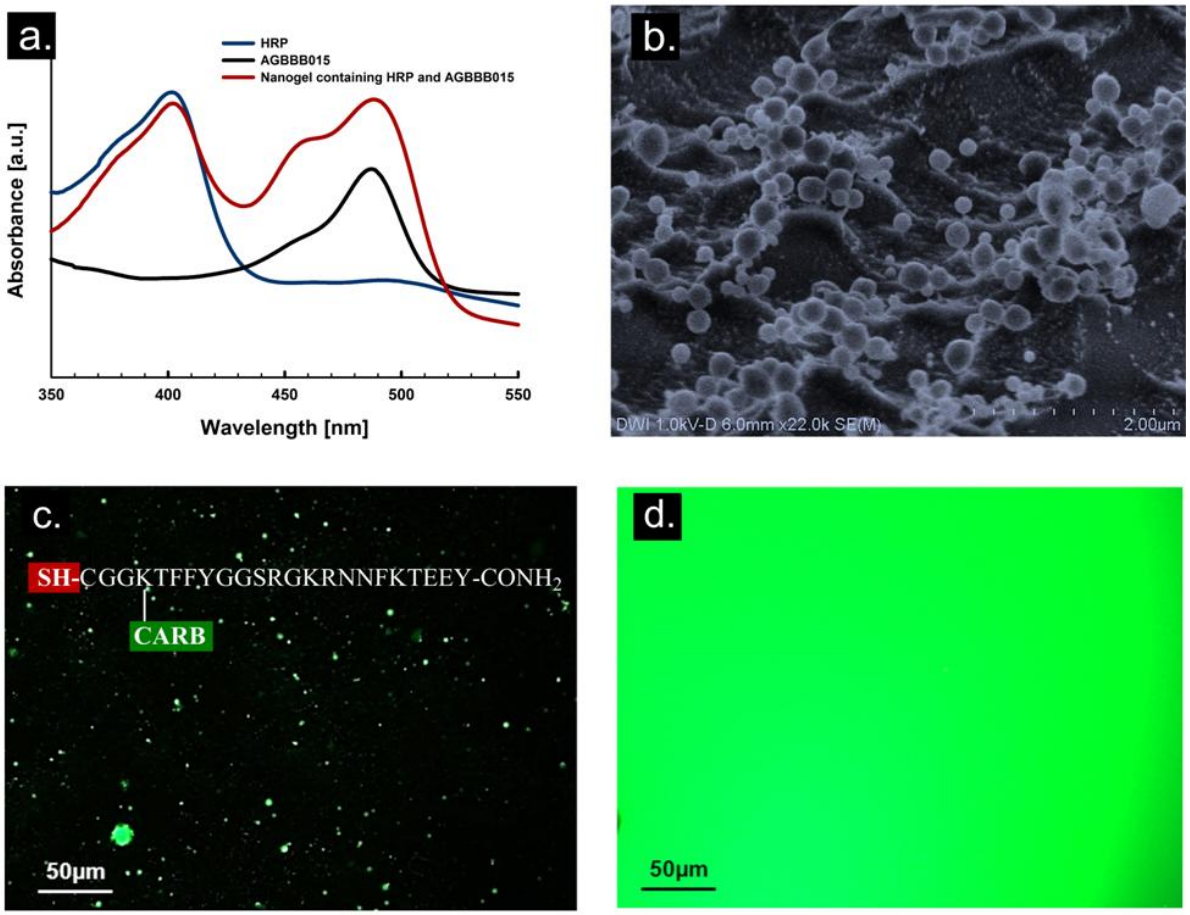

Figure 6.5: a) UV - spectra of HRP, the FAM labeled peptide CGGKTFFYGGSRGKRNNFKTEEY and peptide conjugated HS-PG nanogels prepared

through HRP mediated oxidation; b) cryo-SEM image of peptide labeled nanogels (diameter: 200 - 350 nm). Fluorescence microscopy image of the FAM labeled peptide conjugated nanogels before (c) and after (d) reduction with GSH.

This peptide bears an N-terminal cysteine that allows HRP-mediated covalent conjugation of the peptide to the nanogels. **Figure 6.5 (a)** shows the UV spectrum of native HRP, FAM labeled peptide as well as peptide-conjugated HS-PG nanogels after centrifugation and subsequent dialysis. Native HRP shows an intense band at 403 nm in aqueous solution (Soret band) which is characteristic for heme containing moieties while the peptide exhibits a maximum at 488 nm due to the presence of FAM. In the spectra of purified nanogels both bands are present confirming enzyme encapsulation and the presence of conjugated peptide. The labeling efficiency of the peptide estimated from a standard absorbance calibration curve measured at the 475 nm was 56 %.

Redox sensitivity of peptide labelled nanogels was demonstrated through degradation in the presence of glutathione (GSH). Due to the presence of FAM in the conjugated peptide, this process could be visualized by fluorescence microscopy. It was observed that before degradation particle aggregates appeared as individual bright green spots on the dark background **(Figure 6.6 c).** This implies that the peptide is conjugated to the particles and the non-bound peptide was successfully removed by dialysis. Upon GSH addition to a final concentration of 10 mM, the fluorescent signal is spread as shown in **Figure 6.6 d** depicting a homogeneous green background, demonstrating nanogel degradation.

Release profiles of HRP from the cross-linked networks as well as enzyme activity assays were performed by means of HRP mediated pyrogallol oxidation to purpurogallin.[19]

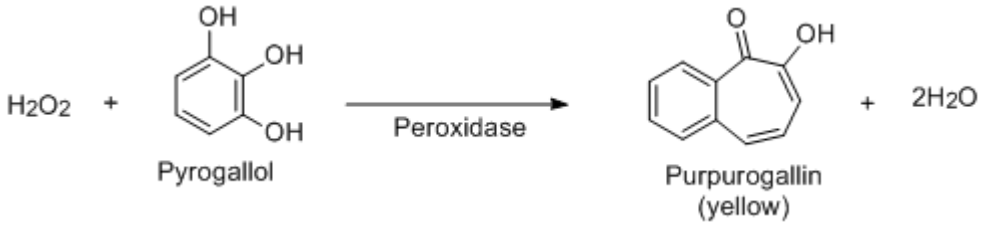

Scheme 6.1: Reaction of of HRP with pyrogallol substrate.

The purpurogallin is yellow in color and can be readily detected spectrophotometrically at 420 nm.

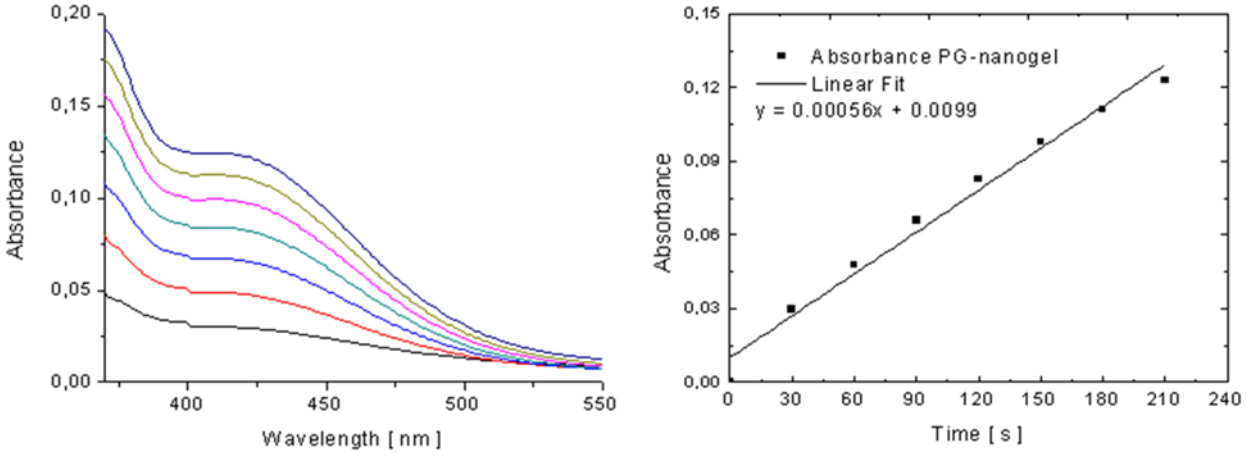

Figure 6.6: Typical UV-Vis spectra of HRP released from **HS-PG**-nanogels (release time was 24 h) (right). The spectra from bottom to top were obtained at 30 s intervals (b) linear fit of the absorbance recorded at 420 nm (left).

HRP release analysis from the hydrogels reveals that > 98% of HRP was released within 24 h **(Figure 6.7 left)**.

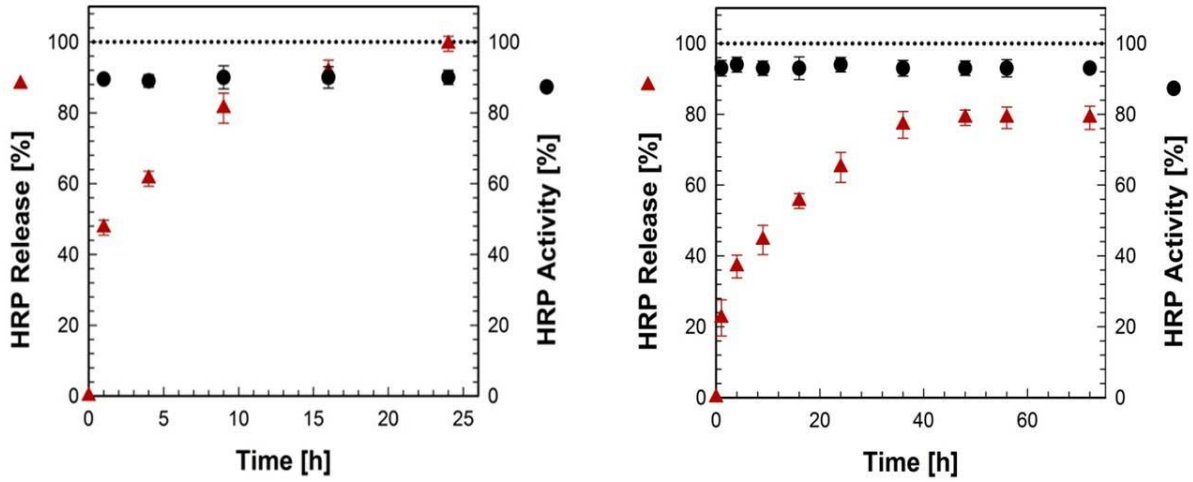

Figure 6.7: HRP release profile and activity assay from (left) bulk hydrogels and (right) nanogels.

In contrast, the release from the nanogels was slower and incomplete, reaching a plateau at 80% after 36 h **(Figure 6.7 right).** While for hydrogels ~ 45 % of the encapsulated HRP was released within 1 h, in the case of nanogels 45 % release was reached after 9 h. Therefore the cross-linking density of hydrogels and nanogel were

calculated. This may eventually be exploited for combination therapies with drugs that are activated through oxidation with HRP. In the field of drug delivery, recent studies[20] have shown that HRP can be used to convert a non-toxic prodrugs (indole-3-acetic acid (IAA) and the halogenated derivative 5-bromo-IAA) to a cytotoxin, which is a very promising drug delivery approach for example for tumor therapy, where side-effects of traditional drugs are severe. Hence, co-delivery of HRP with such drugs in separate particles leads to activation of the drugs only at the site of delivery, which is an extremely promising strategy to significantly lower side reactions of anti-tumor drugs. HRP released from hydro- and nanogels showed in all cases a catalytic activity above 90% in comparison to pure enzyme control.

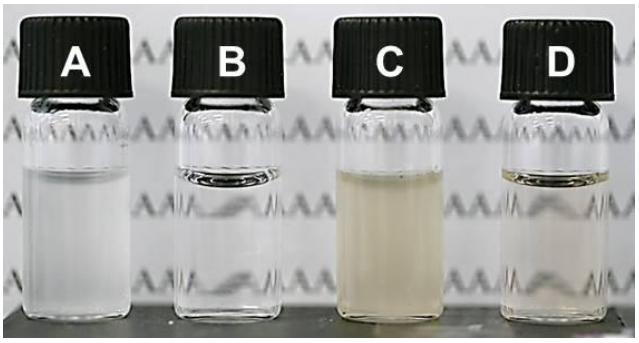

Figure 6.8: Nanogel suspensions before (A, C) and after (B, D) reduction with GSH, prepared by cross-linking with H_2O_2 (A, B) or HRP (C, D). The picture of particles prepared by the HRP mediated cross-linking was taken after 72 h HRP release studies. Slightly brownish color of these particles indicates HRP remaining in the particles. In contrast nanogels prepared by the cross-linking with H_2O_2 show white-milky coloration

Enzymatic activity was thus maintained after the thiol oxidation reactions and the cross-linked networks provide a suitable environment for enzyme encapsulation. When visually observed, a slight brownish color (from HRP) of the nanogels was seen after 2 days **(Figure 6.8)** which also indicates that the lacking 20 % of HRP remains in the nanogels.

Mesh Size Calculation. The average mesh size (distance between tow entanglement points) ξ for bulk hydrogels was calculated from elastic modulus G' based on Rubber Elasticity Theory (RET) through the following equation **(Equation 6.1)**.

$$\xi = \left(\frac{G' N_A}{RT}\right)^{-1/3} \qquad \text{Eq.6.1}$$

Where G' is the elastic modulus, N_A, R and T have their usual meanings.

There are several methods of estimating the mesh size of a nanogel; however, the Flory-Rehner model was selected due to the difficulty of measuring such parameters as the relaxed volume for different models (i.e., for the Peppas–Merrill or Brannon–Peppas equation). Thus, these values are rough estimates of the actual values.

Following the calculation of the ratio of swollen mass to dry mass, *q,* the polymer volume fraction in the swollen state, $v_{2,s}$ was calculated with **Equation 6.2**:

$$v_{2,s} = \frac{m\bar{v}}{m\bar{v} + mq/\rho_w} \qquad \text{Eq. 6.2}$$

Where m is the mass of dry nanogel particles, $\bar{v}$ is the specific volume of the polymer (0.785 g/cm^3), and ρ_w is the density of water. The average molecular weight between cross-links was calculated through the following equation:

$$\frac{1}{\bar{M}_c} = \frac{2}{\bar{M}_n} - \frac{\left[ln(1-v_{2,s}) + v_{2,s} + \chi_1 v_{2,s}^2\right]}{\left(\frac{V_1}{\bar{v}}\right)\left[v_{2,s}^{1/3} - \frac{v_{2,s}}{2}\right]} \qquad \text{Eq. 6.3}$$

Where V_1 is the molar volume of the swelling agent (for water; 18 cm^3/mol), χ_1 is the Flory polymer-solvent interaction parameter (0.25 for PG) and the $\bar{M}_n$ is the number of average of the polymer chains before cross-linking. Once $\bar{M}_c$ was known, the mesh size can be calculated from **Equation 6.4**:

$$\xi = v_{2,s}^{-1/3}\left(\frac{C_n \bar{M}_c}{M_r}\right)^{1/2} l \qquad \text{Eq. 6.4}$$

Where C_n is the Flory characteristics ratio (14.6 for vinyl polymers), M_r is the average molecular weight of the repeating units, and l is the length of the bond along the polymer backbone (0.154 nm for vinyl polymers). The mesh size for hydrogels was found as 4.9 nm, on calculation the average mesh size of HS-PG nanogels was found to be 3.0 nm. Since the radius of gyration of HRP is in the range of 2.5-3 nm, these calculations support the different release profiles of HRP. This may eventually be exploited for combination therapies with drugs that are activated through oxidation with HRP.

Unfolding and Refolding of HRP

To see the effect of reduction on released HRP from nanogels, HRP was reduced with 10mM GSH. On reduction a decrease in its activity was observed. This reduction in activity of HRP could be attributed to the reduction of four intramolecular disulphide bridges Cys 11- Cys91, Cys 44- Cys 49, Cys 97-Cys 301 and Cys 177- Cys 209 of HRP[20] which are also responsible for the stabilization of HRP's conformation and

hence resulting in its unfolding. The activity of unfolded HRP was 50% compared to the ≥ 90% activity of HRP released from the nanogel after 72 h incubation. During the course of reduction it was observed that the heme center of HRP was not disturbed. This was seen by an unaltered Soret band at 403 nm.

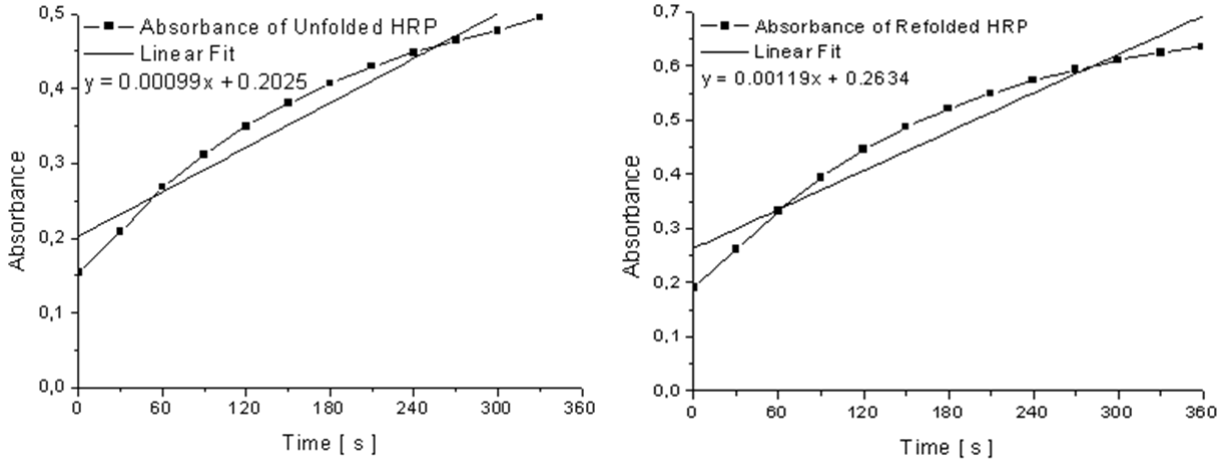

Figure 6.9: Linear fit of the absorbance recorded at 420 nm of unfolded HRP (left) and refolded HRP (right).

The activity of HRP was regained up to 65 % after it was dialyzed against PBS buffer at pH 7.4 in presence of 1mM caffeine. Caffeine which is a very mild oxidizing agent[21] is supposed to enhance the process of disulphide bond formation but for enzyme activity it is critical that on refolding, the cysteine residues should be correctly paired. Due to complexity of measurement it was not determined, so the complete cause for loss of remaining 25% activity of HRP could not be estimated.

β-Galactosidase Loading and Activity

The bacterial enzyme, β-galactosidase, catalyzes the breakdown of the complex sugar lactose into its component simple sugars - galactose and glucose. Its a 460 kDa large tetrameric protein that loses its function upon intermolecular disulfide bridge formation.[22]

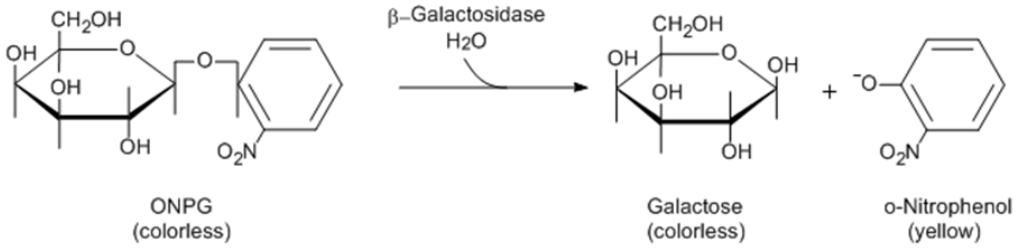

Scheme 6.2: Reaction of of β-galactosidase with ONPG substrate

For an assay for β-Gal activity synthetic substrate ortho-nitrophenyl-beta-D-galactopyranoside (ONPG)[23] with a similar structure to lactose was chosen. ONPG gets cleaved in presence of β-Gal giving yellow coloured o-nitrophenol (ONP) and colourless galactose.The amount of ONP formed can be measured by determining the absorbance at 420 nm and is proportional to the amount of β-Gal and the time of the reaction. The reaction is stopped by adding Na_2CO_3 which shifts the reaction mixture to pH 11. At this pH most of the ONP is converted to the yellow coloured anionic form and β-Gal is inactivated.

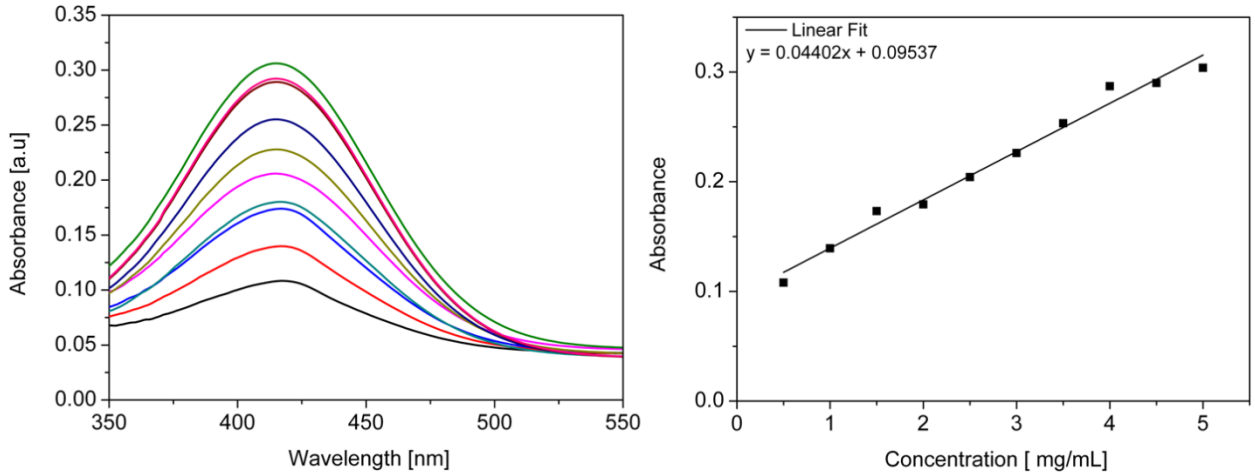

Figure 6.10: a) Typical UV-Vis spectra of ONPG assay of β-galactosidase with concentrations in range of 0.5mg/ mL to 5 mg/ mL b) Linear fit of the absorbance recorded at 420 nm.

Table 6.1 β-galactosidase encapsulation efficiency and activity estimation

β-Gal loading [wt%]	β-Gal loaded [mg]	Loading estimated [mg]	Encapsulation Efficiency %	% Activity	Z-Average [nm]	PDI
5	7.5	3.2	43	85	310±35	0.43±0.09
10	15.0	6.1	40	83	405±25	0.40±0.05

β-Gal activity was retained in the range of 83-85%, while encapsulation efficiency of 40-43% was estimated in the nanogels. Prior to loading of β-Gal in nanogels, stability of only β-Gal was checked with and without sonication for 120s, which is the time required

for preparation of nanogels via miniemulsion. It was found that, 2.5% activity of the enzyme decreased by sonication which can marginally affect enzyme activity. Low encapsulation efficiency could be attributed to the steric hindrance caused by HRP which also gets encapsulated during the nanogel synthesis. As oxidative conditions strongly affect function of this protein, it is shown that by using HRP mediated cross-linking, β-Gal could be loaded into nanogels and released with ca. 85% activity preservation. This demonstrates applicability of HRP cross-linking also to large and oxidation sensitive proteins and underlines the importance of this mechanism.

Cytocompatibility

Nanogels prepared by HRP catalysis (HRPap (undialysed), HRPdi (dialysed)), nanogels prepared through H_2O_2 mediated cross-linking (H_2O_2ap (undialysed) at concentrations of 1 mg/mL and 0.1 mg/mL as well as the used HRP solutions (HRPsol) were assessed for cytocompatibility using human fibroblast cell line 84-9. After incubating the cells for 24 and 48 h, LIVE/DEAD staining showed no differences in cell viability when comparing control cells to nanogel treated cells.

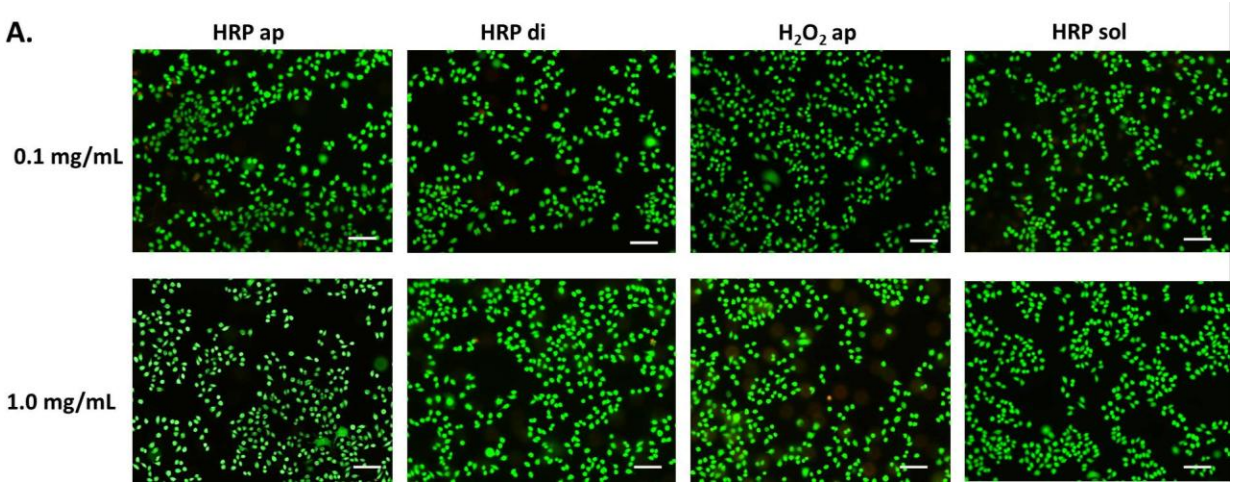

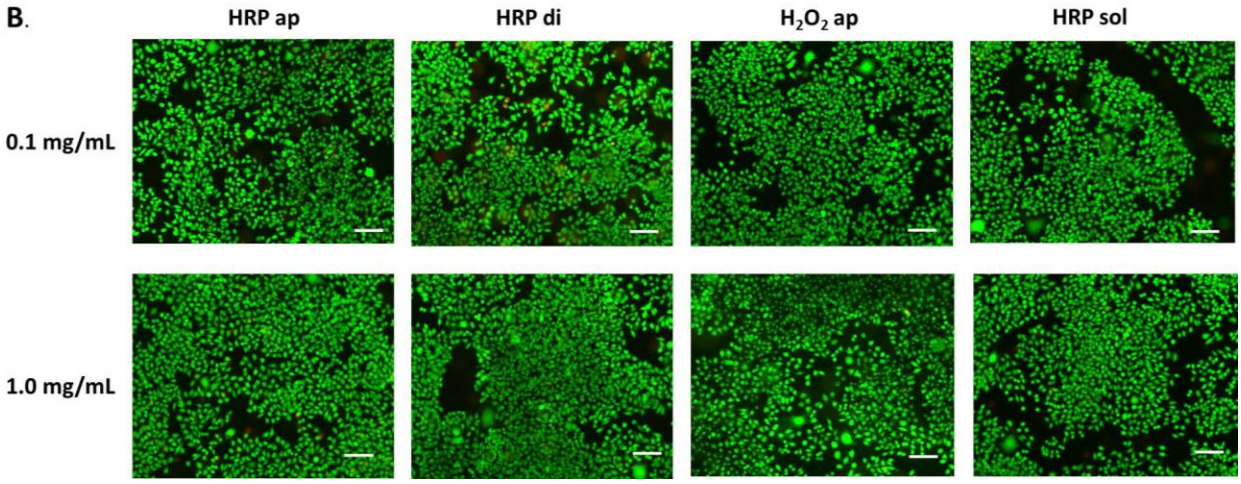

Figure 6.11: LIVE/DEAD staining for cytocompatibility assessment for nanogels prepared by HRP catalysis (HRPap, HRPdi), nanogels prepared through H_2O_2 mediated cross-linking (H_2O_2ap) at concentrations of 1 mg/mL and 0.1 mg/mL as well as the used HRP solutions (HRPsol) using human fibroblast cell line 84-9. After incubating the cells for 24 h(A) and 48 h(B). Scale bar 100μm.

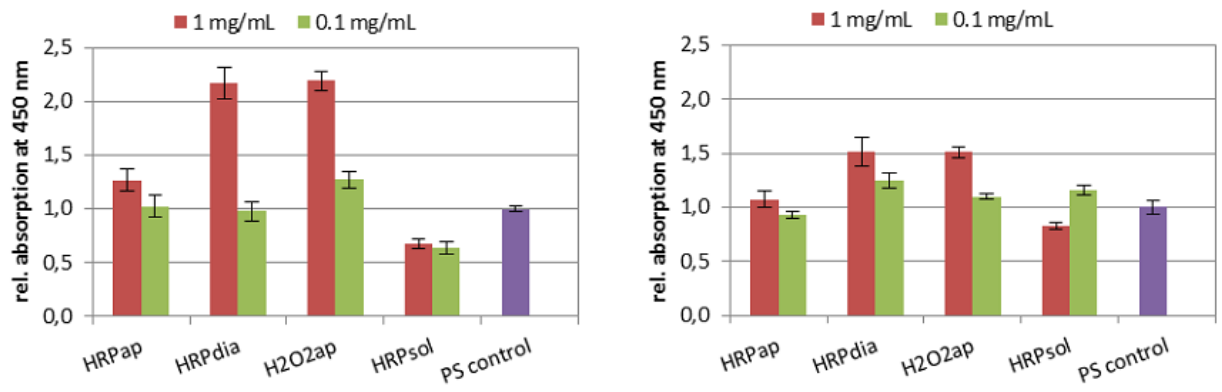

Figure 6.12: WST activity per cell after incubation of the different nanogel samples on human fibroblasts for 24 h (left) and 48 h (right).

Cell activity as assessed by the WST test was calculated in relation to cell numbers as relative absorption per cell. Cells incubated with the three different kinds of nanogel showed no significant decrease in cell activity compared to control cells after 24 and 48 h. Addition of 1 mg/mL of HRPdi) and nanogel with H_2O_2 (H_2O_2ap) to the cell culture medium resulted in a pronounced increase of cell activity after 24 h that lowered again after another 24 h. Cells supplemented with HRPsol showed a decrease of cell activity after 24 h. After 48 h cell activity increased again to levels similar to the ones of control

cells. Nanogels prepared with HRP and H_2O_2 did not affect cell activity and viability negatively. The results show that during the course of incubation no cytotoxic compound was released and that the nanogels are cytocompatible **(Figure 6.12)**

Cell Encapsulation

Preliminary studies were performed to see the potential of cell encapsulation in HRP crosslinked hydrogel. **Figure 6.13** clearly indicates the presence of living cells in the hydrogel even after 18 h of encapsulation.

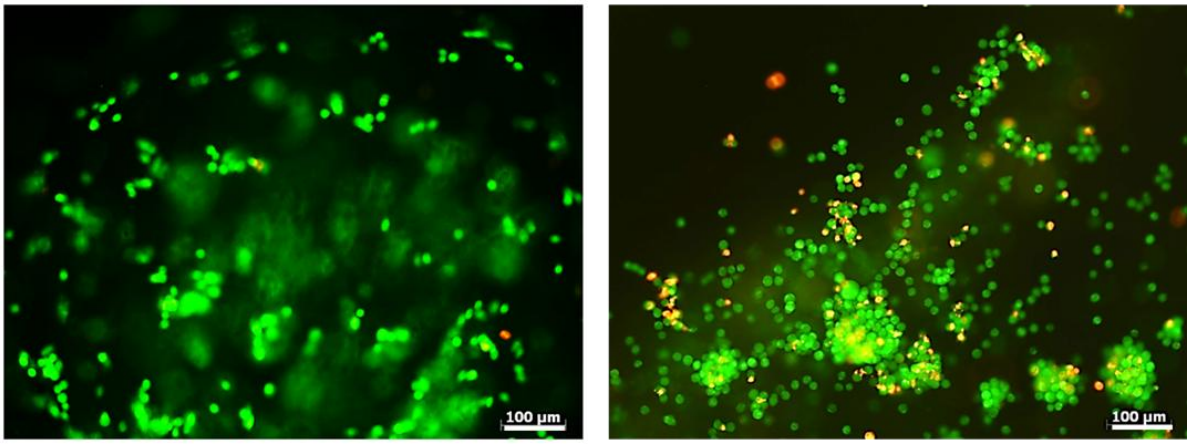

Figure 6.13: Fluorescence microscopic image of the cells encapsulated in the hydrogel after 2h (right) and after 18 h (left) with LIVE/DEAD staining. Green- and red-color cells represent the living and dead cell, respectively.

These first experiments show very high cell survival and proliferation rates, even without addition of adhesion sites. LIVE/ DEAD staining was performed to show the living cells stained with calcei n-AM (green color) versus the dead cells stained with ethidium homo dimer (EthD -1) (red color) by fluorescence microscopy. These results suggest that the cell viability in the hydrogel is retained and they can further be investigated as scaffolds for tissue engineering.

6.4 Conclusion

In conclusion, this chapter for the first time reports enzymatically mediated cross-linking of a redox-sensitive, reversible hydrogel that can be degraded through mild chemical stimuli. HRP can be used for mild enzymatic cross-linking of thiofunctional polymers to hydrogels and nanogels without the need for addition of hydrogen peroxide and can be degraded through mild chemical stimuli. This allows

cleavage of the network under cytocompatible conditions. Suitability of enzyme to create hydrogels as well as nanogels is shown which could embed (bio-) functional moieties such as peptide sequences. Linking of low molecular weight compounds to the network demonstrates that this key (bio-) chemical novelty is not restricted to polymers. Self-encapsulation of the enzyme horseradish peroxidase (HRP) into the nanogels in functional form, is an extremely interesting aspect for drug delivery, sensing and catalysis, and is thus promising candidate as controlled delivery systems. Further HRP crosslinked hydrogels also showed potential for cell encapsulation which could be later exploited for tissue engineering purposes.

6.5 References

[1] F. Meng, W. E. Hennik, Z. Zhong, *Biomaterials* **2009**, 30, 2180.

[2] G. Saito, J. A. Swanson, K. D. Lee, *Adv. Drug. Deliv. Rev.* **2003**, 55, 19.

[3] W. Tang, N. Y. Tsarevsky, K. Matyjaszewski, *J. Am. Chem. Soc.* **2006**, 128, 5578.

[4] J. H. Ryu, R. T. Chacko, S. Jiwpanich, S. Bickerton, R. P. Babu, S. Thayumanavan, *J. Am. Chem. Soc.* **2010**, 132, 17227.

[5] H. Lee, H. Mok, S. Lee, Y-K. Oh, T. A. Park, *J. Control. Rel.* **2007**, 119, 245.

[6] K. Albrecht, M. Moeller, J. Groll. *J. Adv. Polym. Sci.* **2011**, 234, 65.

[7] A. H. Krotz, R. C. Mehta, G. E. Hardee, *J. Pharm. Sci.* **2005**, 94, 341.

[8] S. Toledanom R. J. Williams, V. Jayawarna, R. V. Ulijn, *J. Am. Chem. Soc.* **2006**, 128, 1070.

[9] K. A. Mosiewicz, K. Johnsson, M. P. Lutolf, *J. Am. Chem. Soc.* **2010**, 132, 5972.

[10] Z. M. Yang, P. L. Ho, G. L. Liang, K. H. Chow, Y. Cao, Z. H. Guo, B. Xu, *J. Am. Chem. Soc*. **2007**, 129, 266.

[11] M. Ehrbar, S. C. Rizzi, R. G. Schoenmakers, B. S. Miguel, J. A. Hubbel, F. E. Weber, M. P. Lutolf, *Biomacromolecules* **2007**, 8, 3000.

[12] L. S. M.Teixeira, J. Feijen, C. A. van Blitterswijk, P. J. Dijkstra, M. Karperien, **2012**, 33, 1281.

[13] B. Halliwell, M. V. Clement, L. H. Long, *FEBS Lett.* **2000**, 486, 10.

[14] R. Jin, L. S. M. Teixeira, P. J. Dijkstra, C. A. Karperien, F. J. Jan, *J. Control. Rel.* **2011**, 152, 186.

[15] F. Lee, J. E. Chung, M. Kurisawa, Soft Matter **2008**, 4, 880.

[16] M. Kurisawa, J. E. Chung, Y. Y. Yang, S. J. Gao, H. Uyama, *Chem. Comm.* **2005**, 4312.

[17] J. Groll, S. Singh, K. Albrecht, M. Moeller, *J. Polymer Sci. Part A: Polym. Chem.* **2009**, 47, 5543.

[18] C. Obinger, U. Burner, R. Ebermann, R. *Phyton* **1997**, 37, 219.

[19] www.sigmaaldrich.com : Enzymatic Assay of Peroxidase (EC 1.11.1.7)

[20] J. Tupper, R. M. Stratford, S. Hill, M. G. Tozer, U. G. Dachs, *Cancer Gene Ther.* **2010**, 17, 420.

[21] AplaGen, US Patent Application 20100203001 – Process for Forming Disulphide Bridges US Patent Application 20100203001, August 12, **2010.**

[22] W. B. Snyder, T. J. Silhavy, *J. Bacteriol*.**1995**, 177, 953.

[23] J. Miller, Experiments in Molecular Genetics, 352; Cold Spring Harbor Laboratory, NY, **1972**.

CHAPTER 7

Biohybrid Nanogels by Crosslinking of Ovalbumin with Reactive Star-PEGs in W/O Emulsions

Part of this work is published in Journal of Polymer Science Part A: Polymer Chemistry 2012, 50, 4288.

7.1 Introduction

There has been a great deal of attention toward increasing the chemical diversity and the complexity of nanogels to design and tailor them for specific applications.[1-3] One of the possible strategies is using biomolecules and synthetic polymers as building blocks for nanogel synthesis. This allows not only for production of biologically active material but also to introduce domains with high degree of spatial organization into the polymer based system. The biohybrid nanogel systems can offer several benefits. Apart from the tunable dimension and the rapid response, the high surface-to-volume ratio of nanogel with incorporated biomolecules like proteins makes it useful for sensorics and catalysis as it can load a large amount of compounds (single or multiple) within the gel network as well as on the surface, resulting in a variety of detection methods with respect to photonic/plasmonic intensity, energy distribution, and temporal distribution.[4] As drug-delivery carriers they impart good stability, and reversible volume change in response to environmental stimuli, such as pH, temperature, and glucose level that are unprecedented for common pharmaceutical carriers.[5] Thus biohybrid nanogels provide a platform based on synthetic polymers where the biomolecule can be immobilized by covalent bonding and inherit properties of both the synthetic polymer and the biomolecule (secondary structure, functionality, hydrophobicity and biocompatibility). A system based on PEG as synthetic unit has further known advantages in drug delivery as PEG enhances the solubility of hydrophobic drugs or carriers when conjugated with it. It enhances the physical and chemical stability of drugs and prevents aggregation of the drugs *in vivo*, as well as during storage.[6,7] The main advantages of PEG based nanogel are reduced protein immunogenicity, increased residence time of particles in the body and reduced

enzymatic degradation. All these features ensure that the drug reaches the site of action and is its clearance from the body is prevented. Reactive star-PEG prepolymers have recently been used for the synthesis of variety of nanogels. Colloidal particles with average size of 100 nm were formed upon Michael-type conjugation between amine functionalities of bovine serum albumin (BSA) and vinyl sulfone end-groups of eight-arm star-shaped PEG[8] using phase separation method. The prepolymer condensation concept based on chemical crosslinking methods for biohybrid nanogel synthesis by use of reactive polymers with pre-defined architecture, chemical composition and functionalities is particularly suitable for incorporating peptides and proteins in particles. The selection of reactive building blocks allows very exact adjustment of nanogel properties like ability to vary flexibly the swelling and mechanical properties of nanogels during crosslinking step. Since the crosslinking reactions can occur at very mild conditions, this is probably the best strategy to design biohybrid nanogels or to directly load polymer colloids with proteins or enzymes.

This chapter focuses on nanogels that are constructed by immobilization of protein by crosslinking with reactive prepolymer in inverse miniemulsion and hence resulting in the formation of biohybrid nanogel. The polymer used was based on acrylate functionalized star shaped poly (ethylene oxide-*stat*-propylene oxide) (**Acrylate-sP(EO-*stat*-PO)**). Two different types of nanogel particles were prepared; one by crosslinking the polymer in inverse miniemulsion via Michael addition of its acrylate group with PEG-diamine (model system) and the other with free lysine group of Ovalbumin (biohybrids), a chicken hen protein with a molecular weight of 45kDa. The purpose of making nanogels based on PEG-diamine was to optimize the reaction conditions (droplet size, stability of emulsion, reaction time, etc.) and compare their properties with the biohybrid nanogels prepared with Ovalbumin.

Synthesis and characterization of the gel precursor, preparation of the nanogels, and their characterization regarding particle size, size distribution in solution and in dry state, swelling and chemical composition are herein presented and discussed.

7.2 Experimental

7.2.1 Materials and Methods

Hydroxy terminated, six arm, star shaped poly (ethylene oxide-*stat*-propylene oxide) (sP(EO-*stat*-PO) with a backbone consisting of 80% ethylene oxide and 20% propylene

oxide (Mn=12000 g/mol, Mw/Mn=1.12) was obtained from Dow Chemicals (Terneuzen, NL). Prior to functionalization, sP(EO-*stat*-PO) was purified by precipitation in THF/cold diethylether as solvent/non-solvent system. n-hexane (99%, VWR), Span 80 (Sigma), Tween 80 (Sigma), α,ω-Bis-amino octa(ethylene glycol)(M*w*: 368.5 g/mol) (Iris Biotech), α,ω--Bis-amino 20(ethylene glycol)(M*w*: 897.1 g/mol) (Iris Biotech), Polyoxyethylene bis(amine) (M*w*: 3000 g/mol) (Aldrich), Poly(ethylene glycol)-*bis*-amine (M*w*: 6000 g/mol) (Aldrich), Ovalbumin (M*w*: 45,000 g/mol ,Sigma) HCl (38%, VWR), NaOH (97%, VWR), NaCl (99%, VWR) $CaCl_2$ (96%, VWR) $FeCl_3$ (97%, VWR) Ethanolamine (98%, Fluka), Tetrahydrofuran (99%, Sigma Aldrich) were used as received. Dry toluene, pyridine (>99%, Aldrich), acrylic acid anhydride (99%, Polysciences) were used without additional purification. BCA Assay kit (Thermo Scientific) Dialysis membrane (MWCO = 3.5 kDa, 25kDa and 100kDa) was purchased from Spectrum Laboratories.

Fourier Transform Infra-Red Spectroscopy (FT-IR) FTIR spectra were recorded on a Nexus 470 FTIR spectrometer with an attenuated total reflectance adapter installed (Thermo Nicolet, Madison, WI) by photo acoustic method. The spectrum represents an average of 400 to 600 scans with CO_2 peaks removed.

Circular Dichroism Spectroscopy CD measurements were carried out with an Olis 17 DSM; a Cary 17 monochromater was used with a spectral output of 184-260 nm. CD spectra were measured at protein concentrations of 0.5 mg/mL using a cell with 0.090 mm light path in the wavelength range of 190-260 nm with a bandwidth of 2.00 nm and with number of increments of 50 with an integration time of 20s. CD spectra were expressed in terms of mean residue ellipticity (deg cm^2 $dmol^{-1}$). The data presented is an average of 5 scans.

ZetaPotential measurement Measurements were performed using a Malvern Zetasizer Nano ZS as a function of pH at 20°C. The electrophoretic mobility was measured and the zeta potential was calculated using Henry's equation. 'Expert System' software was used for data interpretation. Disposable poly (styrene) cuvettes were used for measurement in water.

7.2.2 Synthesis of Acrylate Functionalized 6 arm sP(EO-*stat*-PO)

The functionalization of 6 arm sP(EO-*stat*-PO) with acrylate groups was performed according to literature.[9] In short, 17.11g (1.43 mmol) of 6 arm s(EO-*stat*-PO) was dissolved in 51 mL of dry toluene under N_2 and 1.03 mL (13.02 mmol, 1.5 eq.) pyridine was added to it followed by drop wise addition of 1.28 mL (10.14 mmol, 1.3 eq.) of acrylic acid anhydride for 15 min. The reaction mixture was stirred at room temperature for 24 h and the reaction was performed under dark. After the reaction was complete, solvents were removed under vacuum. The product obtained was purified by precipitation in cold diethyl ether; this process was repeated several times. Yield of the final product obtained was 12.4 g (1.03 mmol, 72%). Degree of functionalization was determined by NMR.

1H-NMR(400 MHz,CDCl3): δ = 1.14 (t, 108-H, H1); 3.2-4.0 (m, 964-H, H-3,4,5), 4.23 - 4.45 (m, 10-H, H2), 5.80 - 5.92 (m, 6-H, H7, *cis*), 6.07 - 6.20 (m, 6-H, H6), 6.38 - 6.48 (m,6-H, H7, *trans*) ppm ; 13C-NMR(400 MHz,CDCl3): 70.6, 76.7 - 77.3 ppm ; THF ,GPC: Mn/Mw = 1.10

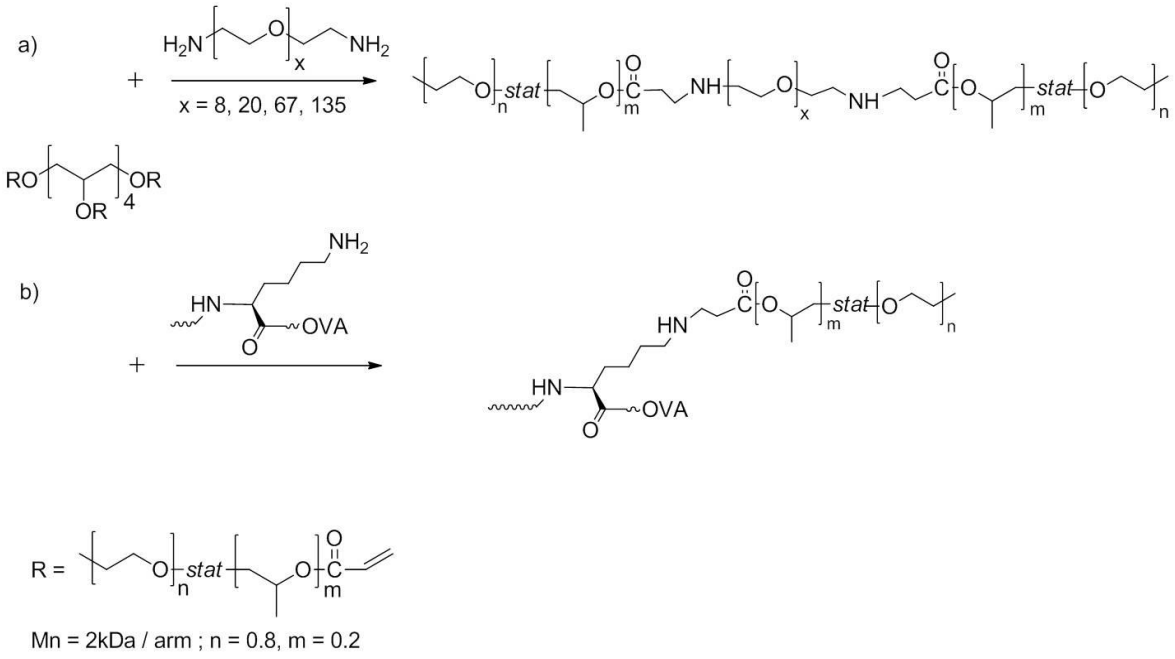

Scheme 7.1: Schematic representation of Michael type addition reaction of **Acrylate-sP(EO-*stat*-PO)** with a) PEG-diamine and b) Ovalbumin.

7.2.3 Synthesis of Acrylate-sP(EO-*stat*-PO)–PEG Diamine Nanogels

Nanogels were synthesized by crosslinking of **Acrylate-sP(EO-*stat*-PO)** with PEG-diamine (368.5 g/mol) (**Scheme1a**). The standard procedure for the synthesis of the

nanogel is as follows. A 5 vol% w/o miniemulsion was prepared by mixing the aqueous phase with **Acrylate-sP(EO-*stat*-PO)** (25 mg, 2.1 × 10^{-3} mmol, 12.5 × 10^{-3} mmol with respect to 6 acrylate functionalities) in 65 μL of phosphate buffer (pH 8) and organic phase consisting of Span 80 (6.5 × 10^{-4} mmol) and Tween 80 (9.0 × 10^{-3} mmol), having a HLB of overall 5.6, in 1.25 mL of n-hexane. After pre-emulsification the mixture was ultrasonicated using a Branson sonifier W450 with a ¼ ″ horn at duty cycle of 40% and amplitude of 360W for 60 s under ice cooling. The sonication was performed under ice cooling to prevent the solution from being heated up during the course of sonication. After 60 s of sonication PEG-diamine 368.5 g/mol (2.3 mg, 12.5 × 10^{-3} mmol dissolved in 20 μL of pH 8 buffer was added to initiate the crosslinking and the solution was sonicated for another 60 s. After sonication the emulsion was stirred for 25 min at room temperature. To separate the formed nanogels from the emulsion, the emulsion was centrifuged for 30 min at a speed of 10000 rpm. The organic rest was decanted and the settled nanogels were washed with 1 ml of THF twice and later dispersed in water. Further the nanogels were purified by dialysis (MWCO 25 kDa) for 24h.

Utilizing the procedure described above nanogels were synthesized by using PEG-diamine with four different spacer lengths of 8 (368.5 g/mol), 20 (897.1 g/mol), 67 (3000 g/ mol) and 135 (6000 g/mol). Preparation of nanogels was carried out according to standard procedure. To investigate the effect of sonication parameters like output and duty cycle on size of Diamine nanogels, synthesis with output of 200W, 280W and 360 W with Duty cycles of 30, 40, 50 and 60% were carried out.

Fourier Transform Infra-Red Spectroscopy (FT-IR)

PEG-diamine (M*w* : 368.5 g/mol): IR(KBr): *v* = 3365 [s, v_{as} NH_2], 3302 [s, v_s -NH_2], 2868 [s, *v*(CH_2, CH_3)], 2131 (w), 1600 [s, δ -NH_2], 1455 (s), 1349 (s), 1109 [vs, *v*(-C-O-C-)], 993 (s), 948 (s), 850 (w, *v* NH_2 (wag)), 523 (w).

Diamine nanogel: IR (KBr): *v* = 3351 (s, v_{as} NH), 2924 (s), 2858 [s, *v* (CH_2, CH_3)], 1763 [m, *v*(-CO-)], 1458 (s), 1112 [vs, *v* (-C-O-C-)], 951 (w), 723 (w, δ, NH), 532 (w).

Acrylate -sP(EO-*stat*-PO): IR (KBr): *v* = 3576 (w), 3514 (w), 2868[s, v (CH2, CH3)], 1964 (w) , 1724 [m, v (-CO)], 1635 [w, v (-C=C)-], 1456 (s), 1349 (s), 1296 (s), 1250 (s), 1109 [*vs*, *v* (-C-O-C-)], 1042 (s), 995 [s, δ (Rs-CH=CH_2)*oop*], 950 [s, δ (R-CH=CH_2)*oop*], 880 (s), 847 (s), 812 (m), 663 (w), 523 (m).

7.2.4 Synthesis of Acrylate-sP(EO-*stat*-PO) - Ovalbumin Nanogels

It has been reported in literature [10] that Ovalbumin has 20 lysine groups out of which 15 are on the surface. Calculation of amount of Ovalbumin required to crosslink **Acrylate-sP(EO-*stat*-PO)** was done taking into consideration these 15 lysine groups

Table 7.1 Amount of **Acrylate-sP(EO-*stat*-PO)** and Ovalbumin used for nanogel preparation

Molar Ratio [mol:mol]	Acrylate-sP(EO-*stat*-PO) [mg]	Ovalbumin [mg]
1.0:0.05	25	1.87
1.0:0.1	25	3.75
1.0:0.2	25	7.50
1.0:0.3	25	11.25
1.0:0.4	25	15.0
1.0:0.5	25	18.75
1.0:0.75	25	28.12
1.0:1.0	25	37.50

Keeping the same procedure as Acrylate-sP(EO-*stat*-PO)-diamine nanogels, Ovalbumin nanogels with a molar ratio of 1.0:0.05, 1.0:0.1, 1.0:0.2, 1.0:0.3, 1.0:0.4, 1.0:0.5, 1.0:0.75 and 1.0:1.0 with respect to 6 acrylate group of Acrylate-sP(EO-*stat*-PO) to 15 free lysine of Ovalbumin were synthesized. The actual amounts are given in **Table 7.1**. Quantification of Ovalbumin in nanogels was done by standard BCA assay.[11]

Fourier Transform Infra-Red Spectroscopy (FT-IR)

Ovalbumin: IR(KBr): *v* = 3297 [vs, *v*(-NH intramol. H-bond)], 3077 [w, *v* (OH)], 2962 [w, *v* (-CH)],1652 [vs,*v*(C=O), δ(OH)], 1540 [s, *v*(C=N), *v*(NH)], 1452 [vw, *δ* (CH)], 1397 [w, *δ*(CH)], 1312 (vw), 1239 [vw, *δ*(NH)].

Ovalbumin nanogel: IR(KBr): *v* = 3299 [vs, *v*(-NH intramolecular. H-bond)], 2925 (s), 2854 [s, *v*(CH_2, CH_3)], 1738 [m, *v*(-CO-)], 1654 [vs, *v*(C=O), *δ*(OH)], 1537 [s, *v*(C=N), *δ*(NH)], 1456 [m, *v*(-C-O-C-)], 1100 [s, *v* (-C-O-C-)], 952 (w).

Raman Spectroscopy

Acrylate-sP(EO-*stat*-PO) : Raman shift: ν = 2933 (s), 2874 (s), 1724 [w, ν(C=O)], 1636 (w), 1470 (m), 1285 (m), 1136 (m).

Ovalbumin: Raman shift: ν = 2933 (s), 1666 [s, ν(C=N), Amide I mode], 1605 [m, ν(CC), phenyl stretching mode], 1448 [s, δ (CH_2, CH_3) scissoring mode], 1339 [m, ν(C=N), Amide III mode], 1003 [s, ν (CC), phenyl stretching mode].

Ovalbumin nanogel: Raman shift: ν = 2928 (s), 1739 [w, ν(C=O)] 1655 [s, ν(C=N), Amide I mode], 1444 [s, ν(CH_2, CH_3) scissoring mode], 1302 [m, ν(C=N), Amide III mode], 1003 [s, ν(CC), phenyl stretching mode].

7.2.5 Influence of pH on Nanogel Size and Zetapotential

Influence of pH on size and zeta-potential of Diamine and Ovalbumin nanogel was investigated. For all the measurements disposable polystyrene cuvettes were used. The pH was maintained by addition of HCl or NaOH. Measurements were carried out at 20°C. For size measurement each sample was measured for 15 runs, each run with 15 repeat cycles. For zetapotential measurement 100 scans were made for each sample. Dialysed nanogels with a concentration of 5mg/ml were used for all measurement.

7.2.6 Influence of Mono and Multivalent Salts on Nanogels Size and Zetapotential

Influence of 0.1M NaCl, $CaCl_2$ and $FeCl_3$ at pH 5.5 on size and zeta-potential of Diamine nanogel was investigated. 0.1M solution of M NaCl, $CaCl_2$ and $FeCl_3$ was prepared and nanogels were dispersed in different salt solutions so that the final concentration of the nanogel was maintained at 5mg/ml.

7.2.7 BCA Assay

A working reagent (WR) which was a mixture of bicinchoninic acid and sodium tartrate in 0.1 M sodium hydroxide plus 4% cupric sulfate was prepared in the ratio of 50:1 as described in the protocol.[11] Range of Bovine Serum Albumin (BSA) standards were added to the WR in the ratio of 1:20 keeping the final concentrations of BSA to 0, 5, 25, 50, 125 and 250 μg/mL. Thereafter, the standards were incubated at 60°C for 30 minutes and then cooled back again to room temperature. To assure accuracy of the test, absorbance at 562 nm was measured for all samples within 10 minutes of cooling. The absorbance measurement of the blank standard was subtracted from the rest of the samples and the absorbance value was plotted against the concentration. A linear

fit was applied and the slope obtained was 0.00248**.** Bicinchoninic acid (BCA) assay was performed on Ovalbumin nanogels for the determination of mass of Ovalbumin crosslinked in nanogels. **Acrylate-sP(EO-*stat*-PO)**-Ovalbumin nanogels were centrifuged to separate them from the aqueous medium. The supernatant (washing cycles repeated until there was no ovalbumin detected) was taken and the amount of Ovalbumin present in it was quantified by measuring the absorbance at 562 nm using UV-Vis spectrophotometer. The amount of Ovalbumin crosslinked in nanogels was determined by subtracting the mass of the Ovalbumin in the supernatant from the initial amount of Ovalbumin added in the recipe.

7.2.8 CD spectra of Ovalbumin Nanogels

CD spectra of nanogels with 1.0:0.3, 1.0:0.4, 1.0:0.5, 1.0:0.75, 1.0:1.0 molar equivalents of **Acrylate-sP(EO-*stat*-PO)** to Ovalbumin was recorded. The spectra were measured at Ovalbumin concentration of 0.5 mg/mL in Millipore water, using a cell with 0.090 mm light. The values presented are average values of five scans for each measurement.

7.3 Results and Discussion

A variety of tests with PEG-diamines and **Acrylate-sP(EO-*stat*-PO)** were made before using an actual protein to optimize the conditions for Michael addition reaction. The influence of different parameters like pH, different ions, sonication setting and spacer length, i.e. molecular weight of the PEG-diamine, on size and polydispersity of the nanogels were tested.

Diamine Nanogel

First, preparation of PEG-diamine (368 g/mol) crosslinked particles from **Acrylate-sP(EO-*stat*-PO)** polymers by Michael type addition in inverse miniemulsion is discussed. Generally, Michael type addition proceeds through the deprotonated of amine group **(Scheme 7.1)**. Thus, in order to maintain slightly basic reaction conditions, 0.04M PBS buffer (pH=8) was used as a dispersed phase. Furthermore, the ionic strength of PBS served as osmotic agent in the droplets to stabilize them against Ostwald ripening.

Table 7.2 Influence of sonication parameters on hydrodynamic diameter and polydispersity index of **Acrylate -sP(EO-*stat*-PO)-PEG diamine** nanogel

Duty Cycle [%]	Output					
	200 W		280 W		360 W	
	Diameter [nm]	PDI	Diameter [nm]	PDI	Diameter [nm]	PDI
30	360±12	0.565±0.008	280±21	0.595±0.012	280±19	0.460±0.020
40	360±19	0.642±0.011	280±22	0.636±0.019	280±21	0.444±0.021
50	300±15	0.670±0.016	280±28	0.570±0.020	280±22	0.440±0.013
60	400±20	0.580±0.020	360±12	0.482±0.021	300±30	0.452±0.014

To optimize the sonication magnitude, Diamine nanogels were synthesized with an output of 200, 280 and 360 W. The ultrasonic energy was pulsed using the Duty Cycle Control with 30, 40, 50 and 60% in order to obtain uniform nanogels. In pulsed mode, ultrasonic vibrations are transmitted to the solution at a rate of one pulse per second. Particles were analyzed via dynamic light scattering **(Table 7.2).**

On comparing the results for different duty cycles it was observed that with increasing duty cycle the hydrodynamic diameter was decreasing from 30 to 50% but duty cycle above 50 % showed start of aggregation rather than further decrease of size. This result was consistent with an output of 200W, 280W as well as for 360W. This observation could be attributed to bulk thermal heating caused due to increase of power as violent collapse of cavitation bubbles in an ultrasonic field result in extremely high local temperatures. Duty Cycle of 50% appeared to be threshold while an output difference of 80 W in the measurements did not influence the particle size significantly. However, to avoid harsh sonication condition while using protein medium, duty cycle (40 %) and a high power (360 W) appeared most relevant and this setting was kept throughout all experiments.

Cryo-scanning electron microscopy (cryo-FESEM) and Cryo- Transmission electron microscopy (Cryo-TEM) were applied to characterize the nanogel particle size in water, i.e. in the swollen state, and Transmission electron microscopy (TEM) was used as a characterization technique for dry particles. **Figure 7.1** shows the cryo-FESEM, cryo-TEM and TEM analysis of **Acrylate-sP(EO-*stat*-PO)-**Diamine nanogels. Particle size

analysis with DLS **(Table 7.2)** gave the z-average particle diameter of 280 nm with a PDI of 0.44.

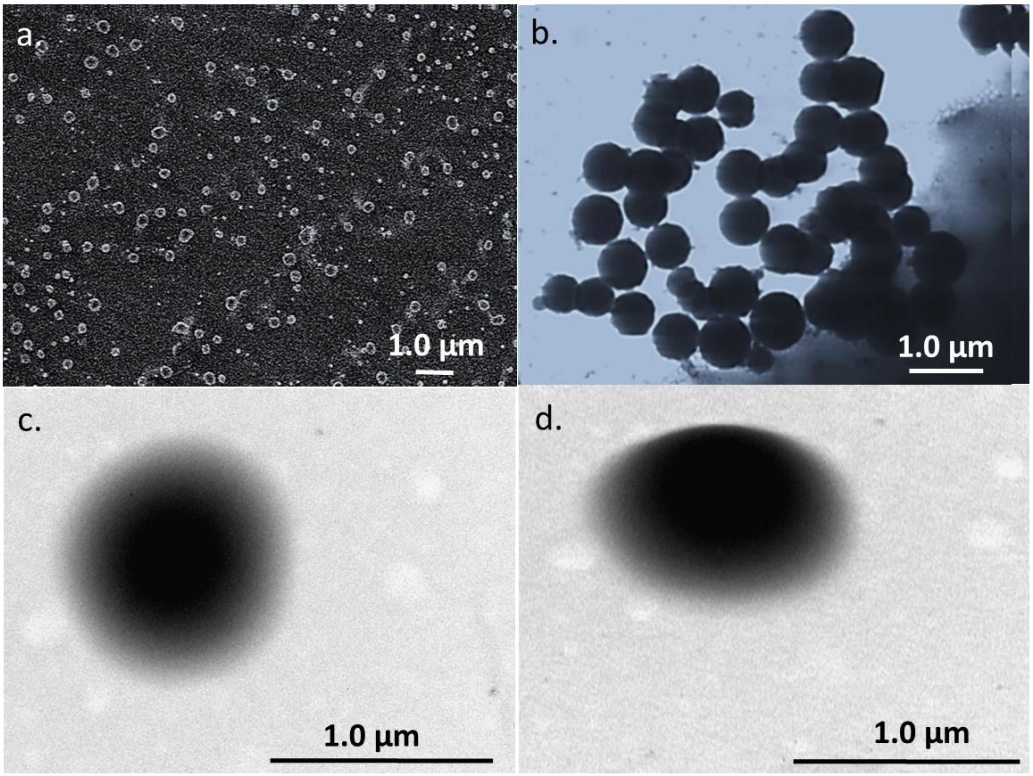

Figure 7.1: a.) Cryo-FESEM, b.) Cryo-TEM c.) TEM (lateral view) d.) TEM (vertical view) images showing **Acrylate-sP(EO-*stat*-PO)**-Diamine (368.5 g/mol) nanogels prepared at duty cycle of 40 % and amplitude of 360 W.

Cryo-FESEM images clearly showed that the particles had well-defined spherical shape, as expected for particles synthesized by miniemulsion techniques, with particle diameters *d* in the range of 230 nm < *d* < 350 nm. Taking into account the freezing-step that might have led to partial volume loss of the nanogels during cryo-FESEM, these two techniques correlated well with each other with respect to size analysis of the nanogels in the hydrated state.

While DLS and cryo-FESEM correlated quite well with respect to particle size, cryo-TEM showed an increase of particle size to 500 nm < *d* < 700 nm although the particles were well defined and appeared spherical. To view into detail the morphology of the particles, particles were viewed under TEM in dry state. **Figure 7.1c** and **7.1d** shows TEM topography images of isolated nanogels in a vertical and a lateral view.The picture demonstrates that the nanogels had a fuzzy interface which is indicative of high water content and soft particles. They were deformable and adopted a flattened, oblate

spheroid shape on the copper grid which apparently gives the perception of increased hydrodynamic diameter.

Figure 7.2 shows a comparison of IR spectra of Diamine nanogel with PEG-diamine and **Acrylate-sP(EO-*stat*-PO)**. The spectrum of PEG-diamine shows two distinct bands at 3302 and 3365 cm^{-1} characteristic of symmetrical and unsymmetrical N-H stretch of primary amine, while its N-H bending vibration is observed at 1600 cm^{-1} which is in close proximity to C=C stretch of **Acrylate-sP(EO-*stat*-PO)** at 1635 cm^{-1}**.** When these two spectra are compared with the spectra of the nanogel only a single band at 3351 cm^{-1} is observed which is characteristic of N-H stretching vibration of secondary amine while the bands at 1600 and 1635 cm^{-1} have disappeared. A strong N-H wag band at 735 cm^{-1} can also be observed in the spectrum of nanogel which gives a clear indication of the secondary amine formation and confirms the Michael addition reaction for the formation of nanogels. The Raman spectra in this case were not very helpful as no significant differences could be observed.

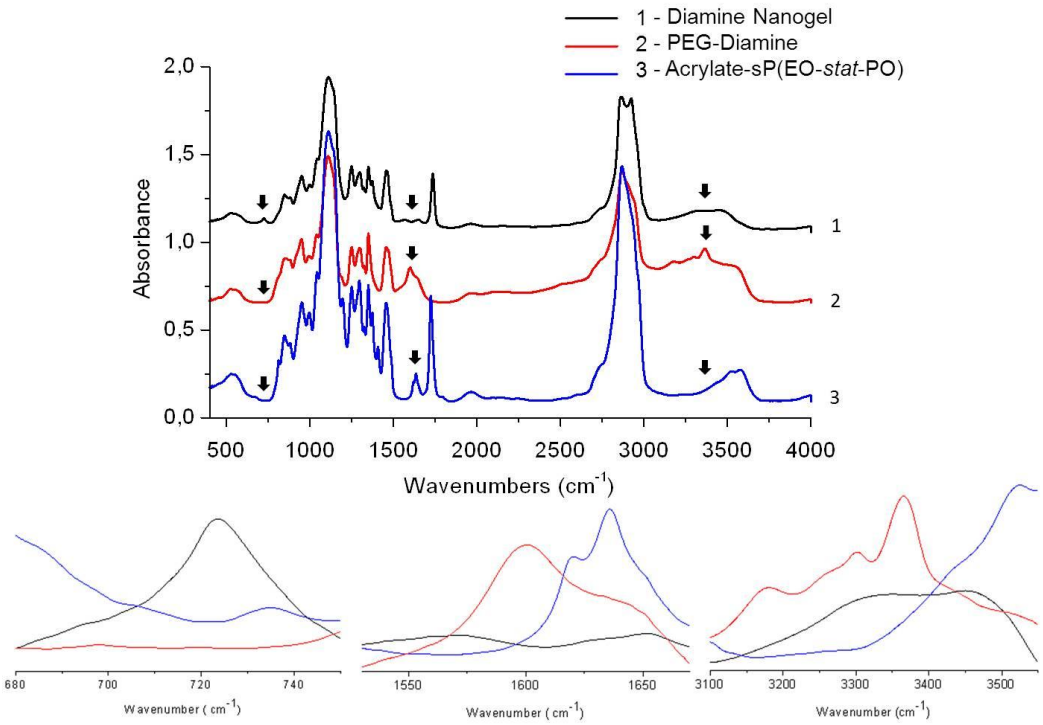

Figure 7.2: IR spectrum for Diamine nanogels with 1.0:1.0 molar ratio of PEG-diamine (368.5 g/mol) and Acrylate -sP(EO-*stat*-PO) (1), PEG-diamine (2) and Acrylate -sP(EO-*stat*-PO) (3).

Nanogels Prepared with Diamines of Different Spacer Length

Table 7.3 Influence of spacer length on hydrodynamic diameter of the Diamine nanogel

PEG-diamine [g/mol]	Diameter [nm]	PDI
368.5	310±12	0.423±0.009
897.1	300±20	0.435±0.010
3000	260±23	0.303±0.015
6000	180±8	0.383±0.017

Particle size analysis of Diamine nanogels in aqueous solution (pH 5.5) are shown in **Table 7.3**. It was observed that with increased spacer length, the nanogel size decreased while the size distribution stayed about the same. This could be due to the effect where longer PEG chains help to stabilize the emulsion and hence result into smaller particles.

Table 7.4 Influence of mono and multivalent salts on hydrodynamic diameter of nanogels prepared with diamines of different spacer length.

Salt	PEG-diamine							
	368.5 g/ mol		897.1 g/mol		3000g/mol		6000g/mol	
	Diameter [nm]	PDI	Diameter [nm]	PDI	Diameter [nm]	PDI	Diameter [nm]	PDI
-	310±12	0.423 ±0.009	300±20	0.435 ±0.010	260±23	0.303 ±0.015	180±8	0.383 ±0.017
NaCl	230±21	0.327 ±0.011	240±17	0.468 ±0.010	220±12	0.482 ±0.016	160±22	0.383 ±0.023
CaC_2	175±24	0.232 ± 0.007	180±13	0.479 ±0.028	160±14	0.152 ±0.017	120±19	0.224 ±0.019
$FeCl_3$	50±23	0.249 ±0.013	50±10	0.212 ±0.020	40±16	0.290 ±0.032	40±12	0.305 ±0.009

DLS measurement data of nanogels with different spacer length in 0.1 M NaCl, $CaCl_2$ and $FeCl_3$ solution shows a decreases of hydrodynamic diameter compared to the particle size in aqueous solution, while there is a difference of 40-60nm due to of Na (I) and Ca (II) ions on particle size, the effect of the Fe (III) ion is far greater as particle size is reduced to a sixth of the initial size in aqueous solution **(Table 7.4).**

This trend was observed for all the Diamine nanogels regardless of the spacer length. The valence of ion affects the electrical double layer of the particles. They accumulate as counter ions in the electrical double layer and consequently compress it. The effect of Na^+ was lower than Ca^{2+} and much lower than Fe^{3+} A trivalent Fe^{3+} ion compresses the double layer to a greater extent and hence reduces the particle size further. Zhao *et al.* also observed that with an increase in charge of the cation, the swelling capacity decreases.[12]

Table 7.5 Influence of mono and multivalent salts on Zetapotential of nanogels prepared with diamines of different spacer length in aqueous solution and ionic solutions (pH 5.5, 0.1M)

Salt	368.5 g/ mol [mV]	897.1 g/mol [mV]	3000g/mol [mV]	6000g/mol [mV]
-	-30.3	-33.4	-36.3	-34.8
NaCl	-7.19	-8.87	-9.62	-8.90
$CaCl_2$	-2.67	-2.79	-2.90	-1.98
$FeCl_3$	2.03	1.15	-0.14	0.75

From **Table 7.5** it is seen that the zeta potential increases to become positive with increasing the valence of the cation at neutral pH. This is due to the ion to nanogel surface interaction which could be ranked in the following order $Na^+ < Ca^{2+} < Fe^{3+}$ corresponding to increasing Gibbs free energy of ion hydration which reflects the propensity of ion to interact with water molecule according to their volume to charge ratio hence the zeta potential change was observed from negative to positive as the valence of cation was increased.[13, 14]

Table 7.6 Influence of pH on size and Zetapotential of Diamine nanogels (PEG diamine M*w*. 368.5 g/mol)

pH	Diameter [nm]	PDI	Zetapotential [mV]
3	260	0.210	13.75
4	265	0.232	3.56
5	280	0.201	1.52
6	280	0.206	-3.81
7	300	0.263	-6.43
8	310	0.254	-9.24
9	310	0.278	-10.20

Table 7.6 shows slight increase in hydrodynamic diameter of the particles with increasing pH with zeta potential ranging between 13.78 mV to -10.20mV. It has been shown that solvated ions may preferentially adsorb to a solvated surface, imparting a strong positive or negative charge to the surface. Poly (ethylene oxide) has been shown to preferentially adsorb hydroxide ion over hydronium ion over the surface.[15] Therefore in basic media the ion imparting a negative charge is hydroxide. These negative charges at elevated pH values are unlikely due to the hydrolysis of the ester group in **Acrylate-sP(EO-*stat*-PO)** since the zeta-potential measurements were performed from basic to acidic pH values and this negative charging was reversible. While the positive charge on the particles at lowers pH is supposed to be mainly due to the protonation of secondary amines in the nanogels

Ovalbumin Nanogels

Ovalbumin nanogels were prepared in the same manner as Diamine nanogels. Ovalbumin was taken in 0.05, 0.10, 0.20, 0.30, 0.40, 0.50, 0.75 and 1.0 molar equivalents. Particles prepared by using Ovalbumin as a crosslinker showed behaviour regarding dispersion stability very similar to Diamine nanogels. However, DLS measurements confirm that in water these nanogels possessed a narrower size distributions compared to Diamine nanogels with the z-average particle diameter in the range of 180 nm to 210 nm for different equivalents of Ovalbumin **(Table 7.7)**.

Table 7.7 Hydrodynamic diameter and zetapotential of Ovalbumin nanogels with varying amount of Ovalbumin.

Ovalbumin Molar Equivalents	Diameter[nm]	PDI	Zetapotential*[mV]
0.05	180	0.345	-30.2
0.10	200	0.342	-29.2
0.20	200	0.367	-31.4
0.30	200	0.367	-30.6
0.40	180	0.316	-31.7
0.50	180	0.321	-30.1
0.75	180	0.300	-29.8
1.0	210	0.310	-30.9

* pH=10

Zetapotential of these nanogels are largely attributed to the presence of deprotonated –COOH residue in Ovalbumin particularly at pH 10. Because of its positive charge in physiologic conditions, the primary amines are usually outward-facing (i.e. on the outer surface) of Ovalbumin; thus, they are accessible for conjugation without denaturing protein structure. Since native Ovalbumin contain compact hydrophobic cores, once the crosslinking is initiated, unfolding of Ovalbumin takes place which exposes the hydrophobic segments and collapse of particle size occurs in hydrophilic environment. This explains the almost constant hydrodynamic diameter of the particles even with increasing Ovalbumin equivalents.

As seen from the cryo-FESEM and cryo-TEM images **(Figure 7.3 a, b)**, the particles have well-defined spherical shapes with particle diameters d in the range of 150 nm < d < 250 nm. These two techniques correlate well with the particle size what is obtained with DLS. In the TEM mode **(Figure 7.3c)** nanogels show a sharp interface and particles appear to be stiffer compared to Diamine nanogels which could be caused due to the hydrophobic nature of Ovalbumin.

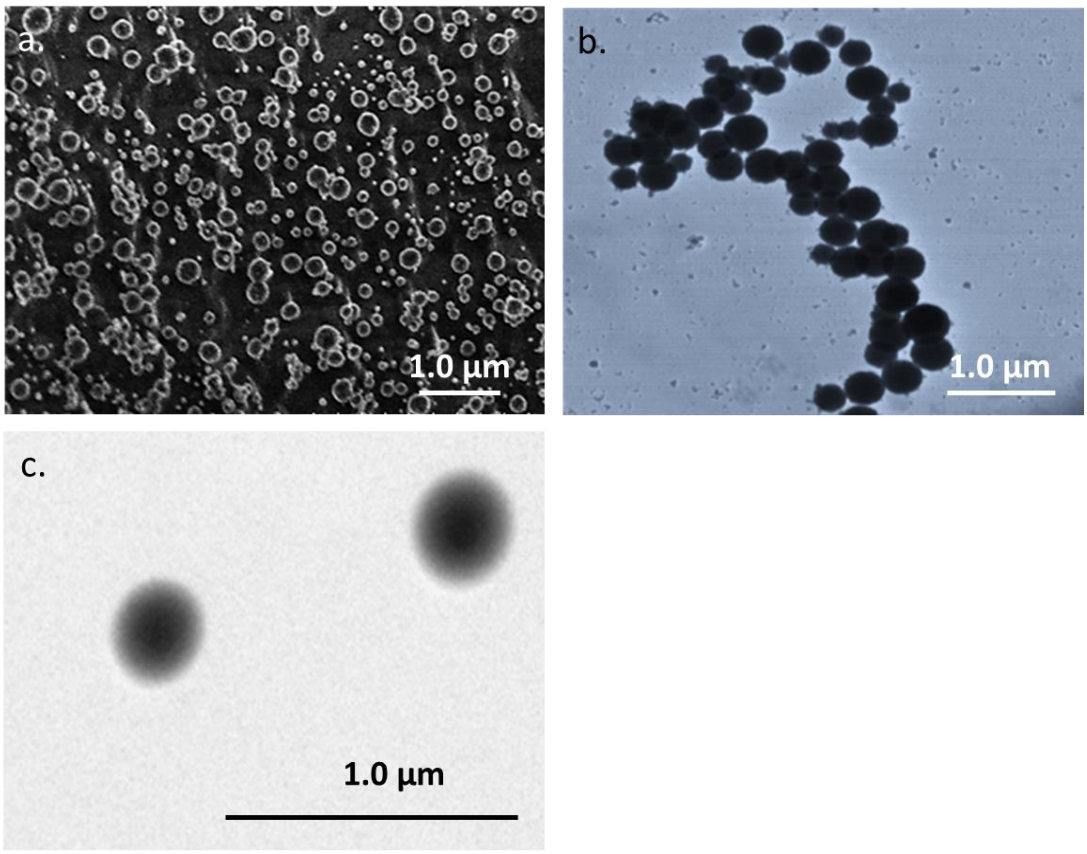

Figure 7.3 a: Cryo-FESEM **b.**Cryo-TEM and **c.**TEM images showing **Acrylate-sP(EO-*stat*-PO)**-Ovalbumin nanogels in the ratio of 1.0:1.0 molar equivalents of **Acrylate-sP(EO-*stat*-PO)** and Ovalbumin.

To determine the loaded amount of Ovalbumin in nanogels, BCA assay was performed. It is an easy way to determine protein concentration in the use of a bicinchoninic acid (BCA) assay. The advantage of this method is its accuracy, easy handling and less interference with common disturbing compounds. The BCA protein assay uses two reagents, a BCA detection reagent and a 4% copper sulfate solution, which are mixed together prior to use in a 50:l ratio.

Step 1: Biuret reaction - Reduction of copper ion from cupric to cuprous, in presence of protein in alkaline environment

BCA is a reagent specific for the cuprous ion (Cu^{+}). It is assumed /postulated that Cu^{2+} existing in the alkaline medium, is reduced by protein when the peptide bonds of a protein forms a blue coloured complex with the copper atoms.

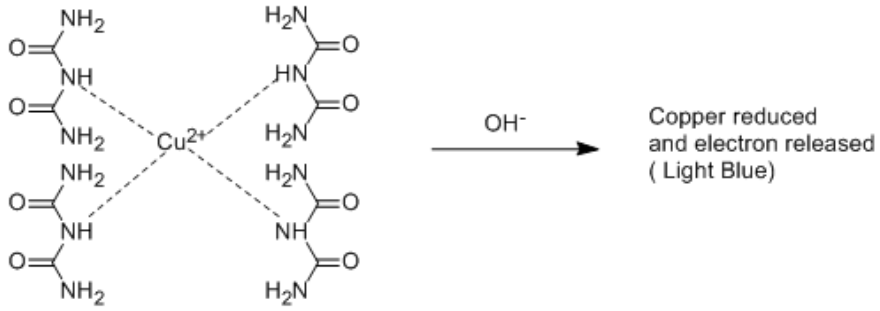

Step 2: Reaction of BCA with cupreous ions

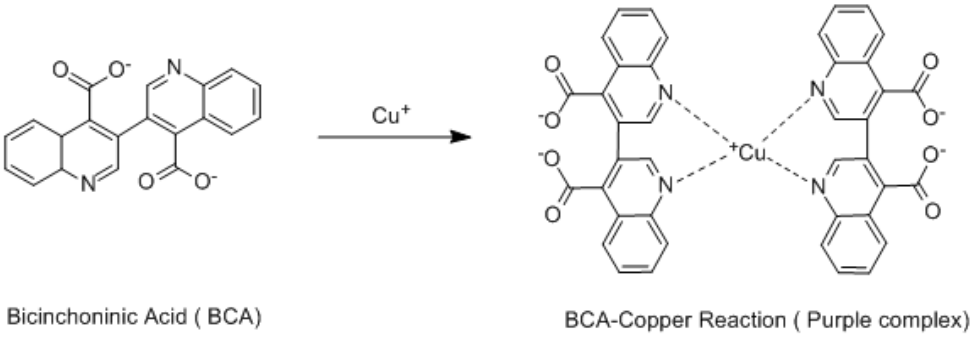

Scheme 7.2: Schematic of BCA assay reaction

Cu^{+} then reacts with two bicinchoninic acid molecules to form an intense purple-colored chelated complex. This BCA/Cu complex is water soluble and absorbs light at a wavelength of 562 nm. The intensity of this absorption increases linearly with increasing protein concentration allowing quantification of protein in solution spectrophotometricaly.

Table 7.8 Amount of Ovalbumin loaded in Ovalbumin nanogel estimated via BCA assay

Acrylate-sP(EO-*stat*-PO) [mg]	Molar Equivalents of Ovalbumin	Ovalbumin in recipe [mg]	Ovalbumin Loaded [mg]	Percentage Loading [%]
25	0.05	1.87	1.70	91
25	0.10	3.75	3.43	92
25	0.20	7.50	6.68	89
25	0.30	11.25	6.75	60
25	0.40	15.0	7.60	51
25	0.50	18.75	8.10	43
25	0.75	28.12	10.13	36
25	1.0	37.50	12.01	30

Working reagent for the assay was prepared as described. To assure the accuracy of the test the absorbance at 562 nm was measured for all samples within 10 minutes. The absorbance measurement of the blank standard was subtracted from the rest of the samples and the absorbance value was plotted against the concentration. A linear fit was applied to find out the concentration of the unknown samples

It was confirmed from the results **(Table 7.8)** that Ovalbumin is crosslinked and not adsorbed as we assume that all non bonded Ovalbumin was removed during repeated centrifugation and later by dialysis using a dialysis membrane with a MWCO of 100,000. With increasing amount of loadings a maximum of 48w/w% of Ovalbumin with respect to **Acrylate-sP(EO-*stat*-PO)** was achieved. The Raman spectra peaks at the wavelength 1003 cm^{-1} are stronger for nanogels prepared with 1.0 eq and 0.75 eq Ovalbumin which correlates to the data obtained by the BCA assay. The rapid decrease of the Ovalbumin loading efficiency at high Ovalbumin concentrations in aqueous droplets can be explained by non-sufficient crosslinking by acrylate-PEG. In this situation non-crosslinked Ovalbumin is removed from the nanogels during purification step.

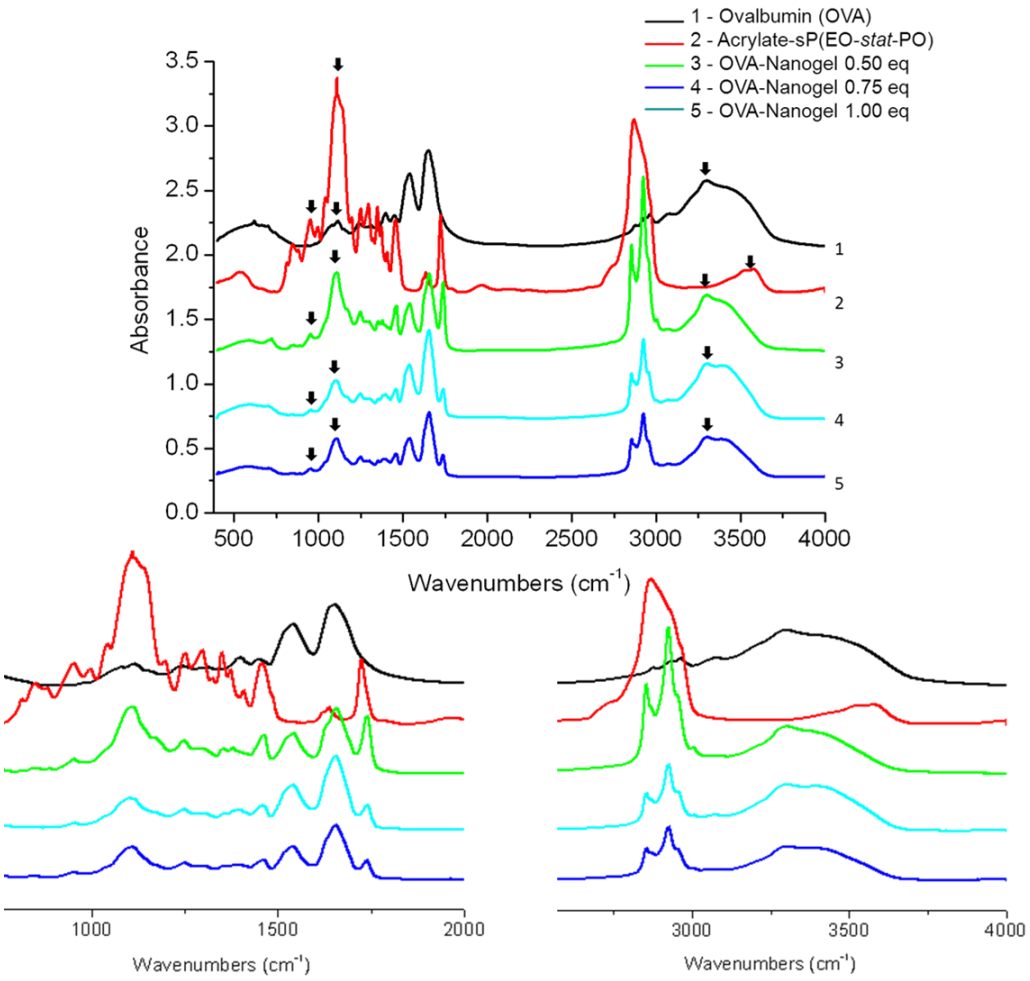

Figure 7.4: IR spectra of Ovalbumin (1) **Acrylate-sP(EO-*stat*-PO)** (2) Ovalbumin nanogels in the ratio of 1.0:0.50 (3) 1.0:0.75 (4) 1.0:1.0 (5) molar equivalents of **Acrylate-sP(EO-*stat*-PO)** and Ovalbumin.

IR spectra analysis was performed for Ovalbumin nanogels and was compared with **Acrylate-sP(EO-*stat*-PO)** and Ovalbumin. All Ovalbumin nanogels show characteristic peaks of the polymer and of the Ovalbumin compound. The peaks at 1108 and 2855 cm^{-1} in the Ovalbumin nanogel samples show that the polymer was incorporated as these vibrations are of the PEG chain. The carbonyl group from **Acrylate-sP(EO-*stat*-PO)** at 1737 - 1739 cm^{-1} could be seen present in all Ovalbumin nanogel samples. The vibrations for the methacrylate group at 1635 cm^{-1} in nanogels samples show a decreasing trend and almost disappear for 1:1.0 molar equivalents of **Acrylate-sP(EO-*stat*-PO)** and Ovalbumin nanogel. While the peak of methacrylate group at 966 cm^{-1} overlaps with Ovalbumin peak. Incorporation of Ovalbumin in the nanogels was clearly

seen by its characteristic peaks at 3297 - 3299, 1654 - 1655 and 1537 - 1540 cm^{-1} and 966 cm^{-1}

Raman Analysis

Raman spectra analysis was also performed for Ovalbumin nanogels and was compared with Acrylate-sP(EO-*stat*-PO) and Ovalbumin Raman spectra in order to see any change in secondary structure changes in Ovalbumin in the nanogel. Ovalbumin nanogels with three different equivalents of crosslinked Ovalbumin were analysed. For Ovalbumin molar equivalents lower than 0.5, the spectral changes were not very distinct so their analysis is omitted here. On comparing the Raman spectra for different Ovalbumin equivalents there was a clear indication that Ovalbumin was bonded to the polymer with changes in its secondary structure.

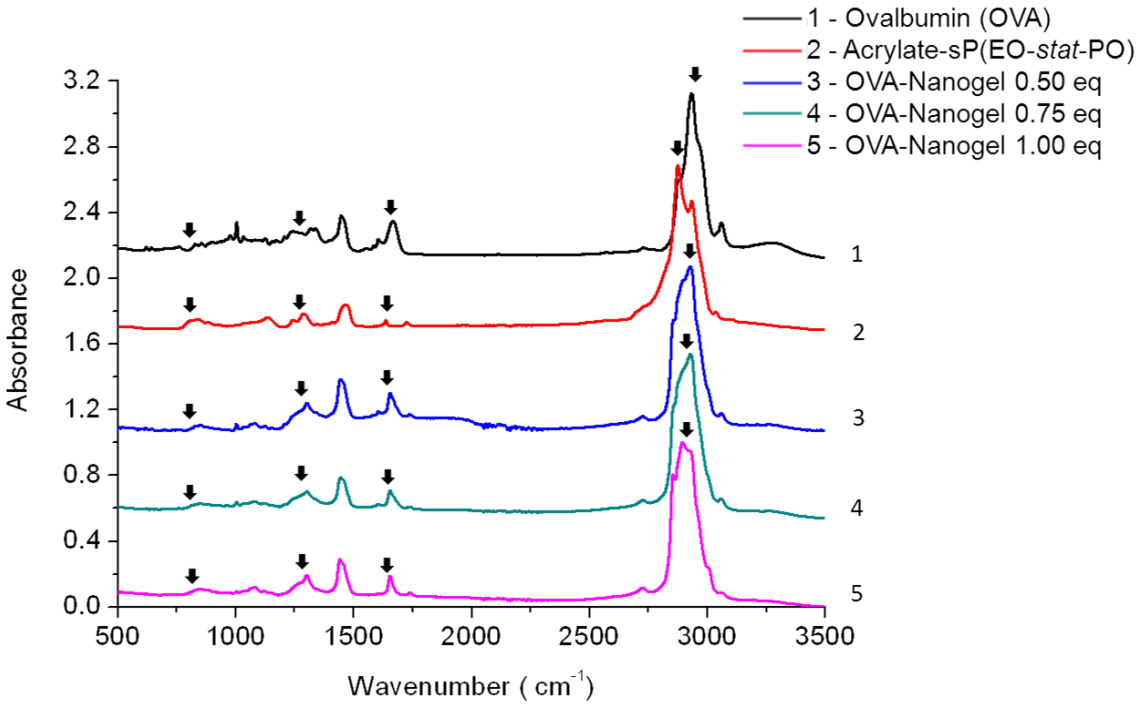

Figure 7.5: Raman spectra of Ovalbumin (1), **Acrylate-sP(EO-*stat*-PO)** (2) Ovalbumin nanogels in the ratio of 1.0:0.50 (3) 1.0:0.75 (4) 1.0:1.0 (5) molar equivalents of **Acrylate-sP(EO-*stat*-PO)** and Ovalbumin.

Ovalbumin has basically peptide bonds that repeat the conformation of the polypeptide backbone forming the secondary structure, like α-helix, β- pleated sheet and random coil. From literature[15] it is known that these three contributions are observed in Raman spectra as a large band centered at 1665 cm^{-1} through the amide I and amide III

contribution. The amide I and amide III modes for the α-helix structure shows a peak at 1658-1640 cm^{-1} and 1310-1260 cm^{-1} respectively.

For the β-sheet the amide I and amide III modes show peak at 1680-1655 cm^{-1} and 1242-1235 cm^{-1} respectively while for random coil Amide I and Amide III are at 1666-1660 cm^{-1} and 1250-1240 cm^{-1}. The phenyl stretching bands at 998, 1027 and 1602 cm^{-1} present in the Raman spectra indicates the aromatic amino acids residues of Ovalbumin. Since the α-helix, β-sheet and random coil Amide I and Amide III bands lie very close to each other, to get a clearer insight into the changes, Circular Dichromism Spectroscopy was performed.

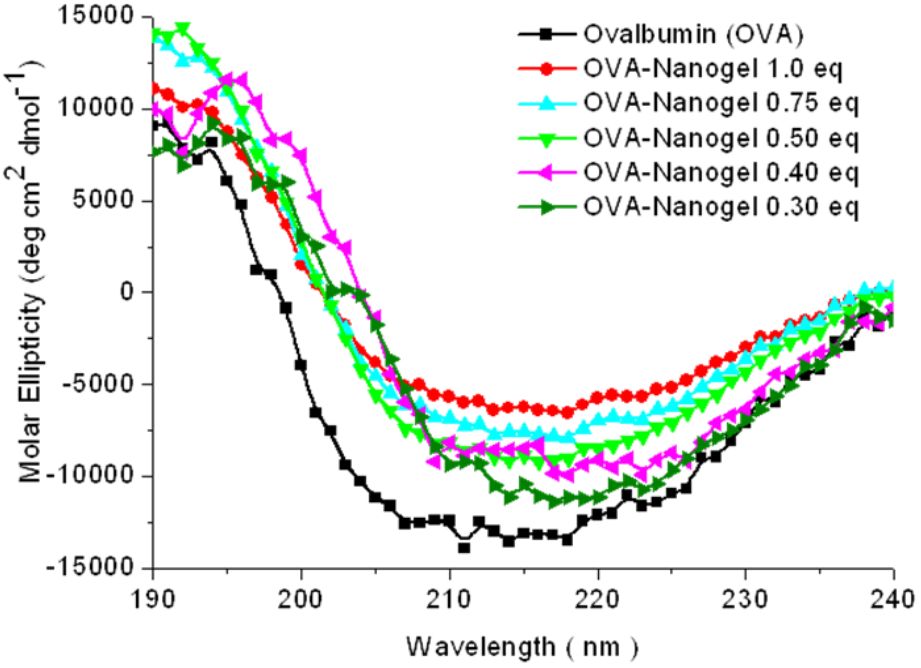

Figure 7.6: CD spectra of Ovalbumin before and after crosslinking in a nanogel.

Ovalbumin contains 33 % α- helix, 5 % β-sheet and 62 % random coil in its native form. The changes in the α-helix content of Ovalbumin were followed by monitoring the ellipticity at 222 nm. A minimum and a shoulder were observed for native Ovalbumin at 222 nm and 210 nm, respectively. When Ovalbumin was crosslinked, the amplitude at 222 nm was attenuated and the shoulder at 210 nm got amplified. The change in CD spectra with amount of Ovalbumin in nanogel suggests that the change in the secondary structure of Ovalbumin progresses with increase in crosslinking. Increase in crosslink density significantly amplified the negative deflection in the region between 210 and 220 nm. For model peptides and proteins of known three-dimensional structures, the helical structure gives minima in CD spectra at 222 and 208 nm and the

β-sheet structure gives minimum at 216 nm while a random coil at 200 nm.[16] α- helical content F_h, of Ovalbumin can be estimated from the mean residual ellipticity at 222 nm, θ_{222} (in $deg.cm^2.dmol^{-1}$), using the following equation.[17]

$F_h = (\theta_{222} - \theta c) / (\theta_h - \theta c)$

were θ_h *and* θc are respectively the mean residual ellipticity values determined for the fully α- helical and fully disordered (random coil) polypeptide. If values of -36,000[18] and -280 $deg.cm^2.dmol^{-1}$ [19]are substitute for θ_h and θc respectively, the α- helical content in unmodified Ovalbumin and Ovalbumin –nanogels can be calculated **(Table 7.9).**

Table 7.9 Percentage of α- helix in Ovalbumin nanogel with increasing Ovalbumin content

Molar Equivalents of Ovalbumin	θ_{222} ($deg.cm^2.dmol^{-1}$)	% α- helix
Ovalbumin	-10984.010	30.0
0.30	-10268.288	28.0
0.40	-9036.351	24.5
0.50	-8030.937	21.7
0.75	-6873.476	18.5
1.0	-5681.097	15.1

It is seen from **Table 7.9** that with increase of Ovalbumin amount in nanogels, the α-helical content decreases from 30% in case of unmodified Ovalbumin to 15% for 1.0:1.0 molar ratio nanogel, showing the increase in crosslink density of Ovalbumin in the nanogels with its increasing molar ratio.

To test whether the size of the Ovalbumin nanogel changes in different pH buffers, the hydrodynamic diameter of Ovalbumin nanogels with 1.0 molar equivalent of Ovalbumin was measured by DLS. It can be observed (Table 7.10) that the size of the Ovalbumin nanogels does not increase by any change in pH.

Table 7.10 Influence of pH on size and zetapotential of Ovalbumin nanogels

pH	Z-average [nm]	PDI	Zetapotential [mV]
3	200	0.207	12.00
4	200	0.191	2.01
5	220	0.224	-1.11
6	220	0.245	-2.24
7	220	0.206	-7.76
8	220	0.215	-9.34
9	220	0.231	-9.29

Looking at the zeta potential of the Ovalbumin nanogels, same zeta potential trend which has already been determined for the Diamine nanogels is seen. The Ovalbumin nanogels display a positive charge in acidic buffers and a negative charge in basic buffers caused by deprotonation of functional groups inside the nanogel network. The data also suits to the zeta potential trend which is displayed by Ovalbumin colloids alone [20] with an isoeletric point (pI) of 4.6 which is very close to the pI of native Ovalbumin at pH 4.9.

7.4 Conclusion

In conclusion nanogels by crosslinking six-arm acrylate functionalized star shaped P(EO-*stat*-PO) with different spacer length PEG-diamine and the amine groups of the various amino acids of Ovalbumin was synthesized in inverse miniemulsion. The size of Diamine-nanogels could be tuned by change in spacer length of diamine, pH and cationic valency of the salts. The SEM analysis of particles confirmed that nanogels with a diameter of 230 nm < *d* < 350 nm were formed. The particles were soft and took a flat morphology in the dry state. IR spectroscopy data showed the efficient crosslinking of diamine to the star polymer. Biohybrid ovalbumin nanogels were synthesized with different equivalents of Ovalbumin. It was found that the size of the Ovalbumin nanogels was independent of the equivalent of star polymer to the Ovalbumin and pH. Microscopy images showed formation of well defined spherical particles with particle diameters *d* in the range of 150 nm < *d* < 250 nm. The CD

spectroscopy and BCA assay proved that the Ovalbumin has been effectively crosslinked. From the results of the BCA assay, it can also be concluded that there exists a limiting amount of Ovalbumin which can be incorporated into the nanogels. It was found that for 25 mg of polymer, up to 12mg of Ovalbumin can be bonded.

As a result Ovalbumin nanogels represent an extremely interesting field of biohybrid nano-hydrogels prepared via simple and mild synthesis route. Introduction of synthetic as well as biomolecule into the system further enhances its versatility

7.5 References

[1] L. A. Lyon, J. D. Debord, S. B. Debord, C. D. Jones, J. G. McGrath, M. J. Serpe, *J. Phys. Chem. B* **2004**, 108, 19099.

[2] M. Das, H. Zhang, E. Kumacheva, *Annu. Rev. Mater. Res.* **2006**, 36, 117.

[3] R. Pelton, *Adv. Colloid Interface Sci.* **2000**, 85, 1.

[4] S. Nagl, M. I. J. Stich, M. Schaferling, O. S.Wolfbeis, *Anal. Bioanal. Chem.* **2009**, 393, 1199.

[5] V. A. KAbanov, V. S. Vinogradov, *Angew. Chem. Int. Ed.* **2009**, 48, 5418.

[6] D. Oupicky, M. Ogris, A. K. Howard, R. P. Dash, K. Ulbrich, W. L. Seymour, *Mol. Ther.* **2002**, 5, 463.

[7] A. Aigner, D. Fischer, T. Merdan, C. Brus, T. Kissel, F. Czubayko, *Gene. Ther.* **2002**, 9, 1700.

[8] E. A. Scott, M. D. Nichols, L. H. Cordova, B. J. George, Y. S. Jun, D. L. Elbert, *Biomaterials* **2008**, 29, 4481.

[9] C. M. Lensen, P. Mela, A. Mourran, J. Groll, J. Heuts, H. Rong, M. Moeller, *Langmuir* **2007**, 23, 7841.

[10] F. S. Steven, G. R. Tristram, *Biochem. J.* **1958**, 70, 179.

[11] Thermo Scientific: Pierce BCA Protein Assay Kit. www.piercenet.com

[12] Z. Ying, S. Haijia, L. Fang, T. Tianwei, *Polymer* **2005**, 46, 5368.

[13] R. Zimmermann, W. Norde, M. A. C. Stuart, C. Werner, *Langmuir* **2005**, 21, 5108.

[14] R. Zimmermann, U. Freundenberg, R. Schweiss, D. Kuettner, C. Werner, Current *Opinion Colloid Interface Sci.* **2010**, 15, 196.

[15] S. Cinta-Pinzaru, S. Cavalu, N. Leopold, R. Petry, W. Kiefer, *J. Mol. Str.* **2001**, 565, 225.

[16] P. P. Batra, K. Sasa, T. Ueki, K. Takeda, *J. Protein Chem.* **1989**, 2, 221.

[17] T. Lin, T. P. Quinn, D. Grandgenett, M. T. Walsh, *Proteins* **1989**, 5, 156.

[18] N. Greenfield, G. D. Fasman, *Biochemistry* **1969**, 8, 4108.

[19] W. L. Mattice, J. T. Lo, L. Mandelkern, *Macromolecules* **1972**, *5*, 729.

[20] T. Matsumoto, J. Chiba, H. Inoue, *Coll. Poly. Sci.* **1992**, *270*, 687.

CHAPTER 8

Elastin Polypeptide Nanogels with Dual Stimuli Responsivity

8.1 Introduction

Elastin as a proteintaceous material with ~50 % of the total vascular ECM weight is the primary structural component underlying the elastomeric mechanical response of compliant tissues.[1,2] It has thus vital role for appropriate function of tissues, especially skin, veins, connective tissue proper, and therefore has been involved in numerous studies aimed at unrevealing the relationship between its sequence and conformation, especially with regard to its influence on the mechanism of extension and recovery.[3] Its unusual structure comprises of hydrophobic and cross-linked desmosine domains which are intellectual driving force for structural investigations of elastin to produce novel protein-based materials. Former domain has an abundance of repeating polypenta- and polyhexapeptide sequences, some of which are often defined as peptide mimetic of elasticity, while its protein composition is mainly dominated by nonpolar amino acid residues, like glycine, proline, alanine, and valine.[4] These hydrophobic pockets in elastin polypeptide induce reversible, temperature-dependent, hydrophobic assembly from aqueous solution resulting in spontaneous phase separation of polypeptide above a critical temperature or lower critical solution temperature) (LCST) which depends on elastin composition and as well as on its surrounding conditions.[5,6] This process is called as coacervation and have similarities with analogous temperature phase behavior seen in thermo-responsive polymers like poly(*N*-isopropylacrylamide) and poly(N-vinylcaprolactam) as such.[7]

Since elastin occurs in its functional chemical cross-linked network, unique functional properties of it led to produce solubilized elastin derivatives *via* scission of chemical bonds under relative hard conditions of acid-triggered (α-elastin) or base-triggered (β-elastin) hydrolysis. Although these processes undoubtedly result in structural modifications,[8] initial studies on solubilized derivatives provided the evidence of the thermally responsive behavior of elastin, preserved biological feature like maintaining cell recognition signals and information on its unusual amino acid composition.[9-11]

Soluble elastin derivatives are involved in the production of novel biomaterials, and the cross-linking generally performed over lysine chemically, stabilize the polymeric form of the protein so that resulting material can be produced in any desired shape and size.[4]
Due to the unique functional properties stated above, elastin and its derivatives are promising candidates for use scaffolding materials in tissue engineering, in which critical properties such as phase behavior, macroscopic mechanical response, biocompatibility, and biodegradability are driving forces for introducing of elastin into novel emerging polymeric systems. Overall, tunable phase behavior of elastin presents an interesting opportunity for encapsulation and controlled release applications. In this context, numerous elastin-derivatives based systems were produced for delivery of a number of pharmaceuticals, DNA, and proteins.[12,13] However, the immunogenicity of these materials has not been much explored.[14] Beside the elastin like polymers (ELP) based nanoparticles, to the best of our knowledge; there is no report on chemically cross-linked native elastin based nanogels.
In this sense, herein we report a novel biohybrid nanogels systems based on soluble α-elastin polypeptides *via* facile inverse miniemulsion approach using two different amine-reactive cross-linkers; poly(ethylene glycol) diglycidyl ether (PEG-DGE) and bis(sulfosuccinimidyl) suberate (BS3). Nanogels were fabricated at various composition of precursors (elastin and cross-linker), and nanogel formation was evidenced by cryo-SEM and dynamic light scattering (DLS). Thermo- and pH responsivity was explored by DLS measurements of the hydrodynamic radii of nanogels in water against respective stimuli. The experimental data revealed that the elastin nanogels were sensitive towards temperature changes with a volume phase transition of 37 and 35.5 °C and pH responsivity in the range of 5-7, for nanogels criosslinked with PEG-DGE and BS3 respectively. Moreover, it was observed that these transitions were mainly influenced by cross-linker type and crosslink density. Elastase-triggered degradation profiles of the nanogels were explored by DLS measurements against time. Colloidal stability of the nanogels was investigated by sedimentation analysis. Texas Red conjugated dextran was used as a model drug to load the nanogels and its loading, release kinetics was investigated spectrophotometrically. The cytocompatibility test of the gels was performed using Human umbilical vein endothelial cells (HUVECs) up to 6 days.

Nomenclature. In this work, cross-linkers; poly(ethylene glycol) diglycidyl ether and bis(sulfosuccinimidyl) suberate are respectively named as PEG-DGE and BS3, the

nanogels produced with these cross-linkers are named with cross-linker name, e.g. PEG-DGE nanogels for elastin nanogels prepared by PEG-DGE cross-linker.

8.2 Experimental

8.2.1 Material and Methods

Elastin with molecular weight range of 10-60 kDa was purchased from Elastin Company (USA) dissolved in borate buffer (pH 9). Poly(ethylene glycol) diglycidyl ether (PEG-DGE) (MW= 526 g/mol) and bis(sulfosuccinimidyl) suberate (BS3) were respectively purchased from Sigma Aldrich (Germany) and Piercenet Biotechnology, Inc (USA). N-hexane (99%, VWR), Span 80 (Sigma), Tween 80 (Sigma), Tetrahydrofuran (99% Sigma Aldrich), Texas Red Dextran (MW= 70 KDa, Invitrogen) were used as received. Dialysis membranes (MWCO = 3.5 kDa, 25 kDa and 100 kDa) were purchased from Spectrum Laboratories.

8.2.2 Synthesis of Elastin-PEG DGE and Elastin-BS3 Nanogels

Nanogels were fabricated *via* inverse miniemulsion method using aqueous phase in 1.25 mL n-hexane containing surfactants (37.5 mg of 3:1 weight ratio of Span 80 and Tween 80) (Scheme 1). The aqueous phase consisted of 25 mg (4.166×10^{-4} mmol) of elastin dissolved in 125 μL of 0.04 M PBS buffer (pH = 9). The organic and the aqueous phases were pre-emulsified by magnetic stirring for 10 min. Following the stirring, the system was ultrasonicated using a Branson sonifier W450 with a ¼″ horn at duty cycle of 30% and output control of 90% under ice cooling. Cross-linking reaction was initiated by subsequent addition of PEG-DGE or BS3, and followed by a further sonication. Following this procedure, nanogels with various molar ratios of 1:2, 1:1.5, 1:1 1:0.5 and 1:0.25 (elastin: cross-linker) were produced. The sonication times before and after the addition of cross-linker was kept constant to 60 s. The reaction was allowed to proceed further for 45 min at room temperature with constant stirring followed by addition of 1.5 mL of acidic water (pH = 3). Separation of the nanogels was achieved by centrifugation at 10,000 rpm for 30 min with subsequent decantation of the supernatant. Nanogels present in the aqueous layer were then carefully washed with hexane (2 × 1.5 mL) and THF (4 × 2.5 mL) in order to remove the surfactants and unreacted elastin. The remaining organic solvents and acid were removed by dialysis. Purified nanogels were stored in Millipore water at 4 °C for further use.

1:0.25 and 1:0.5 PEG-DGE and BS3 nanogels respectively were loaded with Dextran. Loaded nanogels were prepared in similar manner with a loading of 15 and 20 wt% of dextran with respect to elastin for each of the nanogels. During nanogels formation dextran was dissolved in aqueous phase of the miniemulsion while keeping the rest of the parameters as described above. After nanogel purification the amount of conjugated Dextran was quantified by means of UV-Vis method.

8.2.3 Influence of Temperature on Nanogels Size. Thermoresponsivity of nanogels was investigated by DLS measurements as a function of temperature between 10 °C - 55 °C. Hydrodynamic radius (R_h) values have been calculated through second order cumulative fit *via* Stokes-Einstein equation. In order to check the reversibility of the hydrodynamic radius with temperature transition, five heating and subsequent cooling cycles were performed at 20 °C and 44 °C.

8.2.4 Influence of pH and Zeta-Potential. Influence of pH on size and on zeta-potential of nanogel was investigated. The pH was maintained in the range of 3 - 10 by addition of 0.01 M HCl or 0.01 M NaOH. Measurements were carried out at 20 °C. For zeta-potential measurement 100 scans were made for each sample. Dialysed nanogels with a concentration of 5 mg/ml were used for all measurements.

8.2.5 Influence of Temperature at pH 3 and 8 on Microgel Size. PEG-DGE and BS3 nanogels with molar ratio of 1:0.25 were swelled at pH 3 and pH 8, and R_h was monitored as a function of temperature from 10 °C to 55 °C heating and 55 °C to 10 °C cooling.

8.2.6 Sedimentation Analysis Sedimentation of nanogels was investigated with a LUMiFuge 114 separation analyser (L.U.M. GmbH, Germany). Measurements were performed in glass tubes at acceleration velocities of 500 - 3000 rpm at 20°C. The slope of the sedimentation curves was used to calculate the sedimentation velocity and the data further used to evaluate the colloidal stability of the samples.

8.2.7 Drug Loading and Release Followed washing steps microgel particles were re-suspended in 10 mL PBS buffer at pH = 5. The extracted amount Texas Red Dextran during the washing was subtracted from the final value to estimate the final loading

using a standard calibration curve by measuring the absorbance at 596 nm, of the non-loaded dextran present in the supernatant and subtracting this value from the total amount of dextran used for loading. To study the release of loaded dextran, the nanogels were incubated at 20°C and 40°C in tubes. The tubes were then shaken at 100 rpm on a shaker. At an interval time of 0, 1, 5, 10, 15, 25, 36, 48 and 72 h nanogels were centrifuged and then re-suspended in fresh buffer solution at respective temperatures. The release was monitored spectrophotometricaly for all the supernatants obtained from microgel sample. All studies were performed in triplicate and the release behaviour was analyzed in terms of cumulative ratio (%) of released dextran. The encapsulation efficiency% of dextran was calculated according to **Equation 8.1.**

Encapsulation efficiency% = $(D_t / D_0) \times 100$. Eq. 8.1

Where D_t = actual amount of the dextran in microgel and D_0 = theoretical amount of dextran in microgel.

8.2.8 Enzymatic Degradation

Degradation of nanogels was performed in 5 mM elastase in PBS (pH = 8.8) at 37 °C. Assessment of reduction kinetics with in the presence of elastase was followed by measuring the hydrodynamic radius of the nanogels by dynamic light scattering after every 180 s for a total time of 24 h.

8.2.9 XTT Cytotoxicity Test

The XTT viability assay (Roche XTT Cell Proliferation Kit II, catalog no. 1465015) were performed according to the manufacturer`s guidelines. The gels were prepared on the bottom of 96-well polystyrene plates. Human umbilical vein endothelial cells (HUVECs) (10,000 per well) and 500 μL of 10% fetal bovine serum medium were added to the wells (1.77 cm^2), and the mixtures were incubated in 5% CO_2 at 37 ^oC for 96 h. To halt the experiment, aliquots of XTT stock solution, 5 mg/mL, were added to the each experimental well group at a ratio of 50 μL/100 μL of medium. Experimental plates were incubated for 4 h, and samples (100 μL) from each well were transferred to 96-well plates and quantified using a TECAN reader at a λ of 490 nm and a reference λ of 655 nm.

8.3 Results and Discussion

Elastin polypeptide nanogels were produced through inverse mini-emulsion technique using two different cross-linking routes shown in **Scheme 8.1**. In the first cross-linking approach, elastin microgel formation was carried out over epoxy ring opening reaction of diepoxide terminated PEG-based cross-linker at basic pH. In this case, basic pH of the polymerization media catalyzes the epoxy/amine reaction, and additionally, the reaction is also auto-catalyzed by the hydroxyl groups generated in the course of epoxy/amine reactions.

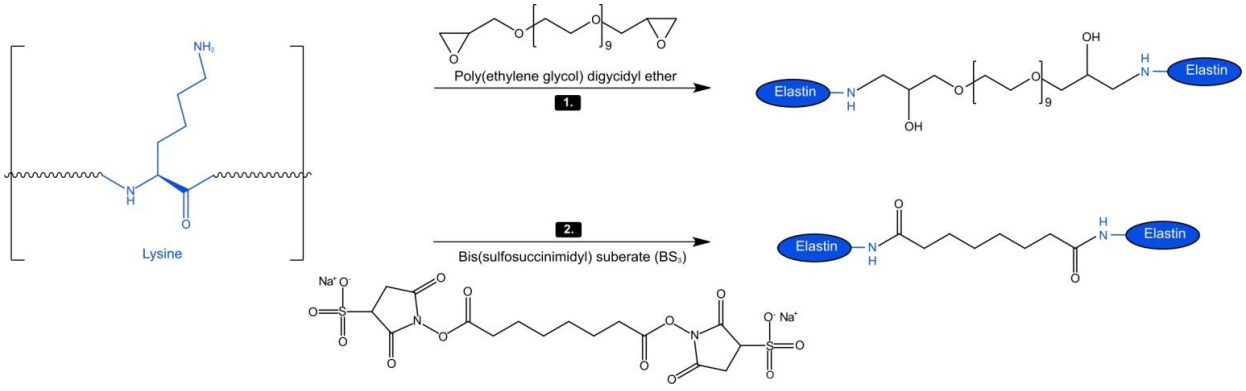

Scheme 8.1: Schematic illustration of nanogels/nanogels formation from elastin polypeptides through inverse miniemulsion technique using two different chemical cross-linking reactions indicated.

The overall mechanism was explained by Rozenberg *et al* (1986) over nucleophilic addition on the epoxy ring, proceeding with preliminary activation of the epoxy ring by amine, which acts both as an electrophilic and as a nucleophilic agent.[15] In the second cross-linking route, cross-linking mechanism go over bis(Sulfosuccinimidyl)suberate (BS3) having terminal sulfonyl substituents. In aqueous media, sulfonyl terminal groups dissociate in water and *N*-hydroxylsiulfosuccinimide (NHS) esters at each end react predominantly with primary amine forming stable amide bonds through S_N2 reaction in which the NHS acts as a leaving group. Elastin nanogels were produced with these cross-linking routes at different cross-linking compositions, and the effect of cross-linking degree was determined through size changes on nanogels by DLS analysis. Relevant data as the molar ratio of cross-linker with respect to elastin are proved in **Table 8.1** in which hydrodynamic radii of nanogels are shown at swollen state of 20 ^{o}C. For both type of cross-linking routes, nanogels with varied hydrodynamic radii in the

range of 170 - 890 with polydispersity index of about 0.50 were obtained, changes on size were remarkable and it was observed that the microgel size decreased with increasing cross-linking density. Lower molar ratio gave nanogels with higher hydrodynamic radius due to low cross-linking density and therefore pronounced swelling. For instance, eight fold increases in molar concentration of PEG-DGE and BS3 (1:2) respectively resulted in ~18 and ~86 folds volumetric decrease in nanogels. Since obtained nanogels are temperature responsive, the ratio of their hydrodynamic radii measured at 50 °C and 20 °C (R_h^{50}/R_h^{20}) reflects to some extent their swelling ability. Since in collapsed state nanogels may contain some water, the swelling ratio $(R_h^{50}/R_h^{20})^3$ is not equal to the swelling degree. To calculate $(R_h^{20}/R_h^{50})^3$ ratio we used average R_h values measured at respective temperature. Further more, we calculated swelling in [%] based on change of the hydrodynamic radius upon temperature change. As shown in Table 1, for both microgel types similar trend is observed, namely the swelling ratio increases with increase of the crosslinker amount, what means that microgel swelling ability is reduced due to the increase of the crosslink density. For the same elastin concentration with varying PEG-DGE amount the swelling - was around 180-200% for molar ratio of 1:0.25, 1:0.5 and 1:1 while for 1:1.5 and 1:2 molar ratios the swelling % decreased to 150. In case of BS3-cross-linked nanogels 1:0.25 and 1:0.5 molar ratio particles showed swelling up to 160 % while the nanogels with 1:1, 1:1.5 and 1:2 molar ratios did not swell remarkably. The difference in hydrodynamic radius and swelling ratios of these two types of nanogels can be attributed to the different chemical structure of crosslinking agents. PEG-DGE exhibits water-soluble hydrophilic PEG spacer, therefore when this crosslinker integrated into microgel network it will enhance the swelling in water.

Table 8.1 Hydrodynamic radii as a function of cross-linker concentration. (PEG-DGE / BS3)

Elastin : Crosslinker [mol:mol]	PEG-DGE				BS3			
	R_h[nm]/$_{PDI}$ at 20°C	Swelling Ratio, V_{rel} $(R_{h50°}/R_{h20°})^3$	Swelling % $(R_{h20°}/R_{h50°}) \times 100$	S.V* [µm/s]	R_h[nm]/$_{PDI}$ at 20°C	Swelling Ratio, V_{rel} $(R_{h50°}/R_{h20°})^3$	Swelling % $(R_{h20°}/R_{h50°}) \times 100$	S.V* [µm/s]
1 : 0.25	878/$_{0.48}$	0.149	190	8.655	752/$_{0.47}$	0.239	160	6.053
1 : 0.5	735/$_{0.47}$	0.114	206	8.466	431/$_{0.48}$	0.232	160	6.156
1 : 1	680/$_{0.49}$	0.169	180	8.521	225/$_{0.48}$	0.701	112	6.485
1 : 1.5	370/$_{0.47}$	0.265	150	8.232	215/$_{0.38}$	0.768	109	6.595
1 : 2	334/$_{0.46}$	0.223	160	7.102	170/$_{0.47}$	0.863	104	5.178

*S.V = Sedimentation Velocity

Contrary, BS3 exhibits short hydrophobic alkyl chain as a spacer, what may enhance hydrophobic interactions in microgel network and lead to smaller size and reduced swelling in water. Additionally, there is a strong difference in cross-linking mechanism of PEG-DGE and BS3 to elastin and their reaction kinetics. In case of BS3 based cross-linking, the reaction took place much faster than PEG-DGE based cross-linking. This was proved by bulk hydrogels level through rheological analysis revealed that the cross-linking was much faster for BS3 (data not shown). This difference in reactivity may lead to more efficient incorporation of BS3 into microgel network compared to PEG-DGE and finally to the reduction of the size and swelling degree of BS3-based nanogels.

The morphology of nanogels was investigated by FESEM in cryo-mode to characterize the microgel size in water, i.e. in the swollen state. Nanogels prepared with elastin to cross-linker molar ratio of 1:2 are shown in **Figure 8.1**. Cryo-FESEM images clearly showed that the particles had well-defined spherical shape, as expected for particles synthesized by miniemulsion techniques, with particle diameters d in the range of 300 nm < *d* < 550 nm for PEG-DGE and 200 nm < *d* < 300 nm for BS3 based cross-linking for 1:2 molar ratio nanogels. Taking into account the freezing-step that might have led to partial volume loss of the microgel during cryo-FESEM, DLS and FESEM correlated well with each other with respect to size analysis of the microgel in the hydrated state.

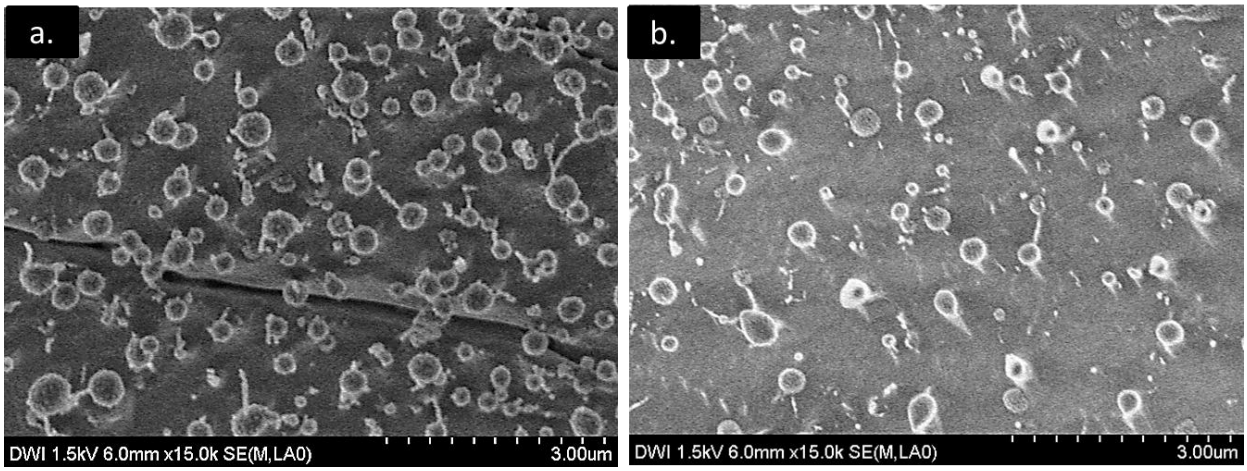

Figure 8.1: Cryo-FESEM images showing a) elastin-PEGDGE and b) elastin-BS3 microgel in the molar ratio of 1:2 of respective precursors.

Thermoresponsive Properties of Microgel.

Thermoresponsivity of both type of elastin nanogels were investigated in aqueous solution by DLS in a temperature range of 10 °C to 55 °C. The relative change of hydrodynamic radii (R_h) as a function of temperature is shown in **Figure 2** for both types of nanogels. As expected, elastin undergo a induced by temperature as external stimulus. The temperature sensitivity of the nanogels is provided by the phase transition temperature of the elastin chains, which occurs at approximately 37 °C (the lower critical solution temperature (LCST)).[16] This phenomenon occurs due to the different solvation of elastin chains by water molecules at temperatures below and above the phase transition temperature, and is also influenced by the introduction of another co-monomer.[17,18] It is believed that the volume phase transition in the microgel occurs as a result of reduced hydrogen bonding between water molecules and the peptide. The temperature at which this transition occurs is dependent on the sensitive hydrophobic/hydrophilic or entropy/enthalpy balance of the protein. Below VPT hydrophobic solvation results into undesired entropic changes which are compensated by the favorable entropy arising from peptide water hydrogen bonding. But as the temperature rises the hydrogen bonding weakens and the peptide chain contracts to compensate the effect of unfavorable entropic changes.[19]

The temperature dependent hydrodynamic radius shows a continuous decrease when approaching the volume phase transition temperature (VPTT). As expected the nanogels with lower cross-linker content were more swellable, while the VPTT was nearly independent of the cross-linking density. Since the VPT of nanogels is affected

by cross-linking density, solvent nature, composition and type of the functional groups in the protein, incorporation of hydrophilic species increases and broadens the phase transition temperature while incorporation of hydrophobic group generally reduces the VPTT. Similar phenomenon was shown for *N*-isopropylacrylamide (NIPAM) with incorporation of hydrophilic co-monomer, acrylamide (AAm) in which the incorporation of AAm was significantly influenced the LCST to higher values.[20, 21]

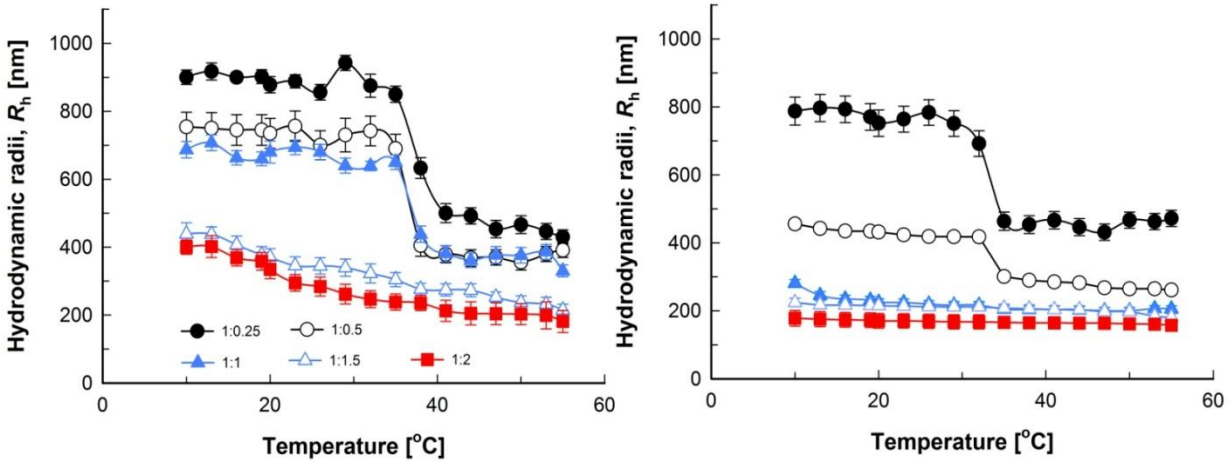

Figure 8.2: Hydrodynamic radius (R_h) of PEG-DGE (left), and BS3 (right) cross-linked microgel as a function of temperature (10°C – 55°C).

Figure 8.2 revealed that VPTT of PEG-DGE nanogels was well defined for 1:0.25, 1:0.5 and 1:1 while for 1:1.5 and 1.2 samples the transition was not observed. For BS3 cross-linked nanogels the transition was only observed for 1:0.25 and 1:0.5 molar ratios. It was further seen that the VPT for PEG-DGE nanogels was around 37.5 °C which is quite close to that of free elastin[22] while for BS3 nanogels the VPTT decreased and shifted to 35 °C which could be attributed to the introduction of hydrophobicity into the system because of the hydrophobic cross-linker and change in polarity balance caused by increased in cross-linking density. Also as the cross-linking density increased the temperature induced shrinkage decreased for both type of nanogels due to their restricted swelling.

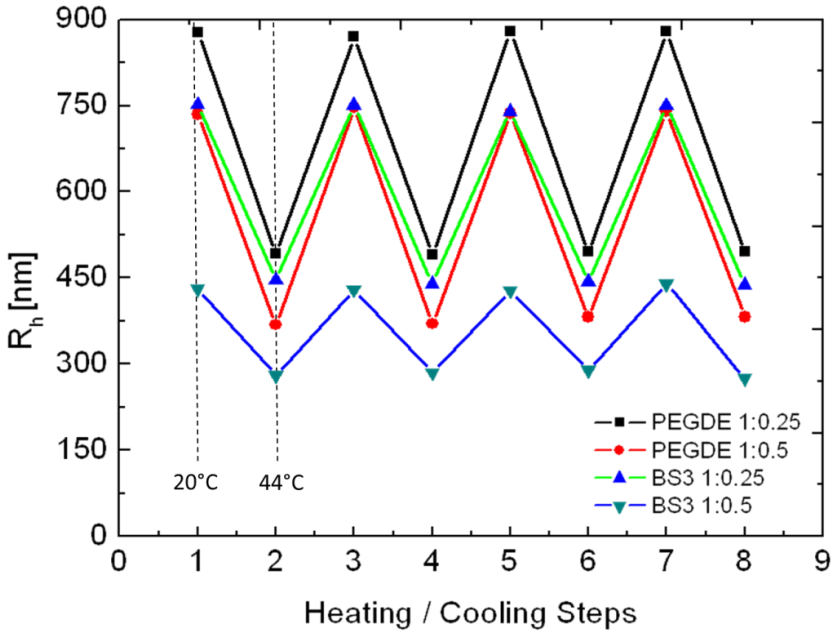

Figure 8.3: Hydrodynamic radii (R_h) during repeated heating and cooling cycle for PEG-DGE (1:0.25, 1:0.5) and BS3 (1:0.25, 1:0.5) microgel between 20 °C and 44 °C.

Four repeated heating and cooling cycles for 1:0.25 PEG-DGE and BS3 nanogels were performed at alternate temperatures; 20 °C and 44 °C and the relevant data are shown in **Figure 8.3**. Data reveals that the swelling/deswelling intensity was not weakened as the alternate temperature cycles increased. It was found that repeated heating and cooling did not significantly affect the R_h and PDI of the microgel. Thus ruling out the possibility of non-cross-linked free chains in the nanogels which could escape out of the microgel, subjected to such temperature cycling.

Influence of pH and Zetapotential

The pH sensitivity of the microgel was demonstrated by measuring the R_h in the pH range of 3 to 11. The ionization of -COOH group or -NH_2 group in basic and acidic pH could result in increase of microgel size due to electrostatic repulsion and induced particle swelling. Figure 8.4 shows that pH dependent-hydrodynamic radii (R_h) changes for both nanogels prepared at different cross-linking density. It was observed that from pH 3 to pH 6 the microgel size decreased and then increased from pH 7 to 11 for PEG-DGE nanogels while for BS3, the decreasing trend was from pH 3 to 7 and increasing from 8 to 11.

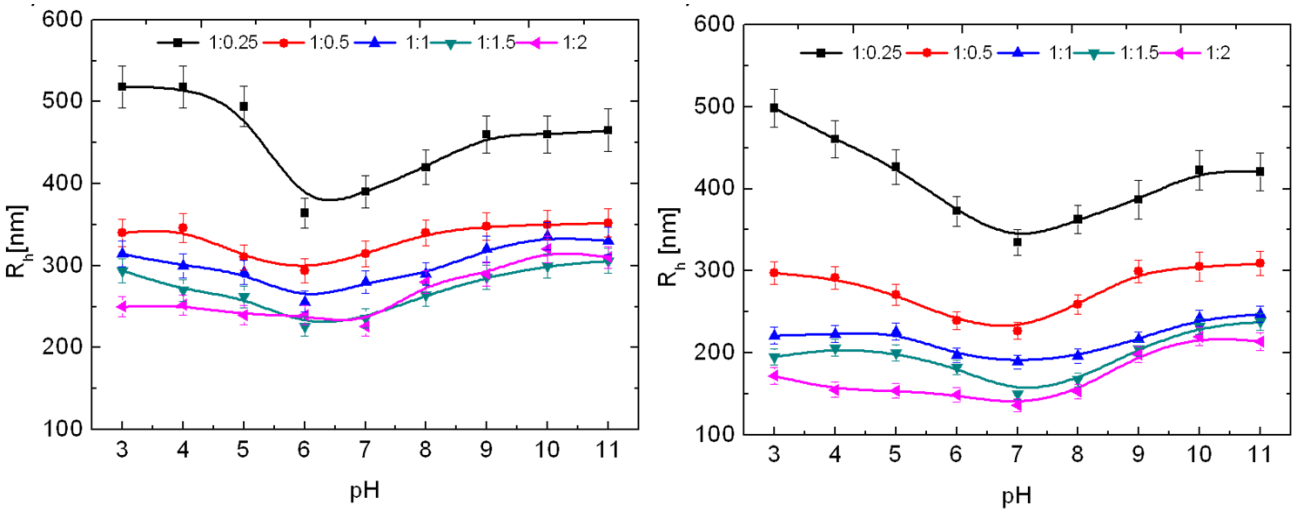

Figure 8.4: Change in hydrodynamic radius (R_h) as a function of pH 3-11 for **a)** PEG-DGE (left) and **b)** BS3 (right) cross-linked microgel.

pH switch was fully reversible in the particle owing to the gel nature of the system at 20 °C for both type of nanogels. The fractions of positively and negatively groups in the microgel play an important role in swelling behavior thus making them amphoteric in character. Such nanogels swell at both high and low pH when they possess an excess of either positive or negative charge. This swelling is due to electrostatic repulsion and osmotic pressure created within the nanogels by the counter ions to the charged functional groups.[23] The minimum size of the microgel is observed at pH were the net charge of the nanogels tends to be zero, that is, when the positive and negative charges in the nanogels are exactly balanced, defined as the isoelectric point (pI), and corresponds to their smallest size in the zwitterionic regime. In this region a large fraction of both cationic and anionic groups in the nanogels exist in their charged state. Hence ion pairing between them dominates over repulsion between un-paired like charges, leading to microgel shrinkage and a net reduction in charge. However flocculated nanogels could be easily re-dispersed by either increase or decrease in pH of the medium. It was observed that at low pH and high pH, the extent of swelling is enhanced by repulsion between protonated cationic groups and deprotonated anionic groups respectively. Two swelling regions on either side of the isoelectric point was observed with pronounced swelling at lower pH than at higher pH for lower mole ratio (1:0.25), which is believed to be due to outnumbering of $–NH_2$ groups to –COOH groups in the protein. The swelling and deswelling of nanogels with high cross-linking density showed more symmetric profile. The pI for the PEG-DGE and BS3 nanogels

with respect to change in their hydrodynamic radius were in the range of 5-7 and 6-8 respectively.

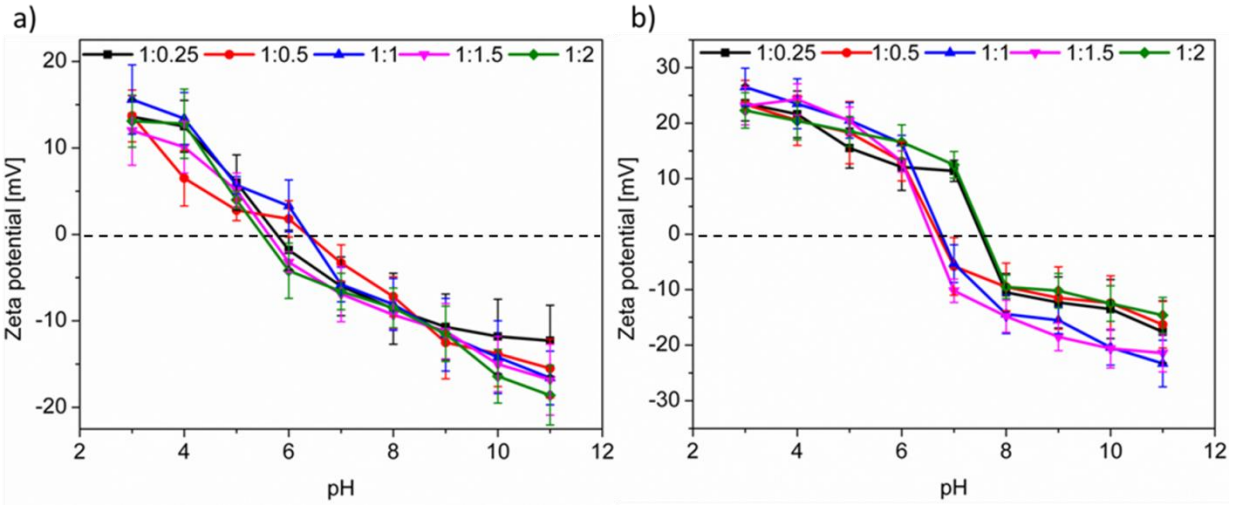

Figure 8.5: Zeta-potential of PEG-DGE (right) and BS3 (left) microgel as a function of pH.

Zeta-potential also followed the trend as the variation of microgel size with maximum value of zeta-potential observed at pH 3 which shows the dominance of Columbic force on variation of hydrodynamic diameter. The zeta potential approach to zero in the pH range of 5 to 7 with increasing the pH the zeta potential further decreases and becomes negative. The distribution of functional groups throughout the nanogels is also a very important parameter with determines the swelling extent and value of pI. These data coincide well with pH-dependent nanogels swelling at which minimum swelling was observed at pH range of 5-7 and 6-8 for PEG-DGE and BS3 microgel respectively **(Figure 8.5).**

CD spectra The change in the α-helix content of Elastin was followed by monitoring the ellipticity at 222 nm for PEG-DGE and BS3 microgel with different molar ratios. In all the microgel system it was seen that on microgel formation the pure elastin underwent a conformational change, which was observed by change in the ellipticity of two negative bands near 222 nm and 208 nm. With increase in crosslinking the curves become distorted, and in general there was reduction of amplitude at 222 nm. The change in CD spectra also suggests that the change in the secondary structure of Elastin progresses with increase in crosslinking.

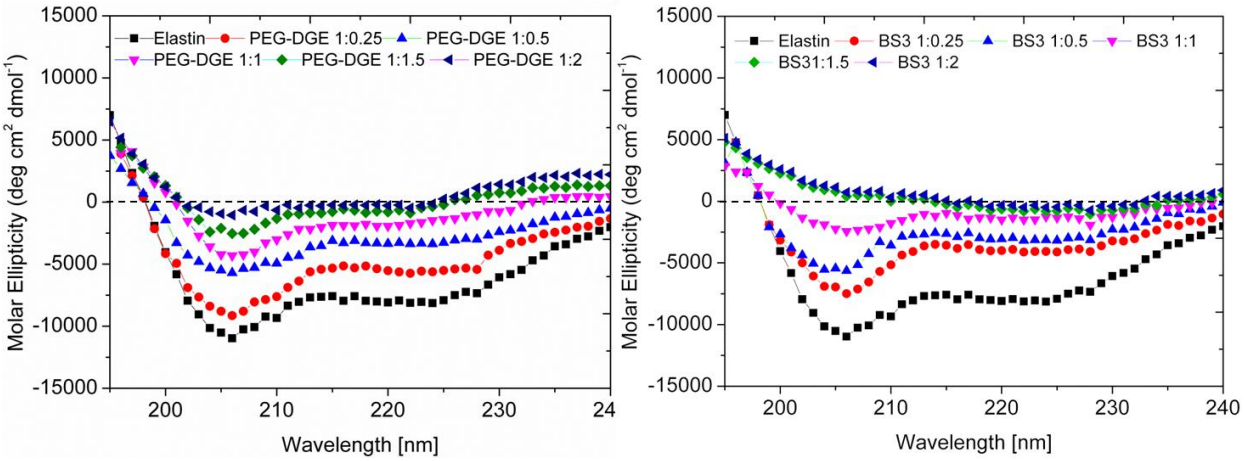

Figure 8.6: CD spectra of Elastin before and after crosslinking in a PEG-DGE and BS3 microgel.

For model peptides and proteins of known three-dimensional structures, the α-helical structure gives minima in CD spectra at 222 and 208 nm and the β-sheet structure gives minimum at 216 nm while a random coil at 200 nm.[24] α- helical content F_h, of Elastin can be estimated from the mean residual ellipticity at 222 nm, θ_{222} (in deg.cm^2.dmol^{-1}), using the following **Equation 8.2**.[25]

$$F_h = (\theta_{222} - \theta c) / (\theta_h - \theta c) \qquad \text{Eq. 8.2}$$

were θ_h and θc are respectively the mean residual ellipticity values determined for the fully α- helical and fully disordered (random coil) polypeptide. If values of -36,000 [26] and -280 deg.cm^2.dmol^{-1} [27] are substitute for θ_h and θc respectively, the- helical content in unmodified Elastin and Elastin nanogels can be calculated **(Table 8.2).** The results in **Table 8.2** show a considerable conformational change with increase in crosslink density which could be due to inter and intra-molecular interactions causing changes in the homogeneous phase of elastin on crosslinking.

Table 8.3 Percentage of α- helix content in PEG-DGE and BS3 nanogels

Elastin / Nanogels	θ_{222} (deg.cm^2.dmol^{-1})	% α- helix content
Elastin	-7925.52	21.4
PEG-DGE 1:0.5	-5312.14	14.1
PEG-DGE 1:1	-4126.05	10.8
BS3 1:0.5	-2795.22	7.0
BS3 1:1	-1005.31	2.0

Colloidal Stability of Nanogels To investigate the colloidal stability of amphoteric nanogels, sedimentation velocity measurements were performed on LUMIfuge which is a separation analyzer that allows detection of microgel sedimentation in a centrifugal field. Higher sedimentation velocity results in lower colloidal stability of particles. Amphoteric nanogels with 1: 0.25, 1: 0.5, 1: 1, 1: 1.5, and 1: 2 molar ratio of elastin to PEG-DGE / BS3 were analyzed at pH 5. From the **Table 8.1** it could be seen that both PEG-DGE and BS3 nanogels exhibited high colloidal stability as reflected by low values of sedimentation velocity. PEG-DGE cross-linked nanogels exhibited higher values of the sedimentation velocity due to their larger size compared to BS3 nanogels. PEG-DGE and BS3 (1:0.25) nanogels were also analyzed as a function of pH. The experimental results **(Table 8.3)** show that both nanogels show lower sedimentation velocity (and better colloidal stability) in acidic and basic medium. Contrary, at pH 6 and 7 the PEG-DGE- und BS3-crosslinked nanogels show sudden increase in sedimentation velocity due to charge neutralization and reduction of the colloidal stability. This is in a good agreement with DLS data presented in **Figure 8.4** and zeta potential data (**Figure 8.5**).

Table 8.3 Sedimentation Velocity Data as a function of pH

Elastin : Cross-linker (1:0.25)	Sedimentation Velocity [μm/s]			
	pH = 3	pH = 6	pH = 7	pH = 11
PEGDE	3.913	37.453	1.378	6.984
BS3	2.342	6.546	13.456	4.321

Enzymatic Degradation of Nanogels

Degradability of nanogels was investigated by DLS in the presence an enzyme elastase. Typical degredation profile was shown in **Figure 8.6** for nanogels prepared at elastin/cross-linker molar ratio of 1: 0.25 were the y-axis corresponds to decrease in size in the presence of elastase at time‘t’. The particles were incubated with 5 mM elastase at 37 °C and pH 8.8. The dispersion contained 5 wt-% of dried microgel. The degradation effect is based on the cleavage of elastin chains between the cross-linking points by the enzyme and degradation leads to reduction of size with partial dissolution of elastin chain in water. In the early stages of enzymatic treatment the particles

showed increase in hydrodynamic diameter due to particle swelling caused by loosening of network. In case of BS3 particles with high cross-linking density the particle had smaller mesh size which decreased the accessibility of elastin chain in the network due to hindered diffusion of the enzyme into the network and lead to enzymatic degradation at the surface. Also the relatively large size of the enzyme (60 kDa) is assumed to hinder its diffusion into the particle resulting into incomplete particle degradation. At 37°C the activity of the enzyme is optimum while the particles are in the collapsed state, so degradation is presumed to proceeds mainly with surface erosion.[28]

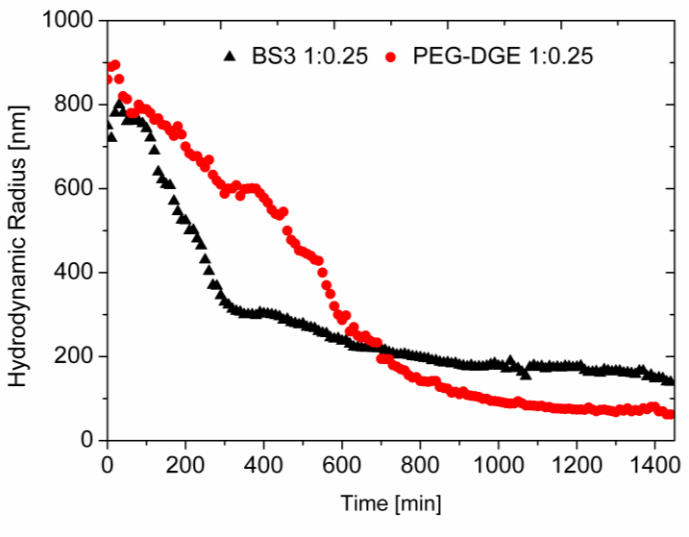

Figure 8.6: Degradability of microgel measured with change on the fractional ratio of hydrodynamic radius (fR_h) as a function of time using 5mM elastase for PEG-DGE (1:0.25) (red) and BS3 (1:0.25) (blue) cross-linked nanogels.

Loading and Release

Table 8.4 summarizes the loading and encapsulation efficiency of Dextran in four of these microgel systems: PEG-DE 1:0.25, 1:0.50 and BS3 1:0.25, 1:0.50. The temperature-triggered release of Dextran from loaded nanogels was examined at two temperatures one below VPTT (20°C) and other above VPTT (40°) of the nanogels at pH 5. At regular intervals the nanogels were centrifuged, followed by their immediate removed and separation from the supernatant.

Table 8.4 Loading and Encapsulation efficiency % for PEG-DGE and BS3 nanogels

Elastin : PEG-DGE [mol:mol]	Elastin : BS3 [mol:mol]	Dextran loading [wt% w.r.t Polymer]	Dextran loaded [mg]	Loading estimated [mg]	Encapsulation efficiency [%]	R_h(nm)/$_{PDI}$	
						20°C	40°C
1:0.25	-	15	3.75	2.41	64.2	890 /0.34	510 /0.26
1:0.5	-	15	3.75	2.89	77.2	750 /0.42	470 /0.21
-	1:0.25	15	3.75	2.75	73.3	765 /0.45	450 /0.31
-	1:0.5	15	3.75	3.01	80.3	456 /0.41	320 /0.30

The absorbance intensities of the supernatant were measured for each sample, and the concentration of Dextran released was calculated with the help of a calibration curve

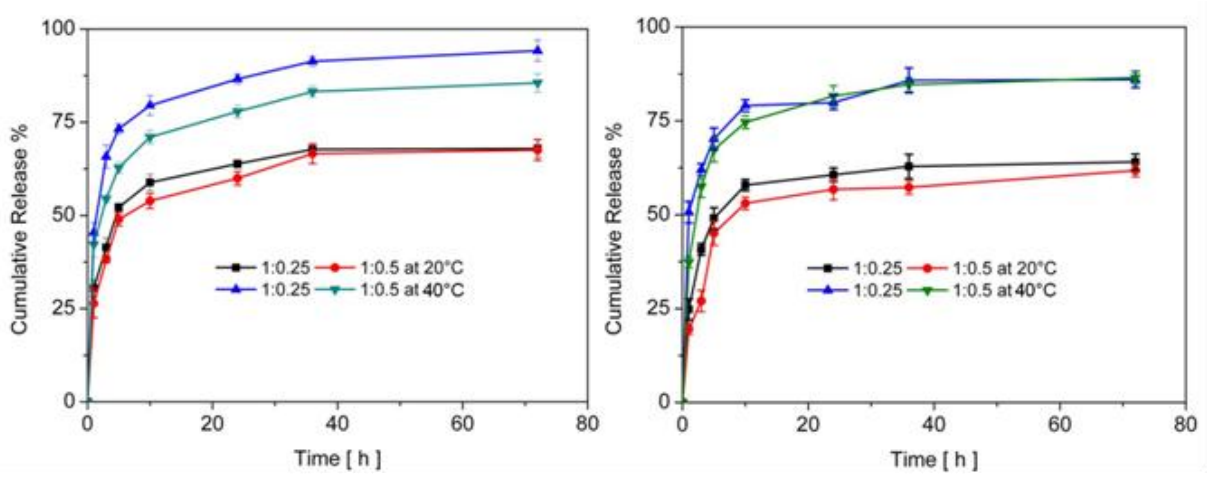

Figure 8.7: Temperature dependent release of dextran form for PEG-DGE 1:0.25, 1:0.50 (left) and BS3 1:0.25, 1:0.50 (right) microgels at 20 and 40°C.

Figure 8.7 shows the summarized results of these experiments for four microgel systems. An encapsulation efficiency of about 64% and 77.2% was obtained for PEG-DE 1:0.25 and 1:0.50 nanogels. There was a slight increase in loading of 9% and 3% for BS3 1:0.25 and 1:0.50 nanogels. This result was used for the evaluation of the cumulative release of Dextran. For PEG-DE 1:0.25 and 1:0.50 nanogels, the amount of released drug after 24h at 20°C was 63 and 59%, while for BS3 1:0.25 and 1:0.50

nanogels, the amount of released after same temperature and time interval was 63 and 59%, respectively, this difference increased markedly at 40 °C to 86 and 77% for PEG-DE 1:0.25 ,1:0.50 and 79 and 81% for BS3 1:0.25, 1:0.50. At this temperature, both types of nanogels show volume-phase transition and the larger release corresponded to a more pronounced shrinking effect occurring in this system (**Table 8.4**). The dextran released by the nanogels was directly related to the swelling state of nanogels. Although, a notable amount of Dextran was released before the onset of the VPTT, a significantly larger amount of dextran was released during the actual deswelling transition at 40°C. The slightly greater amount of released drug than for the BS3 system was most likely due to the presence of hydrophilic PEG channels throughout the hydrophobic network at the transition temperature, which encouraged escape of the dextran. In these systems, the deswelling transition acts as a trigger that tends to squeeze out the loaded drug into the surrounding medium.

Cytotoxicity

The cytotoxicity of the BS3-elastin nanogels with molar ratio of 1:0.5 was investigated by XTT based cell proliferation assay and the results are summarized in **Figure 8.8**, where the samples showed initial little cytotoxicity and for further days; i.e. 6 days after, cell proliferation rate on samples were favourably comparable to the control proving that this microgel system is cytocompatible and can further use as *in vitro* or *in vivo* experiments intra-drug delivery as such. Similar and comparable results were obtainable for other microgel systems.

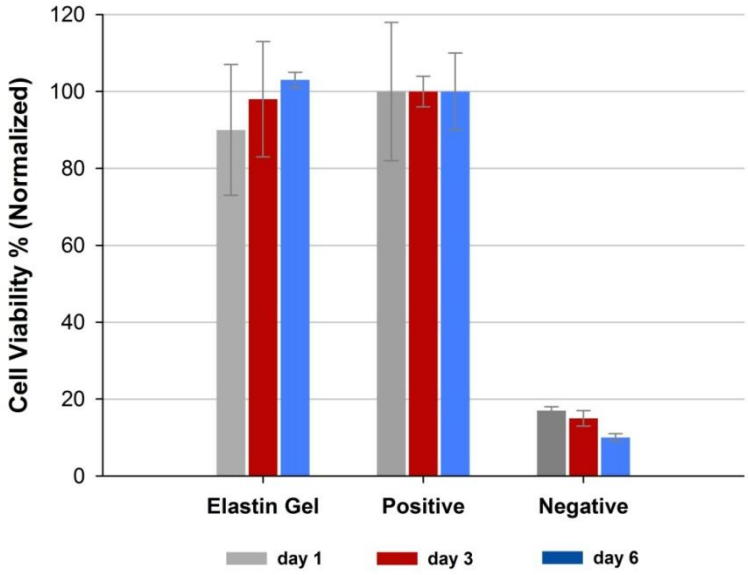

Figure 8.8: Quantitative HUVECs proliferation in elastin gel system.

8.4 Conclusion

In this work hybrid microgels are synthesized by crosslinking of elastin with by amine-reactive cross-linkers; poly(ethylene glycol) diglycidyl ether (PEG-DGE) or bis(sulfosuccinimidyl) suberate (BS3) in W/O emulsion. Elastin microgels with various sizes and tunable properties were prepared and their properties were explored via cryo-SEM, Zetasizer, DLS, and separation analyser (LUMiFuge). Microgels showed dual responsive to temperature and pH. Elastase-mediated degradation and XTT-based cytotoxicity assay evidenced that the resulting microgel were cytocompatible and the microgel network can degrade with elastase introduction. High loading of model drug dextran could be achieved for the microgels which showed a temperature dependent release behavior. Cytocompatible matrices, dual responsivity with further degradability with inherited elastin properties makes these microgels a intriguing candidate for drug delivery systems (DDS).

8.5 References

[1] D. Patel, S. E. Vandromme, M. E. Reid, L. J. Taite, *Biomacromolecules* **2012**, *13*, 1420.

[2] J. C. Rodriguez-Cabello, In *Biomaterials: From Molecules to Engineered Tissues*; Edited by: N. Hasirci, V. Hasirci, Kluwer Academic/Plenum Publ: New York, **2004**, 553, 45.

[3] V. P. Conticello, H. C. D. In *Polymer Science: A Comprehensive Reference*; Edited by: R. Langer, Elsevier: Amsterdam (The Netherlands), **2012**, 9, 71.

[4] K. K. Kumashiro, J. P. Ho, W. P Niemczura, F. W. Keeley, *J. Biol. Chem.* **2006**, 281, 23757.

[5] I. Maeda, Y. Fukumoto, T. Nose, Y. Shimohigashi, T. Nezu, Y. Terada, H. Kodama, K. Kaibara, K. Okamoto, *J. Pept. Sci.* **2011**, 17, 735.

[6] G. C. Yeo, F. W. Keeley, A. S. Weiss, *Adv. Colloid Interface Sci.* **2011**, 167, 94.

[7] L. A. Lyon, Z. Meng, N. Singh, C. D. Sorrell, A. S. John, *Chem. Soc. Rev.* **2009**, 38, 865.

[8] S. M. Partridge, H. F. Davis, G. S. Adair, *Biochem. J.* **1955**, 61, 21.

[9] D. Volpin, D. W. Urry, B. A. Cox, L. Gotte, *Biochim. Biophys. Acta* **1976**, 439, 253.

[10] B. A. Cox, B. C. Starcher, D. W. Urry, *Biochim. Biophys. Acta* **1973**, 317, 209.

[11] S. Ito, S. Ishimaru, S. E. Wilson, *Cardiovasc. Surg.* **1997**, 5, 176.

[12] Z. Megeed, J. Cappello, H. Ghandehari, *Adv. Drug Deliv. Rev.* **2002**, 54, 1075.

[13] R. Anumolu, J. A. Gustafson, J. J Magda, J. Cappello, H. Ghandehari, L. F. Pease, *ACS Nano* **2011**, 5, 5374.

[14] S. Mithieux, J. Rasko, A. Weiss, *Biomaterials* **2004**, 25, 4921.

[15] B. A. Rozenberg, *Adv. Polym. Sci.* **1986**, 75, 113.

[16] X. Sun, R. Rossin, J. L. Turner, M. L. Becker, M. J. Joralemon, M. J. Welch, K. L. Wooley, *Biomacromolecules* **2005**, 6, 2541.

[17] J. E. Chung, M. Yokoyama, T. Aoyagi, Y. Sakurai, T. Okano, *J. Control. Rel.* **1998**, 53, 119.

[18] A. Burmistrova, M. Richter, M. Eisele, C. Uzum, R. Klitzing, *Polymers* **2011**, 3, 1575.

[19] D. W. Urry, *J. Phys. Chem. B* **1997**, 101, 11007.

[20] S. Schachschal, A. Balaceanu, C. Melian, D. E. Demco, T. Eckert, W. Richtering, A. Pich, *Macromolecules* **2010**, 43, 4331.

[21] P. P. Batra, K. Sasa, T. Ueki, K. Takeda, *J. Protein Chem.* **1989***, 2,* 221.

[22] D. W. Urry , C. H. Luan, T. M. Parker, D. C. Gowda, K. U. Prasad, M. C. Reid, A. Safavy, *J. Am. Chem. Soc.* **1991**, 113, 4346.

[23] A. Pich, A. Tessier, V. Boyko, Y. Lu, H. J. P. Adler, *Macromolecules* **2006**, 22, 7701.

[24] P. P. Batra, K. Sasa, T. Ueki, K. Takeda, *J. Protein Chem.* **1989**, 2, 221.

[25] T. Lin, T. P. Quinn, D. Grandgenett, M. T. Walsh, *Proteins* **1989**, 5, 156.

[26] N. Greenfield, G. D. Fasman, *Biochemistry* **1969**, 8, 4108.

[27] W. L. Mattice, J. T. Lo, L. Mandelkern, *Macromolecules* **1972**, 5, 729.

[28] D. Klinger, K. Landfester *J. Poly. Sci. Part A: Polym Chem.* **2012**, 50, 1062.

CHAPTER 9

Radiolabeled Nanogels for Nuclear Molecular Imaging

Part of this work is published in Macromolecular Rapid Communication DOI: 10.1002/marc.201200744

9.1 Introduction

Currently, various types of nanoparticles (e.g. liposomes, nanospheres, nanocrystals) are available as tools for drug delivery.[1] In recent years, also nanogels (nanometer sized hydrogel particles) have gained increased attention as drug delivery systems of biologically important molecules.[2] These soft and hydrophilic particles have a three-dimensional crosslinked network retaining a large amount of water in the swollen state, and mimic biological fluids.[3] Nanogels can be prepared from a variety of chemical structures either by polymerization of monomers or by modification of prepolymers to obtain particles with varying size, charge, and surface modification. In spite of attractive properties (especially the hydrophilic character combined with the retention of water), which promote their long stay in the bloodstream e.g. by avoiding the recognition by the mononuclear phagocyte system, there is only little known about their behavior in vivo.[4] Nanogels based on polyethylene glycol (PEG) as key component let expect an additional reduced systemic clearance and increased blood circulation time, which has been demonstrated for PEGylated nanoparticles with reduced protein immunogenicity.[5] Additionally, PEGylation is known to prevent the aggregation of nanogels in human plasma.[6]

Selective (passive) targeting of macromolecular drugs to tumor tissue is made possible by the enhanced permeability and retention (EPR) effect in tumors.[7,8] The quick growth of tumor cells results in abnormal tumor vessels with poorly-aligned defective endothelial cells. This wide fenestration enables the size-driven accumulation of macromolecules in tumor cells. The accumulation is increased due to the lack of effective lymphatic drainage in tumor cells, the preferred tissue clearance pathway of

macromolecules. Small molecules, like most of the anticancer agents, are able to penetrate any tissue, whereas macromolecules are not able to diffuse through the endothelia cells of normal tissue. Due to the reduction of the systemic side effect the EPR concept is now widely accepted as a gold standard for anticancer drug designing using macromolecular drugs.

The use of nanogels as nanocarriers in drug development requires detailed knowledge about their biodistribution, pharmacokinetic, and the metabolic pathways of the original and degraded probe in vitro and in vivo. Such information can be accessed by investigating the influence of size, charge and surface modifications of nanogels via an in vivo imaging technique. Among various techniques including MRI, CT, NIR, SPECT and PET, the latter has the advantage of monitoring bio-pathways with non-toxic trace amounts (in the nmol range) of the probe. This allows an in vivo estimation of the biodistribution of biomarkers with high sensitivity and is applicable in animals and humans.[9]

Although various polymeric materials such as polymers[10,11] and nanoparticles[12-14] have been radiolabeled, investigation using radiolabeled nanogels is limited to (pullulan or poly(isopropylacrylamide-co-vinylpyrrolidone)) nanogels as nanocarrier system loaded with a radiolabeled drug.[15,16] After unloading of the radiolabeled drug *in vivo* (carrying the radionuclide as signal for detection) these constructs are not able to provide the essential basic information of the fate of the nanogel. Radiolabeling of macromolecules is often performed in aqueous medium by means of metal-chelators attached to the macromolecules (usually at the surface) resulting in very high radiochemical yields.[17] The porous nature of the nanogel also allows radiolabeling inside of the crosslinked network, whereby modifications at the surface are reserved for an active biological targeting. Gallium-68 (^{68}Ga) is an attractive candidate as a positron emitter with a physical half-life sufficient for the expected biokinetic, a relatively low positron energy (resulting in a sufficient spatial resolution for small animal in vivo imaging using positron emission tomography (PET)) and a high availability of the radionuclide ^{68}Ga from a ^{68}Ge/^{68}Ga-generator.

Herein synthesis of radiolabeled biodegradable nanogels, and physiochemical and biological properties relevant to nuclear molecular imaging is reported. Amphiphilic statistical star shaped PEG based prepolymers are used to synthesize nanogels by their self-assembly in aqueous medium without using organic solvents and surfactants. They are crosslinked via disulfide bonds, which are able to degrade after cell uptake by

the reductive environment in the cytosol.[18] The versatile thiol chemistry is used for both, crosslinking and derivatisation for radiolabeling. We used a simple and efficient ^{68}Ga-labeling procedure to radiolabel nanogels containing chelating groups for ^{68}Ga and other trivalent metals. To the best of our knowledge this is the first report on a covalent bonding of a PET-radionuclide directly to a nanogel. These results are the prerequisite for further in vitro and small animal PET investigations (general biodistribution, fate of nanogel, measuring the EPR-effect) yielding a ^{68}Ga-labeled-nanogel as valuable nuclear molecular imaging probe.

9.2 Experimental

9.2.1 Materials and Method

Hydroxy terminated, six arm, star shaped poly (ethylene oxide-*stat*-propylene oxide) **sP(EO-*stat*-PO**) with a backbone consisting of 90% ethylene oxide and 10% propylene oxide (M_n= 6100 g/mol, M_w/M_n=1.12) was obtained from Dow Chemicals (Terneuzen, NL). **sP(EO-*stat*-PO)** was dissolved in tetrahydrofuran and precipitated in cold diethylether prior to further use. N,N'-dicyclohexyl-carbodiimide (DCC), (99%, Acros), 4-(Dimethylamino)pyridine (DMAP) (99%, Aldrich), 3,3'-dithiodipropionic acid (DTPA) (Aldrich), tris(2-carboxyethyl) phosphine (TCEP) (99%, Aldrich), dichloromethane (HPLC grade, Aldrich), and 5,5'-dithio-*bis*-(2-nitrobenzoic acid) (DTNB) (Merck), 2,2'-(7-(1-carboxy-4-((2-(2,5-dioxo-2,5-dihydro-1H-pyrrol-1-yl)ethyl)amino)-4-oxobutyl)-1,4,7-triazonane-1,4-diyl)diacetic acid (maleimide NODAGA) (94%, CheMatech), 3,6-diamino-9-[2-carboxy-4(or5)-[[[5-(2,5-dihydro-2,5-dioxo-1H-pyrrolyl)pentyl]amino]carbonyl] phenyl]-4,5-disulfo-, inner salt, monosodium salt (Alexa Fluor 488 C_5 maleimide) (Invitrogen), ammonium salt of 8-anilinonaphthalene-1-sulfonic acid (90%, Sigma), water (ultra pure, metal free, Merck), hydrochloric acid (30%, supra pure, Merck), ammonium acetate (p.a. Pharm Eur, Sigma), Sephadex G25 (PD-10 column, GE Healthcare), Sephadex G100 (fine grade, GE Healthcare), gallium nitrate (gallium ICP standard, Merck) were used as received. Dialysis membrane with a molecular weight cut off of 3.5 kDa was purchased from Spectrum Laboratories, Inc. The ^{68}Ge/^{68}Ga-generator was obtained from IDB Holland, where the Germanium-68 is fixed on a modified tin dioxide column. The human monocyte cell line THP-1 was from ATCC. The cell medium RPMI-1640 and supplementary reagents including fetal bovine serum (FBS), L-glutamine, sodium pyruvate and non-essential amino acids (NEA) were

obtained from Biochrom, and the chemical reagents like phorbol 12-myristate 13-acetate (PMA) and dimethyl sulfoxide were from Sigma Aldrich.

Fluorescence Spectroscopy

Critical micellization concentration (CMC) of the polymers was determined via fluorescence spectroscopy on 650-40 Hitachi fluorescence spectrophotometer with a slit width of 5 nm. Ammonium salt of 8-anilinonaphthalene-1-sulfonic acid (ANS) was used as fluorescence probes. We collected emission spectra of polymer solutions at various concentrations ranging from 3.0 to 300.0 mg mL^{-1} in the presence of 5×10^{-4} mM (1.58×10^{-7} mg mL^{-1}) ANS at room temperature. The solutions were stirred for 12 h at room temperature in dark prior to measurements. The emission spectra of samples at 510 nm were obtained at a fixed excitation wavelength of 340 nm in triplicate. Excitation and emission band widths were 10 nm and 3 nm, respectively.

Radio-High Performance Liquid Chromatography (Radio - HPLC)

The radiochemical yield and purity were determined by Radio-HPLC. The HPLC-system assembles a quaternaric HPLC-pump (Knauer GmbH), DAD-detector (Knauer GmbH) and NaI-detector (Raytest GmbH) with a recording and analyse software (Raytest GmbH). As stationer phase were used a LiChrosorb RP18e column (250 × 4mm, CS-Chromatographie Service) and a gradient of acetonitrile and 0.1% trifluoracetic acid as mobile phase (10% to 90% acetonitrile in 30min, flow 1mL min^{-1}). The retention time of free $^{68}Ga^{3+}$ was 2.2min and of ^{68}Ga-NODAGA-NG 12.5min.

Radio-Thin Layer Chromatography (Radio - TLC)

Free $^{68}Ga^{3+}$ after radiolabeling was determined by Radio-TLC with ITLC-silica strips and citrate buffer as mobile phase. The spreading was analysed by a Radio-TLC-Scanner (mini-Gita, Raytest GmbH). Free $^{68}Ga^{3+}$ could be detected as ^{68}Ga-citrate at the front, whereas ^{68}Ga conjugated with nanogels (^{68}Ga-NG) remains at the origin.

9.2.2 Synthesis

Synthesis of Thiol Functionalized **sP(EO-*stat*-PO) was** performed as reported in **Chapter 3.**The free thiol content of the polymer was determined using ^{1}H NMR. SEC (THF): M_n = 6500 g/mol, M_w/M_n = 1.12.

^{1}H NMR (400 MHz, $CDCl_3$, δ): δ = 1.14 (dd, 27H, CH_3), 3.2-4.0 (m, 516-H,-CH_2CH_2O),

4.21 (t, 8-H, CH_2-OCO-), 2.61 (t, 2H, CH_2CH$_2$SH), 2.73 (t, 2H, CH$_2$CH_2SH), 1.5 (t, 1H,SH).

Synthesis of **HS-sP(EO-*stat*-PO)** labeled with NODAGA **(NODAGA-HS-sP(EO-*stat*-PO)**.

HS-sP(EO-*stat*-PO) (0.500g, 7.69 × 10^{-2} mmol; w.r.t 2-SH, 1.538 × 10^{-1} mmol) and NODAGA (0.0764g, 1.536 × 10^{-1} mmol) were reacted in 5mL phosphate buffered saline (0.01 M, pH= 7.2) overnight at room temperature under argon. The product was obtained after dialysis against water and freeze-drying. It was stored at 4°C until further use. M_n = 7500g mol^{-1}.

^{1}H NMR (400 MHz, $CDCl_3$, δ): δ = 1.14 (dd, 27H, CH_3), 3.2-4.0 (m, 516-H,-CH_2CH_2O), 4.21 (t, 8-H, CH_2-OCO-), 2.61 (t, 2H, CH_2CH$_2$SH), 2.73 (t, 2H, CH$_2$CH_2SH), 1.5 (t, 1H,SH), 2.26(s, 12H, C$_6H_{12}N_3$).

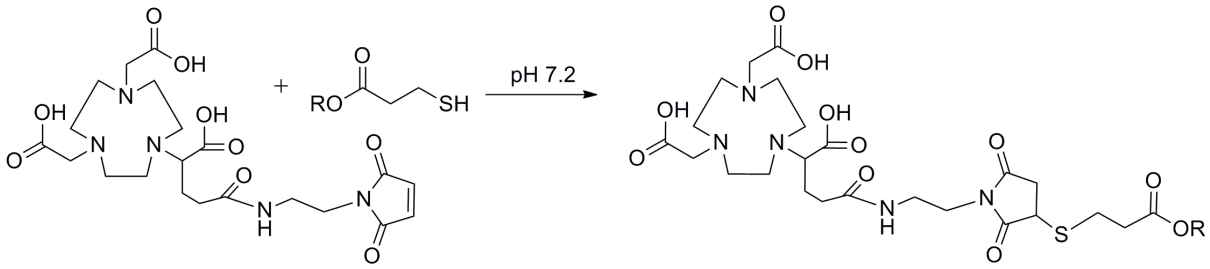

Scheme 9.1: Synthesis of **HS-sP(EO-*stat*-PO)-NODAGA**.

Labeling of **NODAGA-HS-sP(EO-stat-PO)** with Alexa Fluor 488.

NODAGA-HS-sP(EO-*stat*-PO) (1.333 × 10^{-2} mmol, 0.100g, 2.3 free thiols per prepolymer) and Alexa Fluor 488 maleimide (6.666 × 10^{-3} mmol, 0.0048g) in the molar ratio of 1 : 0.5 were reacted in 5mL phosphate buffered saline (0.01M, pH 7.2) in dark for 12 h under argon. The product was obtained after dialysis against water and freeze-drying (calculation of the yield after nanogel formation, see below).

9.2.3 Crosslinking of Polymer Aggregates and Synthesis of Nanogels

NODAGA-HS-sP(EO-*stat*-PO) (0.030 g, 4.0 × 10^{-3} mmol) was dissolved in 1 mL phosphate buffered saline (0.04 M, pH 7.4) and was stirred for 15 min. H_2O_2 (0.020μL, 1.88 × 10^{-3} mmol) was added, and the mixture was stirred for 10 min. The resulting mixture was dialyzed to yield nanogels (NODAGA-NG). Similarly nanogels from

NODAGA-HS-sP(EO-*stat*-PO) labeled with Alexa Fluor 488 (Alexa-NG) were prepared and stored at 4 °C until further use.

9.2.4 Fluorescence measurement of Alexa-NG

Fluorescence measurement were performed for quantification of the conjugated dye by illuminating the samples at an excitation wavelength between 400 and 600 nm with recording the emission at 515 nm. A calibration curve was obtained with different known concentration of Alexa Fluor 488 and conjugation of the dye with the free thiols in polymer was calculated to be 0.3 Alexa Fluor 488 per star by fluorescence measurement (0.3/0.5 = 60% conjugation yield). This results in an available crosslinking capacity of 2.0 thiol groups per prepolymer.

9.2.5 Radiolabeling of NODAGA-NG

In a typical labeling experiment, 250 μL ^{68}Ga-$GaCl_3$ solution (generator elute, 20-150 MBq, 0.6M HCl) was added to 10μL NODAGA-NG (30 mg mL^{-1}) in 83µL 3M NH_4OAc resulting in a pH of 4.0-4.5. In competition experiments $Ga(NO_3)_3$ (56-210 nmol) was mixed before with the generator elute. After mixing for 10-15 min at RT samples were analysed by Radio-TLC and Radio-HPLC. Purification was performed by size exclusion chromatography (SEC) on a Sephadex-PD-10 column (GE Healthcare) with saline by collecting 100μL fractions for determination of the elution profile.

9.2.6 Phagocytosis Assay

The THP-1 cells were grown in RPMI-1640 medium supplemented with 10% FBS, 1% L-glutamine, 1% sodium pyruvate and 1% NEA. In 12-well plates, 105 THP-1 cells were allowed to adhere overnight. Thereafter, medium was replaced by RPMI-1640 without serum. Monocytes were then stimulated with PMA (8nM) for 24 h in a FBS-free medium. To assure opsonisation of nanogels, all phagocytosis assays were conducted in the presence of 10% FBS. Monocytes were incubated with 0.1, 0.5 and 1.0 mg mL^{-1} of Alexa-NG for 1h at 37°C. Plated were washed twice with PBS to remove excess particles. Harvested cells were fixed in 2% paraformaldehyde and analysed by flow cytometry (Cytomics FC 500, Beckman Coulter) For additional microscopy analysis, nuclear counterstaining was accomplished with Hoechst33342 (1 mg mL^{-1}), before being examined by fluorescence microscopy (ZEISS, Axio Scope A1).

9.3 Results and Discussion

The prepolymer for synthesis of gallium-68 labeled nanogels has to bear at least 2 functionalities, one for formation of crosslinked nanogels and another to complex the radiometal. For this purpose we have chosen a six arm, hydroxy terminated, star-shaped poly(ethylene oxide-*stat*-polypropylene oxide) (**sP(EO-*stat*-PO);** 90% EO, 10% PO in molar ratio; M_n = 6100 g mol^{-1}, M_w/M_n = 1.12) as precursor. At first 4 of the 6 hydroxy terminals have been functionalized with thiol groups (**HS-sP(EO-*stat*-PO).** Half of these thiol groups were covalently linked with the chelator NODAGA. The result was a new, star-shaped prepolymer (**NODAGA-HS-sP(EO-*stat*-PO)**) with an average each 2 hydroxy, 2 thiol and 2 NODAGA terminated arm. Crosslinked particles, the NODAGA containing nanogels (NODAGA-NG), were yielded by oxidation of the thiol groups. The remaining hydroxy terminals are reserved for future functionalization modifying biodistribution parameters. For biological experiments **NODAGA-HS-sP(EO-*stat*-PO)** was additionally functionalized (at <1 thiol group) with a dye before nanogel preparation.

In detail, the partially thiolated star shaped prepolymer (**HS-sP(EO-*stat*-PO)** was prepared according to literature[19] via Steglish esterification with the disulfide containing dithiopropionic acid followed by reduction of the disulfide cross-linkage to thiol groups. Incorporation of hydrophobic alkyl-thiols into the amphiphilic **sP(EO-*stat*-PO), (**consists of 10% hydrophobic PPO) retains the amphiphilic behaviour of the polymer. Such amphiphilic polymer shows spontaneous aggregation in aqueous solution and is able to form crosslinked nanogels.[20] ^{1}H-NMR of **HS-sP(EO-*stat*-PO)** indicated a mean of 4.0 thiol groups per prepolymer (**Figure 9.1**).

Estimation of Functionalization by NMR

For calculation of the thiol functionalization and subsequent NODAGA linkage it was important to estimate the exact number of repeating units (precise molar ratio) of the propylene oxide and ethylene oxide units in polymer backbone.[20] CH_3 group of propylene oxide unit in the backbone of prepolymer was used as a reference. The integrals of the CH_3- (I_5) and the CH_2-, CH-groups (I_{1-4}) of the **sP(EO-*stat*-PO)** molecule can be determined with the help of **Equation 9.1**.

$$y / x = (44 \text{ g mol}^{-1} / 58 \text{ g mol}^{-1}) \times [(I_{1-4} / I_5) - 1] \qquad \text{Eq.9.1}$$

x/y : molar ratio of ethylene- and propylene oxide

$I_{1-4,6}$: Integral of H-atoms of the CH_2-, CH-groups of the sP(EO-*stat*-PO)

I_5 : Integral of the H-atoms of the CH_3 group of the sP(EO-*stat*-PO)

The number of repeating units can be calculated with the following **Equation 9.2.**

$$M_{sP\,(EO-stat-PO)} - M_{core} = b \cdot M_{EO} + a \cdot M_{PO} \qquad \text{Eq.9.2}$$

As 'b' is depending on 'a', we can write b = a · y/x and rearrange equation as follows

$$<=> \quad a = (M_{sP\,(EO-stat-EO)} - M_{core})/(y/x \times M_{EO} + M_{PO}) \qquad \text{Eq.9.3}$$

$M_{sP(EO-stat-PO)}$: Molecular weight of sP(EO-*stat* -PO) = 6100 g mol^{-1}

M_{core} Molecular weight of the core of sP(EO-stat -PO) (Sorbitol) = 182 g mol^{-1}

M_{EO} : Molecular weight of ethylene oxide = 44 g mol^{-1}

M_{PO} : Molecular weight of propylene oxide = 58 g mol^{-1}

a : Number of repeating units of propylene oxide

b : Number of repeating units of ethylene oxide

The peak at 1.16 ppm was assigned an integration value of 1.0 and an integration value of 18.77 was obtained for the peak at 3.2-4.0 ppm (**Figure 9.1a**). These values were put into equation (1.1) and result in y/x = 13.32.

The value for y/x was used in **Equation 9.3**:

$$a = (6100\ g\ mol^{-1} - 182\ g\ mol^{-1})/\ 13.32 \times 44\ g\ mol^{-1} + 58\ g\ mol^{-1}$$

which results in the value of 9 for 'a'. Therefore **sP(EO-*stat*-PO)** has 9 repeating units of propylene oxide corresponding to 27 H-atoms (CH_3 group) in the **sP(EO-*stat*-PO).**

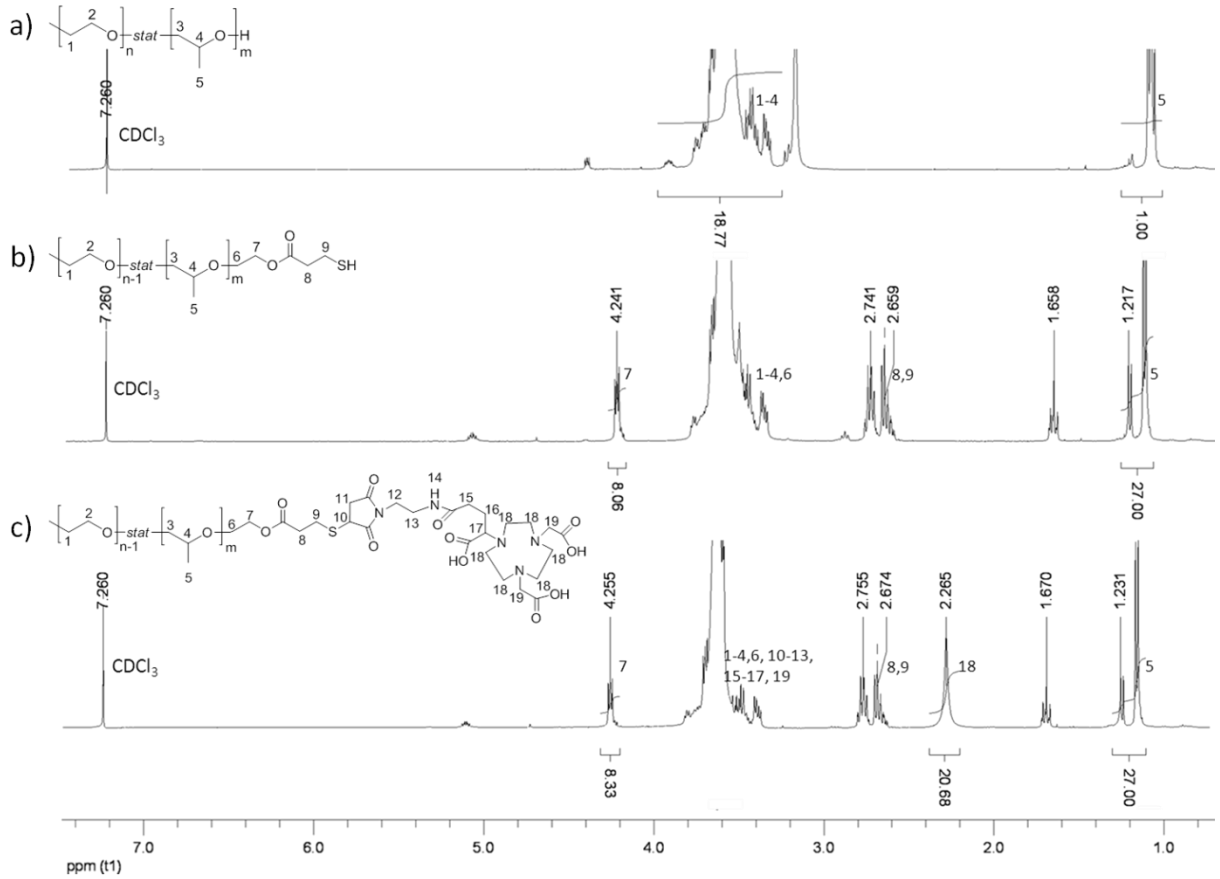

Figure 9.1: ^{1}H NMR spectra of *a)* **sP(EO-*stat*-PO)** *b)* **HS-sP(EO-*stat*-PO)** and *c)* **NODAGA-HS-sP(EO-*stat*-PO)**

Thiol functionalization via Steglish esterification and subsequent reduction the 2H (H-7, CH_2 group adjacent to ester) proton shows a triplet at 4.2 ppm. Using the corresponding 27 H-atoms from the CH_3 group of propylene oxide unit as reference integration of these 2 protons comes out to be 8.06 which indicates that out of 6 arm, 4 arm of the **sP(EO-*stat*-PO)** are thiol functionalised (**Figure 9.1b**).After functionalization with NODAGA, a distinct peak of the imine ring protons (H-18) appears at 2.26 ppm.[21] This peak results from 12 protons and on integration it shows that 1.7 (20.7/12) arm out of 6 are linked with the chelating agent (**Figure 9.1c**). Insertion of the chelator NODAGA into **HS-sP(EO-*stat*-PO)** was achieved via Michael addition of thiols with maleimide linked to the NODAGA functionality. The molar ratio of maleimide to thiols (1 to 2 = 2 NODAGA per prepolymer) ensures the presence of free thiol groups for crosslinking. Conjugation of NODAGA into **HS-sP(EO-*stat*-PO)** led to incorporation of 1.7 NODAGA per prepolymer as evidenced by 1H-NMR (**Figure 9.1c**). The successful incorporation of thiol functionality was also confirmed by the signals in the FT-IR

spectrum positioned at 2559 cm-^{1} (SH-group) and 1750 cm-1 (C=O stretching, from ester bond), respectively (**Figure 9.2a**). While Raman spectroscopy indicated S-H stretching mode at 2578 cm^{-1} (**Figure 9.2b**).

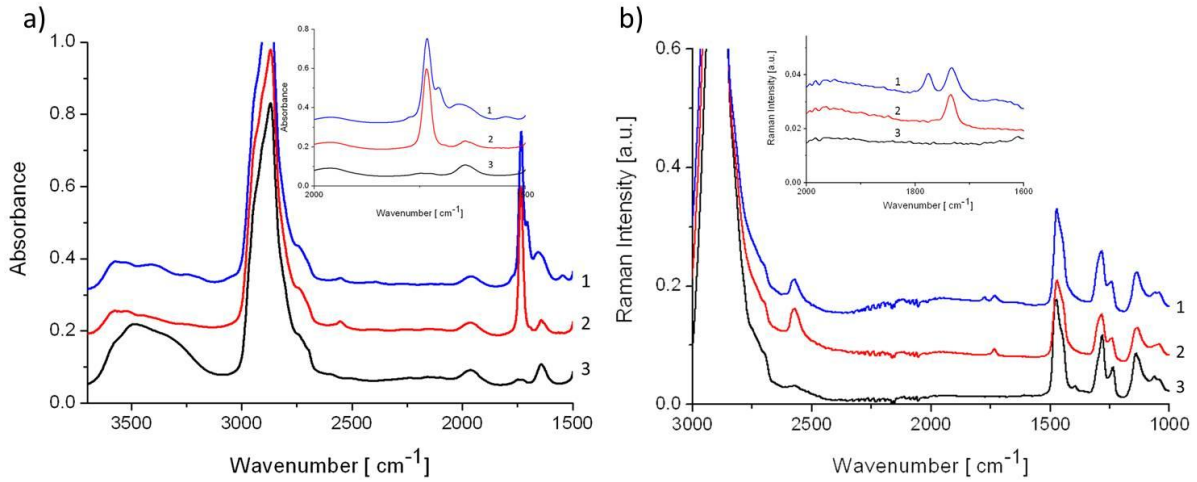

Figure 9.2 a): Normalized FT-IR spectra of 1- **HS-sP(EO-*stat*-PO)-NODAGA** 2- **HS-sP(EO-*stat*-PO)** and 3- **sP(EO-*stat*-PO) b).** Normalized Raman spectra of 1- **HS-sP(EO-*stat*-PO)-NODAGA** and 2- **HS-sP(EO-*stat*-PO)** showing –SH stretch at 2700 cm^{-1}. Inset depicts the C=O stretch of imide group from NODAGA appearing as a sharp band near 1780 cm^{-1}

FT-IR-spectrum of **NODAGA-HS-sP(EO-*stat*-PO)** indicated characteristic signals for NODAGA-maleimide, showing an amide I band at 1650 cm^{-1}, a band due to the five-membered imide ring at 1700 cm^{-1}, and an amide II band at 1550 cm^{-1} involving C-N stretching and C-N-H in plane bending[22] (**Figure 9.2a**). Upon NODAGA conjugation, the intensity of the -SH band (2578 cm^{-1}) in the Raman spectrum was reduced compared to **HS-sP(EO-*stat*-PO)** indicating the presence of thiol in **NODAGA-HS-sP(EO-*stat*-PO)**. Moreover C=O from imide appearing as a sharp band near 1780 cm^{-1} from NODAGA, along with C=O from ester at 1734 cm^{-1} in **NODAGA-HS-sP(EO-*stat*-PO)** confirms the successful conjugation (**Figure 9.2 b, inset).**

NODAGA-HS-sP(EO-*stat*-PO) was further labeled with Alexa Fluor 488 through reaction of maleimide functionalized dye with thiols. The conjugation of the dye to thiol was calculated by fluorescence measurement to be 0.3 Alexa Fluor 488 per star. This results in an available crosslinking capacity of 2.0 thiol groups per prepolymer.

Amphiphilic statistical polymers can perform both intramolecular and intermolecular associations forming simultaneously unimers and multipolymer aggregates. However

their molecular associative behaviour is particularly effected by polymer concentration and macromolecular architecture.[23] For successful self-assembly of **NODAGA-HS-sP(EO-*stat*-PO)** the critical micelle concentration (cmc) was studied using fluorescence spectroscopy. Estimation of the cmc of **NODAGA-HS-sP(EO-*stat*-PO)** was performed using a series of solutions of the functional polymer (concentration varied from 3.0 to 300.0 mg mL^{-1}) and fluorescence probe (8-anilinonaphthalene-1-sulfonic acid ammonium salt, constant concentration of 1.58×10^{-7} mg mL^{-1}, 5×10^{-4} mM). Plotting concentration dependence of emission intensity of **NODAGA-HS-sP(EO-*stat*-PO)** yielded the cmc of the polymer as 30 mg mL^{-1}, similar to the native star **sP(EO-*stat*-PO)** with a cmc of 35 mg mL^{-1} (**Figure 9.3**).

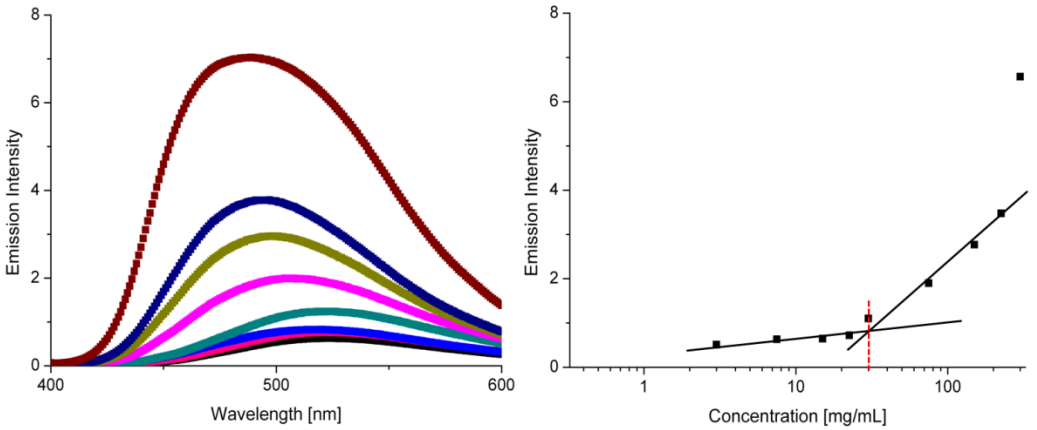

Figure 9.3: Concentration dependence of emission spectra of **NODAGA-HS-sP(EO-*stat*-PO)** (red line denotes the cmc value) at [ANS (fixed)] = 5×10^{-4} mM, $\lambda_{excitation}$= 346 nm $\lambda_{emission}$ = 510 nm. Points correspond to 3.0, 7.5 , 15, 22.5, 30, 75, 150, 225 and 300 mg mL^{-1} respectively.

Knowing critical micellization concentration (cmc) of the functional polymers is critical to determine the concentration of the prepolymers necessary to undergo self-assembly. We used 8-anilinonaphthalene-1-sulfonic acid ammonium salt (ANS) as the fluorescence probe. To estimate cmc of the **NODAGA-HS-sP(EO-*stat*-PO)** a series of solutions with functional polymer and fluorescence probe, in which the concentration of the polymer was varied from 3.0 to 300 mg mL^{-1} and the concentration of the fluorescence probe was kept constant at 1.58×10^{-7} mg mL^{-1} were prepared. ANS has a fluorescence emission at 510 nm (at 296 K) when excited at 346 nm. Therefore the resulting solutions were excited at 346 nm and emission spectrum was collected at 510 nm (**Figure 9.3**). With increasing polymer concentration, the number of the formed

micelles increases and ANS diffuses inside the particles. In this apolar microenvironment, the electron transfer is less limited and the fluorescence is stronger so that the emission intensity increases and simultaneously fluorescence emission is shifted towards blue light. The emission spectra of the solutions containing both **NODAGA-HS-sP(EO-*stat*-PO)** and ANS indicated a shift in the emission maximum from 510 nm to 482 nm. This blue shift was due to decreased local polarity and an increase in the fluorescence lifetime as well as quantum yield arising out of restricted mobility of the fluorophore.[24,25]

It is worth to note that even in the premicellar concentration there is a slight blue shift in the spectrum of ANS which indicates the possibility of the existence of premicellar aggregates. Determining the cmc of the functional polymers using fluorescence emission requires determining the concentration at which abrupt changes in emission intensity takes place. On plotting concentration dependence of emission intensity of **NODAGA-HS-sP(EO-*stat*-PO)**, intercept between the linear extrapolations of the horizontal portion at low polymer concentration and of the rapidly varying portion, yielded the cmc of the polymer as 30 mg mL^{-1}. Similar measurements were also carried out with **sP(EO-*stat*-PO)** prepolymers which also showed a amphiphilic behavious with a cmc close to 35 mg mL^{-1}. This amphiphilicity induces self-assembling in water and as a consequence particles with micellelar type of structure were formed.

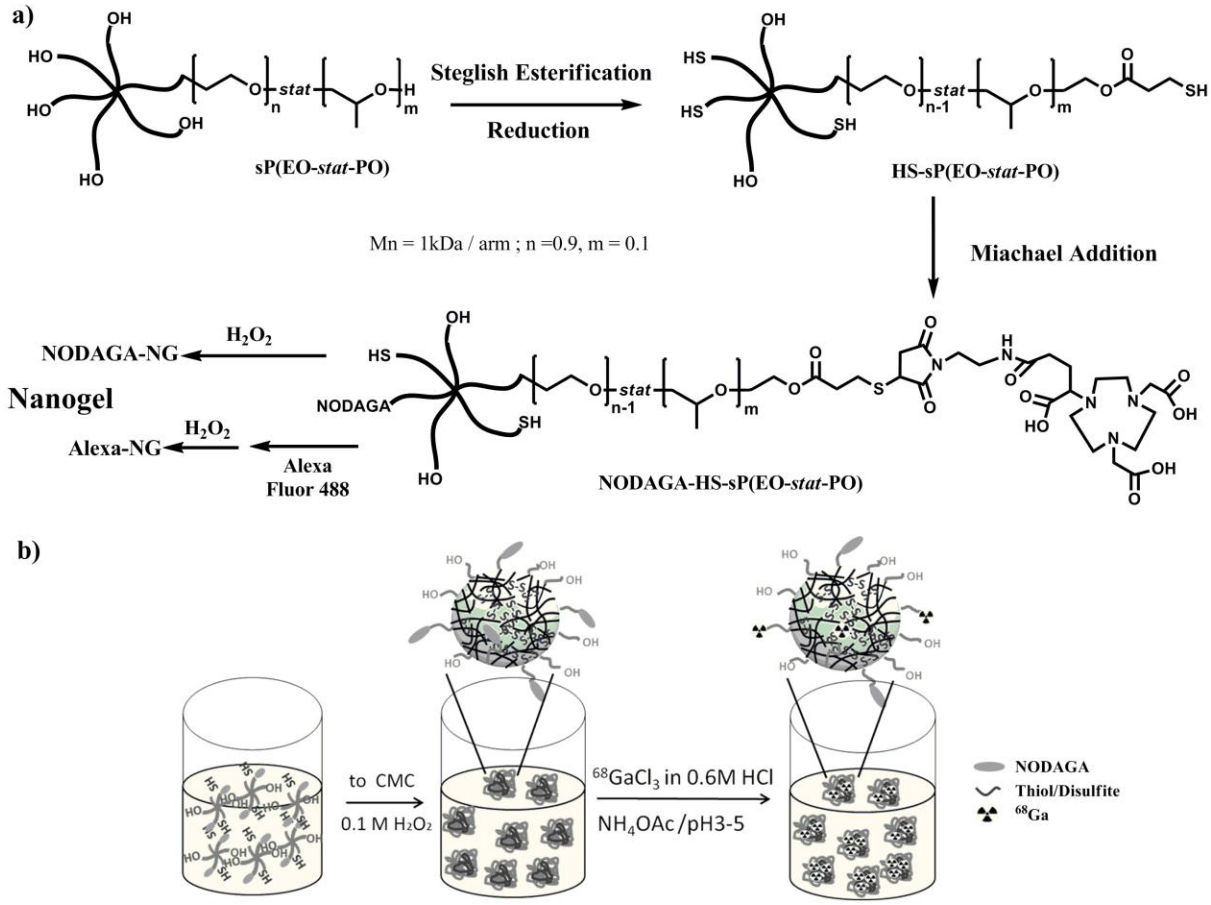

Scheme 9.2: Schematic representation of ^{68}Ga-labeled nanogel synthesis.

The nanogels (NODAGA-NG) were prepared by self-assembly of **NODAGA-HS-sP(EO-*stat*-PO)** in PBS buffer (0.01M, pH 7.4) followed by crosslinking via thiol oxidation with catalytic amount of hydrogen peroxide to ensure the particle stability. Alexa Fluor 488 functionalized prepolymer was converted into nanogel (Alexa-NG) in a similar **(Scheme2).**

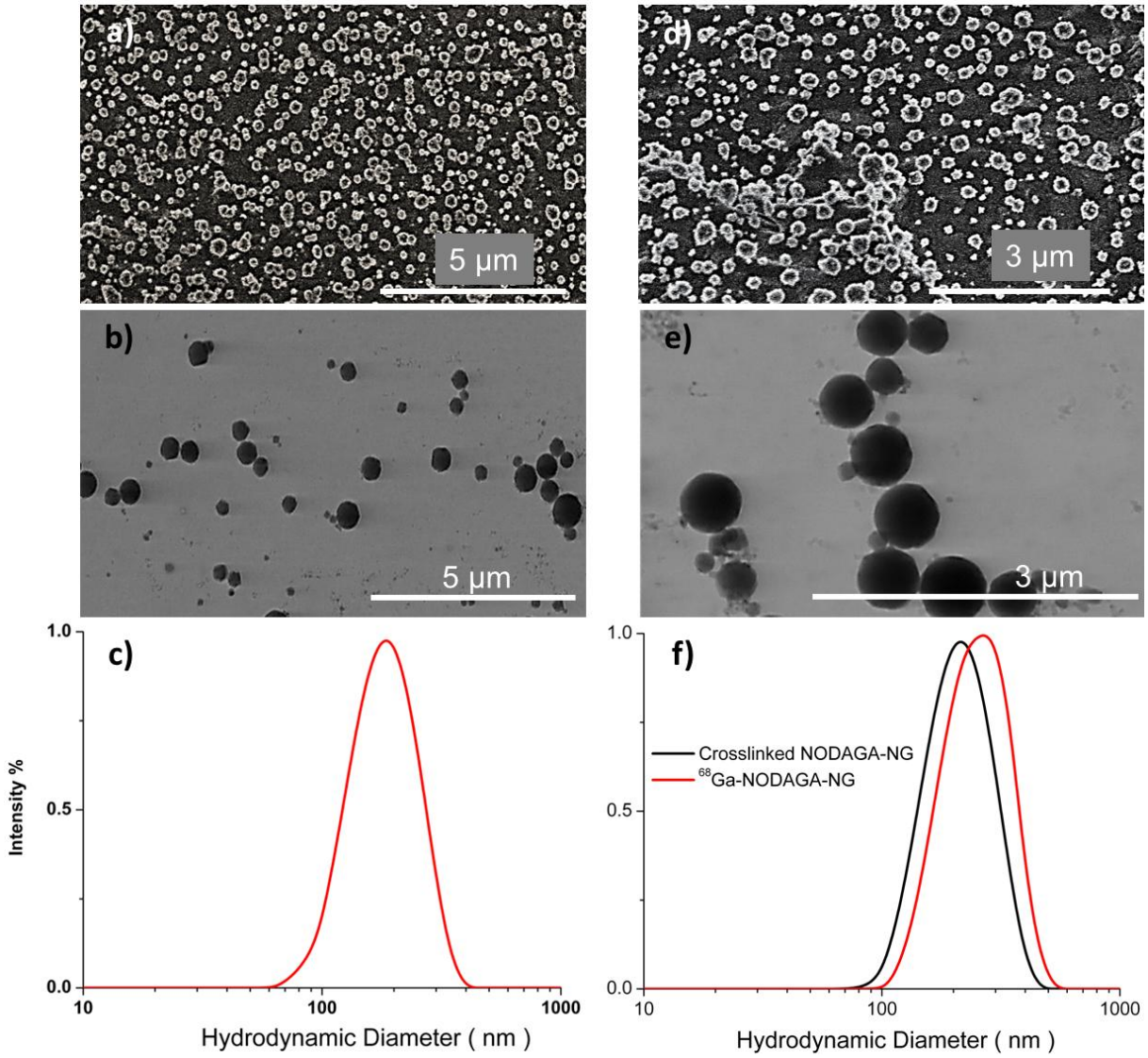

Figure 9.4: Cryo-FESEM image of *a),d)* uncrosslinked and crosslinked **NODAGA-HS-sP(EO-*stat*-PO)**, *b),e)* **Cryo-TEM** image uncrosslinked and crosslinked **NODAGA-HS-sP(EO-*stat*-PO)** nanogels, DLS measurement of c) uncrosslinked, f) crosslinked and ^{68}Ga-labeled **NODAGA-HS-sP(EO-*stat*-PO)** nanogels.

The particle sizes of the NODAGA-NG were investigated using dynamic light scattering (DLS), cryo-field emission scanning electron microscopy (Cryo-FESEM) and cryo-transmission electron microscopy (Cryo-TEM). Hydrodynamic diameter and PDI of nanogels by DLS was 250±50 nm (PDI 0.145) and 270±50 nm (PDI 0.175) before and after crosslinking, respectively. The PDI shows a narrow distribution of the particle size. Cryo-FESEM and Cryo-TEM images showed particles with a diameter *d* in the range of 200 nm < *d* < 300 nm. The nanogels were well defined and spherical. These results indicated that particle size of nanogels did not change significantly upon crosslinking

and they remained monodisperse even after crosslinking. The difference in size obtained from scattering and imaging techniques might be due to partial volume loss of the NODAGA-NG during the freezing step prior to imaging via Cryo-FESEM/TEM (**Figure 9.4**). The fluorescent labeled Alexa-NG showed morphology and comparable size to the unlabeled once, with a hydrodynamic diameter of 310±50 nm (PDI 0.210, **Figure 9.5**).

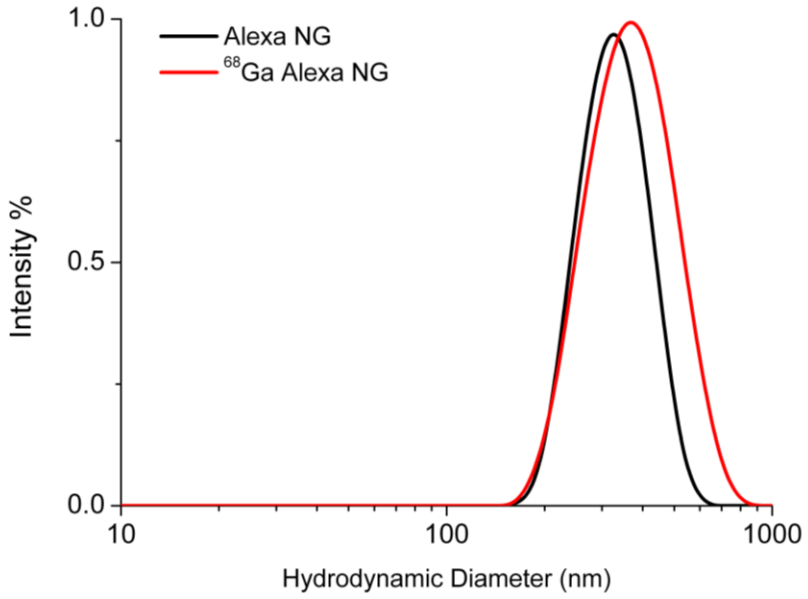

Figure 9.5: DLS measurement of Ga labelled and unlabelled Alexa NG.

Stability of the Nanogels

Stability of the NODAGA-NG was tested by following the change in their size and size distribution upon incubation in radiolabeling buffer (0.6M HCl + 3M NH_4OAc, v/v 3/1; pH 4.5) via DLS. The nanogels showed no decomposition of either polymer or gel structure after remaining 18 days in the buffer (**Figure 9.6**).

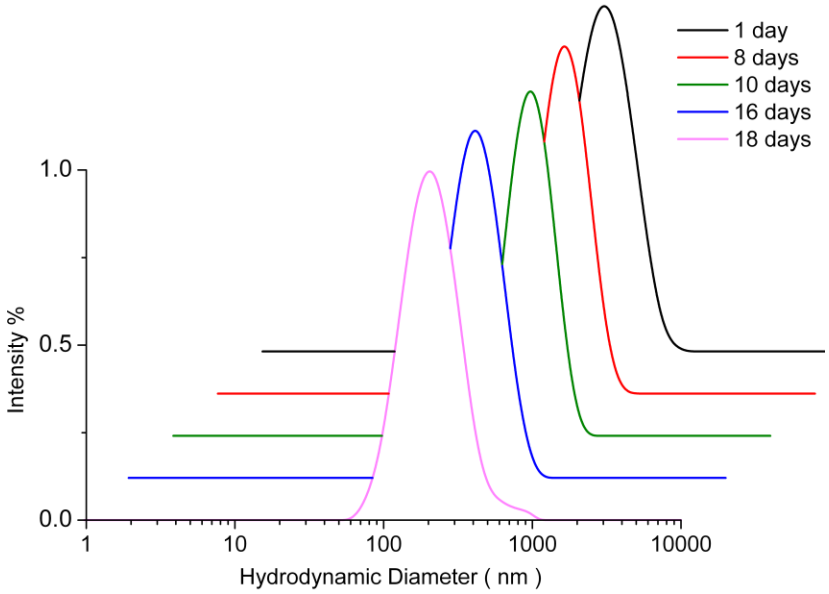

Figure 9.6: Stability of ^{68}Ga labelled NODAGA-NG was tested by following the change in their hydrodynamic diameter upon incubation in radiolabeling buffer (pH 4.5) for 18 days via DLS

Radiolabeling of NODAGA-NG with n.c.a. ^{68}Ga

The ^{68}Ge/^{68}Ga-generator provides no carrier added (n.c.a.) ^{68}Ga as $^{68}GaCl_3$ in 0.6M HCl solution. pH adjustment with NH_4OAc to an optimal pH-range of 3-5 ensures a high radiolabeling yield of the NODAGA-chelator in a biocompatible buffer. Initial tests with the prepolymer (**NODAGA-HS-sP(EO-*stat*-PO)**) indicate, that chelation of n.c.a. $^{68}GaCl_3$ results in high radiochemical yields at room temperature (RT) (**Table 9.1**, **entry 1**). For radiolabeling the generator elute was added to 250 nmol NODAGA-NG dissolved in NH_4OAc (3M) resulting in a pH of 4.5. This was allowed to stand at RT for 15min. ^{68}Ga-NODAGA-NG was purified by SEC on a PD10-Sephadex column receiving a pure product in saline. Using this methodology, NODAGA-NG and Alexa-NG were successfully labeled with nearly quantitative radiochemical yields at RT (**Table 9.1, entry 2-3**). These results for ^{68}Ga-labeling of nanogels confirm the advantageous labeling conditions for ^{68}Ga of the chelator NODAGA compared to DOTA (e.g. RT vs. 85-95°C for ^{68}Ga-labeling of peptides[17]). The size of the nanogels is preserved by radiolabeling demonstrated by an unchanged hydrodynamic diameter and PDI (**Figure 9.4f**, DLS: 270±30 nm, PDI 0.187 vs. 290±50 nm, PDI 0.175). Reducing the amount of NODAGA-NG to 50 nmol (**Table 9.1, entry 3-5**) has no effect on the high radiolabeling efficiency and is comparable with often used amount for NODAGA-

peptide labeling (5-30 nmol).[17] The specific radioactivity of the ^{68}Ga-NODAGA-NG was determinate as up to 1500 GBq/$g_{nanogel}$, so that no pharmacological or toxic effects are expected for in vivo experiments.

Table 9.1 Radiochemical yield of ^{68}Ga-labeling of NODAGA-NG (reaction conditions: 0.3-1.5μg / 0.05-0.25μmol NODAGA-NG + 83μL NH_4OAc (3M) + 250μL $^{68}GaCl_3$ (+ x nmol Ga^{3+}) in 0.6M HCl, 10-15min room temperature, analysis by radio-TLC and radio-HPLC)

	NG [nmol[b]]	**Ga^{3+} [nmol]**	**RCY[a] ^{68}Ga-NODAGA-NG**	**RCY[a] ^{68}Ga-prepolymer**	**RCY[a] ^{68}Ga-Alexa-NG**
1	225			>95%	
2	160				>95%
3	250		>95%		
4	150		>95%		
5	50		>95%		
6	50	56	88%		
7	50	70	62%		
8	50	98	53%		
9	50	126	38%		
10	50	210	18%		

[a]) RCY: radiochemical yield; [b]) nmol prepolymer

In a competition experiment with non radioactive Ga^{3+} the labeling yield of ^{68}Ga-NODAGA-NG decreased from >95% to 18% (**Table 9.1, entry 5 -10**) by increasing the amount of Ga^{3+}. Due to the insignificant amount of radioactive ^{68}Ga (5 pmol carrier free) the NODAGA concentration attached to the nanogel corresponded to Ga^{3+} concentration at a radiochemical yield of 50% (approx. 100 nmol, **Table 9.1**). This calculates 2.0 NODAGA per **NODAGA-HS-sP(EO-*stat*-PO)** (molar ratio of NODAGA-conjugation was 2:1, NODAGA-maleimide to **HS-sP(EO-*stat*-PO)**) and is consistent with the value obtained from ^{1}H-NMR (1.7, **Figure 9.1c**). These results demonstrate a) the number of available labeling position correlates well with the estimated NODAGA concentration, b) all NODAGA-chelators (both inside and outsides of the nanogel

structure) are accessible by diffusion for ^{68}Ga-ions and c) unspecific adsorption of ^{68}Ga is insignificant. In short, specific ^{68}Ga-labeling of NODAGA-NG was achieved with an efficient procedure resulting in radiolabeled nanogels ready to use for small animal PET.

Biological Properties of Alexa-NG

As nanoparticles are suitable vehicles for delivery of therapeutic agents, the mechanisms determining biodistribution and cellular fate should be carefully evaluated. The internalization of nanogels by circulating macrophage precursor cells, the monocytes, and mostly tissue resident phagocytosing macrophages is a predictive indicator of the blood clearance in vivo.

The unstimulated THP monocytes only marginally engulfed Alexa-NG, which suggests an almost non-existent phagocytosis (**Figure 3a**). Stimulation with phorbol-12-myristate-13-acetate (PMA) led to Alexa-NG concentration dependent increase of the phagocytosis rate. In contrast to unstimulated THP monocytes, the ingestion of Alexa-NG in activated macrophages was increased from 9% to 73% by PMA stimulation (**Figure 3**) due to the upregulation of the phagocytosis capacity.

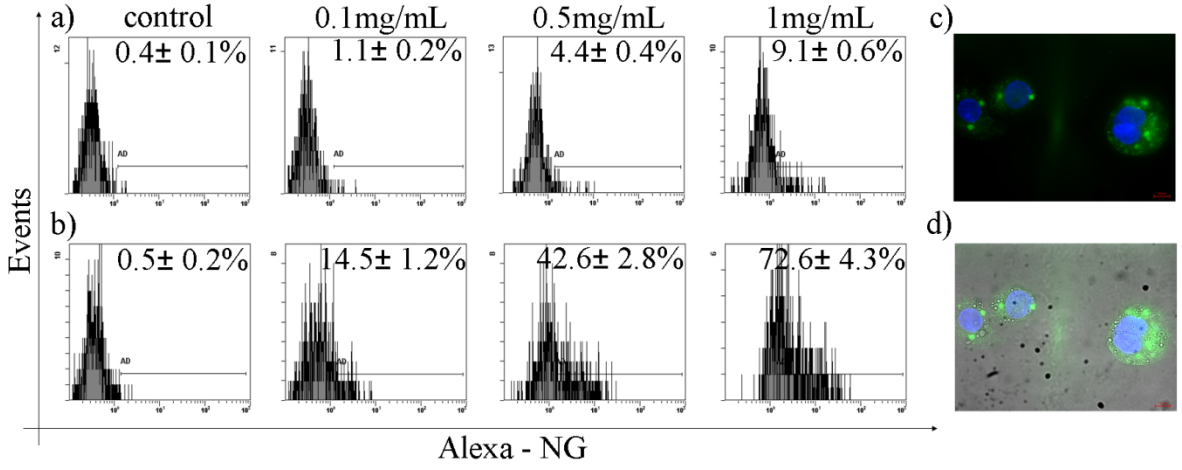

Figure 9.7: Flow cytometric phagocytosis analysis of Alexa-NG particles in a) unstimulated THP-1 cells and b) PMA stimulated THP-1 cells after incubation with 0.1 mg/mL, 0.5 mg/mL and 1.0 mg/mL of Alexa-NG´s for 1h at 37°C. Fluorescence microscopy analysis of PMA stimulated THP-1 macrophages after incubation with 1.0 mg/mL of Alexa-NG´s for 1h at 37°C and counterstaining with Hoechst c) overlay of Alexa-NG´s with Hoechst and d) overlay of fluorescence with bright field (100-fold magnification).

These results visualized an efficient internalization of Alexa-NG by phagocytosing cells like macrophages. Importantly, nanogels remain largely unrecognized for monocytes. This will probably result in a desired slow clearance and prolonged blood circulation of nanogels. No general cytotoxic effects were observed in cells after incubation with NODAGA-NG or Alexa-NG. However, for in vivo application, the possible cytotoxic effects on liver or kidneys due to the hepatic or renal retention and clearance of ^{68}Ga-NODAGA-NG have to be considered.

9.4 Conclusion

Radiolabeling of nanogels is a new approach for nuclear molecular imaging with a high scientific potential. Derivatisation of the nanogel with the chelator NODAGA results in a highly efficient and specific ^{68}Ga-labeling. The high stability and the mild radiolabeling conditions allow a preservation of the nanogel structure evidenced by the negligible change of polymer properties. Due to their surface properties the nanogels are basically unrecognizable for monocytes. The PEG based radiolabeled-nanogel concept allow easily additional modifications with biomarkers (e.g. peptides) for additional active targeting in vivo.

^{68}Ga-nanogels will enable preclinical studies to understand the in vivo behaviour of nanogel, especially fate of the nanogel and measuring of the EPR-effect.

9.5 References

[1] R. Duncan, *Nat. Rev. Drug Discovery* **2003**, 2, 347.

[2] D. J Siegwart, J. K. Oh, K. Matyjaszewski, *Prog. Polym. Sci.* **2012**, 37, 18.

[3] K. Albrecht, M. Moeller, J. Groll, *Adv. Polym. Sci.* **2010**, 234, 65.

[4] D. E. Owens, N. E. Peppas, *Int. J. Pharm*. **2006**, 307, 93.

[5] R. Gref, Y. Minamitake, M. T. Peracchia, V. Trubetskoy, V. Torchilin, R. Langer, *Science* **1994**, 263, 1600.

[6] B. Naeye, K. Raemdonck, J. Demeester, S. C. DeSmedt, *J. Control. Rel.* **2010**, 148, e90.

[7] H. Maeda, G. Y Bharate, J. Daruwalla, *Eur. J. Pharm. Biopharm*. **2009**, 71, 409.

[8] Y. Matsumura, H. Maeda, *Cancer Res.* **1986**, 46, 6387.

[9] M. Allmeorth, D. Moderegger, B. Biesalski, K. Koynov, F. Rösch, O. Thews, R. Zentel, *Biomacromolecules* **2011**, 12, 2841.

[10] J. Thevenot, A. L. Troutier, L. David, T. Delair, C. Ladaviere, *Biomacromolecules* **2007**, 8, 3651.

[11] K. Fukukawa, R. Rossin, A. Hagooly, E. D. Pressly, J. N. Hunt, B. W. Messmore, K. L. Wooley, M. J. Welch, C. J. Hawker, *Biomacromolecules* **2008**, 9, 1329.

[12] D. W. Barlett, H. Su, I. Hildebrandt, W. A. Weber, M. E. Davis, *Proc. Natl. Acad. Sci.* **2007**, 104, 15549.

[13] X. Sun, R. Rossin, J. L. Turner, M. L. Becker, M. J. Joralemon, M. J. Welch, K. L. Wooley, *Biomacromolecules* **2005**, 6, 2541.

[14] M. Sarparanta, E. Meakilea, T. Heikkilea, J. Salonen, E. Kukk, V. P. Lehto, H. A. Santos, J. Hirvonen, A. J. Airaksinen, *Mol. Pharmaceutics* **2011**, 8, 1799.

[15] T. Nochi, Y. Yuki, H. Takahashi, S. Sawada, M. Mejima, T. Kohda, N. Harada, G. Kong, A. Sato, N. Kataoka, D. Tokuhara, S. Kurokawa, Y. Takahashi, H. Tsuda, S. Kozaki, K. Akiyoshi, H. Kiyono, *Nat. Materials* **2010**, 9, 572.

[16] S. Soni, A. K. Babbar, R. K. Sharma, A. Maitra, *J. Drug Targeting* **2006,** 14, 87.

[17] M. Fani, L. D. Pozzo, K. Abiraj, R. Mansi, M. L. Tamma, R. Cescato, B. Waser, W. A. Weber, J. C. Reubi, H. R. Maecke, *J. Nucl. Med.* **2011**, 52, 1110.

[18] A. Meister, M. E. Anderson, *Annu. Rev. Biochem.* **1983**, 52, 711.

[19] J. Groll, S. Singh, K. Albrecht, M. Moeller, *J. Polym. Sci. Part A: Polym. Chem*. **2009**, 47, 5543.

[20] ((Highly functional star shaped prepolymers for ultrathin layer formation)) Peter Gasteier, PhD thesis, RWTH University ((Aachen)), October, **2009**.

[21] K. P. Eisenwiener, M. I. M. Prata, I. Buschmann, H. W. Zhang, A. C. Santos, S. Wenger, J. C. Reubi, H. R. Maecke, *Bioconjugate Chem.* **2002**, 13, 530.

[22] D. Lin-Vien, N. B. Colthup, W. G. Fateley, J. G. Grasselli, The handbook of infrared and Raman characteristic frequencies of organic molecules, Academic Press, San Diego, USA **1991**.

[23] A. Hashidzume, A. Kawaguchi, A. Tagawa, K. Hyoda, T. Sato, *Macromolecules* **2006**, 39, 1135.

[24] A. C. Kumar, H. Erothu, H. B. Bohidar, A. K. Mishra, *J. Phys. Chem. B* **2011**, 115, 433.

[25] S. A. Ferreira, P. J. G. Coutinho, F. M. Gama, *Langmuir* **2010**, 26, 11413.

Acknowledgements

The practical work forming the basis of this PhD thesis was mainly carried out at the Interactive Materials Research – DWI at the RWTH Aachen from September 2008 to October 2012 under the supervision of Professor Dr. Martin Möller. I would like to express my deep gratitude to him for giving me the opportunity to work on such an interesting topic and for the discussions critical to the progress of the research. I consider myself very fortunate that he taught me critical scientific thinking. I have learned a lot from him.

My sincere thanks goes to Prof. Dr. Jürgen Groll for his whole hearted support during my studies when he was in Aachen as well as when he moved to Würzburg. I really appreciate his encouragement during my studies and for my successful integration here in Aachen. All these were extremely essential for the completion of this dissertation. I am particularly grateful to Dr. Krystyna Albrecht for the good communication, discussions and suggestions during the work and teaching me all the preliminary things, proof reading my publications and helping me with AFM. Not only professionally but personally also she was a great support.

I would also like to thanks Prof. Andrij Pich for his constant support and being available all the time for critical discussion and valuable suggestions.

Special thanks go to Dr. Joern Schmaljohann and Natascha Drude from Department of Nuclear Medicine, University Hospital, RWTH Aachen for a very fruitful co-operation.

I am also thankful to Stefan Ruetten and Dr. Ho Phan for great help with Cryo-FESEM measurements.

I gratefully acknowledge Artur Henke, Micheal Meurathrath, Claudia Poerschke, Haika Heidelbrand, Heidrun Keul, Fuat Topuz, Naveed Anwar, Matthias Kuhlmann, Sabrina Ullman and Juliana Kurniadi for their valuable advice and support during the everyday laboratory life and for providing a comfortable working atmosphere and perfect working conditions.

I am very thankful to all my friends, especially Harsh Sankhla and Manisha Gupta who supported me all through my ups and downs and for giving me a helping hand during this whole process. Thank you very much!

Last but not the least I am so very grateful to my family for their encouragement, unconditional love, and support throughout the years. Without the support of all of you this work would have been hardly possible.

List of Publications

Parts of this thesis are published, submitted to be published or presented at conferences.

Articles:

1. **Smriti Singh**, Krystyna Albrecht, Martin Moeller, Juergen Groll: Biodegradable Nanogels for Targeted Delivery of Proteins, *BIOmaterialien* **2008**, 9, 135.

2. Matthias Bartneck, Heidrun A. Keul, **Smriti Singh,** Gabriele Zwadlo-Klarwasser, Juergen Groll: Surface chemistry of gold nanorods determines uptake by human primary immune cells, *BIOmaterialien* **2008**, 9, 136.

3. Juergen Groll, **Smriti Singh**, Krystyna Albrecht, Martin Moeller: Biocompatible and degradable nanogels via oxidation reactions of synthetic thiomers in inverse miniemulsion, *Journal of Polymer Science Part A: Polymer Chemistry* **2009**, 47, 5543.

4. Matthias Bartneck, Heidrun A. Keul, **Smriti Singh**, K. Czaja, J. Bornemann, M. Bockstaller, Martin Moeller, Gabriele Zwadlo-Klarwasser, Juergen Groll: Rapid uptake of gold nanorods by primary human blood phagocytes and immunomodulatory effects of surface chemistry, *ACS Nano* **2010**, 4, 3073.

5. Delia Projahn, Elisa A. Liehn, **Smriti Singh**, Birgit Kramp, Doris Klee, Jeurgen Groll, A. Zernecke, Christian Weber, Rory R. Koenen; Generation of biodegradable protease-resistant CXCL12-and MET-RANTES-derivatized gels for the therapy of myocardial infarction, *Journal of Vascular Research* **2011**, 48, 298.

6. **Smriti Singh**, Julia Bloehbaum, Martin Moeller, Andrij Pich: Biohybrid Nanogels by Crosslinking of Ovalbumin with Reactive Star-PEGs in W/O Emulsions, *Journal of Polymer Science Part A: Polymer Chemistry* **2012**, 50, 4288.

7. Matthias Kuhlmann, **Smriti Singh,** Juergen Groll**:** Controlled ring-opening polymerization of substituted episulphide for side chain functional polysulphide-based amphiphiles, *Macromolecule Rapid Communication* **2012**, 33, 1482.

8. **Smriti Singh,** Ilona Zilkowski, Andrea Ewald, Tobias Maurell-Lopez, Martin Moeller, Krystyna Albrecht, Juergen Groll: Mild oxidation of thiofunctional polymers to cytocompatible and stimuli-sensitive hydrogels and nanogels, *Macromolecule Bioscience* DOI = 10.1002/mabi.201200389

9. **Smriti Singh,** Fuat Topuz, Kathrin Hahn, Krystyna Albrecht, Juergen Groll: Embedding of Active Proteins and Living Cells in Redox-Sensitive Hydrogels and Nanogels through Enzymatic Cross-Linking, *Angewandte Chemie* 2013, 52, 3000.

10. **Smriti Singh,** Bahar Bingoel, Agnieszka Morgenroth, Felix M. Mottaghy, Martin Moeller, Joern Schmaljohan: Radiolabeled Nanogels for Nuclear Molecular Imaging, *Macromolecular Rapid Communication 2013, 34, 562.*

11. **Smriti Singh**, Martin Moeller, Andrij Pich: Highlight- Biohybrid Nanogels, *Journal of Polymer Science Part A: Polymer Chemistry* 2013, 51, 3044

12. Delia Projahn, Sakine Simsekyilmaz, **Smriti Singh**, Isabella Kanzler, Birgit Kramp, Jürgen Bernhagen, Doris Klee, Jeurgen Groll, Christian Weber, Elisa A. Liehn, Rory R. Koenen: Intramyocardial delivery of engineered chemokines using biodegradable hydrogel for prevention of injury extension after myocardial infarction- *Journal of Cellular and Molecular Medicine* doi: 10.1111/jcmm.12225

13. **Smriti Singh,** Fuat Topuz, Krystyna Albrecht, Juergen Groll, Martin Moeller: Stimuli-Sensitive Microgels from Native Elastin: An Easy Approach for a Drug Release System - *Advances in Polymer Science* 2013, 262, 415.

14. Fuat Topuz, **Smriti Singh,** Krystyna Albrecht, Marin Moeller**,** Juergen Groll: DNA microgels for polyaromatic quenching- **to submit**

Poster/Abstract:

1. Krystyna Albrecht, Heidrun Keul, **Smriti Singh**, Helmut Keul, Martin Moeller, Preparation of Biodegradable Nanogels and Gold Rod-Like Nanoparticles Coated with Hydrogel Layer. NanoBiopharmaceutics Graz, Austria, 2008.

2. **Smriti Singh,** Krystyna Albrecht, Juergen Groll, Martin Moeller, Nanogel Particles as Carriers for Peptide and Proteins: Bio and Polymers. New polymer Technologies in water, Aachen, Germany, 2008.

3. Heidrun A. Keul, **Smriti Singh**, Wiktor Steinhauer, Krystyna Albrecht, Michael Bockstaller, Helmut Keul, Martin Möller, Jürgen Groll, Biocompatibilization of Rodlike Gold Nanoparticles. Bio&Polymers, Aachen, 2008.

4. Karola Scheafer, Krystyna Albrecht, **Smriti Singh**, Michael Scharpf, Wiktor Steinhauer, Helmut Keul, Martin Meoller, Synthesis of hydrophilic thiol-functional polymers and applications. Aachen Dresden International Textile Conference, Dresden, Germany, 2008.

5. **Smriti Singh,** Krystyna Albrecht, Juergen Groll, Martin Moeller, Preparation of Novel Nanogel Particles as Carriers for Peptide and Proteins. New Year Symposium, Institute für Organic Chemistry, Aachen, Germany, 2009.

6. **Smriti Singh**, Krystyna Albrecht, Martin Moeller, Juergen Groll: Biodegradable Nanogels via Addition Reactions in Inverse Miniemulsion- Proceedings of the 2nd International Symposium on Advanced Particles, Yokohama, Japan, 2009.

7. **Smriti Singh,** Krystyna Albrecht, Martin Moeller, Juergen Groll, Biocompatible and Degradable Nanogels via Addition Reactions in Inverse Miniemulsion as Delivery Vehicles for Peptides and Proteins. Euro Nano Medicine, Bled, Slovenia, 2009.

8. **Smriti Singh,** Krystyna Albrecht, Martin Moeller, Juergen Groll, Biocompatible and Degradable Nanogels as Delivery Vehicles for Peptides and Proteins. Biomedica, Aachen, Germany, 2010.

9. Heidrun A. Keul, Matthias Bartneck**, Smriti Singh**, Gabriele Zwadlo-Klarwasser, Michael R. Bockstaller, Juergen Groll, Martin Moeller. Properties determining nanoparticle clearance by primary human leukocytes. Abstracts of Papers, 239th ACS National Meeting, San Francisco, CA, United States, 2010.

10. Juergen Groll, **Smriti Singh,** Krystyna Albrecht, Martin Moeller, Redox-Sensitive Nanogels for Targeted Delivery of Proteins. Polymers in Biomedicine and Electronics, Berlin-Dahlem, Germany, 2010.

11. Delia Projahn, E. Liehn, **Smriti Singh**, B. Kramp, Doris. Klee, Juergen. Groll, A. Zernecke, C. Weber, R. R. Koenen-Generation of a biodegradable protease-resistant CXCL12- and METRANTES-1 derivatized gels for the therapy of myocardial infarction**.** Cardiac Stem Cell and Tissue Engineering Conference, Venice, Italy, 2011.

12. **Smriti Singh**, Krystyna Albrecht, Martin Moeller, Juergen Groll, Biocompatible and Degradable Nanogels as Delivery Vehicles for Peptides and Proteins, 24th European Congress on Biomaterials, Dublin, Ireland, 2011.

13. Matthias Kuhlmann, **Smriti Singh**, Krystyna Albrecht, Martin Moeller, Juergen Groll, Polyglycidol-based Nanogels for Targeted Protein-Delivery. 9th world Biomaterial Congress, Chengdu, China, 2012.

14. **Smriti Singh,** Krystyna Albrecht, Martin Moeller, Juergen Groll, Nanogel as Carriers for Proteins. S-PolyMart, Kerkrade, Netherlands, 2012.

15. Matthias Kuhlmann, **Smriti Singh**, Krystyna Albrecht, Juergen Groll, Polyglycidol-based Nanogels for Targeted Protein Delivery. Proceedings of the 4th International Conference on Strategies in Tissue Engineering. Würzburg, Germany, 2012.

16. Matthias Kuhlmann, **Smriti Singh**, Krystyna Albrecht, Juergen Groll, Redox-Sensitive Nanogels for Targeted Delivery of Proteins. Proceedings of the 9th World Biomaterials Congress, Chengdu, China, 2012

17. **Smriti Singh,** Krystyna Albrecht, Martin Moeller, Juergen Groll, Enzyme triggered Hydrogel / nanogel formation. Warwick Polymer Conference, Coventry, UK, 2012.

18. Fuat Topuz, **Smriti Singh**, Krystyna Albrecht, Martin Moeller, Juergen Groll - Design and engineering of DNA nanogels as PAH scavengers. Biomedica Summit, Liege, Belgium, 2012.

19. **Smriti Singh**, Fuat Topuz, Krystyna Albrecht, Martin Moeller, Juergen Groll - Dual sensitive elastin polypeptide microgels. European Polymer Fedration (EPF) Pisa, Italy, 2013.